creative commons
COMMONS DEED

저작자표시-비영리-변경금지 2.0 대한민국

이용자는 아래의 조건을 따르는 경우에 한하여 자유롭게

- 이 저작물을 복제, 배포, 전송, 전시, 공연 및 방송할 수 있습니다.

다음과 같은 조건을 따라야 합니다:

저작자표시. 귀하는 원저작자를 표시하여야 합니다.

비영리. 귀하는 이 저작물을 영리 목적으로 이용할 수 없습니다.

변경금지. 귀하는 이 저작물을 개작, 변형 또는 가공할 수 없습니다.

- 귀하는, 이 저작물의 재이용이나 배포의 경우, 이 저작물에 적용된 이용허락조건을 명확하게 나타내어야 합니다.
- 저작권자로부터 별도의 허가를 받으면 이러한 조건들은 적용되지 않습니다.

저작권법에 따른 이용자의 권리는 위의 내용에 의하여 영향을 받지 않습니다.

이것은 이용허락규약(Legal Code)을 이해하기 쉽게 요약한 것입니다.

Disclaimer

dCollection

이학박사학위논문

Shift in the dominant red-tide species, establishment of two new dinoflagellate genera, and ecophysiology of the mixotrophic dinoflagellate *Biecheleria cincta* from Shiwha bay, Korea

시화호에서 우점 적조종의 변화 및 와편모류 두개의 신속 수립과 혼합영양성 와편모류인 *Biecheleria cincta*의 생태생리에 대한 연구

2016년 02월

서울대학교 대학원

지구환경과학부 해양학전공

강 남 선

Shift in the dominant red-tide species, establishment of two new dinoflagellate genera, and ecophysiology of the mixotrophic dinoflagellate *Biecheleria cincta* from Shiwha bay, Korea

시화호에서 우점 적조종의 변화 및 와편모류 두개의 신속 수립과 혼합영양성 와편모류인 *Biecheleria cincta*의 생태생리에 대한 연구

지도교수 정 해 진

이 논문을 이학박사 학위논문으로 제출함

2016 년 02 월

서울대학교 대학원
지구환경과학부 해양학 전공
강 남 선

강남선의 박사 학위논문을 인준함

2016 년 02 월

위 원 장 _____ (인)

부위원장 _____ (인)

위 원 _____ (인)

위 원 _____ (인)

위 원 _____ (인)

Abstract

Shift in the dominant red-tide species, establishment of two new dinoflagellate genera, and ecophysiology of the mixotrophic dinoflagellate *Biecheleria cincta* from Shiwha bay, Korea

Nam Seon Kang

Oceanography

School of Earth and Environmental Sciences

College of Natural Sciences

Seoul National University

Red tides, discoloration of sea surface due to plankon blooms, have often caused large scale mortality of fin-fish, shellfish, and marine mammals and sometimes destroy the balance in marine ecosystems. To understand red tide dynamics and economic impact in a certain area, red-tide causative species should be identified and variations in their abundances investigated. Furthermore, if they were not previously reported, their taxonomy should be explored. Moreover, their ecophysiology should be investigated.

Restricted water circulation and/or high nutrient load from freshwater in bays and estuaries have been known to be favorable for outbreaks of red tides. However, intense turbulence and/or vigorous mixing have been shown to prevent outbreaks of red tides in some cases. Shiwha bay is an ideal place to explore effects of restricted

water circulation, high nutrient load, and turbulence and/or vigorous mixing on red tide outbreaks. In 1994, a 12.7-km dike with a 100-m water gate was constructed in the mouth of the bay and water exchange between inside and outside the dike occurred only through the water gate, but water circulation was highly restricted and the tidal range inside the dike was reduced to 3-5 m. However, in 2011, the world's largest tidal power plant was constructed in the middle of the dike and water exchange began to occur through the turbines of the tidal power plant.

To understand red tide dynamics in Shiwha Bay, shift in the dominant species of red tides before and after establishment of the tidal power plant was explored by analyzing samples collected from 3 fixed stations inside the dike on a monthly basis from 2008 to 2012 and measured physical, chemical, and biological properties (Chapter 2). In the research period, I isolated and set up clonal cultures of two new dinoflagellates isolated from Shiwha Bay and established new genera, *Paragymnodinium* and *Gyrodiniellum* through intensive morphological and genetic analyses (Chapter 3 and 4). Furthermore, I found the phototrophic dinoflagellate, *Biecheleria cincta* which had not been reported in Korean water and explored its ecophysiology (Chapter 5). I revealed that this dinoflagellate is a mixotrophic dinoflagellates feeding on diverse algal prey species. The combined results of these subtopics provide a basis on better understanding red tide dynamics in Shiwha Bay.

In Chapter 2, I focused on effects of water circulation on red tide dynamics. Restriction of water circulation at Station 1 (in the innermost part of the bay) may cause more frequent red tides due to phototrophic dinoflagellates than those at Station 3, where water exchange between the inside and outside of the dike occurs through a water gate. After the tidal power plant was established in 2011, red-tide causative species switched from phototrophic dinoflagellates such as *Gymnodinium aureolum*, *Heterocapsa rotundata*, *Heterocapsa triquetra*, *Karlodinium veneficum*, *Paragymnodinium shiwhaense*, and *Prorocentrum minimum* to diatoms such as *Chaetoceros* spp., *Skeletonema costatum*, and *Thalassiosira* spp.. Exchange of

seawater between the inside and outside of the dike through the tidal power plant may have resulted in this change in the species composition. Inorganic nitrogen concentrations for the growth of phototrophic dinoflagellates and small flagellates during red tides were likely unlimited, but inorganic phosphorus concentrations may be limited. Thus, some phototrophic dinoflagellates and flagellates may be driven to acquire phosphorus from prey. The maximum grazing coefficients of the heterotrophic dinoflagellates *Pfiesteria piscicida*, *Gyrodiniellum shiwhaense*, *Gyrodinium dominans, Gyrodinium moestrupii*, and *Protoperidinium bipes* feeding on red-tide causative taxa including cryptophytes, *Eutreptiella gymnastica*, *P. minimum*, and *S. costatum*, were found to be 0.14-0.77 h^{-1}. Therefore, heterotrophic protistan grazers in Shiwha Bay may, at times, have considerable grazing impact on populations of co-occurring red-tide organisms.

In Chapter 3, I established a new phototrophic dinoflagellate species in a new genus. The phototrophic dinoflagellate *Paragymnodinium shiwhaense* n. gen., n. sp. is described from living cells and from cells prepared by light, scanning electron, and transmission electron microscopy. In addition, sequences of the small subunit (SSU) and large subunit (LSU) rDNA and photosynthetic pigments are reported. The episome is conical, while the hyposome is hemispherical. Cells are covered with polygonal amphiesmal vesicles arranged in 16 rows and containing a very thin plate-like component. There is neither an apical groove nor apical line of narrow plates. Instead, there is a sulcal extension-like furrow. Cell length and width of live cells fed *Amphidinium carterae* were 8.4-19.3 and 6.1-16.0 μm, respectively. *P. shiwhaense* does not have a nuclear envelope chamber nor a nuclear fibrous connective (NFC). Cells contain chloroplasts, nematocysts, trichocysts, and peduncle, though eyespots, pyrenoids, and pusules are absent. The main accessory pigment is peridinin. The sequence of the SSU rDNA of this dinoflagellate is 4% different from that of *Gymnodinium aureolum*, *Lepidodinium viride*, and *Gymnodinium catenatum*, the three closest species, while the LSU rDNA was 17-18% different from that of *G. catenatum*, *Lepidodinium chlorophorum*, and

Gymnodinium nolleri. The phylogenetic trees show that this dinoflagellate belongs within the *Gymnodinium* sensu stricto clade. However, in contrast to *Gymnodinium* spp., cells lack nuclear envelope chambers, NFC, and an apical groove. Unlike *Polykrikos* spp., which have a taeniocyst-nematocyst complex, *P. shiwhaense* has nematocysts without taeniocysts. In addition, *P. shiwhaense* does not have ocelloids in contrast to *Warnowia* spp. and *Nematodinium* spp. Therefore, based on morphological and molecular analyses, I suggest that this taxon is a new species, also within a new genus.

In Chapter 4, I established a new heterotrophic dinoflagellate species in a new genus. The heterotrophic dinoflagellate *Gyrodiniellum shiwhaense* n. gen., n. sp. is described from live cells and from cells prepared for light, scanning electron, and transmission electron microscopy. Also, sequences of the SSU and LSU of rDNA have been analyzed. The episome is conical, while the hyposome is ellipsoid. Cells are covered with polygonal amphiesmal vesicles arranged in 16 horizontal rows. Unlike other *Gyrodinium*-like dinoflagellates, the apical end of the cell shows a loop-shaped row of five elongate amphiesmal vesicles. Cells that were feeding on the dinoflagellate *Amphidinium carterae* Hulburt were 9.1–21.6 μm long and 6.6–15.7 μm wide. Cells of *G. shiwhaense* contain nematocysts, trichocysts, a peduncle, and pusule systems, but they lack chloroplasts. The SSU rDNA sequence is >3% different from that of the six most closely related species: *Warnowia* sp. (FJ947040), *Lepidodinium viride* Watanabe, Suda, Inouye, Sawaguchi & Chihara, *Gymnodinium aureolum* (Hulburt) Hansen, *Gymnodinium catenatum* Graham, *Nematodinium* sp. (FJ947039), and *Gymnodinium* sp. MUCC284 (AF022196), while the LSU rDNA is 11–12% different from that of *Warnowia* sp., *G. aureolum,* and *Nematodinium* sp. (FJ947041). The phylogenetic trees show that the species belongs in the *Gymnodinium* sensu stricto clade. However, in contrast to *Gymnodinium* spp., cells lack nuclear envelope chambers and a nuclear fibrous connective. Unlike *Polykrikos* spp., cells of which possess a taeniocyst–nematocyst complex, *G. shiwhaense* has nematocysts but lacks taeniocysts. It differs from *Paragymnodinium shiwhaense*

Kang, Jeong, Moestrup & Shin by possessing nematocysts with stylets and filaments. *Gyrodiniellum shiwhaense* n. gen., n. sp. furthermore lacks ocelloids, in contrast to *Warnowia* spp., *Nematodinium* spp., and *Proterythropsis* spp. Based on morphological and molecular data, I suggest that the taxon represents a new species within a new genus.

In Chapter 5, I explored ecophysiology of the phototrophic dinoflagellate *Biecheleria cincta* which had not been reported in Korean waters. *Biecheleria* species are dinoflagellates in the order Suessiales inhabitingmarine or freshwater environments; their ecophysiology has not been well investigated, in particular, their trophic modes have yet to be elucidated. Previous studies have reported that all *Biecheleria* species are photosynthetic, although their mixotrophic abilities have not been explored. I isolated a dinoflagellate from coastal waters in western Korea and established clonal cultures of this dinoflagellate. On the basis of morphology and analyses of the small/large subunit rRNA gene, I identified this dinoflagellate as *Biecheleria cincta* (previously *Woloszynskia cincta*). I further established that this dinoflagellate is a mixotrophic species. I found that *B. cincta* fed on algal prey using a peduncle. Among the diverse prey provided, *B. cincta* ingested those algal species that had equivalent spherical diameters (ESDs) ≤12.6 μm, exceptions being the diatom *Skeletonema costatum* and the dinoflagellate *Prorocentrum minimum*. However, *B. cincta* did not feed on larger algal species that had ESDs ≥15 μm. The specific growth rates for *B. cincta* increased continuously with increasing mean prey concentration before saturating at a concentration of ca. 134 ng C ml^{-1} (1,340 cells ml^{-1}) when *Heterosigma akashiwo* was used as food. The maximum specific growth rate (i.e. mixotrophic growth) of *B. cincta* feeding on *H. akashiwo* was 0.499 d^{-1} at 20 °C under illumination of 20 μE m^{-2} s^{-1} on a 14:10 h light-dark cycle, whereas its growth rate (i.e. phototrophic growth) under the same light conditions without added prey was 0.040 d^{-1}. The maximum ingestion and clearance rates of *B. cincta* feeding on *H. akashiwo* were 0.49 ng C $grazer^{-1}$ d^{-1} (4.9 cells $grazer^{-1}$ d^{-1}) and 1.9 μl $grazer^{-1}$ h^{-1}, respectively. The calculated grazing coefficients for *B. cincta*

on co-occurring *H. akashiwo* were up to 1.1 d^{-1}. The results of the present study suggest that grazing by *B. cincta* can have a potentially considerable impact on prey algal populations.

Conclusively, this study clearly shows that a shift in the dominant red tide causative species after establishment of the tidal power plant occurred. Furthermore, discovery of new dinoflagellate genera may stimulate researches on eco-physiology, evolution, and utilization of these dinoflagellates. Moreover, unveiling mixotrophic ability of the small phototrophic dinoflagellate *Biecheleria cincta* provide a clue to understanding ecological roles of small mixotrophic dinoflagellates in marine ecosystems.

Keywords: Ecology, Harmful Algal bloom, Physiology, Proist, Red tide, Taxonomy

Student Number: 2005-23246

Contents

Chapter 1 Introduction……....1

Chapter 2 Shifted dynamics of red tides organisms following a huge dike and tidal power plant established in shiwha Bay, western Korea.....6

2.1 Abstract…….....6

2.2 Key words…….....7

2.3 Introduction…….....7

2.4 Materials and methods…….....9

2.4.1 Abundances of protists and bacteria in Shiwha Bay…….....9
2.4.2 Physical and chemical properties in Shiwha Bay…….....12
2.4.3 Grazing impact of heterotrophic protists on red-tide organisms..13

2.5 Results…….....14

2.5.1 Physical and chemical properties in Shiwha Bay……....14
2.5.1.1 Station 1……..14
2.5.1.2 Station 2……..15
2.5.1.3 Station 3……..15
2.5.2 Frequency of red tides and dominant groups……...16
2.5.3 Temporal and spatial variations in red-tide causative species….19
2.5.4 Conditions when red-tide causative species formed red tide in Shiwha Bay.....25
2.5.5 Spatial distribution of *Paragymnodinium shiwhaense* and *Biecheleria cincta* in Shiwha Bay…….....30
2.5.6 Dominant species of heterotrophic protists…….30

2.5.7 Grazing impact by protistan grazers on red-tide organisms…….31
2.5.8 Correlation coefficients at all three stations…….....43

2.6 Discussion……...44

2.6.1 Physical, chemical, and biological properties in Shiwha Bay….44
2.6.2 Trends in frequency and causative species of red-tide events in Shiwha Bay……...44
2.6.3 Effects of physical and chemical factors on frequency and causative species of red-tide events……..49
2.6.4 Grazing impact……..52

2.7 Conclusion……..53

Chapter 3 Taxonomy of the new planktonic mixotrophic dinoflagellate *Paragymnodinium shiwhaense* n. gen., n. sp. from Korean waters……..58

3.1 Abstract……...58

3.2 Key words……...59

3.3 Introduction……..59

3.4 Materials and methods……60

3.4.1 Collection and culturing of *Paragymnodinium shiwhaense*……60
3.4.2 Morphology of *Paragymnodinium shiwhaense*…….61
3.4.3 DNA extraction, PCR amplification, and sequencing…….62
3.4.4 Sequence availability and phylogenetic analysis……..63
3.4.5 Pigment analysis……..64

3.5 Results……..69

3.5.1 Morphology of *Paragymnodinium shiwhaense*……69
3.5.2 Molecular characterization of *Paragymnodinium shiwhaense*.....87
3.5.3 Date and locality of isolation……....87
3.5.4 Remarks on culturing and behavior……..87

3.6 Discussion……...96

Chapter 4 *Gyrodiniellum shiwhaense* n. gen., n. sp., A new planktonic heterotrophic dinoflagellate from the coastal waters of western Korea……103

4.1 Abstract……..103

4.2 Key words……104

4.3 Introduction……...104

4.4 Materials and methods……..105

4.4.1 Collection and culturing of *Gyrodiniellum shiwhaense*.....105
4.4.2 Morphology……106
4.4.3 DNA extraction, PCR amplification, sequencing, and data analysis.....107
4.4.4 Sequence availability and phylogenetic analysis……108

4.5 Results……...109

4.5.1 Morphology……109
4.5.2 Gene sequence of *Gyrodiniellum shiwhaense* and phylogenetic analysis……...129
4.5.3 Date and locality of isolation……..133
4.5.4 Remarks on culturing and behavior……133

4.6 Discussion……..133

Chapter 5 Mixotrophy in the newly described phototrophic dinoflagellate *Biecheleria cincta* (=*Woloszynskia cincta*) from western Korean waters: Taxonomy and ecology ……150

5.1 Abstract……..150

5.2 Key words……151

5.3 Introduction……...151

5.4 Materials and methods……..153

5.4.1 Experimental organisms…….153
5.4.2 Morphology of *Biecheleria cincta*……..154
5.4.3 DNA extraction, PCR amplification, sequencing, and data analysis……155
5.4.4 Sequence availability and phylogenetic analysis……156
5.4.5 Prey species…….157
5.4.6 Feeding mechanisms……...163
5.4.7 Comparison of growth and ingestion rates for edible prey at single prey concentrations……..163
5.4.8 Effects of prey concentration……..165
5.4.9 Potential grazing impact…….167
5.4.10 Swimming speed…….168

5.5 Results……...168

5.5.1 Morphology and rDNA sequences of the Korean strain of *Biecheleria cincta*……...168
5.5.2 Prey species…….170

5.5.3 Feeding behavior……171
5.5.4 Comparison of growth and ingestion rates at a single prey concentration……...171
5.5.5 Effects of prey concentration……..179
5.5.6 Potential grazing impact……182
5.5.7 Swimming speed……182

5.6 Discussion……..182

5.6.1 *Biecheleria cincta* isolated from Korean waters……182
5.6.2 Prey species and feeding mechanism……..183
5.6.3 Comparison of growth and ingestion rates for the 6 edible prey species……..191
5.6.4 Effect of prey concentration……...192
5.6.5 Grazing impact……199

Chapter 6 Overall conclusion……..203

Bibliography……208

Abstract (in Korean)……237

List of Tables

Table 1.1 The range of physical and chemical properties at three different stations from May 2008 to July 2012 in Shiwha Bay, Korea…….....17

Table 1.2 The maximum abundance (MA) and biomass (MB) of the red-tide causative species during each red-tide event in Shiwha Bay, Korea from May 2008 to July 2012…….....32

Table 1.3 Calculated grazing impacts (GI, h^{-1}) of the dominant heterotrophic protists on red-tide species in Shiwha Bay, Korea, from May 2008 to July 2012 and the predators' maximum ingestion rate and K_{IR} (half-saturation) at given prey concentrations in the literature…….....42

Table 1.4 Correlations between physical and chemical properties in Shiwha Bay, Korea, from May 2008 to July 2012…….....46

Table 1.5 Correlations between the physical and chemical properties and the biomass of protists and bacteria in Shiwha Bay, Korea, from May 2008 to July 2012…….....47

Table 1.6 Half-saturation constants (Ks, μM) for uptake of ammonium (NH_4), nitrate (NO_3), phosphate (PO_4), and silicate (SiO_2) by selected red-tide organisms in Shiwha Bay, Korea, from May 2008 to July 2012…….....55

Table 1.7 Correlations between physical and chemical properties in Shiwha Bay, Korea from May 2008 to July 2012…….....56

Table 2.1 List of species used in constructing phylogenetic trees. GenBank accession numbers are listed to the right of each species…….65

Table 2.2 Comparison of *Paragymnodinium* gen. nov with other gymnodinioid and woloszynskioid dinoflagellates……..99

Table 3.1 List of species used in constructing phylogenetic trees. GenBank accession numbers are listed to the right of each species……...111

Table 3.2 Comparison of the number of rows of amphiesmal vesicles (AVs) in *Gyrodiniellum shiwhaense*, *Paragymnodinium shiwhaense*, and woloszynskioid dinoflagellates……138

Table 3.3 Comparison of *Gyrodiniellum shiwhaense* with other gymnodinioid, warnowiid, and woloszynskioid dinoflagellates……142
Table 3.4 Comparison of nematocysts and nematocyst-taeniocyst complex in dinoflagellates……145
Table 4.1 List of species used in constructing phylogenetic trees. Genbank accession numbers are listed to the right of each species……...158
Table 4.2 Taxa, sizes, and concentration of prey species offered as food to *Biecheleria cincta* in Expt 1……160
Table 4.3 Comparison in growth (GR, d^{-1}) and ingestion rates (IR, ng C $predator^{-1} d^{-1}$) [means (± standard errors), n=3] of *Biecheleria cincta* on 6 edible prey species at single mean prey concentrations (MPC, ng C ml^{-1})……181
Table 4.4 Comparison in prey species and the maximum growth and ingestion rates of the peduncle feeding mixtotrophic (MTD) and heterotrophic dinoflagellates (HTD)……..193
Table 4.5 Optimal prey, maximum mixotrophic growth (MGR), ingestion (MIR), and clearance rates (MCR) of each mixotrophic dinoflagellate predator species at the light intensity of 20 µE m^{-2} s^{-1}……...201
Table 4.6 The maximum growth, ingestion, and clearance rates of mixotrophic and heterotrophic dinoflagellate predators on *Heterosigma akashiwo* which was the optimal or suboptimal prey for the predators……202

List of Figures

Figure 1 Outline of this thesis .....……..5

Figure 2.1 Map of Shiwha Bay, Korea (**A**), and three sampling stations during low (**B**) and high tide (**C**). The numbers indicate bathymetry (meters)…….....11

Figure 2.2 Physical and chemical properties of Shiwha Bay at St. 1 from May 2008 to July 2012……..18

Figure 2.3 Physical and chemical properties of Shiwha Bay at St. 2 from May 2008 to July 2012……..20

Figure 2.4 Physical and chemical properties of Shiwha Bay at St. 3 from May 2008 to July 2012……..21

Figure 2.5 Red-tide events at three stations in Shiwha Bay, Korea, from May 2008 to July 2012……...22

Figure 2.6 Biomass of red-tide causative protist groups and bacteria at St. 1 in Shiwha Bay from May 2008 to July 2012……23

Figure 2.7 Biomass of phototrophic dinoflagellate species at St. 1 in Shiwha Bay from May 2008 to July 2012…….26

Figure 2.8 Biomass of the species or taxa diatoms, raphidophytes, euglenophytes, prasinophytes, and cryptophytes at St. 1 in Shiwha Bay from May 2008 to July 2012……...27

Figure 2.9 Biomass of heterotrophic protists at St. 1 in Shiwha Bay from May 2008 to July 2012……..41

Figure 3.1 Micrographs of *Paragymnodinium shiwhaense* n. gen., n. sp. taken using light microscopy, epifluorescent microscopy and scanning electron microscopy……71

Figure 3.2 Micrographs of *Paragymnodinium shiwhaense* n. gen., n. sp. taken using scanning electron microscopy…….73

Figure 3.3 Micrographs of *Paragymnodinium shiwhaense* n. gen., n. sp. taken using scanning electron microscopy…….74

Figure 3.4 Micrographs of *Paragymnodinium shiwhaense* n. gen., n. sp. taken using scanning electron microscopy……75
Figure 3.5 Drawings of *Paragymnodinium shiwhaense* n. gen., n. sp. to show the external morphology……76
Figure 3.6 Micrograph of *Paragymnodinium shiwhaense* n. gen., n. sp. taken using transmission electron microscopy……...78
Figure 3.7 Micrographs of *Paragymnodinium shiwhaense* n. gen., n. sp. taken using transmission electron microscopy……...79
Figure 3.8 Transversely sectioned micrograph of *P. shiwhaense* n. gen., n. sp., taken using transmission electron microscope, showing nuclear pores (NP) in the nuclear envelope (NE)……...80
Figure 3.9 Diagrammatic drawing of *P. shiwhaense* n. gen., n. sp., based mainly on serially sectioned transmission electron microscope from the apex to the antapex and SEM……....81
Figure 3.10 Electron micrographs of serially sectioned *Paragymnodinium shiwhaense* n. gen., n. sp. showing the longitudinal basal body (LB), longitudinal flagellum (LF), nucleus (N), and Root 1 (R1)…….....…..83
Figure 3.11 Electron micrographs of serially sectioned *Paragymnodinium shiwhaense* n. gen., n. sp. showing the longitudinal basal body (LB), transverse basal body (TB), Root 1 (R1), Root 3 (R3), $C1_{LB/R1}$ and $C2_{LB/R1}$, and bbc1, 2, 3, which connect the LB and TB……...84
Figure 3.12 Electron micrographs serially sectioned *Paragymnodinium shiwhaense* n. gen., n. sp. showing the relative positions (angles) of the longitudinal basal body (LB), transverse basal body (TB), Root 1 (R1), $C1_{LB/R1}$ and $C2_{LB/R1}$, and Root 4 (TSR+TSRM), striated root connectives (SRC), transverse striated root (TSR), and transverse striated root microtubule (TSRM) ……..85
Figure 3.13 Diagrammatic reconstruction of the flagellar apparatus of *Paragymnodinium shiwhaense*, based mainly on transverse transmission electron microscope serially sectioned layers……....86
Figure 3.14 Serially sectioned transmission electron microscope micrographs of

Paragymnodinium shiwhaense n. gen., n. sp. showing the shape and position of nematocysts (arrows)……....88
Figure 3.15 Micrographs of nematocysts of *Paragymnodinium shiwhaense* n.gen., n.sp……....89
Figure 3.16 Micrographs of *P. shiwhaense* showing a peduncle (PE) and ventral ridge (VR)…….....90
Figure 3.17 Chromatogram derived by high performance liquid chromatography of the major pigments of *Paragymnodinium shiwhaense* n. gen., n. sp. satiated with the cryptophyte *Rhodomonas salina* and then starved for 2wk compared with that of the prey organism *R. salina*……....91
Figure 3.18 Bayesian and Maximum likelihood (ML) phylogenetic tree based on SSU rDNA……....92
Figure 3.19 Bayesian and Maximum likelihood (ML) phylogenetic tree based on LSU rDNA.....94
Figure 4.1 Micrographs of *Gyrodiniellum shiwhaense* n. gen., n. sp. showing the whole cell……....114
Figure 4.2 Micrographs of *Gyrodiniellum shiwhaense* n. gen., n. sp. taken using scanning electron microscopy…….115
Figure 4.3 Micrographs of *Gyrodiniellum shiwhaense* n. gen., n. sp. taken using scanning electron microscopy…….116
Figure 4.4 Micrographs of *Gyrodiniellum shiwhaense* n. gen., n. sp. in the scanning electron microscope…….117
Figure 4.5 *Gyrodiniellum shiwhaense* n. gen., n. sp. using scanning electron microscopy……..118
Figure 4.6 Drawings of *Gyrodiniellum shiwhaense* n. gen., n. sp. to show the external morphology.....119
Figure 4.7 *Gyrodiniellum shiwhaense* n. gen., n. sp. taken using transmission electron microscopy……121
Figure 4.8 *Gyrodiniellum shiwhaense* n. gen., n. sp., photographed using transmission electron microscopy……....122

Figure 4.9 *Gyrodiniellum shiwhaense* n. gen., n. sp., photographed using transmission electron microscopy……...123
Figure 4.10 Micrographs showing slightly oblique transverse sections of the flagellar apparatus of *Gyrodiniellum shiwhaense* n. gen., n. sp……..125
Figure 4.11 Micrographs showing slightly oblique longitudinal sections of the flagellar apparatus and the relative positions of the longitudinal basal body (LB), transverse basal body (TB), Root1 (R1), Root 4 (transverse striated root+transverse striated root microtubule), striated root connectives (SRC) and pusule system (PS) of *Gyrodiniellum shiwhaense* n. gen., n. sp……....126
Figure 4.12 Diagrammatic reconstruction of the flagellar apparatus of *Gyrodiniellum shiwhaense* n. gen., n. sp., based mainly on transverse serial sections (70-nm-thick sections)……....127
Figure 4.13 Serial sections of *Gyrodiniellum shiwhaense* n. gen., n. sp. showing shape and position of the nematocysts, using transmission electron microscopy……..128
Figure 4.14 Micrographs of *Gyrodiniellum shiwhaense* n. gen. n. sp……...130
Figure 4.15 Transmission electron micrographs of *Gyrodiniellum shiwhaense* n. gen., n. sp. showing trichocyst and membrane-like lamellae (MLL)…….131
Figure 4.16 Diagrammatic drawing of *Gyrodiniellum shiwhaense*……...132
Figure 4.17 Bayesian and Maximum likelihood (ML) phylogenetic tree based on SSU rDNA……..134
Figure 4.18 Bayesian and Maximum likelihood (ML) phylogenetic tree based on LSU rDNA…….136
Figure 4.19 Schematic illustrations showing the organization of nematocysts of *Gyrodiniellum shiwhaense*, *Paragymnodinium shiwhaense*, and *Nematodinium* sp. and the nematocyst-taeniocyst complex of *Polykrikos schwartzii*……146
Figure 5.1 Micrographs of *Biecheleria cincta* isolated from Shiwha Bay, Korea……..172
Figure 5.2 Micrographs of *Biecheleria cincta* taken using a scanning electron microscope and drawing of the elongate apical vesicles (EAV)……174

Figure 5.3 Bayesian and Maximum likelihood (ML) phylogenetic tree based on SSU rDNA……..……..175
Figure 5.4 The feeding by *Biecheleria cincta* on *Heterosigma akashiwo* and *Teleaulex* sp. Photomicrographs were taken using a transmission electron microscope……..……..177
Figure 5.5 The feeding by *Biecheleria cincta* on *Isochrysis galbana* and *Eutreptiella gymnastica*. ……178
Figure 5.6 Feeding process of *Biecheleria cincta* (Bc) on *Heterosigma akashiwo* (Ha)…….…...180
Figure 5.7 The ingestion rate (IR) and growth rate (GR) of *Biecheleria cincta* feeding on 6 edible prey species as a function of prey size and the GR as a function of the IR as in Table 4.3……..……184
Figure 5.8 Specific growth rates of *Biecheleria cincta* feeding on *Heterosigma akashiwo* as a function of mean prey concentration…….…...185
Figure 5.9 Ingestion rates of *Biecheleria cincta* feeding on *Heterosigma akashiwo* as a function of mean prey concentration……...……..…...186
Figure 5.10 Calculated grazing coefficients for *Biecheleria cincta* feeding on co-occurring *Heterosigma akashiwo*……...187
Figure 5.11 The prey and predators of *Biecheleria cincta* so far reported……190
Figure 5.12 Maximum ingestion rate, specific ingestion rate, maximum mixotrophic growth rateand autotrophic growth rate as control, and maximum mixotrophic growth rate minus autotrophic growth rate of 7 mixotrophic dinoflagellates feeding on their optimal prey (*Heterosigma akashiwo* for *Biecheleria cincta*, *Lingulodinium polyedrum* for *Fragilidium* cf. *mexicanum*, and *Teleaulax* sp. for the other mixotrophic dinoflagellate predators) as a function of equivalent spherical diameter (ESD, μm), obtained under illumination of 20 μE m^{-2} s^{-1} on a 14:10 h light-dark cycle. ……197
Figure 5.13 Maximum swimming speed of 7 mixotrophic dinoflagellates feeding on their optimal prey species as a function of equivalent spherical diameter,

obtained under illumination of 20 µE m^{-2} s^{-1} on a 14:10 h light-dark cycle……..200

Chapter 1: Introduction

Marine ecosystems consist of living organisms and their abiotic environments (Holling et al. 1995). Marine ecosystems play diverse roles in the earth; they contain many and diverse organisms; they circulate materials; they provide food and/or useful materials to human (Alexander et al. 1997). Thus, we have spent a lot of time and money on maintaining healthy marine ecosystems. However, some natural or artificial impacts have caused destruction of healthy marine ecosystems. To maintain healthy marine ecosystems, we must fully understand the structure and function of marine ecosystems and their changes due to harmful impacts.

Red tides, discoloration of sea surface due to plankton blooms, have often caused large scale mortality of fin-fish, shellfish, and marine mammals and sometimes destroy the balance in marine ecosystems (Burkholder and Glasgow 1995; ECOHAB 1995: Steidinger 1983). Thus, understanding and managing red tides are critical concerns to scientists, officials, and people in the aquaculture and tourism industries. However, some unknown red tide or harmful species make us to have difficulty in managing red tides or harmful algal blooms. Therefore, we must find these unknown species and conduct taxonomic work. In addition, we should explore ecophysiology and genetics of these new species. Furthermore, their distributions and environmental factors affecting their distributions should be explored.

My thesis consists of 6 chapters including this introduction chapter (Fig. 1). In chapter 2, I explored red tides in Shiwha Bay, western Korea: a huge dike and tidal power plant established in a semi-closed embayment system. Furthermore, I established the new planktonic mixotrophic dinoflagellate *Paragymnodinium shiwhaense* from Shiwha Bay in chapter 3 and the new heterotrophic dinoflagellate *Gyrodiniellum shiwhaense* in chapter 4. Moreover, I explored eco-physiology, in particular, mixotrophy in the newly described phototrophic dinoflagellate

Biecheleria cincta (=*Woloszynskia cincta*) from Shiwha bay in chapter 5. Finally, I provided overall conclusions and an insight on red tide dynamics and discovery of new dinoflagellate species in chapter 6.

Chapter 2: Red tides have occurred often in semiclosed bays and estuaries, although huge red tides have also occurred in oceanic waters (Cheng et al. 2005; Choi et al. 1997; Huang and Qi 1997; Jeong et al. 2013a; Kishi and Ikeda 1986; Kononen 1992; Reid 1980; Xingyu et al. 2009). Restricted water circulation and/or high nutrient load from freshwater in bays and estuaries have been known to be favorable for outbreaks of red tides (Balkis 2003; Tsutsumi et al. 2003). However, intense turbulence and/or vigorous mixing have been shown to prevent outbreaks of red tides in some cases (Smayda 2002). Tidal currents in shallow-water regions, where tidal range is large, can produce high-intensity turbulence or vigorous mixing (Chen and Jirka 1998; Jirka 2001). Shiwha Bay (43.8 km^2 in area), located on the western coast of the central Korean peninsula. Shiwha Bay is an ideal place to explore effects of restricted water circulation, high nutrient load, and turbulence and/or vigorous mixing on red tide outbreaks (Baek et al. 2011; Choi et al. 1997). In 1994, a 12.7-km dike with a 100-m water gate was constructed in the mouth of the bay and water exchange between inside and outside the dike occurred only through the water gate, but water circulation was highly restricted and the tidal range inside the dike was reduced to 3-5 m. However, in 2011, the world's largest tidal power plant was constructed in the middle of the dike and water exchange began to occur through the turbines of the tidal power plant. To explore the dynamics of red tides in Shiwha Bay and effects of water exchange through the power plant, I took water samples at 3 fixed stations inside the dike on a monthly basis from 2008 to 2012 and measured physical, chemical, and biological properties. I concluded that exchang of seawater between the inside and outside of the dike through the tidal power plant may have resulted in this change in the species composition.

Chapter 3: Phototrophic dinoflagellates are ubiquitous protists in marine

environments and have sometimes formed red tides or harmful algal blooms (Jeong 1995). Interest in phototrophic dinoflagellates is increasing because many phototrophic dinoflagellates that had been thought to be exclusively autotrophic have been revealed to be mixotrophic and they have been revealed to play diverse ecological roles in marine planktonic communities (Carvalho et al. 2008; Stoecker et al. 2006). The phototrophic dinoflagellates are in turn important prey for diverse predators (Jacobson and Anderson 1986; Jeong et al. 2005e; Kamiyama and Matsuyama 2005; Stoecker and Sanders 1985). Our correct understanding of the structure and functioning of marine ecosystems makes the correct identification and description of their biodiversity, including novel phototrophic dinoflagellates, and the exploration of their role in marine food webs essential research. I isolated a dinoflagellate from Shiwha Bay and established a clonal culture. After conducting intensive morphological and genetical analyses, I concluded that it is a new species in a new genus and described it.

Chapter 4: Heterotrophic dinoflagellates are ubiquitous protists in marine environments and play diverse ecological roles in marine plankton food webs (Jeong 1999; Jeong et al. 2010c; Lessard 1991; Sherr and Sherr 2007); they feed on a diverse array of prey and in turn serve as prey for diverse predators (Gransden and Lewitus 2003; Jeong et al. 2004a; Stoecker et al. 2002). To understand the structure and function of the marine ecosystems, it is important to identify heterotrophic dinoflagellates, describe their diversity, and explore their role in marine food webs. I isolated a dinoflagellate from Shiwha Bay and established a clonal culture. After conducting intensive morphological and genetical analyses, I concluded that it is a new species in a new genus and described it.

Chapter 5: Dinoflagellates are among the major components of marine ecosystems (Hansen 1991; Jacobson and Anderson 1986; Jeong 1995; Lessard 1984, 1991; Sherr and Sherr 2007; Terrado et al. 2009). They play diverse roles in marine food webs, feeding on diverse prey items and, in turn, serving as prey for diverse

predators (reviewed by Jeong et al. 2010c). In the last decade, several novel dinoflagellates, the cell lengths of which are 5-20 μm, have been identified (e.g. Kang et al. 2010). Although it is very difficult to identify these small dinoflagellates under the light microscope, recent developments in molecular techniques and detailed morphological descriptions using electron microscopes have enabled us to identify small dinoflagellates and describe novel species. However, the ecophysiology of many of these small dinoflagellates has yet to be explored. Thus, it is difficult to assess the roles played by these organisms in marine ecosystems. *Biecheleria* species have a wide geographical distribution, including Europe (Siano et al. 2009; Woloszynska 1917), the United States (Thompson 1951), India (Shyam and Sarma 1975), and Japan (Takano and Horiguchi 2003). However, the ecophysiology of species in this genus has not been investigated. In particular, their trophic modes have yet to be elucidated. Previous studies had reported that all *Biecheleria* species are photosynthetic, and mixotrophy was unknown (Lindberg et al. 2005). Therefore, it is worthwhile exploring the possibility of mixotrophy in *Biecheleria* species. I isolated a dinoflagellate from Shiwha Bay and established a clonal culture. After conducting intensive morphological and genetic analyses and ecophysiology study. I concluded that it is a newly described mixotrophic dinoflagellate in Korean waters.

Chapter 6: The results of my studies will provide a basis on understanding red tide dynamics in the waters where artificial construction and changes in red tide causative species to environmental changes. In addition, discovery of the new dinoflagellate genera and unveil of mixotrophy in the newly described dinoflagellates may stimulate researches on taxonomy and evolution of dinoflagellates and their commercial uses.

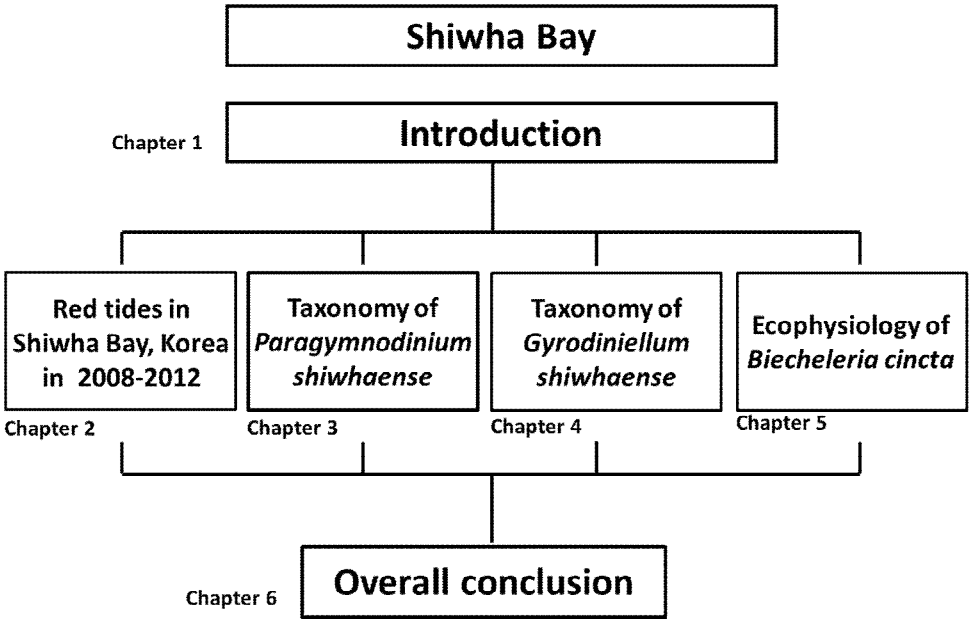

Fig. 1 Outline of this thesis.

Chapter 2: Shifted dynamics of red tides organisms following a huge dike and tidal power plant established in Shiwha Bay, western Korea

2.1 Abstract

To investigate red tides in Shiwha Bay, Korea, where a 12.7-km dike with two outlets (at the water gate and tidal power plant) was constructed, I measured physical, chemical, and biological properties at 3 fixed stations inside the dike on a monthly basis from May 2008 to July 2012. During the study period, red tides were present in Shiwha Bay during 33 of 46 (i.e., 72%) sampling events. Clearly, red tides are common in the bay. Red tides occurred 33, 12, and 10 times at Stations 1, 2, and 3, respectively.

Restriction of water circulation at Station 1 (in the innermost part of the bay) may cause more frequent red tides due to phototrophic dinoflagellates than at Station 3, where water exchange between the inside and outside of the dike occurs through a water gate. After the world's largest tidal power plant was established in 2011, red-tide causative species switched from phototrophic dinoflagellates such as *Gymnodinium aureolum*, *Heterocapsa rotundata*, *Heterocapsa triquetra*, *Karlodinium veneficum*, *Paragymnodinium shiwhaense*, and *Prorocentrum minimum* to diatoms such as *Chaetoceros* spp., *Skeletonema costatum*, and *Thalassiosira* spp. Exchange of seawater between the inside and outside of the dike through the tidal power plant may have resulted in this change in the causative species. *Biecheleria cincta* did not cause the red tide during the study period and observed between 2008 and 2009 at Station 1 but not at later times. Inorganic nitrogen concentrations for the growth of phototrophic dinoflagellates and small flagellates during red tides were likely unlimited, but inorganic phosphorus concentrations may be limited. Thus, some phototrophic dinoflagellates and flagellates may acquire phosphorus from prey.

The maximum grazing coefficients of the heterotrophic dinoflagellates *Pfiesteria piscicida*, *Gyrodiniellum shiwhaense*, *Gyrodinium dominans, Gyrodinium moestrupii*, and *Protoperidinium bipes* feeding on red-tide causative taxa including cryptophytes, *Eutreptiella gymnastica*, *P. minimum*, and *S. costatum*, were found to be 0.14-0.77 h^{-1}. Therefore, heterotrophic protistan grazers in Shiwha Bay may, at times, have considerable grazing impact on populations of co-occurring red-tide organisms.

2.2 Key words

Food web, Harmful Algal Bloom, Mixotrophy, Tidal power plant, Protist, Red tide

2.3 Introduction

Red tides have occurred often in semiclosed bays and estuaries (Choi et al. 1997; Huang and Qi 1997; Jeong et al. 2013a; Kishi and Ikeda 1986; Reid 1980; Xingyu et al. 2009), although huge red tides have also occurred in oceanic waters (Cheng et al. 2005; Kononen 1992). Restricted water circulation and/or high nutrient load from freshwater in bays and estuaries have been known to be favorable for outbreaks of red tides (Balkis 2003; Tsutsumi et al. 2003). In addition, seasonality of water temperature, precipitation, salinity, and/or nutrient loads in semiclosed bays and estuaries of temperate regions have resulted in seasonal changes in red-tide causative species (Honer et al. 1997; Smayda 1997; Jeong et al. 2013a, 2013b).

Water movements such as currents, turbulence, internal wave, and mixing are known to affect formation of red tide patches (Fermin et al. 1996; Franks 2005; Juhl et al. 2000; Omand et al. 2011: Smayda 2002; Thomas and Gibson 1990; Tynan 1993). Intense turbulence and/or vigorous mixing have been shown to prevent outbreaks of red tides in some cases (Smayda 2002). Tidal currents in shallow-water regions, where tidal range is large, can produce high-intensity turbulence or

vigorous mixing (Chen and Jirka 1998; Jirka 2001). Tidal range in the coastal waters of western Korea (i.e., the Yellow Sea side) is approximately 9-10 m. The frequency of outbreak of red tides in western Korea was much lower than that in southern Korea, where the tidal range is 2-4 m (Jeong et al. 2013b; Park et al. 2013). However, huge dikes constructed in the mouths or middles of bays and estuaries in western Korean prevent tidal excursion and restrict water circulation (Yih et al. 2005; Yoo et al. 2002). Since the construction of these dikes, red tides have occurred frequently in these waters. Bays and estuaries in western Korean act as nurseries for diverse marine organisms; in fact, some bays have been used for aquaculture farms (Kim 1997, 1998). However, red tides in these regions have been known to cause great losses for the aquaculture industry (Kim 1997, 1998).

Many red tides have occurred in Shiwha Bay, which is located on the west coast of central Korea (Baek et al. 2011; Choi et al. 1997). This bay is surrounded by 3 highly populated large cities: Ansan, Shiheung, and Hwasung. Several small streams enter the bay (Shin et al. 2000a, 2000b), which is long and narrow, restricting water circulation inside the bay. In 1994, a 12.7-km dike with a 100-m water gate was constructed in the mouth of the bay. Thus, water exchange between inside and outside the dike occurred only through the water gate; water circulation was highly restricted and the tidal range inside the dike was reduced to 3-5 m. In addition, the world's largest tidal power plant was constructed in the middle of the dike in 2011. Water exchange began to occur through the turbines of the tidal power plant. To explore the dynamics of red tides in Shiwha Bay, I took water samples at 3 fixed stations inside the dike on a monthly basis from 2008 to 2012 and measured physical, chemical, and biological properties. This study provides an improved understanding of redtide dynamics in semiclosed bay systems, in waters with high tidal ranges, and in regions where the emplacement of artificial structures has resulted in restriction or relaxation of water circulation.

2.4 Materials and methods

2.4.1 Abundances of protists and bacteria in Shiwha Bay

Shiwha Bay (43.8 km^2 in area) is located on the western coast of the central Korean peninsula (Fig. 2.1). A 12.7-km dike crossing the mouth of the bay was constructed in 1994, and water passed through a 100-m-long water gate before the world's largest tidal power plant was constructed in April 2011. Approximately half the water inside the Shiwha Bay (i.e., ~150 of 320 million tons waters) daily passes through ten 7.5-m diameter turbines of the tidal power plant (Bae et al. 2010). The speed of the water passing the turbines is 12–13 m s^{-1}. I explored red tides at 3 different fixed stations inside the dike: Station 1 (St. 1) was located in the innermost part at the point of entry of a small stream, Station 2 (St. 2) near the tidal power plant, and Station 3 (St. 3) near the water gate. Water depths at St. 1, St. 2, and St. 3 were 3.5-6.0 m, 11.3-13.0 m, and 5.5-10.0 m, respectively, depending on the tide (Fig. 2.1).

Water samples were taken at the surface at each station with water samplers during high tides every month from May 2008 to July 2012, except in frozen months (December 2009-February 2010 and January-February 2011). In addition, nutrient data were unavailable in November 2008 and January and July 2009 and pH data in July and August 2011.

Plankton samples for counting were poured into 500-ml polyethylene (PE) bottles and preserved with acidic Lugol's solution (for diatoms, phototrophic dinoflagellates, cryptophytes, raphidophytes, euglenophytes, prasinophytes, and heterotrophic protists), Bouin's solution (for ciliates), or glutaraldehyde (for nanoflagellates, picoeukaryotes, and bacteria). Dominant species of protists were isolated and established in clonal cultures for identification using morphological and DNA sequencing analysis.

To determine the abundances of diatoms, phototrophic dinoflagellates, heterotrophic protists, and diverse flagellates (cryptophytes, raphidophytes, euglenophytes, etc.), samples preserved with acidic Lugol's solution were concentrated by 1/5–1/10 using settling and siphoning methods (Welch 1948). After thorough mixing, all (or a minimum of 100) cells of each protest species in one to ten 1-ml Sedgwick–Rafter counting chambers were counted under a light microscope.

Small phototrophic or heterotrophic dinoflagellates *Gyrodiniellum shiwhaense*, *Karlodinium veneficum*, *Paragymnodinium shiwhaense*, *Pfiesteria piscicida*, *Stoeckeria algicida*, *Biecheleria cincta*, *Azadinium* cf. *poporum*, and *Gymnodinium aureolum* were only 10-20 μm in cell length and all displayed very similar morphologies (Ballantine 1956; Jeong et al. 2005b, 2006, 2010b; Kang et al. 2010, 2011a, 2011b; Potvin et al. 2012); thus, one species could not be distinguished from the others using only light microscopy. Therefore, I identified these species using their DNA sequences and quantified their abundance using a quantitative PCR (qPCR) method (Park et al. 2009). Total abundances of these dinoflagellates in fixed samples were enumerated and then compared to abundances quantified using the qPCR method. For qPCR analysis, aliquots of 100-250 ml water samples were gently filtered through GF/C filters and preserved at -72 °C until DNA extraction. After the genomic DNA was extracted with phenol chloroform isoamyl alcohol (25:24:1), qPCR was carried out with Platinum qPCR SuperMix-UDG (Invitrogen, Eugene, Oregon, USA) on a Rotor-Gene qPCR detection system (Rotor-Gene 3000, Corbett Research, Sydney, Australia).

In order to determine the abundance of bacteria, picoeukaryotes, and nanoflagellates, aliquots of the water samples were poured into 100-ml PE bottles and preserved with glutaraldehyde (final conc. = 1%, v/v).

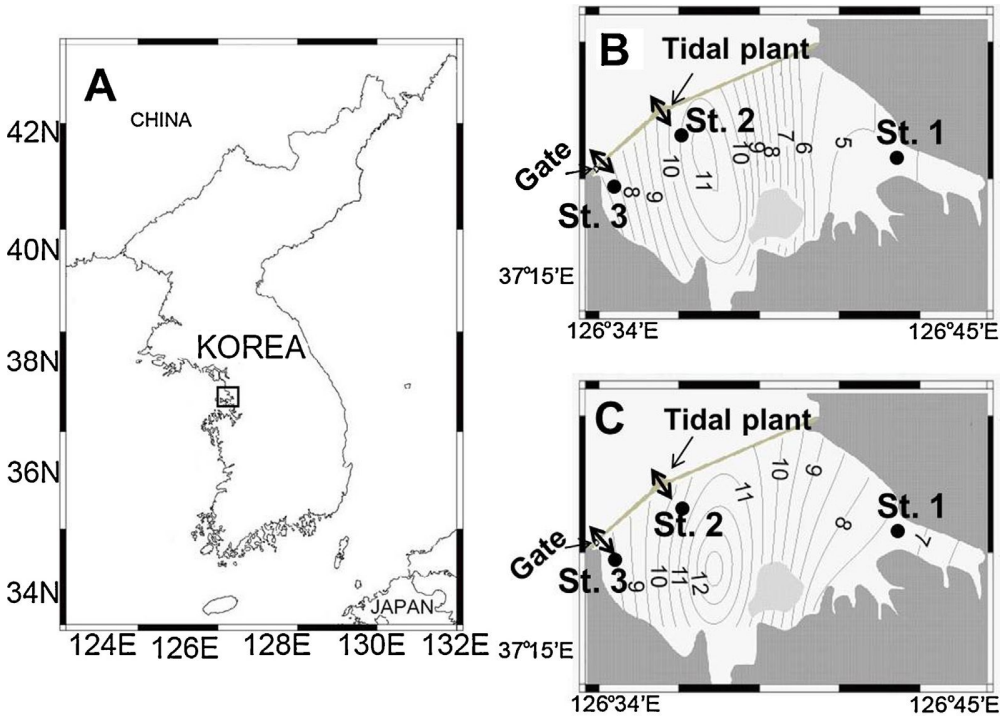

Fig. 2.1 Map of Shiwha Bay, Korea (**A**), and three sampling stations during low (**B**) and high tide (**C**). The numbers indicate bathymetry (meters).

Three to twelve 1-ml fixed aliquots were stained with 4', 6-diamidino-2-phenylindole (DAPI, finalconc. = 1 μM) and then filtered onto 0.2-μm-pore-size polycarbonate (PC) black membrane filters. Bacteria were enumerated under an epifluorescent microscope with ultraviolet light excitation (Porter and Feig 1980). Additionally, three 1-5 ml fixed aliquots were stained with DAPI and then filtered onto 0.2-μm pore- sized PC black membrane filters. Phototrophic nanoflagellates (PNFs; 3-6 μm cell length) that exhibited orange-colored autofluorescence under an epifluorescent microscope with blue light excitation were also enumerated.

I measured the carbon content for each of many protists species cultured in our laboratory using a CHN analyzer (Jeong et al. 2013a). For noncultured species or taxa, the length and width of cells preserved in 5% acidic Lugol's solution were measured using a light microscope and cell volume was then calculated according to geometry. The carbon content for each species of protists was calculated from the cell volume according to Menden- Deuer and Lessard (2000).

During the study period, red-tide patches were generally visible when the biomass of total red-tide causative species exceeded 200 ng C ml^{-1}. In fact, when the biomass of red-tide organisms exceeds 200 ng C ml^{-1}, a red-tide warning is announced by the National Fisheries Research and Development Institute, Korea (NFRDI 2012). Thus, I defined red tides here as the biomass of one or sum of the top 3 causative species $\geq$ 200 ng C ml^{-1}.

2.4.2 Physical and chemical properties in Shiwha Bay

Water temperatures and salinities in surface waters were measured using a YSI 30 (YSI, LA, USA) and pH and dissolved oxygen (DO) was measured using pH-11 (Schott HandyLab, Mainz, Germany) and Oxi 197i (WTW, Weilheim, Germany), respectively. For inorganic nutrient analysis, the water samples were gently filtered through GF/F filter papers and moved to the laboratory and analyzed immediately. When the samples could not be analyzed immediately, they were

preserved at -20 ℃ in a freezer until analysis could take place. Ammonium (NH_4), nitrate plus nitrite ($NO_3 + NO_2$, hereafter NO_3), phosphate (PO_4), and silicate (SiO_2) were detected using a nutrient auto-analyzer system (QuAAtro, Seal Analytical GmbH, Werkstrasse, Norderstedt, Germany).

The precipitation used for correlation was based on the database of the Korea Meteorological Administration (KMA http://web.kma.go/kr). I used the precipitation for 14 days from the sampling date. Correlation coefficients between protists and physical, chemical, and biological properties were calculated using the Pearson's correlation (Conover 1980; Zar 1999).

2.4.3 Grazing impact of heterotrophic protists on red-tide organisms

Based on several assumptions, it was possible to estimate grazing coefficients attributable to a dominant protistan grazer feeding on a co-occurring red-tide organism. I did this by combining field data on the abundances of the protistan grazer and red-tide organism with rates of ingestion of the red-tide prey by the protistan grazer based on the literature. The heterotrophic dinoflagellates *Gyrodinium dominans* and *Gyrodinium moestrupii* could not be distinguished from each other under a light microscope because they are morphologically very similar (Yoon et al. 2012). Thus, I used the term *G. dominans*/*G. moestrupii*.

Furthermore, I assumed that the ingestion rates of *Eutreptiella gymnastica* by naked ciliates ≤50 μm and of *Prorocentrum minimum* by naked ciliates >50 μm were the same as those for ingestion of *Strobilidium* sp. and *Strombidinopsis* sp. by the same prey species (Jeong et al. 1999a, 2011a).

The grazing coefficient g (h^{-1}) was calculated as follows:

$$g = CR \times GC \qquad (1)$$

where CR is the clearance rate (ml $predator^{-1}$ h^{-1}) for a predator of a red-tide organism at a given prey concentration and GC is the predator concentration (cells

ml^{-1}). CR values were calculated as follows:

$$CR = IR/X \quad (2)$$

where IR is the ingestion rate (cells eaten $predator^{-1}$ h^{-1}) of the predator on the prey and X is the prey concentration (cells ml^{-1}). CR values were corrected using Q_{10} = 2.8 (Hansen et al. 1997) because the in situ water temperatures and the temperature used in the laboratory for this experiment (20 ^{o}C) were sometimes different.

2.5 Results

2.5.1 Physical and chemical properties in Shiwha Bay

2.5.1.1 Station 1

The range of water temperature in the surface waters of St. 1 from May 2008 to July 2012 was 0.2-28.4 °C (mean ± standard error = 16.6 ± 1.3 °C, Table 1.1; Fig. 2.2); the highest temperature was observed in July 2010 and the lowest in January 2012. In addition, precipitation summed for 2 weeks was 0-481 mm (mean ± SE = 64 ± 15 mm) and salinity was 3.4-31.7 (mean ± SE = 23.4 ± 1.0). Furthermore, water temperature was significantly posi-tively correlated with precipitation and the concentration of PO_4, but significantly negatively correlated with salinity (Table 1.7). The pH was 7.9-9.6 (mean ± SE = 8.6 ± 0.1). The NH_4 concentration was 0.4-80.5 μM (mean ± SE = 10.3 ± 2.2 μM, Table 1.1; Fig. 2.2), while NO_3 concentration was undetectable (UD)-133.9 μM (mean ± SE = 17.4 ± 3.8 μM). In addition, PO_4 concentration was UD-2.4 μM (mean ± SE = 0.3 ± 0.1 μM), while SiO_2 concentration was UD-67.7 μM (mean ± SE = 15.0 ± 2.7 μM). The NO_3 and SiO_2 concentrations were significantly positively correlated with precipitation, but negatively correlated with salinity (Table 1.7). However, the PO_4 concentration was uncorrelated with salinity. This evidence suggests that rain

increased NO_3 and SiO_2 concentrations, but not PO_4 concentration, at St. 1.

2.5.1.2 Station 2

The range of water temperature in the surface waters at St. 2 from May 2008 to July 2012 was 1.2–29.5 °C (mean ± SE = 16.2 ± 1.3 °C, Table 1.1; Fig. 2.3); the highest water temperature was observed in July 2010 and the lowest in January 2012, as in St. 1. In addition, salinity was 3.1-31.9 (mean ± SE = 26.0 ± 1.0). Like St. 1, water temperature at St. 2 was significantly positively correlated with precipitation, but significantly negatively correlated with salinity (Table 1.7).

The pH was 7.8-9.2 (mean ± SE = 8.5 ± 0.1). The NH_4 concentration at St. 2 was 0.1-44.2 μM (mean ± SE = 6.6 ± 1.5 μM, Table 1.1; Fig. 2.3) and the NO_3 concentration was UD-135.2 μM (mean ± SE = 8.4 ± 3.2 μM). In addition, the PO_4 concentration was UD-0.8 μM (mean ± SE = 0.2 ± 0.03 μM) and the SiO_2 concentration was UD-135.9 μM (mean ± SE = 10.0 ± 3.2 μM). Similar to St. 1, NO_3 and SiO_2 concentrations were significantly positively correlated with precipitation but significantly negatively correlated with salinity (Table 1.7). However, PO_4 concentration was uncorrelated with salinity.

2.5.1.3 Station 3

The range of water temperature in the surface waters at St. 3 from May 2008 to July 2012 was 1.2-29.1 °C (mean ± SE = 16.0 ±1.3 °C, Table 1.1; Fig. 2.4); the highest water temperature was observed in July 2010 and the lowest in January 2009. In addition, salinity was 3.1-32.3 (mean ± SE = 26.0 ± 1.0). Like St. 1 and St. 2, water temperature at St. 3 was significantly positively correlated with precipitation, but significantly negatively correlated with salinity (Table 1.7).

The pH was 7.8-9.1 (mean ± SE = 8.4 ± 0.1). The NH_4 concentration at St. 3 was 0.3–30.4 μM (mean ± SE = 8.0 ± 1.3 μM, Table 1.1; Fig. 2.4) and the NO_3 concentration was UD–90.9 μM (mean ± SE = 8.0 ± 2.2 μM). The PO_4

concentration was UD–1.2 μM (mean ± SE = 0.2 ± 0.04 μM) and the SiO_2 concentration was UD–95.4 μM (mean ± SE = 8.9 ± 2.4 μM). Like St. 1 and St. 2, NO_3 and SiO_2 concentrations were significantly positively correlated with precipitation, but significantly negatively correlated with salinity (Table 1.7). However, PO_4 concentration was uncorrelated with salinity.

2.5.2 Frequency of red tides and dominant groups

During the study period, red tides at St. 1, St. 2, and St. 3 occurred 33, 12, and 10 times, respectively (Table 1.2; Fig. 2.5). From 2008 to 2012, the frequency of red-tide occurrence at St. 1 varied little, but that at both St. 2 and St. 3 increased (Fig. 2.5).

At St. 1, 6 red-tide events were dominated by phototrophic dinoflagellates, 7 events by diatoms, 2 events by picoeukaryotes, 1 event by euglenophytes, 1 event by prasinophytes, and the remaining events by mixtures of 2-4 taxonomical groups (Table 1.2; Fig. 2.6). However, at St. 2, 1 red-tide event was dominated by phototrophic dinoflagellates, 7 events by diatoms, 1 event by mixotrophic ciliate *Mesodinium rubrum,* and 3 events by mixed groups. At St. 3, 3 red-tide events were dominated by phototrophic dinoflagellates, 4 by diatoms, 1 by *Noctiluca scintillans*, 1 by *M. rubrum*, and 1 by cyanobacteria. Thus, phototrophic dinoflagellates were comparably responsible for red-tide events to diatoms at St. 1 and 3, fewer events than diatoms at St. 2. However, red-tide causative taxa at all stations were phototrophic dinoflagellates and picoeu- karyotes before the establishment of the tidal power plant in 2011, with diatoms becoming the dominant causative species afterward. Cryptophytes formed red tides at St. 1, but not at St. 2 or St. 3 (Table 1.2; Fig. 2.6). In addition, these red-tide organisms caused red tides more frequently in 2010-2012 than in 2008–2009. Euglenophytes also formed red tides at St. 1 and not at St. 2 and 3 (Table 1.2; Fig. 2.6).

Table 1.1 The range of physical and chemical properties at three different stations from May 2008 to July 2012 in Shiwha Bay, Korea

Component	St. 1			St. 2			St. 3		
	range	mean ± SE	n	range	mean ± SE	n	range	mean ± SE	n
T	0.2-28.4	16.6 ± 1.3	46	1.2-29.5	16.2 ± 1.3	46	1.2-29.1	16.0 ± 1.3	46
P	0-481	64 ± 15	46	0-481	64 ± 15	46	0-481	64 ± 15	46
S	3.4-31.1	22.9 ± 1.0	46	3.1-31.9	26.0 ± 1.0	46	3.1-32.3	26.0 ± 1.0	46
pH	7.9-9.6	8.6 ± 0.1	44	7.8-9.2	8.5 ± 0.1	44	7.8-9.1	8.4 ± 0.1	44
NH_4	0.4-80.5	10.3 ± 2.2	43	0.1-44.2	6.6 ± 1.5	43	0.3-30.4	8.0 ± 1.3	43
NO_3	UD-133.9	17.4 ± 3.8	43	UD-135.2	8.4 ± 3.2	43	UD-90.9	8.0 ± 2.2	43
PO_4	UD-2.4	0.3 ± 0.1	43	UD-0.8	0.2 ± 0.03	43	UD-1.2	0.2 ± 0.04	43
SiO_2	UD-67.7	15.0 ± 2.7	43	UD-135.9	10.0 ± 3.2	43	UD-95.4	8.9 ± 2.4	43

UD: undetectable.

T: temperature (°C), P: precipitation (mm), S: salinity, NH_4: ammonium (μM), NO_3: nitrite plus nitrate (μM), PO_4: phosphate (μM), SiO_2: silicate (μM).

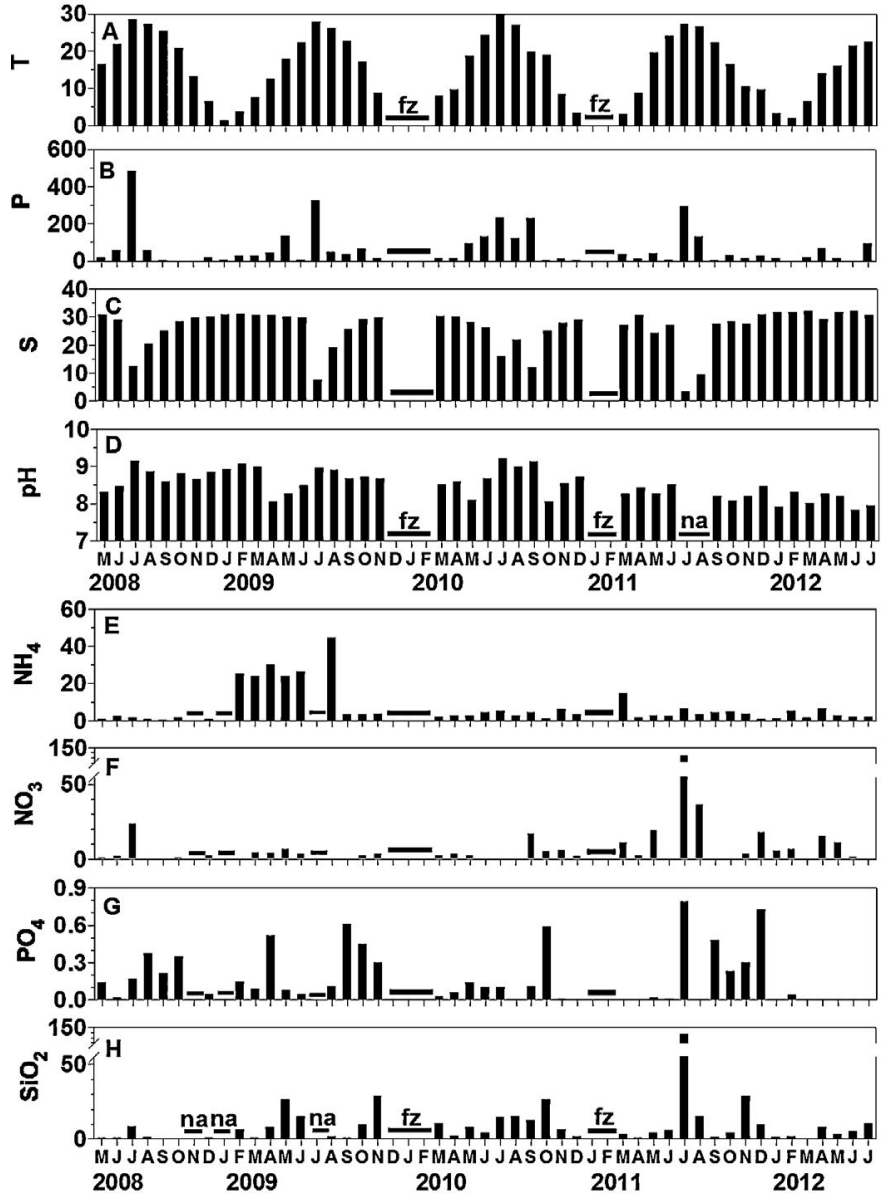

Fig. 2.2 Physical and chemical properties of Shiwha Bay at St. 1 from May 2008 to July 2012. (**A**) Water temperature (T, °C), (**B**) precipitation (P, mm), (**C**) salinity (S), (**D**) pH, (**E**) ammonium (NH4, μM), (**F**) nitrite plus nitrate (NO3, μM), (**G**) phosphate (PO4, μM), and (**H**) silicate (SiO2, μM). fz indicates months when water was frozen and na indicates months when data were not available.

2.5.3 Temporal and spatial variations in red-tide causative species

During the study period at St. 1, *Gymnodinium aureolum*, *Paragymnodinium shiwhaense*, and *Karlodinium veneficum* formed red tides between May and June 2008 but did not form red tides at later times (Table 1.2; Fig. 2.7). Furthermore, *Prorocentrum micans*, *Prorocentrum minimum*, and *Heterocapsa triquetra* formed red tides between 2008 and 2010 but not at later times. *Heterocapsa rotundata* was the only phototrophic dinoflagellate forming red tides in 2012. Conversely, the diatoms *Thalassiosira* spp., *Skeletonema costatum*, *Chaetoceros* spp., *Cylindrotheca closterium*, and *Cyclotella* sp. did not form red tides in 2009-2010, but these species did form red tides in 2011–2012 (Table 1.2; Fig. 2.8). In addition, a red tide dominated by the raphidophyte *Heterosigma akashiwo* first occurred in 2012.

The numbers of red-tide causative species at St. 2 and St. 3 were considerably lower than at St. 1 (Table 1.2). At St. 2, *Prorocentrum micans* and *Prorocentrum minimum* formed red tides in 2008-2010 but not at later dates (Table 1.2). However, *Cylindrotheca closterium*, *Stephanopyxis palmeriana*, and *Chaetoceros* spp. did not form red tides in 2008–2010 but did in 2011-2012; *Skeletonema costatum* and *Thalassiosira* spp. formed red tides in 2008, 2011, and 2012, while *Thalassiothrix frauenfeldii* formed a red tide in 2008 only (Table 1.2).

At St. 3, *Gymnodinium aureolum*, *Prorocentrum micans*, and *Prorocentrum minimum* formed red tides between 2008 and 2010 but not later. However, *Skeletonema costatum*, *Cylindrotheca closterium*, *Eucampia zodiacus*, and *Thalassiosira* sp. formed red tides in 2011–2012 but not in 2008–2010 (Table 1.2).

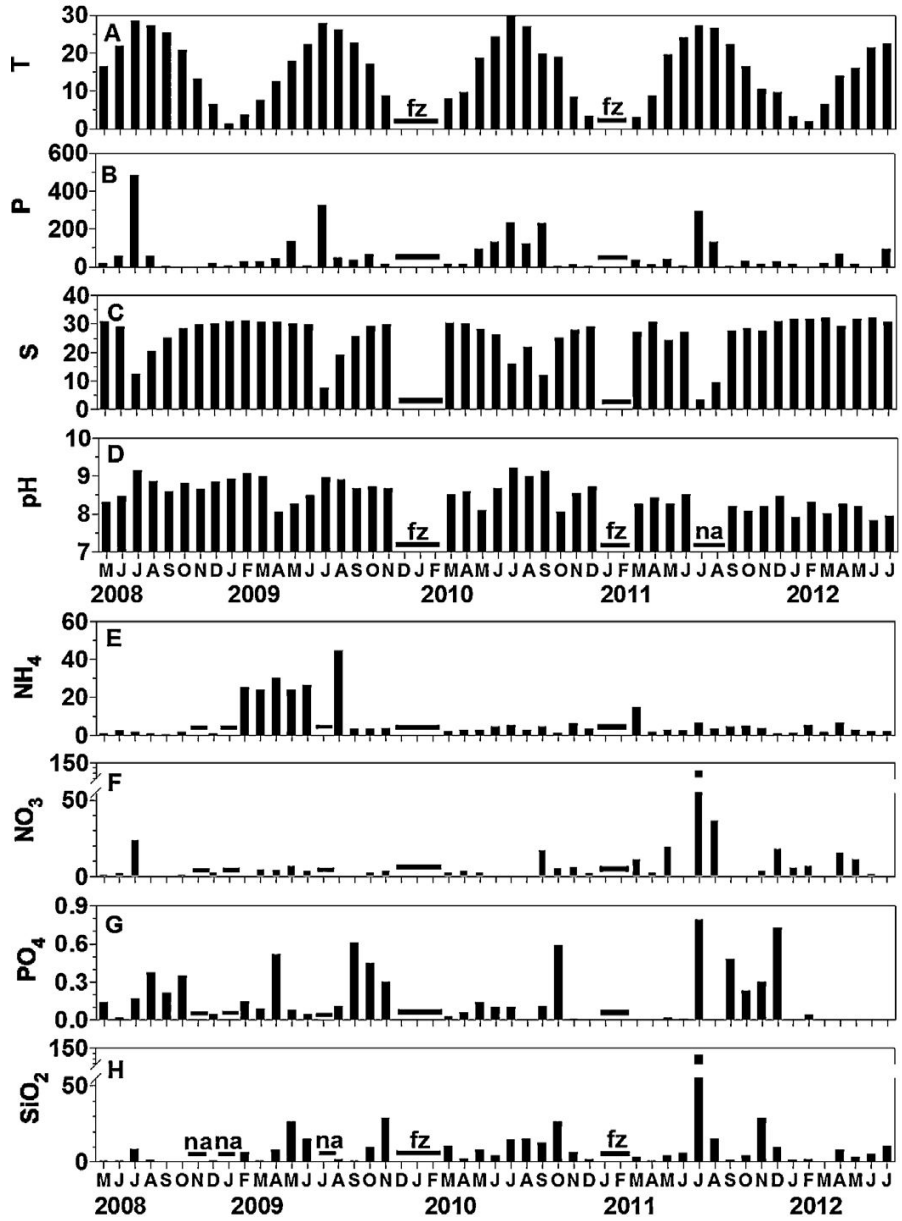

Fig. 2.3 Physical and chemical properties of Shiwha Bay at St. 2 from May 2008 to July 2012. (**A**) Water temperature (T, °C), (**B**) precipitation (P, mm), (**C**) salinity (S), (**D**) pH, (**E**) ammonium (NH4, μM), (**F**) nitrite plus nitrate (NO3, μM), (**G**) phosphate (PO4, μM), and (**H**) silicate (SiO2, μM). fz indicates months when water was frozen and na indicates months when data were not available.

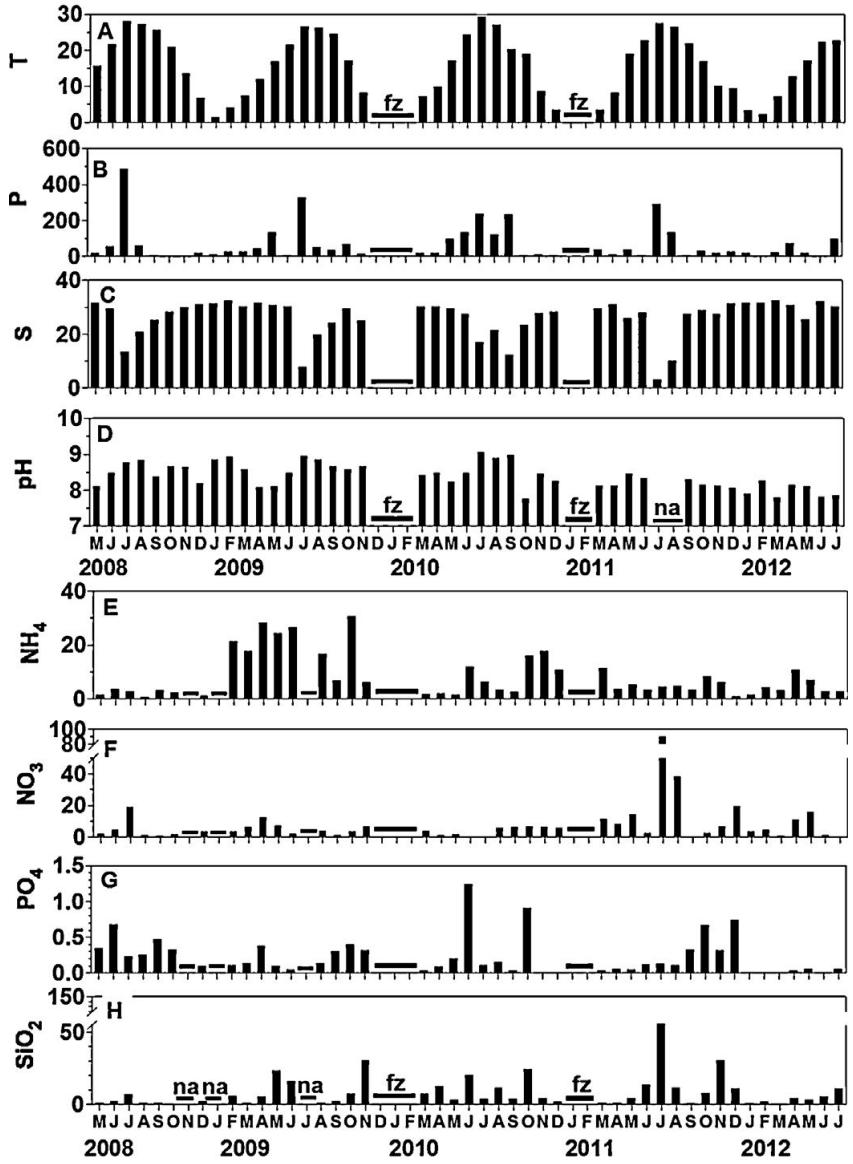

Fig. 2.4 Physical and chemical properties of Shiwha Bay at St. 3 from May 2008 to July 2012. (**A**) Water temperature (T, °C), (**B**) precipitation (P, mm), (**C**) salinity (S), (**D**) pH, (**E**) ammonium (NH4, μM), (**F**) nitrite plus nitrate (NO3, μM), (**G**) phosphate (PO4, μM), and (**H**) silicate (SiO2, μM). fz indicates months when water was frozen and na indicates months when data were not available.

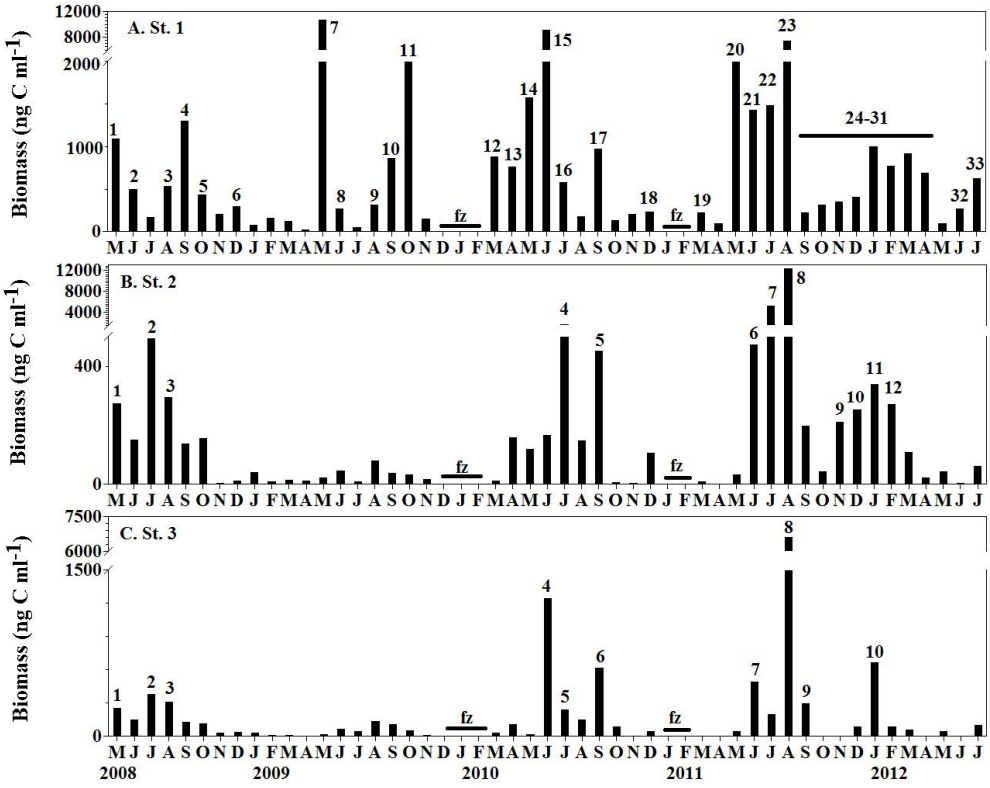

Fig. 2.5 Red-tide events at three stations in Shiwha Bay, Korea, from May 2008 to July 2012. Numbers indicate the sequence of each red-tide event. fz indicates months when water was frozen.

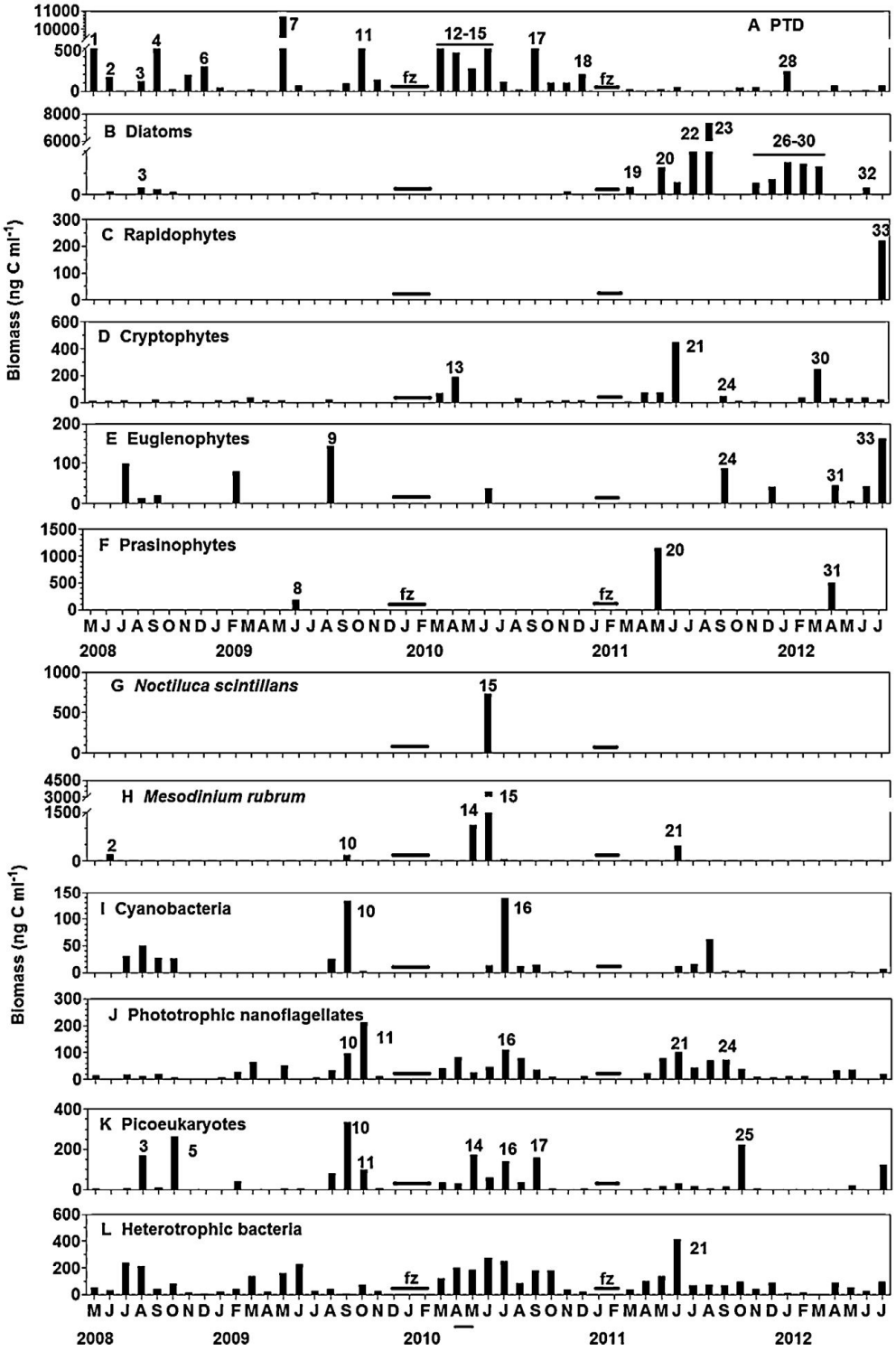
A PTD
B Diatoms
C Rapidophytes
D Cryptophytes
E Euglenophytes
F Prasinophytes
G Noctiluca scintillans
H Mesodinium rubrum
I Cyanobacteria
J Phototrophic nanoflagellates
K Picoeukaryotes
L Heterotrophic bacteria
Biomass (ng C ml-1)
fz
12-15
26-30
M J J A S O N D J F M A M J J A S O N D J F M A M J J A S O N D J F M A M J J A S O N D J F M A M J J
2008
2009
2010
2011
2012

Fig. 2.6 Biomass of red-tide causative protist groups and bacteria at St. 1 in Shiwha Bay from May 2008 to July 2012. (**A**) Phototrophic dinoflagellates (PTD), (**B**) Diatoms, (**C**) Raphidophytes, (**D**) Cryptophytes, (**E**) Euglenophytes, (**F**) Prasinophytes, (**G**) the heterotrophic dinoflagellate *Noctiluca scintillans*, (**H**) the mixotrophic ciliate *Mesodinium rubrum*, (**I**) Cyanobacteria, (**J**) Phototrophic nanoflagellates, (**K**) Picoeukaryotes, and (**L**) Heterotrophic bacteria. fz indicates months when water was frozen.

2.5.4 Conditions when red-tide causative species formed red tides in Shiwha Bay

Gymnodinium aureolum: This dinoflagellate formed a red tide once in May 2008 at St. 1 and St. 3 (Table 1.2). The maximum abundance and biomass of *G. aureolum* during the red tides were 386-1,172 cells ml^{-1} and 205-621 ng C ml^{-1}, respectively. Water temperature was 15.5-18.3 °C and salinity 30.4-31.3 (Table 1.2); the concentrations of NH_4, NO_3, PO_4, and SiO_2 were 0.5-1.3, 0.8-2.4, 0.3-0.4, and 0.6-1.3 μM, respectively (Table 1.2).

Karlodinium veneficum formed a red tide in June 2008 at St. 1.; its maximum abundance and biomass were 930 cells ml^{-1} and 167 ng C ml^{-1}, respectively.

However, during this red tide, co-occurring *Mesodinium rubrum* made the abundance of red-tide organisms >200 ng C ml^{-1}. Water temperature during the red tide was 19.3 °C, salinity was 29.4, and concentrations of NH_4, NO_3, PO_4, and SiO_2 2.3, 3.2, 1.1, and 3.7 μM, respectively (Table 1.2).

Prorocentrum minimum formed red tides 6 times (i.e., September 2008, May and October 2009, and June, September, and December 2010) at St. 1 and once (September 2010) at St. 2 and St. 3 (Table 1.2). Its maximum abundance and biomass were 1363-35,770 cells ml^{-1} and 177-4,650 ng C ml^{-1}, respectively. Water temperature was 3.2-26.9 °C, salinity 11.2-27.7; and the concentrations of NH_4, NO_3, PO_4, and SiO_2 0.4-17.2, 0.6-34.5, UD-1.5, and 1.4-43.7 μM, respectively (Table 1.2).

Heterocapsa rotundata formed red tides twice, with *Heterocapsa triquetra* in December 2008 and *Thalassiosira* spp. in January 2012, at St. 1. Its maximum abundance and biomass were 7,867-9,400 cells ml^{-1} and 157-188 ng C ml^{-1}, respectively. Water temperature was 0.2-3.7 °C, salinity 28.9-31.1, and the concentrations of NH_4, NO_3, PO_4, and SiO_2 1.0-1.2, UD-2.7, UD-0.04, and UD- 1.6 μM, respectively (Table 1.2).

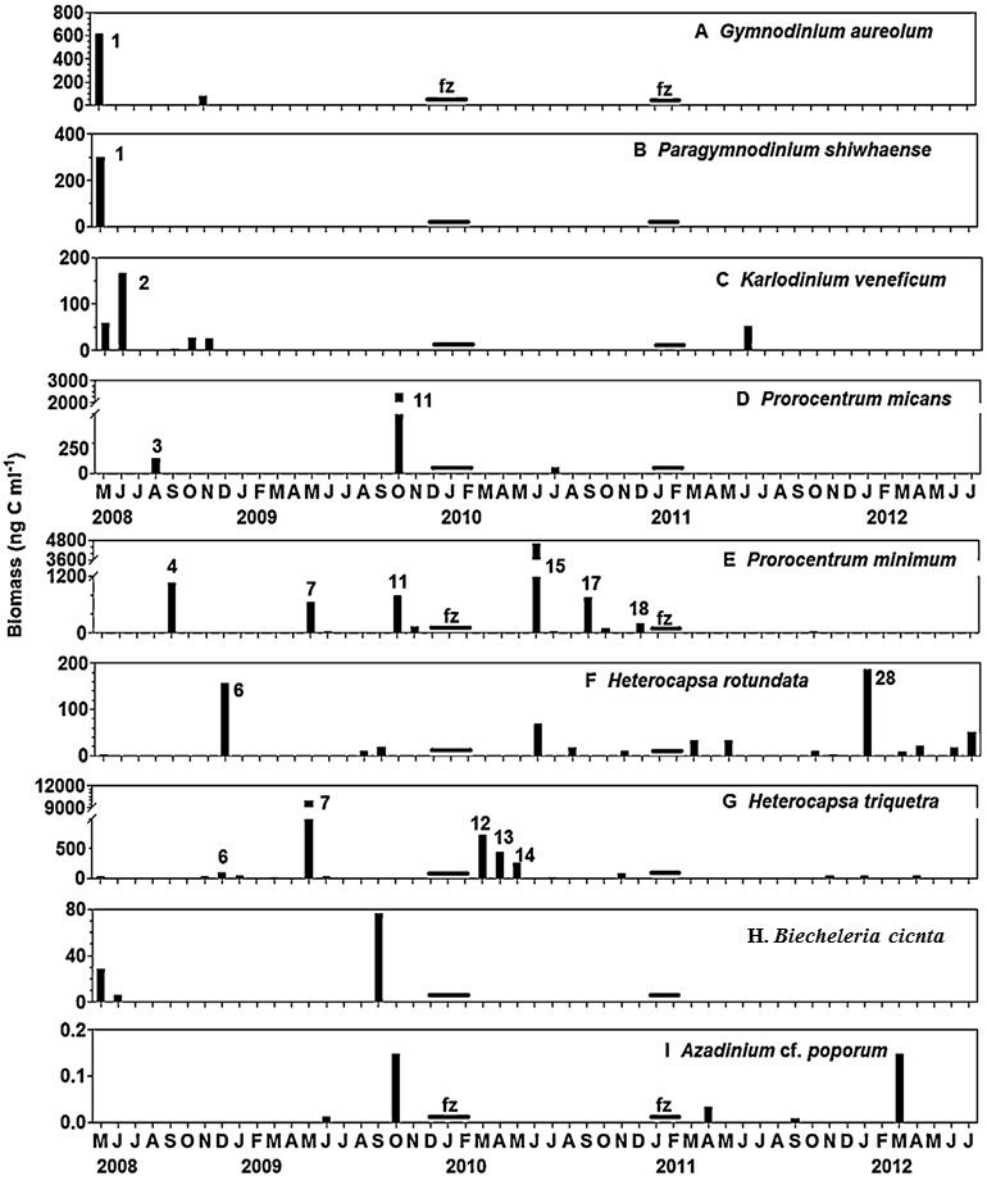

Fig. 2.7 Biomass of phototrophic dinoflagellate species at St. 1 in Shiwha Bay from May 2008 to July 2012. (**A**) *Gymnodinium aureolum*, (**B**) *Paragymnodinium shiwhaense*, (**C**) *Karlodinium veneficum*, (**D**) *Prorocentrum micans*, (**E**) *Prorocentrum minimum*, (**F**) *Heterocapsa rotundata*, (**G**) *Heterocapsa triquetra*, (**H**) *Biecheleria cincta*, and (**I**) *Azadinium* cf. *poporum*. fz indicates months when water was frozen.

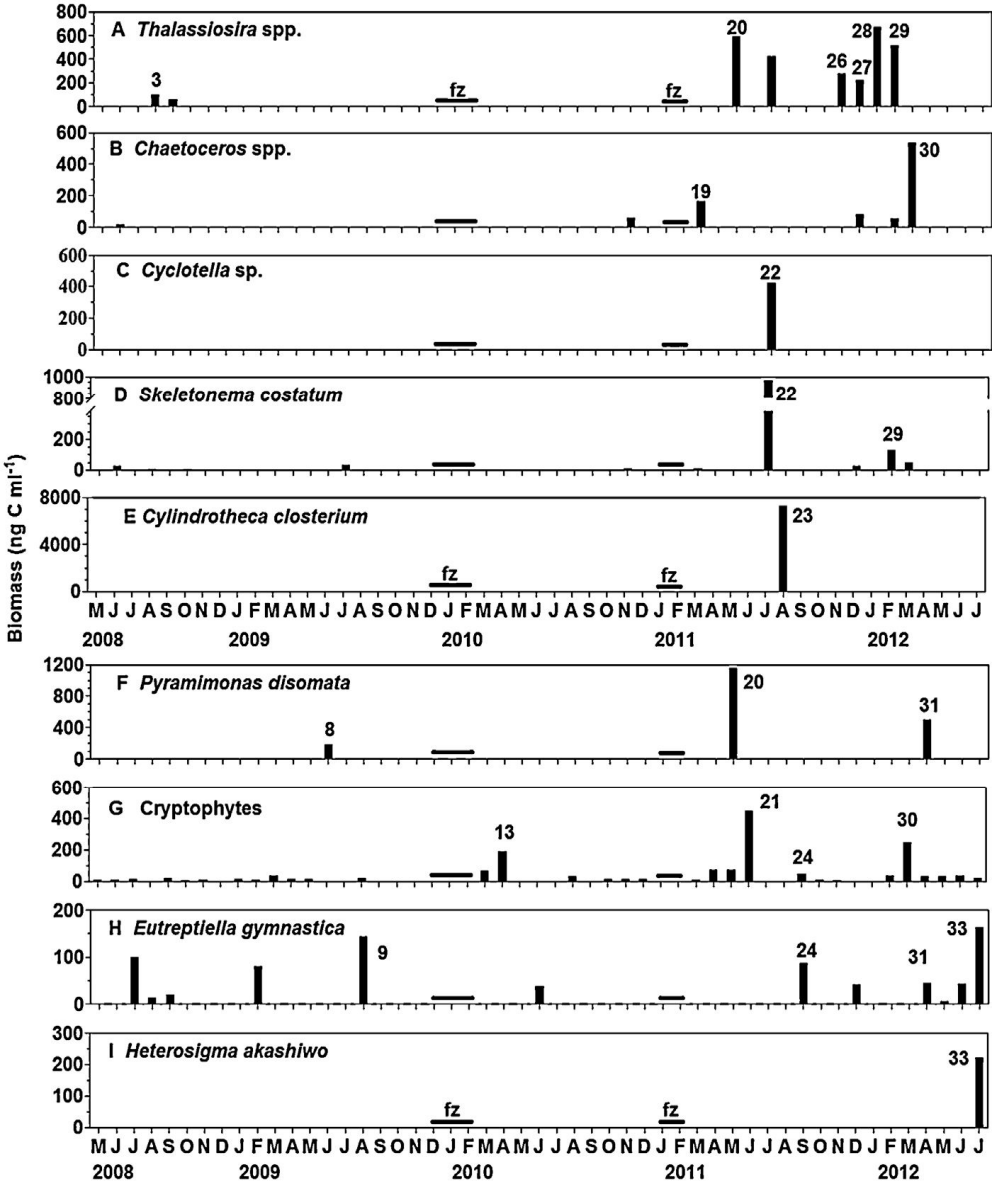

Fig. 2.8 Biomass of the species or taxa of diatoms, raphidophytes, euglenophytes, prasinophytes, and cryptophytes at St. 1 in Shiwha Bay from May 2008 to July 2012. (**A**) *Thalassiosira* spp., (**B**) *Chaetoceros* spp., (**C**) *Cyclotella* sp., (**D**) *Skeletonema costatum*, (**E**) *Cylindrotheca closterium*, (**F**) *Pyramimonas disomata*, (**G**) Cryptophytes, (**H**) *Eutreptiella gymnastica*, and (**I**) *Heterosigma akashiwo*. fz indicates months when water was frozen.

Heterocapsa triquetra formed red tides 5 times (December 2008, May 2009, and March, April, and May 2010). Its maximum abundance and biomass were 470-45,700 cells ml^{-1} and 103-10,054 ng C ml^{-1}, respectively. Water temperature was 3.7-20.6 °C, salinity 19.7-28.9, and the concentrations of NH_4, NO_3, PO_4, and SiO_2 were 1.2-17.2, 2.7-44.1, 0.04-0.6, and 1.6-43.7 μM, respectively (Table 1.2).

Prorocentrum micans formed red tides twice in August 2008 and October 2009 at St. 1, three times (July and August 2008 and July 2010) at St. 2, and once in July 2010 at St. 3 (Table 1.2). Its maximum abundance and biomass were 125-2,457 cells ml^{-1} and 125-2,457 ng C ml^{-1}, respectively. Water temperature was 15.8-29.5 °C, salinity 12.4-21.1, and the concentrations of NH_4, NO_3, PO_4, and SiO_2 0.6-12.7, UD-23.9, 0.1-2.4, and 0.7-14.2 μM, respectively (Table 1.2).

Thalassiosira spp. These diatoms (mainly *T. rotula*, *T. pacifica*, *T. gravida*, and *T. decipiens*) formed 6 red tides at St. 1 (in August 2008, May 2011, and each month from November 2011 to February 2012), 3 times at St. 2 (May 2008, November 2011, and January 2012), and once at St. 3 (January 2012). The maximum abundance and biomass of *Thalassiosira* spp. during the red tides were 208-2,267 cells ml^{-1} and 109-677 ng C ml^{-1}, respectively. The water temperature during the red tides was 0.2-26.1 °C, while the salinity was 21.1-31.7. In addition, the concentrations of NH_4, NO_3, PO_4, and SiO_2 during the red tides were 0.3-25.5, UD-30.3, UD-2.4, and UD-50.0 μM, respectively (Table 1.2).

Chaetoceros spp. These diatoms (mainly *C. curvisetus*, *C. mulleri*, *C. subtilus*, and *C. diadema*) formed red tides twice at St. 1 (in March 2011 and 2012) and once at St. 2 (in February 2012; Table 1.2). The maximum abundance and biomass of *Chaetoceros* spp. were 619-4,925 cells ml^{-1} and 68-542 ng C ml^{-1}, respectively. Water temperature was 1.9-8.9 °C, salinity 19.1-31.6, and the concentrations of NH_4, NO_3, PO_4, and SiO_2 were 4.9-80.5, 4.5-53.4, UD-0.03, and 0.4-30.3 μM, respectively (Table 1.2).

Skeletonema costatum formed two red tides (July 2011 and February 2012) at St. 1, once (in July 2011) at St. 2, and one (in January 2012) at St. 3 (Table 1.2). Its maximum abundance and biomass were 4,550-176,667 cells ml^{-1} and 137-5,300 ng C ml^{-1}, respectively. Water temperature was 2.9-27.0 °C, salinity 3.1-31.5, and the concentrations of NH_4, NO_3, PO_4, and SiO_2 1.2-34.3, 3.6-135.2, UD-1.3, and 0.1-135.9 μM, respectively (Table 1.2).

Cryptophytes. Cryptophytes formed 3 red tides (April 2010, June 2011, and March 2012) at St. 1 (Table 1.2). Their maximum abundance and biomass were 11,324-26,674 cells ml^{-1} and 193-453 ng C ml^{-1}, respectively. Water temperature was 8.9-25.4 °C, salinity 21.5-29.8, and the concentrations of NH_4, NO_3, PO_4, and SiO_2 2.0-8.3, UD-33.8, UD-0.9, and 0.4-27.8 μM, respectively.

Mesodinium rubrum. This mixotrophic ciliate formed 5 red tides (June 2008, September 2009, May 2010, June 2010, and June 2011) at St.1 and one (in June 2011) at St. 2 and St. 3 (Table 1.2). Its maximum abundance and biomass were 179-3,150 cells ml^{-1} and 202-3,560 ng C ml^{-1}, respectively. Water temperature was 19.3-26.4 °C, salinity 20.7-29.4, and the concentrations of NH_4, NO_3, PO_4, and SiO_2 2.0-10.0, UD-16.1, 0.01-1.1, and 1.6-17.5 μM, respectively.

Eutreptiella gymnastica. This euglenophyte formed 4 red tides with picoeukaryotes in August 2009 and September 2011, *Pyramimonas disomata* and *Heterosigma akashiwo* in April and July 2012, respectively, at St. 1 (Table 1.2). Its maximum abundance and biomass were 638-1,171 cells ml^{-1} and 89-164 ng C ml^{-1}, respectively. Water temperature was 15.3-25.9 °C, salinity 17.5-27.7, and the concentrations of NH_4, NO_3, PO_4, and SiO_2 1.0-14.0, 0.4-21.7, UD-0.7, and 1.6-22.7 μM, respectively.

Heterosigma akashiwo formed a red tide in July 2012 at St. 1 (Table 1.2). Its maximum abundance and biomass were 2,029 cells ml^{-1} and 223 ng C ml^{-1}, respectively. Water temperature was 24.1 °C, salinity 27.7, and the concentrations of

NH_4, NO_3, PO_4, and SiO_2 1.0, 6.6, 0.3, and 22.7 μM, respectively.

In addition, the PTD *Paragymnodinium shiwhaense*, the heterotrophic dinoflagellate *Noctiluca scintillan*, and the diatoms *Cyclotella* sp., *Cylindrotheca closterium*, *Melosira* sp., *Thalassiothrix frauenfeldii*, *Stephanopyxis palmeriana*, *Eucampia zodiacus* formed red tides (Table 1.2).

2.5.5 Spatial distribution of *Paragymnodinium shiwhaense* and *Biecheleria cincta* in Shiwha Bay

Paragymnodinium shiwhaense formed a red tide once in May 2008 at St. 1 (Table 1.2). The maximum abundance and biomass of *P. shiwhaense* during the red tide were 1,375 cells ml^{-1} and 303 ng C ml^{-1}, respectively. The water temperature during the red-tide was 18.0 ^{o}C, while the salinity was 30.5. In addition, the concentrations of NH_4, NO_3, PO_4, and SiO_2 during the red tide were 0.5, 0.9, 0.5, and 1.7 μM, respectively.

Biecheleria cincta did not cause the red tide during the study period. However, this dinoflagellate was abundant in May 2008, June 2008, and September 2009 at St. 1 (Table 1.2; Fig. 2.7). The maximum abundance and biomass of *B. cincta* during the red tide were 297 cells ml^{-1} and 76.9 ng C ml^{-1}, respectively. The water temperature during the red-tide was 22.5 ^{o}C, while the salinity was 25.1. In addition, the concentrations of NH_4, NO_3, PO_4, and SiO_2 during the red tide were 2, 0.02, 0.4, and 1.6 μM, respectively.

2.5.6 Dominant species of heterotrophic protists

Pfiesteria piscicida and *S. algicida* were abundant in 2008, while *Gyrodiniellum shiwhaense* was found in 2008-2009 (Fig. 2.9). *Gyrodinium* spp. (mainly *Gyrodinium dominans*/*Gyrodinium moestrupii*) and *Protoperidinium bipes* were abundant in almost all years (Fig. 2.9). Several naked ciliates (mainly the *Strobilidium*, *Strombidiniopsis*, and *Balanion* genera) were present almost all the

year. In addition, the tintinnid ciliates *Tintinnopsis* spp. (mainly *T. beroidea*) were abundant in October 2008-2011. *Favella taraikaensis* and *Eutintinnus tubulosa* were present in July 2010 and June 2011, respectively.

2.5.7 Grazing impact by protistan grazers on red-tide organisms

The range of the calculated grazing coefficients attributable to dominant protistan grazers on co-occurring red-tide organisms in Shiwha Bay during the study period was wide. The grazing coefficients for each red-tide organism were as follows.

Prorocentrum minimum. *Gyrodinium dominans* and *Strombidinopsis* sp. are known to feed on *P. minimum* (Jeong et al. 1999a; Kim and Jeong 2004). When the abundances of *P. minimum* and co-occurring *G. dominans*/*Gyrodinium moestrupii* were 8-3,993 cells ml^{-1} and 128-2,256 cells ml^{-1}, respectively, the grazing coefficients attributable to *G. dominans*/*G. moestrupii* grazing on *P. minimum* were 0.05-0.66 h^{-1} (Table 1.3). When the abundancesof *P. minimum* and co-occurring *Strombidinopsis* spp. were 294 cells ml^{-1} and 1 cell ml^{-1}, respectively, the grazing coefficient of *Strombidinopsis* spp. on *P. minimum* was 0.21 h^{-1} (Table 1.3). The combined grazing coefficients for *G. dominans*/*G. moestrupii*, and *Strombidinopsis* spp. grazing on *P. minimum* were 0.05-0.66 h^{-1}.

Skeletonema costatum. *Protoperidinium bipes* is known to feed on *S. costatum* (Jeong et al. 2004c). When the abundances of *S. costatum* and co-occurring *P. bipes* were 64-1,756 cells ml^{-1} and 7-188 cells ml^{-1}, respectively, the grazing coefficients of *P. bipes* on *S. costatum* were 0.00-0.14 h^{-1} (Table 1.3).

Table 1.2 The maximum abundance (MA) and biomass (MB) of the red-tide causative species during each red-tide event in Shiwha Bay, Korea from May 2008 to July 2012.

A. Station 1

NO.	time	Species	T	S	NH_4	NO_3	PO_4	SiO_2	MA	MB
1	2008.05.17	*Gymnodinium aureolum* (PTD)	18.3	30.4	0.5	0.8	0.4	1.3	1,172	621
		Paragymnodinium shiwhaense (PTD)							**1,375**	**303**
		Amphidinium cf. *carterae* (PTD)							2,094	147
		Karlodinium veneficum (PTD)							338	61
		Heterocapsa triquetra (PTD)							133	29
		Biecheleria cincta (PTD)							**112**	**29**
		Mesodinium rubrum (MC)							17	19
		Cryptophytes (CRY)							733	12
2	2008.06.17	*Mesodinium rubrum* (MC)	19.3	29.4	2.3	3.2	1.1	3.7	200	226
		Karlodinium veneficum (PTD)							930	167
		Skeletonema costatum (DIA)							1,141	34
		Rhizosolenia delicatula (DIA)							200	30
		Chaetoceros spp. (DIA)							200	22
		Cryptophytes (CRY)							917	16
3	2008.08.16	*Thalassiosira* spp. (DIA)	26.3	20.9	12.7	4.1	1.5	3.2	288	180
		Prorocentrum micans (PTD)							125	125
		Thalassiothrix frauenfeldii (DIA)							263	37
		Eutreptiella gymnastica (EUG)							106	15
		Skeletonema costatum (DIA)							419	13
4	2008.09.19	*Prorocentrum minimum* (PTD)	26.8	23.5	35.0	1.2	1.6	1.7	8,222	1,069
		Thalassiosira spp. (DIA)							161	61

		Rhizosolenia fragillisima (DIA)							400	60
		Cryptophytes (CRY)							1,300	22
		Eutreptiella gymnastica (EUG)							156	22
5	2008.10.10	Picoeukaryotes (PE)	20.7	25	21	1.7	0.1	0.0	124,760	267
		Mesodinium rubrum (MC)							29	32
		Karlodinium veneficum (PTD)							161	29
6	2008.12.06	*Heterocapsa rotundata* (PTD)	3.7	28.9	1.2	2.7	0.04	1.6	7,867	157
		Heterocapsa triquetra (PTD)							470	103
		Prorocentrum minimum (PTD)							195	25
		Gymnodinium aureolum (PTD)							19	10
7	2009.05.23	*Heterocapsa triquetra* (PTD)	19.6	22.5	17.2	19.5	0.1	43.7	45,700	10,054
		Prorocentrum minimum (PTD)							5,017	652
		Cryptophytes (CRY)							1,185	20
8	2009.06.08	*Pyramimonas disomata* (PRA)	22.7	17.4	2.5	0.8	0.4	2.9	16,200	194
		Prorocentrum minimum (PTD)							305	40
		Heterocapsa triquetra (PTD)							150	33
9	2009.08.29	*Eutreptiella gymnastica* (EUG)	25.9	17.5	14.0	0.7	0.5	14.9	1,044	146
		Picoeukaryotes (PE)							38,534	82
		Phototrophic nanoflagellates (PNF)							4,878	35
10	2009.09.26	Picoeukaryotes (PE)	22.5	25.1	2.0	0.02	0.4	1.6	157,468	337
		Mesodinium rubrum (MC)							179	202
		Cyanobacteria (CYA)							675,317	134
		Phototrophic nanoflagellates (PNF)							13,739	100
		Biecheleria cincta (PTD)							257	77
11	2009.10.23	*Prorocentrum micans* (PTD)	15.8	20.6	0.8	9.6	0.1	0.8	2,457	2,457
		Prorocentrum minimum (PTD)							6,117	795
		Prorocentrum triestinum (PTD)							407	57

		Phototrophic nanoflagellates (PNF)							13,739	215
		Picoeukaryotes (PE)							29,591	102
12	2010.03.30	*Heterocapsa triquetra* (PTD)	10.0	19.7	3.7	44.1	0.1	39.8	3,341	735
		Cryptophytes (CRY)							4,169	71
13	2010.04.10	*Heterocapsa triquetra* (PTD)	12.3	21.5	2.0	33.8	0.6	27.8	2,063	454
		Cryptophytes (CRY)							11,324	193
14	2010.05.29	*Mesodinium rubrum* (MC)	20.6	24.7	7.5	16.1	0.2	17.5	983	1,111
		Heterocapsa triquetra (PTD)							1,217	268
		Picoeukaryotes (PE)							82,433	176
15	2010.06.23	*Prorocentrum minimum* (PTD)	26.4	20.7	10.0	4.6	0.4	7.1	35,770	4,650
		Mesodinium rubrum (MC)							3,150	3,560
		Noctiluca scintillans (HTD)							21	742
		Eutreptiella gymnastica (EUG)							280	39
		Heterocapsa rotundata (PTD)							3,500	70
		Prorocentrum triestinum (PTD)							420	59
16	2010.07.29	Picoeukaryotes (PE)	28.4	19.1	5.62	4.1	0.2	17.8	67,215	144
		Cyanobacteria (CYA)							699,624	139
		Phototrophic nanoflagellates (PNF)							15,218	110
17	2010.09.30	*Prorocentrum minimum* (PTD)	20.4	11.2	2.1	34.5	0.1	42.4	5,872	763
		Picoeukaryotes (PE)							74,939	160
18	2010.12.23	*Prorocentrum minimum* (PTD)	3.2	27.7	2.6	3.5	UD	1.7	1,544	201
		Cryptophytes (CRY)							1,009	17
19	2011.03.05	*Chaetoceros* spp. (DIA)	4.3	19.1	80.5	53.4	UD	30.3	1,555	171
		Heterocapsa rotundata (PTD)							1,724	34
		Skeletonema costatum (DIA)							573	17
		Cryptophytes (CRY)							656	11

20	2011.05.24	*Pyramimonas disomata* (PRA)	19.6	22.7	4.0	18.5	0.1	9.1	96,640	1,160
		Thalassiosira spp. (DIA)							1,573	598
		Cryptophytes (CRY)							4,489	76
		Heterocapsa rotundata (PTD)							1,724	34
21	2011.06.17	*Mesodinium rubrum* (MC)	25.4	25.5	3.2	UD	0.9	9.7	421	476
		Cryptophytes (CRY)							26,674	453
		Phototrophic nanoflagellates (PNF)							14,267	104
		Karlodinium veneficum (PTD)							295	53
22	2011.07.20	*Skeletonema costatum* (DIA)	26.8	6.5	34.3	76.9	1.3	67.7	32,444	973
		Cyclotella sp. (DIA)							3,550	430
23	2011.08.22	*Cylindrotheca closterium* (DIA)	27	3.4	5.1	133.9	UD	43.4	66,625	7,329
24	2011.09.30	Eutreptiella gymnastica (EUG)	22.1	26.5	4.8	0.4	0.7	1.6	638	89
		Phototrophic nanoflagellates (PNF)							10,146	74
		Cryptophyte (CRY)							3131	53
25	2011.10.18	Picoeukaryotes (PE)	15.3	22.8	27.5	20.6	0.7	15.0	105,079	225
26	2011.11.26	*Thalassiosira* spp. (DIA)	7.7	26.7	12.6	30.3	0.2	50.0	736	545
		Heterocapsa triquetra (PTD)							238	52
27	2011.12.07	*Thalassiosira* spp. (DIA)	7	28.0	0.4	12.5	UD	2.3	600	444
		Chaetoceros spp. (DIA)							755	83
		Eutreptiella gymnastica (EUG)							310	43
		Detonula pumila (DIA)							135	43
		Skeletonema costatum (DIA)							1,135	34
		Thalassiothrix frauenfeldii (DIA)							70	11
28	2012.01.04	*Thalassiosira* spp. (DIA)	0.2	31.1	1.0	UD	UD	UD	1,781	677
		Detonula pumila (DIA)							950	299
		Heterocapsa rotundata (PTD)							9,400	188

		Thalassiothrix frauenfeldii (DIA)							431	69
		Heterocapsa triquetra (PTD)							212	47
		Pseudonitzschia spp. (DIA)							419	14
29	2012.02.24	*Thalassiosira* spp. (DIA)	2.9	30.3	25.5	10.4	UD	0.1	1,380	524
		Skeletonema costatum (DIA)							4,550	137
		Chaetoceros spp. (DIA)							530	58
		Cryptophytes (CRY)							2,400	41
30	2012.03.29	*Chaetoceros* spp. (DIA)	8.9	29.8	8.3	4.5	UD	0.4	4,925	542
		Cryptophytes (CRY)							14,915	254
		Skeletonema costatum (DIA)							1,725	52
		Thalassiothrix frauenfeldii (DIA)							415	66
		Heterocapsa rotundata (PTD)							520	10
31	2012.04.28	*Pyramimonas disomata* (PRA)	15.3	27.4	4.6	21.7	UD	14.8	42,333	508
		Eutreptiella gymnastica (EUG)							1,133	159
		Heterocapsa triquetra (PTD)							333	51
		Cryptophytes (CRY)							2,000	34
		Heterocapsa rotundata (PTD)							233	23
32	2012.06.18	*Melosira* sp. (DIA)	22.4	31.7	1.7	UD	UD	5.6	993	167
		Eutreptiella gymnastica (EUG)							321	45
		Cryptophytes (CRY)							2,286	39
		Heterocapsa rotundata (PTD)							929	19
33	2012.07.04	*Heterosigma akashiwo* (RAP)	24.1	27.7	1.0	6.6	0.3	22.7	2,029	223
		Eutreptiella gymnastica (EUG)							1,171	164
		Heterocapsa rotundata (PTD)							2,564	51
		Cryptophytes (CRY)							1,390	24
		Prorocentrum minimum (PTD)							136	18

B. Station 2

NO	time	Species	T	S	NH_4	NO_3	PO_4	SiO_2	MA	MB
1	2008.05.17	*Thalassiosira gravida* (DIA)	16.3	30.8	0.3	0.9	0.1	0.2	281	149
		Skeletonema costatum (DIA)							1,756	53
		Amphidinium cf. *carterae* (PTD)							750	38
2	2008.07.31	*Prorocentrum micans* (PTD)	28.3	12.4	1.3	23.9	0.2	7.9	161	161
		Cyanobacteria (CYA)							779,943	155
		Phototrophic nanoflagellates (PNF)							9,268	67
		Prorocentrum minimum (PTD)							250	33
		Skeletonema costatum (DIA)							589	18
		Cryptophytes (CRY)							656	11
		Rhizosolenia delicatula (DIA)							67	10
3	2008.08.16	*Prorocentrum micans* (PTD)	27.1	20.4	0.6	0.3	0.4	0.7	144	144
		Thalassiothrix frauenfeldii (DIA)							744	119
4	2010.07.29	*Prorocentrum micans* (PTD)	29.5	15.8	5.1	UD	0.1	14.2	1,809	1,809
		Prorocentrum triestinum (PTD)							124	17
5	2010.09.30	*Prorocentrum minimum* (PTD)	19.6	11.7	4.3	17.2	0.1	12.3	1,363	177
		Picoeukaryotes (PE)							59,447	127
		Cryptophytes (CRY)							2,283	39
		Heterocapsa rotundata (PTD)							1,858	37
6	2011.06.17	*Mesodinium rubrum* (MC)	24.2	27.4	11.6	UD	1.2	19.8	275	311
		Picoeukaryotes (PE)							59,447	63
		Phototrophic nanoflagellates (PNF)							5,548	54
7	2011.07.20	*Skeletonema costatum* (DIA)	27.0	3.1	6.1	135.2	0.8	135.9	176,667	5,300

		Cryptophytes (CRY)							2164	37
8	2011.08.22	*Cylindrotheca closterium* (DIA)	26.5	9.3	2.9	36.3	UD	14.9	112,714	12,399
9	2011.11.26	*Thalassiosira rotula* (DIA)	10.4	27.4	3.3	3.8	0.3	28.4	208	154
		Chaetoceros curvisetus (DIA)							272	30
		Stephanopyxis palmeriana (DIA)							14	20
10	2011.12.07	*Stephanopyxis palmeriana* (DIA)	9.6	30.9	0.6	18.0	0.7	9.3	124	181
		Thalassiosira decipiens (DIA)							162	33
		Eucampia zodiacus (DIA)							104	26
11	2012.01.14	*Thalassiosira* sp. (DIA)	3.1	31.7	0.8	5.5	UD	1.1	1,944	235
		Skeletonema costatum (DIA)							2,917	88
12	2012.02.24	*Ditylum brightwellii* (DIA)	1.9	31.6	4.9	6.8	0.03	1.6	11	90
		Thalassiosira sp. (DIA)							663	80
		Chaetoceros sp. (DIA)							619	68
		Skeletonema costatum (DIA)							1,000	30
		Thalassionema nitzschioides (DIA)							625	25

C. Station 3

NO	Time	Species	T	S	NH_4	NO_3	PO_4	SiO_2	MA	MB
1	2008.05.17	*Gymnodinium aureolum* (PTD)	15.5	31.3	1.3	2.4	0.3	0.6	386	205
2	2008.07.31	Cyanobacteria (CYA)	28.0	13.2	2.6	19.2	0.2	6.2	741,897	148
		Prorocentrum micans (PTD)							88	88
		Phototrophic nanoflagellates (PNF)							7,247	53
3	2008.08.16	*Thalassionema frauenfeldii* (DIA)	27.1	20.6	0.3	1.2	0.2	0.6	933	149
		Phototrophic nanoflagellates (PNF)							7,833	57

		Cyanobacteria (CYA)							257,445	51
2	2010.06.23	*Noctiluca scintillans* (HTD)	24.2	27.4	11.6	UD	1.2	19.8	33	1,166
3	2010.07.29	*Prorocentrum micans* (PTD)	29.1	16.8	6.1	0.02	0.1	3.4	250	250
		Prorocentrum minimum (PTD)							103	13
4	2010.09.30	*Prorocentrum minimum* (PTD)	20.1	12.0	2.3	6.5	0.03	3.4	3,993	519
5	2011.06.17	*Mesodinium rubrum* (MC)	22.6	27.7	3.1	2.6	0.1	13.1	347	392
6	2011.08.22	*Cylindrotheca closterium* (DIA)	26.3	9.9	4.5	38.0	0.1	11.0	59,857	6,584
7	2011.09.24	*Eucampia zodiacus* (DIA)	21.8	27.3	3.3	0.0	0.3	0.3	1,086	272
		Guinardia delicatula (DIA)							108	16
		Chaetoceros denticularis (DIA)							120	13
8	2012.01.04	*Skeletonema costatum* (DIA)	3.0	31.5	1.2	3.6	UD	0.1	11,358	341
		Thalassiosira sp. (DIA)							2,267	274
		Chaetoceros sp. (DIA)							317	35
		Psedonitzschia pungens (DIA)							444	15

T (temperature, ^{o}C), S (salinity), NH_4 (ammonium, μM), NO_3 (nitrite plus nitrate, μM), PO_4 (phosphous, μM), SiO_2 (silicate, μM), MA (maximum abundance, cells ml^{-1}), MB (maximum biomass, ng C ml^{-1}), PTD (phototrophic dinoflagellates), DIA (diatoms), CRY (cryptophyte), RAP (raphidophyte), EUG (euglenophyte), PRA (prasinophyte), MC (mixotrophic ciliate), HTD (heterotrophic dinoflagellates).

Cryptophytes. *Gyrodiniellum shiwhaense*, *Pfiesteria piscicida*, and *Mesodinium rubrum* are known to feed on cryptophytes (Jeong et al. 2006, 2011b; Yih et al. 2004). When the abundances of cryptophyte and co-occurring *P. piscicida* were 213-2,463 cells ml^{-1} and 0.2-488 cells ml^{-1}, respectively, the calculated grazing coefficients of *P. piscicida* grazing on cryptophytes were 0.00-0.77 h^{-1} (Table 1.3). When the abundances of cryptophyte and co-occurring *G. shiwhaense* were 129-2,500 cells ml^{-1} and 0.3-2,929 cells ml^{-1}, respectively, the grazing coefficients of *G. shiwhaense* grazing on cryptophytes were 0.00-0.74 h^{-1} (Table 1.3). Furthermore, when the abundances of cryptophytes and co-occurring *M. rubrum* were 300-26,674 cells ml^{-1} and 14–421 cells ml^{-1}, respectively, the calculated grazing coefficients attributable to *M. rubrum* grazing on co-occurring cryptophytes were 0.00-0.01 h^{-1} (Table 1.3). During the study period, the combined calculated grazing coefficients for *G. shiwhaense*, *P. piscicida*, and *M. rubrum* grazing on co-occurring cryptophyte were 0.00-0.79 h^{-1}.

Eutreptiella gymnastica. *Gyrodinium dominans*, *Protoperidinium bipes*, and naked ciliates (i.e., *Strobilidium* sp. and *Strombidinopsis* sp.) are known to feed on *E. gymnastica* (Jeong et al. 2011a). When the abundances of *E. gymnastica* and co-occurring *P. bipes* were 8-1,171 cells ml^{-1} and 11-233 cells ml^{-1}, respectively, the grazing coefficients of *P. bipes* on *E. gymnastica* were 0.04–0.54 h^{-1} (Table 1.3). When the abundances of *E. gymnastica* and co-occurring *G. dominans*/*Gyrodinium moestrupii* were 8-1,171 cells ml^{-1} and 7-150 cells ml^{-1}, respectively, the grazing coefficients of *G. dominans*/*G. moestrupii* grazing on *E. gymnastica* were 0.01-0.51 h^{-1} (Table 1.3). Furthermore, when the abundances of *E. gymnastica* and co-occurring naked ciliates (≤ 50 μm) were 50-1,171 cells ml^{-1} and 1-87 cells ml^{-1}, respectively, the grazing coefficients of naked ciliates (≤ 50 μm) on *E. gymnastica* were 0.000–0.003 h^{-1} (Table 1.3). During this study, the combined calculated grazing coefficients for *G. dominans*/*G. moestrupii*, *P. bipes*, and naked ciliates grazing on co-occurring *Eutreptiella gymnastica* were 0.00-0.57 h^{-1}.

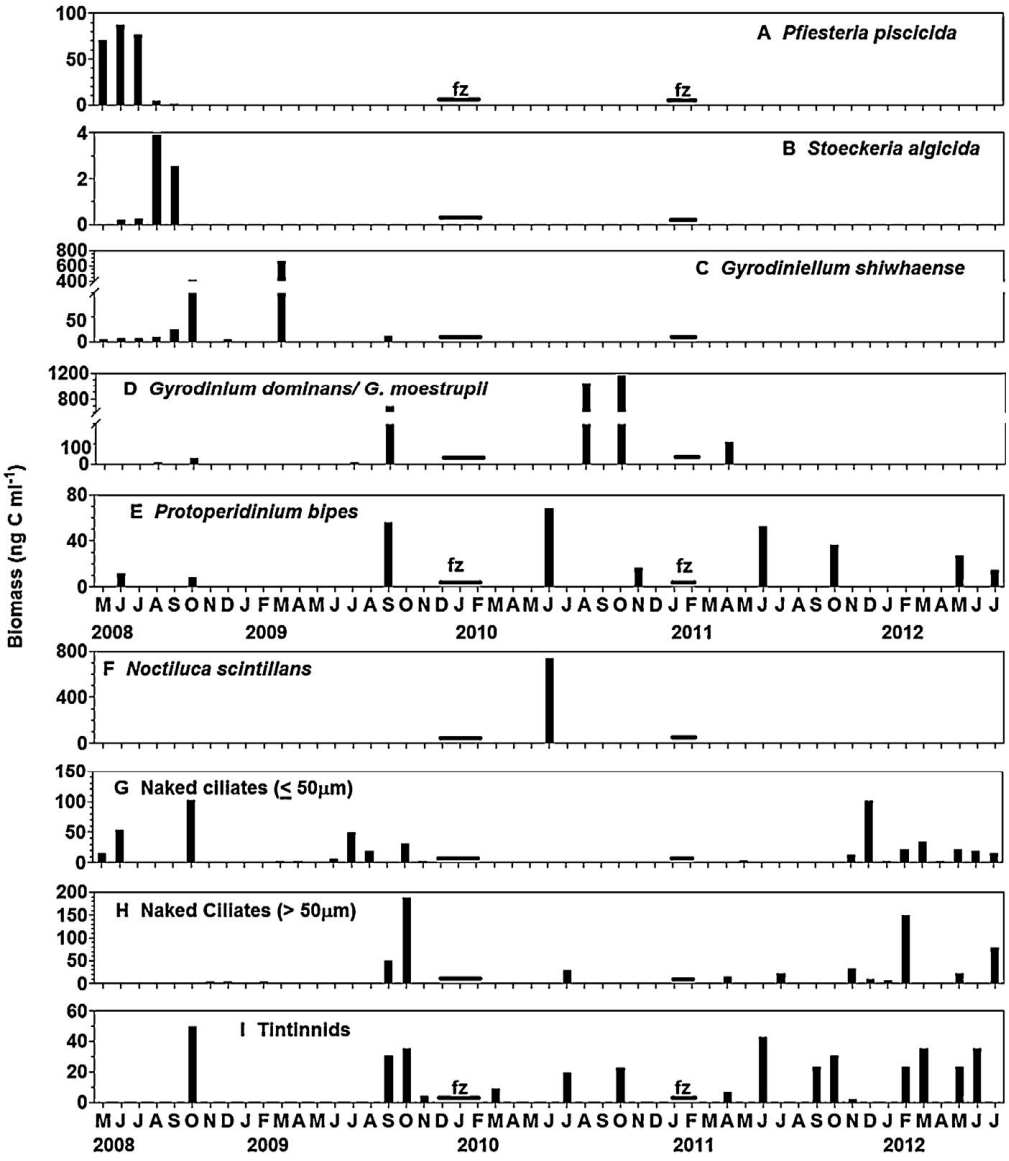

Fig. 2.9 Biomass of heterotrophic protists at St. 1 in Shiwha Bay from May 2008 to July 2012. (**A**) *Pfiesteria piscicida*, (**B**) *Stoeckeria algicida*, (**C**) *Gyrodiniellum shiwhaense*, (**D**) *Gyrodinium dominans*/*G. moestrupii*, (**E**) *Protoperidinium bipes*, (**F**) *Noctiluca scintillans*. (**G**) Naked ciliates (≤50 μm), (**H**) naked ciliates (>50 μm), and (**I**) total tintinnids. fz indicates months when water was frozen.

Table 1.3 Calculated grazing impacts (GI, h^{-1}) of the dominant heterotrophic protists on red-tide species in Shiwha Bay, Korea, from May 2008 to July 2012 and the predators' maximum ingestion rate and K_{IR} (half-saturation) at given prey concentrations in the literature.

Red-tide organisms	Predator	GI	M_{IR}	K_{IR}	Ref
Prorocentrum minimum	*Gyrodinium dominans*	0.05-0.66	1.2	31	Kim and Jeong (2004)
	Strombidiniopsis sp.	0.21	267	82	Jeong et al. (1999a)
Skeletonema costatum	*Protoperidinium bipes*	0.00-0.14	2.9	355	Jeong et al. (2004c)
cryptophytes	*Gyrodiniellum shiwhaense*	0.00-0.74	0.35	30.3	Jeong et al. (2011b)
	Pfiesteria piscicida[b]	0.00-0.77	1.1[a]	450.5	Jeong et al. (2006)
	Mesodinium rubrum	0.00-0.01	0.15		Yih et al. (2004)
Eutreptiella gymnastica	*Gyrodinium dominans*	0.01-0.51	2.7	229	Jeong et al. (2011a)
	Protoperidinium bipes	0.04-0.54	3.3	109	Jeong et al. (2011a)
	Naked ciliates (≤50μm)	0.000-0.003	2.2	722	Jeong et al. (2011a)

M_{IR}: maximum ingestion rate (ng C $predator^{-1}$ d^{-1}). K_{IR}: prey concentration sustaining 1/2 M_{IR}.

[a] Given prey concentrations in the literature. [b] M_{IR}: linear equation, IR=0.00031(x)+0.0083.

The calculated grazing coefficients attributable to heterotrophic protistan grazers feeding on the other red-tide causative species were negligible.

2.5.8 Correlation coefficients at all three stations

I calculated correlation coefficients among physical, chemical, and biological properties by pooling data obtained from all 3 stations (Tables 1.4 and 1.5).

Precipitation summed for 2 weeks was significantly and positively correlated with water temperature, but negatively correlated with salinity (Table 1.4). Salinity was significantly and negatively correlated with the concentrations of NO_3, PO_4, and SiO_2, and the concentrations of PO_4 and SiO_2 were significantly and positively correlated with temperature. pH was significantly negatively correlated with salinity.

The biomass of *Heterocapsa rotundata* was significantly and negatively correlated with water temperature (Table 1.5A). In addition, the biomass of *Skeletonema costatum* and *Thalassiosira* spp. were significantly negatively correlated with salinity and significantly positively correlated with concentrations of NO_3 and SiO_2 (Table 1.5A). *Prorocentrum minimum*, *Prorocentrum micans*, *P. triestinum*, and *Noctiluca scintillans* biomass were significantly positively correlated with pH. However, the biomass of *Mesodinium rubrum* and *N. scintillans* were significantly negatively correlated with salinity (Table 1.5A).

The biomass of phototrophic nanoflagellates (PNFs), picoeukaryotes, cyanobacteria, and heterotrophic bacteria were significantly positively correlated with water temperature, unlike the biomass of PNFs, picoeukaryotes, cyanobacteria, and heterotrophic bacteria which was significantly and negatively correlated with salinity (Table 1.5B). Biomass of picoeukaryotes and heterotrophic bacteria were significantly positively correlated with the concentration of PO_4 (Table 1.5B), and the biomass of PNFs, cyanobacteria and heterotrophic bacteria was significantly positively correlated with pH.

The biomass of *Protoperidinium bipes* and heterotrophic nanoflagellates (HNFs) was significantly positively correlated with water temperature and precipitation, but significantly negatively correlated with salinity (Table 1.5C). Biomass of *Noctiluca scintillans* was significantly positively correlated with pH, but significantly negatively correlated with salinity (Table 1.5C).

2.6 Discussion

2.6.1 Physical, chemical, and biological properties in Shiwha Bay

During this study, the concentrations of NO_3 and SiO_2 at all 3 stations were significantly negatively correlated with salinity. This suggests that freshwater drainage into Shiwha Bay after rainfall may increase the concentrations of NO_3 and SiO_2. In addition, the biomass of dominant diatoms was significantly positively correlated with concentrations of NO_3 and SiO_2. This suggests that rain may increase the biomass of dominant diatoms in Shiwha Bay by delivering NO_3 and SiO_2 from land surrounding the bay. However, the PO_4 concentration was not correlated with salinity at any site, but was weaker correlated with salinity when the data from all 3 stations were pooled. Thus, rain may not always increase PO_4 concentration.

The biomass of dominant phototrophic dinoflagellates was significantly positively correlated with pH, which suggests that CO_2 uptake by dominant phototrophic dinoflagellates may increase pH during their red tides. Thus, blooms of these dominant phototrophic dinoflagellates may play an important role in relaxing ocean acidification.

2.6.2 Trends in frequency and causative species of red-tide events in Shiwha Bay

During the study, 33 red tides were observed in a total of 46 sampling times (i.e., in 72% of sampling events). Clearly, red tides are common in Shiwha Bay, and their frequency of occurrence is increasing overall. Nutrient concentrations did not

increase markedly after construction of a huge tidal power plant. The red-tide causative groups in Shiwha Bay changed from phototrophic dinoflagellates and picoeukaryotes to diatoms and/or cryptophytes after construction of the tidal power plant in the middle of a dike in 2011, which resulted in the exchange of water between the inside and outside of the dike.

Ten huge turbines of the tidal power plant are likely to generate turbulent waters. However, it is difficult to quantify turbulence intensity of the waters. Theoretically, all the waters inside the Shiwha Bay pass the turbines at the speed of 12-13 m s^{-1} every two days and become turbulent flow. The rates of turbulent energy dissipation (ε) in tidal a front and a tidal estuary (Severn) have been reported to be 0.1 cm^{-2} s^{-3} and 0.02-0.08 cm^{-2} s^{-3}, respectively (Estrada and Berdalet 1998; Kiørboe and Saiz 1995; Reynolds 1994). The dinoflagellates *Akashiwo sanguinea*, *Cochlodinium polykrikoides*, and *Lingulodinium polyedrum* had negative growth at the $\varepsilon > 0.05$ cm^{-2} s^{-3}, while the diatoms *Chaetoceros* and *Psedonitzshia* had positive growth at similar ε (Arin et al. 2002; Kim 2001; Thomas et al. 1995). Therefore, an increase in turbulence may have been responsible for the change in the red-tide causative species from phototrophic dinoflagellates to diatoms. In addition, the smaller flagellates are known to be more tolerant to turbulence (Arin et al. 2002; Smayda 2002; Thomas and Gibson 1990). Thus, smaller cryptophytes may have come to prevail over larger phototrophic dinoflagellates under the more turbulent conditions in Shiwha Bay when the tidal power plant became operational. The growth rates of diatoms are much greater than those of phototrophic dinoflagellates of similar size (Banse 1982). For example, the diatom *Skeletonema costatum* is able to divide 2-4 times per day, but *Prorocentrum minimum* only once per day. Thus, if red-tide causative species change from slow-growing phototrophic dinoflagellates to fast-growing diatoms, red tides are likely to occur more frequently.

Table 1.4 Correlations between physical and chemical properties in Shiwha Bay, Korea, from May 2008 to July 2012.

Component	T	P	S	pH	NH_4	NO_3	PO_4	SiO_2
T								
P	0.523**							
S	-0.591**	-0.749**						
pH		0.301**	-0.472**					
NH_4								
NO_3		0.417**	-0.679**					
PO_4	0.338**		-0.198*					
SiO_2	0.187*	0.378**	-0.558**			0.790**		

*p<0.05, **p<0.01.

T: temperature, P: precipitation, S: salinity, NH_4 (ammonium,), NO_3 (nitrite plus nitrate), PO_4 (phosphous), SiO_2 (silicate).

Table 1.5 Correlations between the physical and chemical properties and the biomass of protists and bacteria in Shiwha Bay, Korea, from May 2008 to July 2012.

A. Physical and chemical properties and the biomass of red-tide causative species

	Ht	Hr	Pmn	Pmc	Pt	Sc	Ts	Eg	Mr	Ns
T		-0.459*								
P										
S						-0.477**	-0.451*		-0.554*	-0.784*
pH			0.448*	0.760**	0.649*					0.867*
NH_4							0.730**		0.585*	
NO_3						0.763**	0.747**			
PO_4										
SiO_2	0.490*					0.778**	0.550**	0.655**		

B. Physical and chemical properties and the biomass of small protists and bacteria

	PNF	PE	CYA	HB
T	0.309**	0.250**	0.422**	0.493**
P	0.218*		0.517**	0.349**
S	-0.311**	-0.210*	-0.417**	-0.358**
pH	0.371**		0.273**	0.198*
NH_4				

NO_3			
PO_4	0.197*		0.208*
SiO_2			

C. Physical and chemical properties and the biomass of heterotrophic dinoflagellate species

	Gs	Pb	Ns	HNF
T		0.429*		0.280**
P		0.414*		0.444**
S		-0.464*	-0.784*	-0.248**
pH			0.867*	
NH_4	0.758*			
NO_3				
PO_4				0.189*
SiO_2				

*p<0.05, **p<0.01

T: temperature, P: precipitation, S: salinity, NH_4: ammonium, NO_3: nitrate plus nitrite, PO_4: phosphate, SiO_2: silicate.

Ht: *Heterocapsa triquetra*, Hr: *Heterocapsa rotundata*, Pmn: *Prorocentrum minimum*, Pmc: *Prorocentrum micans*, Pt: *Prorocentrum triestinum*, Sc: *Skeletonema costatum*, Ts: *Thalassiosira* spp., Eg: *Eutreptiella gymnastica*, Mr: *Mesodinium rubrum*, Ns: *Noctiluca scintillans*, PNF: phototrophic nanoflagellate, PE: picoeukaryote, CYA: cyanobacteria, HB: heterotrophic bacteria, Gs: *Gyrodiniellum shiwhaense*, Pb: *Protoperidinium bipes*, HNF: heterotrophic nanoflagellates.

In addition, *Gymnodinium aureolum*, *Paragymnodinium shiwhaense*, *Karlodinium veneficum*, *P. minimum*, *Prorocentrum micans*, and *Heterocapsa triquetra* formed red tides before the tidal power plant was constructed in 2011, but not after. However, *Heterocapsa rotundata* formed red tides in 2012. This suggests that *H. rotundata* may possess a tolerance against highly turbulent conditions that allows it to continue to form red tides in Shiwha Bay.

2.6.3 Effects of physical and chemical factors on frequency and causative species of red-tide events

During the study, 7 phototrophic dinoflagellate taxa (*Gymnodinium aureolum*, *Karlodinium veneficum*, *Heterocapsa triquetra*, *Heterocapsa rotundata*, *Paragymnodinium shiwhaense*, *Prorocentrum micans*, and *Prorocentrum minimum*), 10 diatom taxa (*Chaetoceros* spp., *Cyclotella* sp., *Cylindrotheca closterium*, *Skeletonema costatum*, and *Thalassiosira* spp.), one raphidophyte (*Heterosigma akashiwo*), one euglenophyte (*Eutreptiella gymnastica*), one prasinophyte (*Pyramimonas disomata*), and one mixotrophic ciliate (*Mesodinium rubrum*) were primarily responsible for the formation of red tides. Cryptophytes were also the primary organisms forming red tides in several instances.

During this study, *Prorocentrum micans* and *Skeletonema costatum* red tides occurred over a wide range of temperature and salinity (i.e., ranges >20 °C and >20, respectively), while *Gymnodinium aureolum*, *Heterocapsa rotundata*, and *Cyclotella* sp. in narrow ranges of temperature and salinity (i.e., <5 °C and <5, respectively). However, cryptophytes caused red tides over a wide range of temperature and a narrow range of salinity (i.e., >20 °C and <5, respectively)., while *Heterocapsa triquetra*, *P. micans*, and *Thalassiosira* spp. caused red tides over a wide range of temperature and moderate range of salinity (i.e., >20 °C and ~10, respectively). Thus, the effects of temperature and salinity in Shiwha Bay are likely to be critical to some red-tide species, but negligible to others.

Prorocentrum minimum, *Heterocapsa triquetra*, *P. micans*, *Skeletonema costatum*, and *Cylindrotheca closterium* red tides occurred over a wide range of NO_3 concentration (i.e., >20 μM), and *Gymnodinium aureolum* and *Heterocapsa rotundata* red tides over a narrow range (i.e., <3 μM), and *P. minimum*, *S. costatum*, and *Mesodinium rubrum* over a wide range of PO_4 concentration (i.e., >1.0 μM), while *G. aureolum*, *H. triquetra*, and *Eutreptiella gymnastica* red tides occurred over narrow ranges (i.e., <0.3 μM). Therefore, the effects of NO_3 and PO_4 concentrations in Shiwha Bay are likely to be critical to some red-tide species, but negligible to others.

Phototrophic dinoflagellates and diatoms can co-occur in most coastal environments (Allen 1949; Yoo et al. 2009). For a long time, the primary interaction between these two functional groups has been thought to be competition for nutrients (Smayda 1997). In general, diatoms have been known to grow faster than similarly sized PTDs when nutrient concentrations are high (Banse 1982). In addition, when nutrient uptake (U) is considered, values of $K_{1/2}$ (the nutrient concentration sustaining $1/2U_{max}$) for diatoms are lower than those for PTDs (Table 1.6); thus, diatoms are able to grow faster than PTDs as nutrient concentrations increase (Smayda 1997). However, PTDs are known to feed on diverse prey, such as bacteria, diatoms, other PTDs, and heterotrophic protists (e.g., Burkholder et al. 2008; Jeong et al. 2005c, 2010b, 2010c, 2012; Yoo et al. 2009, 2010). Thus, predominance between PTDs and diatoms can be affected by feeding ability as well as nutrient concentrations. Therefore, exploration of the mechanisms responsible for the outbreak of a red tide associated with a certain red-tide taxa or species should be conducted with consideration of both $K_{1/2}$ and the phototrophic ability of the organism.

Prorocentrum minimum formed red tides in all seasons when water temperatures were 3.2-26.9 °C. *P. minimum* also formed red tides in both summer and winter in Masan Bay, Korea (Jeong et al. 2013a). Thus, this dinoflagellate is

likely to exhibit tolerance of extreme hot and cold temperatures. Concentrations of NO_3 (0.6-34.5 μM) during its red tides were higher than the reported values for $K_{1/2}$ (1.4-20.5 μM), but concentrations of PO_4 (UD-1.5 μM) during red tides were comparable to or lower than the reported values for $K_{1/2}$ (1.4-2.0 μM) (Table 1.6). In addition, the biomass of *P. minimum* was not correlated with the concentration of any inorganic nutrient. *P. minimum* has been known to feed on bacteria, small flagellates, and diatoms (Jeong et al. 2005d, 2010b; Seong et al. 2006; Stoecker et al. 1997; Yoo et al. 2009). Thus, *P. minimum* may acquire phosphorus from its prey.

Heterocapsa triquetra formed red tides in winter and spring when water temperatures were 3.7-20.6 °C; demonstrating that this dinoflagellate can form red tides over a wide range of water temperature. The concentrations of NO_3 (2.7-44.1 μM) during red tides were relatively high, while those of PO_4 (0.04-0.6 μM) were very low. I could not investigate the effects of these inorganic nutrients on the growth of *H. triquetra* because $K_{1/2}$ values were not available. During the red tides, *Heterocapsa rotundata* and *Prorocentrum minimum* were abundant (Table 1.2). *H. triquetra* is known to feed on *H. rotundata* and *P. minimum* (Jeong et al. 2005d); therefore, *H. triquetra* may form and/or maintain its red tide by feeding on these co-occurring dinoflagellates.

Heterosigma akashiwo formed a red tide once in summer 2012, when water temperature was 24.1 °C. An optimal temperature for growth of a Korean strain of *H. akashiwo* is 23-25.4 °C (Jeong et al. 2013b). To date, *H. akashiwo* red tides have occurred primarily at latitudes lower than Shiwha Bay (Jeong et al. 2013b), but warming of local waters may have provided a chance for this species to form a red tide in Shiwha Bay. It is worthwhile exploring red tides dominated by *H. akashiwo* in Shiwha Bay because it is known to be harmful to marine organisms (Black et al. 1991; Clough and Strom 2005; Honjo 1993; Imai et al. 1996; MacKenzie 1991). The concentration of NO_3 (6.6 μM) during the red tide was higher than the reported values for $K_{1/2}$ (1.5-2.5 μM), but concentration of PO_4 (0.3 μM) during the red tide

was lower than the reported values for $K_{1/2}$ (1.0-2.0 μM) (Table 1.6). During this red tide, heterotrophic bacteria and cyanobacteria were abundant (Fig. 2.6). *H. akashiwo* is known to feed on bacteria and *Synechococcus* (Jeong 2011; Jeong et al. 2010a; Seong et al. 2006). Thus, water temperature, heterotrophic bacteria, and *Synechococcus* may affect outbreak and maintenance of its red tides.

Mesodinium rubrum formed red tides in summer and autumn, when water temperatures were 19.9-26.4 and 22.5 °C, respectively. The concentration of NO_3 (UD-16.1 μM) during red tides covered a wide range, but the concentration of PO_4 (0.01-1.1 μM) was low. I could not evaluate the effects of these inorganic nutrients on growth of *M. rubrum* because $K_{1/2}$ values were not available. However, the biomass of *M. ruburm* exhibited significant positive correlations with the biomass of cryptophytes. *M. ruburm* is known to feed on cryptophytes (Yih et al. 2004); therefore, it may form and/or maintain red tides by feeding on cryptophytes, even when nutrient concentrations are low.

Skeletonema costatum formed red tides in summer and winter after the hydraulic turbine of the tidal power plant became operational. During red tides, water temperatures were 2.9-27.0 °C. The concentrations of NH_4 (1.2-34.3 μM), NO_3 (3.6-135.2 μM), and SiO_2 (0.1-135.9 μM) during red tides exceeded reported $K_{1/2}$ values (0.8-3.6 μM, 0.4-0.5 μM, and 0.03-0.05 μM) (Table 1.6). Thus, *S. costatum* may form its red tides by utilizing these inorganic nutrients. In addition, *S. costatum* is eaten by a diverse range of PTDs. After the construction of the tidal power plant, the abundance of PTDs decreased rapidly, and the low abundance of PTDs may have enabled this diatom to form red tides easily.

2.6.4 Grazing impact

In Shiwha Bay during this study, the protistan grazer exhibiting the highest grazing coefficient differed for almost every red-tide organism. For example, *Pfiesteria piscicida* and *Gyrodiniellum shiwhaense* exhibited the highest grazing

impact on populations of cryptophytes; *Gyrodinium dominans*/*Gyrodinium moestrupii* on *P. minimum* and *Eutreptiella gymnastica*, and *Protoperidinium bipes* on *E. gymnastica*. Therefore, certain protistan grazers may be specialized to control populations of specific red-tide species in Shiwha Bay.

The maximum grazing coefficients of *Pfiesteria piscicida*, *Gyrodiniellum shiwhaense*, *Gyrodinium dominans*/*Gyrodinium moestrupii*, and *Protoperidinium bipes* for cryptophytes, *Prorocentrum minimum*, and *S. costatum*, respectively, were 0.14-0.77 h^{-1} (i.e., 13–54% of their prey populations were consumed in 1 h). Therefore, heterotrophic protistan grazers in Shiwha Bay may sometimes have considerable grazing impact on the populations of co-occurring red-tide organisms.

The maximum grazing impact of heterotrophic protistan grazers on *Prorocentrum minimum* in Shiwha Bay (0.66 h^{-1}) was greater than that on *Skeletonema costatum* (0.14 h^{-1}). Therefore, heterotrophic protistan grazers may control dinoflagellate red tides more effectively than diatom red tides.

2.7 Conclusion

The results of the present study can be summarized as follows. (1) Red tides in Shiwha Bay between 2008 and 2012 occurred in 33 of 46 (i.e., 72%) sampling events. Clearly, red tides are a common occurrence in Shiwha Bay. (2) The causative species of red tides in Shiwha Bay switched from phototrophic dinoflagellates to diatoms and/or cryptophytes after a huge tidal power plant was constructed in the middle of the dike in 2011, allowing waters inside and outside the dike to be exchanged. An increase in turbulence may have been responsible for the change in red-tide causative species from phototrophic dinoflagellates to diatoms. (3) Inorganic nitrogen concentrations during red tides were higher than $K_{1/2}$ values for the red-tide causative species, but inorganic phosphorus concentrations were lower than $K_{1/2}$ values. Thus, some PTDs and flagellates may form red tides by feeding on prey. (4) The protistan grazer exhibiting the highest grazing coefficient

was different for almost every red-tide organism in Shiwha Bay during the study period. Therefore, certain protistan grazers may be specialized to control populations of specific redtide species in Shiwha Bay. In addition, the maximum grazing coefficients of *Pfiesteria piscicida*, *Gyrodiniellum shiwhaense*, *Gyrodinium dominans*/*Gyrodinium moestrupii*, and *Protoperidinium bipes* for cryptophytes, *Prorocentrum minimum*, and *Skeletonema costatum*, respectively, were considerable; thus, heterotrophic protistan grazers in Shiwha Bay may sometimes exert considerable grazing impact on the populations of co-occurring red-tide organisms.

Table 1.6 Half-saturation constants (Ks, μM) for uptake of ammonium (NH_4), nitrate (NO_3), phosphate (PO_4), and silicate (SiO_2) by selected red-tide organisms in Shiwha Bay, Korea, from May 2008 to July 2012.

Red-tide organisms	NH_4	NO_3	PO_4	SiO_2	Ref.
Prorocentrum minimum (MTD)			2.0		Cembella et al. (1984)
		20.5	1.4		Hu et al. (2011)
	2.4-9.8	1.4-7.8			Fan et al. (2003)
		5			Lomas and Glibert (2000)
Heterocapsa triquetra (MTD)			3.1		Doremus (1982)
Heterosigma akashiwo (RAP)	2.0-2.3	2.0-2.5	1.0-2.0		Tomas (1979)
	1.44	1.47			Herndon and Cochlan (2007)
Skeletonema costatum (DIA)	0.8-3.6	0.4-0.5			Eppley et al. (1969)
	0.04			0.05	Conway and Harrison (1977)
	0.03			0.03	Conway et al. (1976)
				0.03	Paasche (1973)

MTD: mixotrophic dinoflagellates, RAP: raphidophyte, DIA: diatoms.

Table 1.7 Correlations between physical and chemical properties in Shiwha Bay, Korea from May 2008 to July 2012.

A. Station 1

	T	P	S	pH	NH_4	NO_3	PO_4	SiO_2
T								
P	0.500*							
S	-0.511**	-0.714**						
pH								
NH_4								
NO_3		0.364*	-0.706**		0.317*			
PO_4	0.467**							
SiO_2		0.376*	-0.574**			0.708**		

B. Station 2

	T	P	S	pH	NH_4	NO_3	PO_4	SiO_2
T								
P	0.539**							
S	-0.639**	-0.797**						
pH		0.446**	-0.539**					
NH_4								
NO_3		0.499**	-0.662**					
PO_4						0.408**		
SiO_2		0.422**	-0.564**			0.890**	0.491**	

C. Station 3

	T	P	S	pH	NH_4	NO_3	PO_4	SiO_2
T								
P	0.530**							
S	-0.638**	-0.768**						
pH	0.309*	0.431**	-0.571**					
NH_4								
NO_3		0.465**	-0.667**					
PO_4								

SiO_2	0.346*	-0.502**	0.787**

*p<0.05, **p<0.01

T: temperature, P: precipitation, S: salinity, NH_4 (ammonium,), NO_3 (nitrite plus nitrate), PO_4 (phosphous), SiO_2 (silicate).

Chapter 3: Taxonomy of the new planktonic mixotrophic dinoflagellate *Paragymnodinium shiwhaense* from Korean waters

3.1 Abstract

The mixotrophic dinoflagellate *Paragymnodinium shiwhaense* n. gen., n. sp. is described from living cells and from cells prepared by light, scanning electron, and transmission electron microscopy. In addition, sequences of the small subunit (SSU) and large subunit (LSU) rDNA and photosynthetic pigments are reported. The episome is conical, while the hyposome is hemispherical. Cells are covered with polygonal amphiesmal vesicles arranged in 16 rows and containing a very thin plate-like component. There is neither an apical groove nor apical line of narrow plates. Instead, there is a sulcal extension-like furrow. The cingulum is displaced by 0.2-0.3 x cell length. Cell length and width of live cells fed *Amphidinium carterae* were 8.4-19.3 and 6.1-16.0 μm, respectively. *Paragymnodinium shiwhaense* does not have a nuclear envelope chamber nor a nuclear fibrous connective (NFC). Cells contain chloroplasts, nematocysts, trichocysts, and peduncle, though eyespots, pyrenoids, and pusules are absent. The main accessory pigment is peridinin. The sequence of the SSU rDNA of this dinoflagellate (GenBank AM408889) is 4% different from that of *Gymnodinium aureolum*, *Lepidodinium viride*, and *Gymnodinium catenatum*, the three closest species, while the LSU rDNA was 17-18% different from that of *G. catenatum*, *Lepidodinium chlorophorum*, and *Gymnodinium nolleri*. The phylogenetic trees show that this dinoflagellate belongs within the *Gymnodinium* sensu stricto clade. However, in contrast to *Gymnodinium* spp., cells lack nuclear envelope chambers, NFC, and an apical groove. Unlike *Polykrikos* spp., which have a taeniocyst-nematocyst complex, *P. shiwhaense* has nematocysts without taeniocysts. In addition, *P. shiwhaense* does not have ocelloids in contrast to *Warnowia* spp. and *Nematodinium* spp. Therefore, based on

morphological and molecular analyses, I suggest that this taxon is a new species, also within a new genus.

3.2 Key words

LSU, nematocyst, peduncle, dinoflagellate taxonomy, SSU

3.3 Introduction

Phototrophic dinoflagellates are ubiquitous protists in marine environments and have sometimes formed red tides or harmful algal blooms (Jeong 1995). Interest in phototrophic dinoflagellates is increasing because (1) many phototrophic dinoflagellates that had been thought to be exclusively autotrophic have been revealed to be mixotrophic and (2) they have been revealed to play diverse ecological roles in marine planktonic communities (Carvalho et al. 2008; Stoecker et al. 2006): Mixotrophic dinoflagellates are now known to prey upon on diverse taxa (Bockstahler and Coats 1993; Jeong et al. 2005c, 2005d; Li et al. 2000; Seong et al. 2006; Smalley et al. 1999; Yoo et al. 2009). The phototrophic dinoflagellates are in turn important prey for diverse predators (Jacobson and Anderson 1986; Jeong et al. 2005e; Kamiyama and Matsuyama 2005; Stoecker and Sanders 1985). Recent work on dinoflagellate taxonomy has resulted in the description of several novel phototrophic dinoflagellate genera and species. Our correct understanding of the structure and functioning of marine ecosystems makes the correct identification and description of their biodiversity, including novel phototrophic dinoflagellates, and the exploration of their role in marine food webs essential research.

Recently, several new phototrophic dinoflagellate species belonging to gymnodinioid and woloszynskioid genera, such as *Baldinia, Biecheleria, Borghiella, Cochlodinium, Esoptrodinium*, *Gymnodinium, Jadwigia, Karenia, Karlodinium, Lepidodinium, Takayama,* and *Tovellia* and have been established (e.g. Bergholtz et al. 2005; Botes et al. 2003; Calado et al. 2006; Chang and Ryan 2004; de Salas et al. 2004a, 2004b, 2005, 2008; Fariman et al. 2007; Hansen et al. 2007a, 2007b;

Haywood et al. 2004; Iwataki et al. 2007; Kremp et al. 2005; Lindberg et al. 2005; Moestrup et al. 2006, 2008; Yang et al. 2001). While gymnodinioid genera are in general unarmoured, woloszynskioids have hexagonal or pentagonal amphisiemal plates arranged in rows.

Recently, I found a new mixotrophic dinoflagellate in Shiwha Bay, Korea, a highly eutrophic bay. This species has an amphiesmal plate pattern similar to woloszynskioid dinoflagellates, though it does not have the Apical Line of narrow Plates (ALP), the Pair of Elongate amphiesmal Vesicles (PEV), or apical groove and also does not have eyespots. Also, this dinoflagellate has none of the 3 characters that define *Gymnodinium* [i.e. nuclear envelope chambers, horseshoe-like apical groove, and a nuclear fibrous connective (NFC)]. Surprisingly, it instead has both chloroplasts and nematocysts. Only very few dinoflagellates (e.g. *Polykrikos lebourae*) have been reported to have both of these organelles (Hoppenrath and Leander 2007a). Therefore, nematocysts may be an important character for the taxonomy of the phototrophic dinoflagellates. I present here a description of the morphology of the planktonic mixotrophic dinoflagellate *Paragymnodinium shiwhaense* n. gen. n. sp., observed using light microscope, scanning electron microscope (SEM), and transmission electron microscopy (TEM) and report its small subunit (SSU) rDNA, internal transcribed spacers (ITSs, including ITS 1, 5.8S rDNA, and ITS2), and large subunit (LSU) rDNA sequences from cultured cells. Finally, I provide data on its pigment profile.

3.4 Materials and methods

3.4.1 Collection and culturing of *Paragymnodinium shiwhaense*

Plankton samples collected with water samplers were taken from the waters in Shiwha Bay, Korea (37°18’ N, 126° 36’E), during May 2006 when the water temperature and salinity were 18.8 ºC and 30.4, respectively. The samples were filtered gently through a 154-μm Nitex mesh and placed in 6-well tissue culture

plates. A clonal culture of *P. shiwhaense* was established by two serial single cell isolations. The mixotrophic dinoflagellate *Amphidinium carterae* was provided as prey at 5,000-8,000 cells ml^{-1}. As the concentration of *P. shiwhaense* increased, cells were subsequently transferred to 32, 270, and 500-ml polycarbonate (PC) bottles of fresh *A. carterae*. The bottles were filled to capacity with filtered seawater, capped, and placed on a rotating wheel at 0.9 rpm at 20 ^{o}C under an illumination of 20 μE m^{-2} s^{-1} of cool white fluorescent light on a 14:10 h light–dark cycle. Once dense cultures of *P. shiwhaense* were obtained, they were transferred daily to 500-ml PC bottles of fresh *A. carterae* at ~20,000 cells ml^{-1} or the cryptophyte *Rhodomonas salina* as prey at ~15,000-20,000 cells ml^{-1}

3.4.2 Morphology of *Paragymnodinium shiwhaense*

The morphology of live cells and cells preserved in 4% (v/v) glutaraldehyde were examined with a compound microscope. For SEM, a 20-ml aliquot of a dense culture of *P. shiwhaense* was fixed with osmic tetroxide (final concentration = 2%) in seawater for 1.5 h. The fixed cells were collected on a polycarbonate membrane filter (pore size = 5 μm) without additional pressure and rinsed 3 times with distilled waters to remove the salt. They were dehydrated in an ethanol series, and finally dried using a critical point dryer (BAL-TEC, CPD 300, Balzers, Liechtenstein, Germany). The dried filters were mounted on a stub and coated with gold-palladium. Cells were viewed with a FE-SEM (S-4800, HORIBA: EX-250, HITACHI, Hitachinaka, Japan) and SEM (JSM-840A, SEM JEOL Ltd., Tokyo, Japan) and photographed using a digital camera. I measured cell length and cell width of live vegetative flagellated cells, some fed *A. carterae* and some starved for 2d, using an image analysis system on images collected with a compound microscope (Image-Pro Plus 4.5, Media Cybernetics**,** Silver Spring, MD 20910**,** USA). For TEM, cells from a dense culture were transferred to a 10-ml tube and fixed in 2.5% glutaraldehyde (final concentrations) in culture medium. One and half to 2 h later, all the contents of the tube were placed in a 10-ml centrifuge tube and concentrated at 1,610 g for 10 min in a Vision Centrifuge VS-5500 (Vision Scientific Company.,

Bucheon, Korea). A pellet from the tube was then transferred into a 1.5-ml tube and rinsed in 0.2 M sodium cacodylate buffer at pH 7.4. After several rinses in 0.2 M sodium cacodylate buffer, the cells were postfixed in 1% (final concentrations) osmic tetroxide in deionized water for 90 min. The pellet was then embedded in agar. Dehydration was accomplished using a graded ethanol series (50, 60, 70, 80, 90, and 100% ethanol, followed by two 100% ethanol steps). The material was embedded in Spurr's low-viscosity resin (Spurr 1969). Sections were obtained with a RMC MT-XL ultramicrotome (Boeckeler Instruments Inc., Tucson, AZ, USA) and stained with 3% (final concentrations) aqueous uranyl acetate followed by lead citrate. The sections were viewed with a JEOL-1010 transmission electron microscope (JEOL Ltd., Tokyo, Japan).

3.4.3 DNA extraction, PCR amplification, and sequencing

Approximately 20 ml of a dense culture of *P. shiwhaense* was concentrated by centrifugation (2190 *g*) for 5-10 min at room temperature, and the pellet was transferred to a 1.5-ml tube and resuspended in tris-ethylenediaminetetraacetic acid (TE) buffer. Sodium dodecyl sulfate (final conc. 0.5% [w/v]) and proteinase K (final conc. 0.1 mg ml^{-1}) were added, and the mixture was incubated at 37 °C for 1 h. DNA was extracted by adding 800 μl of phenol:chloroform:isoamyl alcohol (25:24:1) to the incubated material and the residual phenol was removed by adding 700 μl of chloroform:isoamyl alcohol (24:1). Extracted DNA was precipitated by adding isopropyl alcohol and washed in cold 70% ethanol. DNA yield was quantified by a spectrophotometer. The extracted DNA was divided into two PCR tubes, and two independent PCR reactions were conducted. The small subunit (SSU) rDNA was amplified using eukaryotic primers (forward: 5´-AAC CTG GTT GAT CCT GCC AGT-3´; reverse: 5´-TGA TCC TTC TGC AGG TTC ACC TAC-3´) and approximately 1,000 bp large subunit (LSU) rDNA was amplified using forward primer Dino 1500F (5'-GTT GTT GCG GTT AAA AAG C-3') and reverse primer LSUB (5'-ACG AAC GAT TTG CAC GTC AG-3'), following Medlin et al.

(1988). The 50- μl PCRs were mixed with the following reactants: 1X PCR buffer with 1.5 mM $MgCl_2$, 0.2 mM dNTP, 0.5 μM each primer, 5U of Taq DNA polymerase (Bioneer, Daejeon, Korea), and 200 ng template DNA. The PCR reactions were performed under the following conditions: 1 initial denaturating step of 3 min at 94 °C, 40 cycles of 45 sec at 95 °C, 1 min at 55 °C, and 3 min at 72 °C in series, and then 1 extension at 72 °C for 5min in a GeneAmp PCR System 2700 (Perkin-Elmer, Boston, USA). PCR products were cloned into the pCR®2.1-TOPO® vector using the TA Cloning® Kit (Invitrogen, Carlsbad, USA). The cloned material was incubated in liquid LB media at 37 °C overnight. Plasmids were extracted using the AccuPrep® Plasmid Extraction Kit (Bioneer, Daejeon, Korea). The presence of inserts in the plasmids was ascertained by adding *Eco*RI restriction endonuclease (Promega, Madison, USA) into the extracted plasmids. To determine the sequence of internal fragments inside the inserts, the reverse primer Euk1209R (5′-GGG CAT CAC AGA CCT G-3′) and ITSR2 (5′-TCC CTG TTC ATT CGC CAT TA-3′) were used. Sequencing the SSU rDNA and LSU rDNA was performed using an ABI PRISM® 3700 DNA Analyzer (Applied Biosystems, Foster City, USA). All sequences were aligned using the ContigExpress alignment program (InforMax, Frederick, USA).

3.4.4 Sequence availability and phylogenetic analysis

The sequence for the nuclear SSU rDNA were aligned in the Genetic Data Environment (GDE 2.2) program (Smith et al. 1994) by eye, with the alignment based on secondary structure using the nuclear SSU rDNA of *Karenia brevis* (C.C. Davis) G. Hansen & Ø. Moestrup (Wuyts et al. 2001) as a guide. The entire conserved areas of the nuclear SSU rDNA genes were readily alignable across taxa and were used for phylogenetic analyses (Table 2.1). The sequence for the nuclear LSU rDNA was also aligned manually in the Genetic Data Environment (GDE 2.2) program (Table 2.1). For Bayesian analyses, I performed a likelihood ratio test using MODELTEST 3.7 (Posada and Crandall 1998) to determine the best available

model for the SSU and LSU rDNA data. The selected models were a TrN+I+ Γ model with a gamma correction for among-site rate variation (SSU; α=0.6001, LSU; α=0.7368) and invariant sites (SSU; I = 0.3608, LSU; I=0.1766). Bayesian analyses were run using an MrBayes 3.1.2 version (Huelsenbeck and Ronquist 2001). Four independent Markov chain Monte Carlo simulations were run simultaneously for 2,000,000 generations and trees were sampled every 1,000 generations and the first 800 trees were deleted to ensure that the likelihood had reached convergence. A majority-rule consensus tree was created from the remaining 1,201 trees in order to examine the posterior probabilities of each clade.

The Maximum likelihood phylogenetic analyses were done using the RAxML 7.0.4 program (Stamatakis 2006) with the general time reversible (GTR) + Γ model. I used 200 independent tree inferences using -# option of the program to identify the best tree. Bootstrap values (MLBS) were calculated using 1,000 replicates using the same substitution model.

3.4.5 Pigment analysis

I analyzed pigments of *Paragymnodinium shiwhaense* satiated with the cryptophyte *Rhodomonas salina* and then starved for 2 weeks and *Rhodomonas salina* only (control) using HPLC (LC-10A system, Shimadzu Co., Kyoto, Japan) as in Zapata et al. (2000). A dense culture of 8,000-10,000 cells ml^{-1} of *P. shiwhaense* growing mixotrophically on *R. salina* in f/2 media and under 14:10 h light-dark cycle of cool white fluorescent light at 20 μE $m^{-2}s^{-1}$ was transferred to one 1-L PC bottle containing f/2 medium when *R. salina* was undetectable. The bottle was filled to capacity with freshly filtered seawater, capped, placed on a rotating wheel at 0.9 rpm, and incubated under the conditions described above. After a 2-week incubation, a 1-ml aliquot from the bottle was placed on a 1-ml Sedgwick-Rafter (SR) chamber and then it was confirmed that there were no prey cells outside *P. shiwhaense* cells and there were chloroplasts inside *P. shiwhaense* cells.

Table 2.1 List of species used in constructing phylogenetic trees. GenBank accession numbers are listed to the right of each species

Taxon	Accession no.	
	SSU rDNA	LSU rDNA
Adenoides eludens	AF274249	
Akashiwo sanguinea	AJ415513	AF260397
Alexandrium affine		AY338753
Alexandrium catenella		AF200667
Babesia microti	AB219802	
Baldinia anauniensis	EF052682	EF052683
Borghiella tenuissima		AY571374
Cochlodinium polykrikoides	AY421782	
Esoptrodinium gemma		DQ289020
Glenodiniopsis steinii	AF274257	
Gymnodinium aureolum	AF172713	AF200670
Gymnodinium bei	U41087	
Gymnodinium catenatum	AB265962	AF200672
Gymnodinium cf. *placidum*		AF260383
Gymnodinium falcatum		AY320049
Gymnodinium fuscum	AF022194	AF200676
Gymnodinium impudicum		AF200674
Gymnodinium microreticulatum	AB265964	AY036078
Gymnodinium nolleri	AB265963	AF200673
Gymnodinium palustre		AF260382
Gymnodinium simplex	U41086	
Gymnodinium sp.	AF022196	EF192412
Gymnodinium venator		AY455681
Gyrodinium dominans		AY571370

Gyrodinium dorsum	AF274261	
Gyrodinium fusiforme	AB120002	
Gyrodinium helveticum	AB120004	
Gyrodinium instriatum	AY443015	
Gyrodinium rubrum	AB120003	
Gyrodinium spirale	AB120001	AY571371
Gyrodinium uncatenum	AF274263	AY916541
Haplozoon axiothellae	AF274264	
Heterocapsa rotundata	DQ388464	AF260400
Jadwigia applanata	EF058240	AY950447
Karenia asterichroma		AY590123
Karenia bidigitata		AY947662
Karenia brevis	AJ415518	AF200677
Karenia brevisulcata		AY243032
Karenia mikimotoi	Af022195	AF200678
Karenia papilionacea		AY590124
Karenia selliformis		U92250
Karenia umbella		AY263962
Karlodinium armiger		DQ114467
Karlodinium australe		DQ151559, DQ151560
Karlodinium veneficum	AJ415516	AY263964, AF200675
Kryptoperidinium foliaceum	AF274268	
Lepidodinium chlorophorum		EF010974, AF200669
Lepidodinium viride	AF022199	AY464689
Noctiluca scintillans	AF022200	
Nematodinium sp.	FJ947038, FJ947039	FJ947041
Paragymnodinium shiwhaense	AM408889	AM408889

Pentapharsodinium tyrrhenicum	AF022201	
Peridinium willei		AF260384
Pheopolykrikos beauchampii	DQ371295	EF616463
Polarella glacialis	EF417317	AY571373
Polykrikos hartmannii	AY421789	AY526521
Polykrikos herdmanae	DQ975470	
Polykrikos kofoidii		EF192411, FJ947043
Polykrikos lebourae	DQ975472	FJ947044
Polykrikos schwartzii		EF192408
Prorocentrum micans		AF260377
Protoceratium reticulatum	AF274273	
Proterythropsis sp.	FJ947036, FJ947037	
Pyrocystis lunula	AF274274	
Pyrodinium bahamense	AF274275	
Sarcocystis muris	M64244	
Scrippsiella trochoidea var. *aciculifera*		AF260393
Symbiodinium californium	AF225965	
Symbiodinium corculorum	L13717	
Symbiodinium meandrinae	L13718	
Symbiodinium microadriaticum		AF060896
Symbiodinium pilosum	X62650	
Symbiodinium sp.	AY443023	
Takayama helix		AY284950
Takayama pulchella	AY800130	U92254
Takayama tasmanica		AY284948
Thoracosphaera heimii	AF274278	
Togula britannica		AY455679
Togula compacta		AY568562

Togula jolla		AY455680
Tovellia coronata		AY950445
Tovellia sanguinea		DQ320627
Toxoplasma gondii	U00458	
Warnowia sp.	FJ947040, FJ947046	FJ947042
Woloszynskia halophila	EF058252	AY628430
Woloszynskia leopoliensis	AY443025	
Woloszynskia pascheri	EF058253	EF058276
Woloszynskia pseudopalustris		AF260402
Woloszynskia sp.		EF616464
Uncultured eukaryote	AY664896, AY664911 AY664912, AY664914 AY664983, AY665026 EF527120	

Another 150-ml aliquot was filtered onto a 1.2 μm-pore-sized GF/C filter. Three ml of 95% methanol were used for extraction and a Waters C8 column (150 mm x 4.6 mm, 3.5 μm particle size, 0.01 μm pore size) for separation. Pigments were identified by retention times and absorption spectra identical to those of authentic standards, and quantified against standards purchased from DHI Water & Environment (Hørsholm, Denmark).

3.5 Results

3.5.1 Morphology of *Paragymnodinium shiwhaense*

The episome is somewhat conical and smaller than the hemispherical hyposome (Fig. 3.1A-B, 3.1E, 3.4A). There is a wide (2.3-2.9 μm and 0.2-0.3 x cell length), distinct, descending cingulum, which is displaced by 0.2-0.3 x cell length (Fig. 3.1A-B, 3.5A). The sulcus becomes wider toward the antapex (Fig. 3.1A, 3.1D, 3.1H). The chloroplasts were brown-yellowish and arranged in bands (Fig. 3.1C, 3.1F, 3.1G). The ranges (and mean $\pm$ standard error, n=240) of cell length and cell width of living cells growing photosynthetically and starved for 2d were 8.4-15.2 μm (10.9$\pm$0.4) and 5.2-11.6 μm (8.6$\pm$0.3), respectively, while live cells fed with *Amphidinium carterae* (n=240) measured 8.4-19.3 μm (13.9$\pm$0.1) and 6.1-16.0 μm (11.0$\pm$0.1), respectively. The ratios of cell length to cell width of living cells fed *A. carterae* (mean $\pm$ standard error = 1.2 $\pm$0.01; range = 0.7-1.7, n=240) were slightly greater than those of the cells of the photosynthetically growing cells (mean $\pm$ standard error = 1.3 $\pm$ 0.05; range = 1.1-1.8, n=240).

Cells are covered with very thin and transparent hexagonal or pentagonal amphiesmal vesicles (AVs), which are easily removed under physical or osmotic stress (Fig. 3.1H-L). When the outer AV membranes are removed, there are the inner amphiesmal vescicle membrane (IAVM) and one more thin plate lying on the top of the IAVM (Fig. 3.1K-L). There are many pores among the AVs (Fig. 3.1K-L).

The AVs were arranged in 16 rows; 6 rows on the episome, 5 rows in the cingulum, and 5 rows on the hyposome (Fig. 3.2- 3.5). The total number of AV was ~250. Also, there was a sulcal extension-like furrow (SEF) on the episome containing 8 AVs (Fig. 3.2D-E, 3.5A). The length of the SEF was ~7 μm. The SEF was ~2 μm wide near the cingulum and became very narrow toward the apex, disappearing before reaching the apex (Fig. 3.2A-C, 3.5A, 3.5C). There was neither an apical groove nor an apical line of narrow plates (Fig. 3.2A-D, 3.5A, 3.5C). The size of each side of the hexagonal or pentagonal AV was ~1-2.5 μm. Of the five horizontal rows of AVs in the cingulum (Fig. 3.2D, 3.3C, 3.5F), one row covered the cingulum ceiling, three rows were present in the middle of the cingulum, and the last row covered the cingulum floor. The anterior rim of the cingulum was very sharp and well defined, in particular near the ventral ridge, while the posterior rim was somewhat rounded (Fig. 3.3A). The sulcus became wider toward the antapex and comprised ~20 AVs arranged in 3-4 longitudinal rows (Fig. 3.4E-F, 3.5D-E).

Longitudinal serial sections for TEM showed the length and width of the nucleus to be ~1/2 of the whole cell and containing many chromosomes, each measuring ~2 μm x 0.5 μm x 0.5 μm (Fig. 3.6). The few chloroplasts were located in the cell periphery or near the nucleus (Fig. 3.6).

When ~200 transverse TEM serial sections were analyzed, the details of the shape, width, and depth of the SEF and the sulcus were observed (Fig. 3.7). On the episome, the depth of the SEF near the cingulum was 30 nm, becoming shallower toward the apex (Fig. 3.7A). Near the cingulum there was a small ridge (Fig. 3.7C). On the hyposome, the sulcus was 1.5 μm wide and 2 μm deep just below the cingulum, becoming wider and deeper toward the antapex (Fig. 3.7D). The nucleus was oval and located in the center or dorsal side of the cell (Fig. 3.7).

The nuclear envelope possessed typical nuclear envelope with nuclear pores but lacked nuclear envelope chambers (Fig. 3.8).

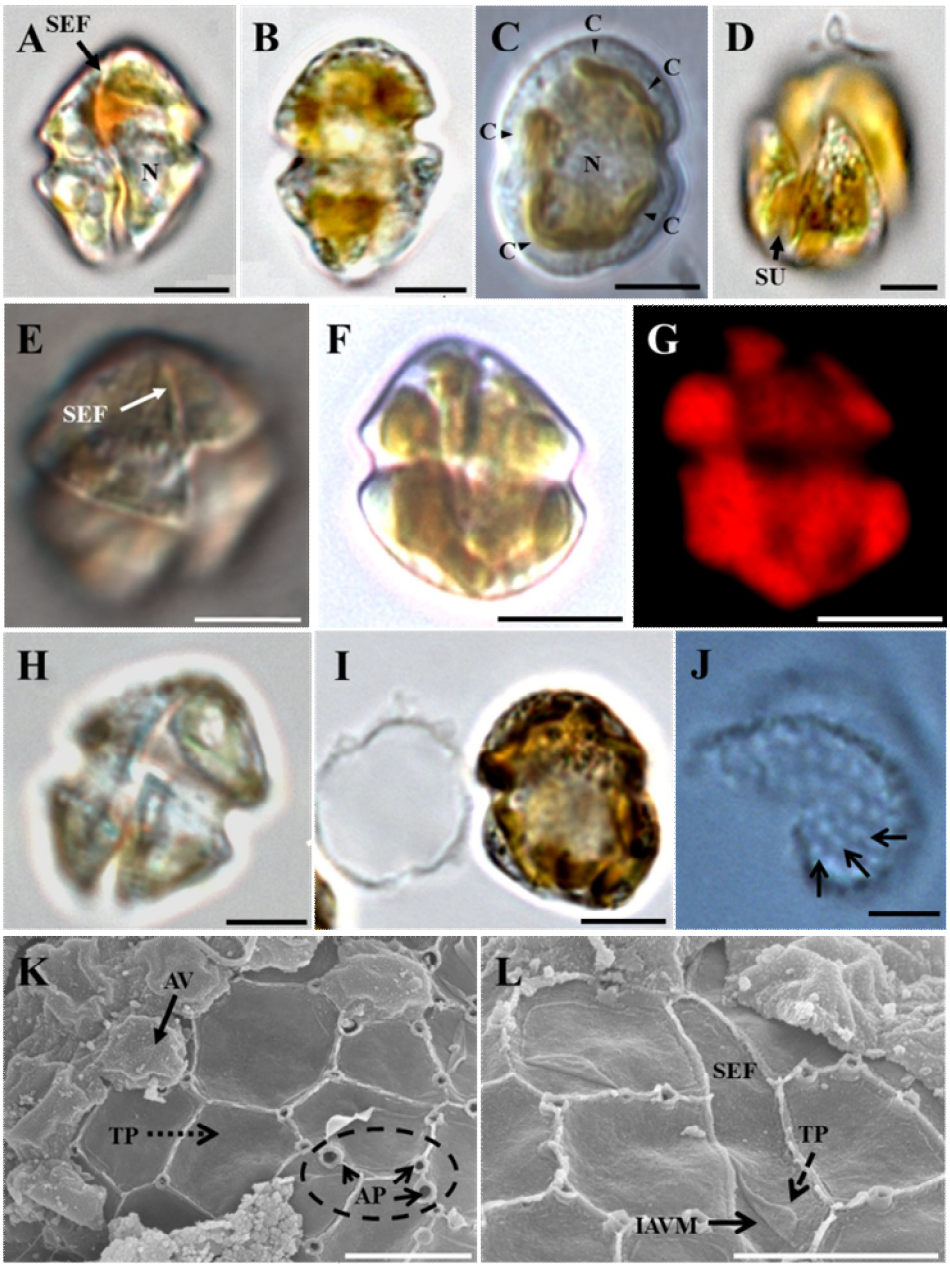

Fig. 3.1 Micrographs of *Paragymnodinium shiwhaense* n. gen., n. sp. taken using light microscopy (**A-F**, **H-J**), epifluorescent microscopy (Fig. **G**) and scanning electron microscopy (**K**, **L**). **A.** Ventral view. SEF: sulcal extension like furrow

(arrows). **B.** Lateral view. **C.** Dorsal view. **D.** Antapical view. **E.** Ventral view of a SEF. **F, G.** The brown-yellowish chloroplasts, located in the cell periphery or near the nucleus. **H-L.** Amphiesmal vesicles. Before and after the thin amphiesmal vesicles (AVs) are shed. **H.** Before shedding of the AVs. **I.** After shedding of the AVs. **J.** Shed AVs. The arrow indicates hexagonal AVs of cell surface. **K, L.** AVs, the inner amphiesmal vescicle membrane (IAVM), and a thin plate (TP). When the outer AV membranes are removed, there are IAVM and TP lying on the top of the IAVM. There are many pores (AP) among the AVs. C: Chloroplast. N: Nucleus. SU: Sulcus. Scale bars = 5 μm for Fig. **A-J**, and 1 μm for Fig. **K, L**.

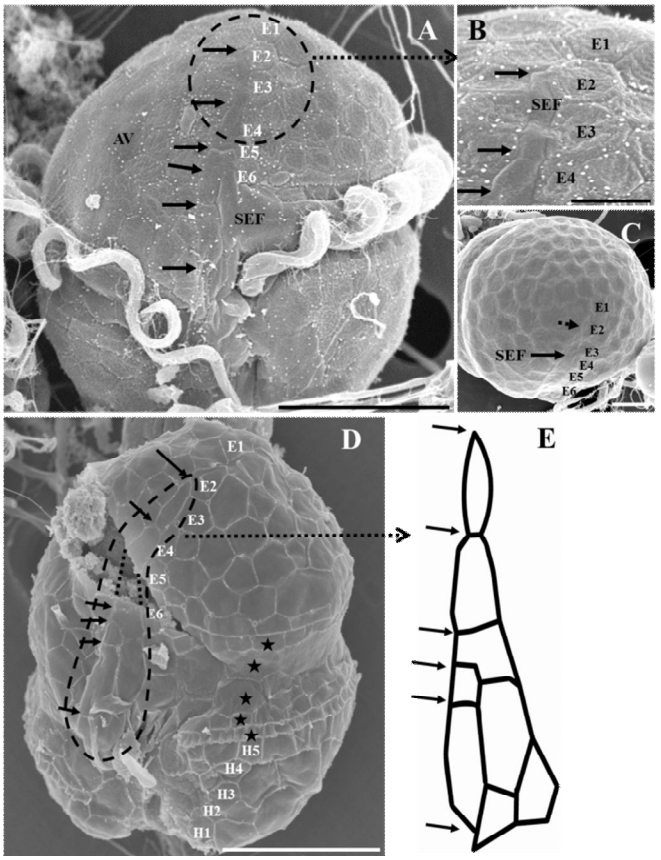

Fig. 3.2 Micrographs of *Paragymnodinium shiwhaense* n. gen., n. sp. taken using scanning electron microscopy. **A.** Ventral view showing that the epicone and cingulum of *P. shiwhaense* have numerous pentagonal and hexagonal amphiesmal vesicles (AVs) on the surface. On the episome, there is the sulcal extension-like furrow (SEF), in which there are 8 AVs (arrows). **B.** Enlarged from Fig. **A. C.** Apical view showing that *P. shiwhaense* has the SEF, which does not reach the apex. The dashed arrow indicates the end of the SEF. **D.** Ventral-lateral view showing a whole cell whose AVs were removed. Arrows indicate the border line of each AV. Dashed lines connect two separated parts. The AVs are arranged in 16 rows; 6 rows on the episome (E1-E6, Fig. **A, C**), 5 rows on the cingulum, and 5 rows on the hyposome (H1-H5, Fig. **D**). **E.** Restored SEF from Fig. **D**. There were 8 AVs in the SEF. Scale bars = 5 μm for Fig. **A, D**, and 2 μm for Fig. **B, C**.

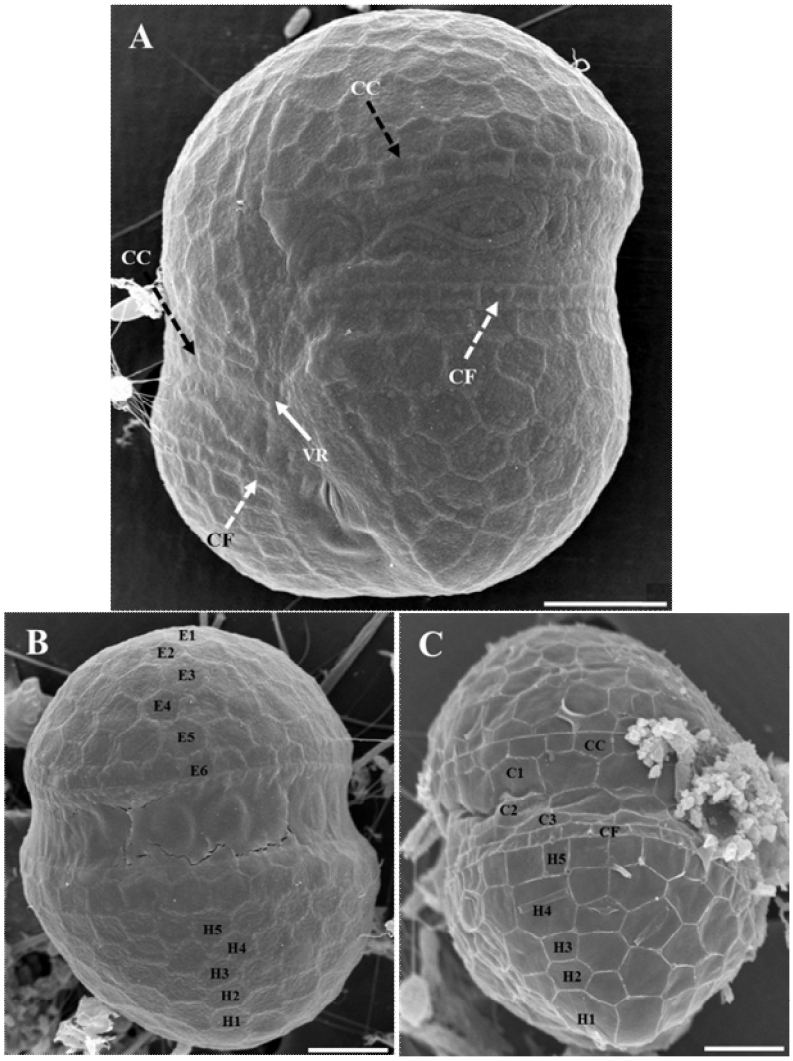

Fig. 3.3 Micrographs of *Paragymnodinium shiwhaense* n. gen., n. sp. taken using scanning electron microscopy. **A.** Ventral-lateral view showing the whole cell. CC, cingulum ceiling (black dashed arrows); CF, cingulum floor (white dashed arrows); VR, ventral ridge (white solid arrow). **B.** Dorsal view showing a cell with amphiesmal vesicles (AVs). **C.** Dorsal view showing a cell without AVs. The AVs are arranged in 16 rows; six rows on the episome (E1–E6, Fig. **B**), five rows on the cingulum (CC, C1-C3, CF, Fig. **C**), and five rows on the hyposome (H1-H5, Fig. **B, C**). Scale bars = 2 μm.

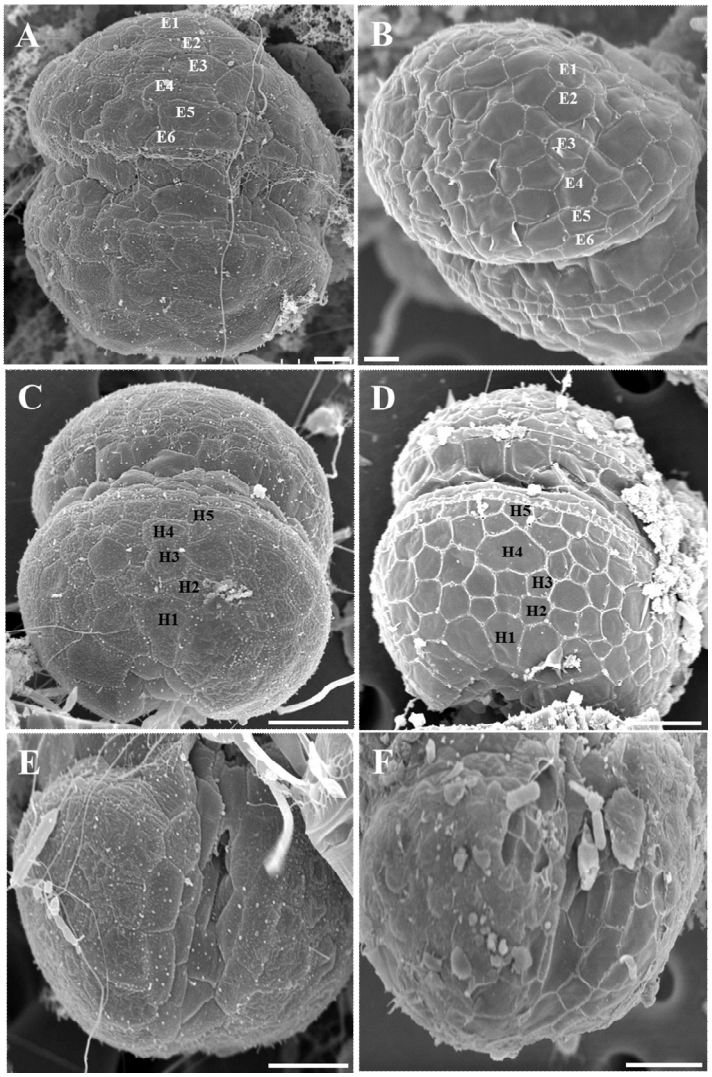

Fig. 3.4 Micrographs of *Paragymnodinium shiwhaense* n. gen., n. sp. taken using scanning electron microscopy. **A.** Lateral view showing a cell with amphiesmal vesicles (AVs). **B.** Lateral view showing a cell without AVs. **C.** Dorsal–antapical view showing a cell with AVs. **D.** Dorsal–antapical view showing a cell without AVs. **E.** Sulcus view showing a cell with AVs. **F.** Sulcus view showing a cell in which the AVs were partially removed. The AVs are arranged in six rows on the episome (E1–E6, Fig. **A, B**) and five rows on the hyposome (H1–H5, Fig. **C, D**). Scale bars = 2 μm.

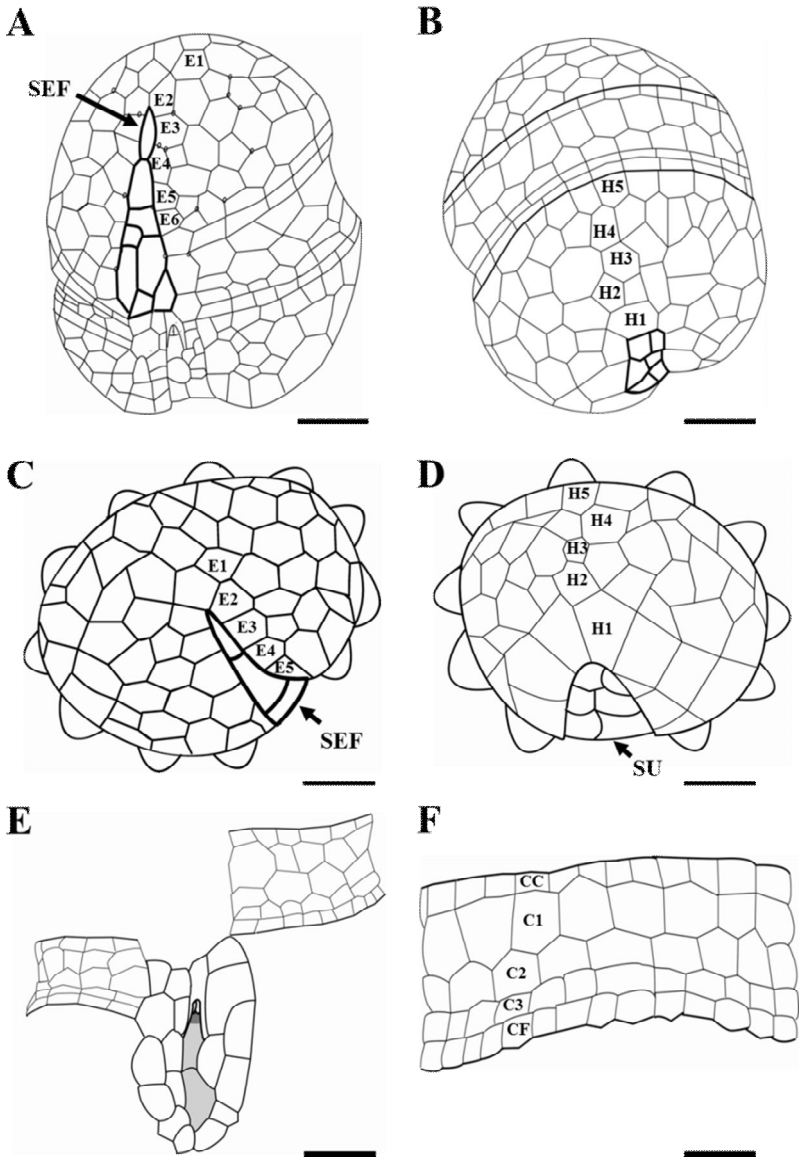

Fig. 3.5 Drawings of *Paragymnodinium shiwhaense* n. gen., n. sp. to show the external morphology. **A**. Ventral view. **B**. Dorsal view. **C**. Apical view. **D**. Antapical view. **E**. Ventral view of the cingulum and sulcus. **F**. Dorsal view of the cingulum. SEF, sulcal extension-like furrow; SU, sulcus; ‘‘E1-6,’’ ‘‘H1-5,’’ and ‘‘CC-CF’’ indicate episomal, hyposomal, and cingular amphiesmal vesicles, respectively. Scale bars = 2 μm.

I examined the flagellar apparatus of several cells (Fig. 3.10-3.13). The first set of serial sections showed the presence and position of components of the flagellar apparatus (Fig. 3.10-3.11); the flagellar root system comprises a large multi-membered microtubular root (R1), located to the left of the longitudinal basal body (LB) (viewer's right) (Fig. 3.11A); the transverse basal body (TB) is located to the right of the LB (viewer's left) and TB and LB were located at an angle of approximately 160° to each other (Fig. 3.11B); two fibrous connectives are involved in connecting the LB with the R1 (Fig. 3.11B); the C1 (LB/R1) and the C2 (LB/R1) attach R1 to adjacent triplets of the LB. The R2 was not observed; the R3, a single-membered microtubular root, was located to the right of the TB (Fig. 3.11C); three connectives, the bbc1, bbc2, and bbc3, interlink the two basal bodies (Fig. 3.11C). If the triplets of the TB (viewed from tip to base) are labeled anticlockwise starting with the triplet associated with the R3 root, then the bbc1, bbc2, and bbc3 attach to triplet number 4, 5, and 6, respectively (Fig. 3.11C). I examined the space between nucleus and flagellar apparatus in many serial sections (> 50 cells) under TEM, but no nuclear fibrous connective (NFC) was observed (Fig. 3.10-3.11). Also, no pusule was observed. In addition, the transverse microtubular root extension (TMRE) was not observed. The 2nd set of serial sections confirmed the presence of two fibrous connectives (Fig. 3.12A-C). The 3rd set of serial sections showed that the R4 consists of a prominent striated fiber, the transverse striated root (TSR) with an associated single microtubule, the transverse striated root microtubule (TSRM) and is associated with the left proximal part of the TB (Fig. 3.12D-F). The R1 and R4 roots are interlinked by a striated root connective (SRC) (Fig. 3.12E). Additional photos confirmed the presence and position of the TB, LB, R1, R4, and SRC (Fig. 3.12G-I).

Several nematocysts were located near the surface (Fig. 3.14-3.15). Each nematocyst had an anterior operculum (OP) covering an anterior chamber (AC), and an ovoid posterior body (PB) (Fig. 3.14, 3.15A-F).

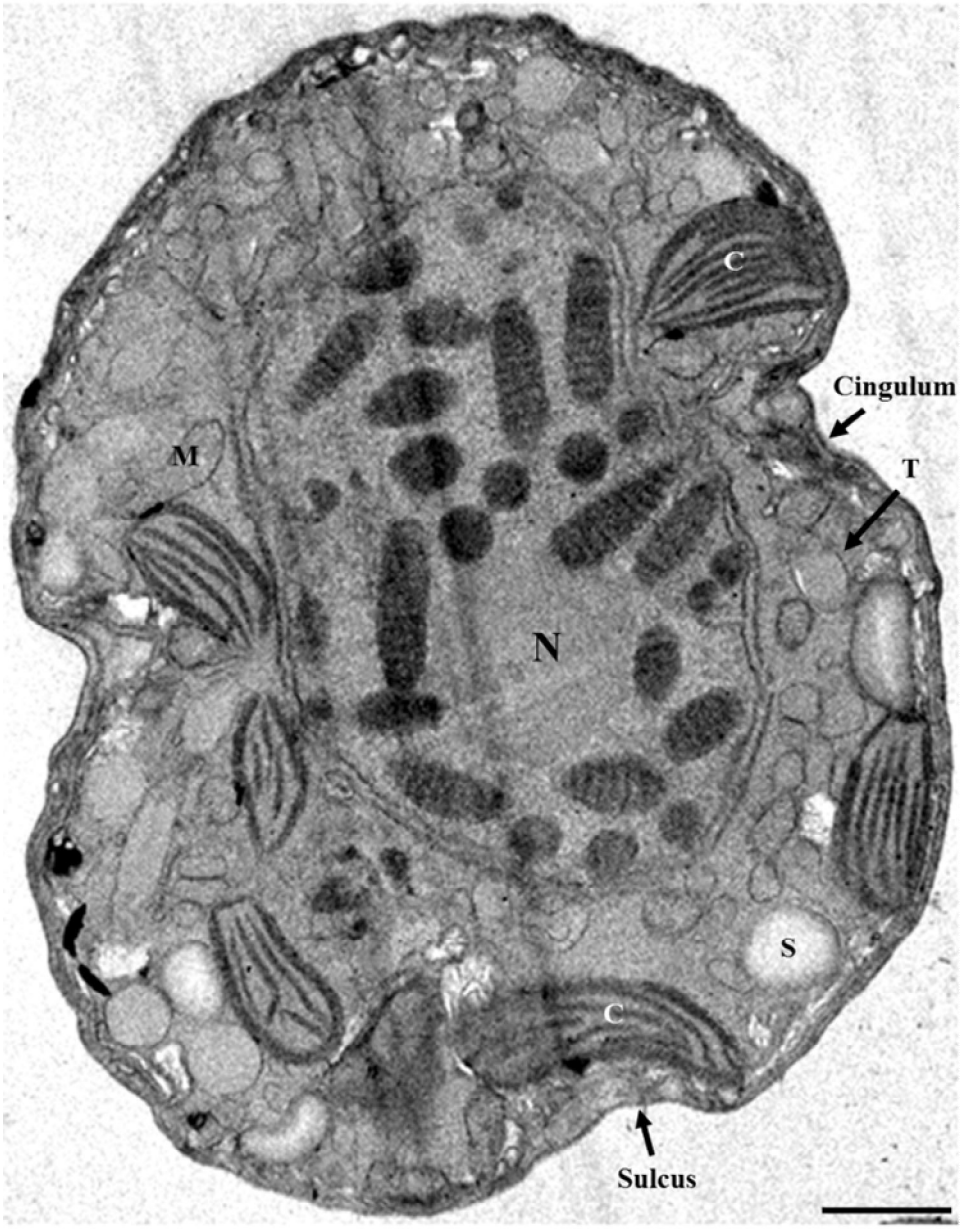

Fig. 3.6 Micrograph of *Paragymnodinium shiwhaense* n. gen., n. sp. taken using transmission electron microscopy. Longitudinal section, which shows several organelles inside the protoplasm. C, chloroplast; N, nucleus; M, mitochondrion; S, starch; T, trichocyst. Scale bars = 2 μm.

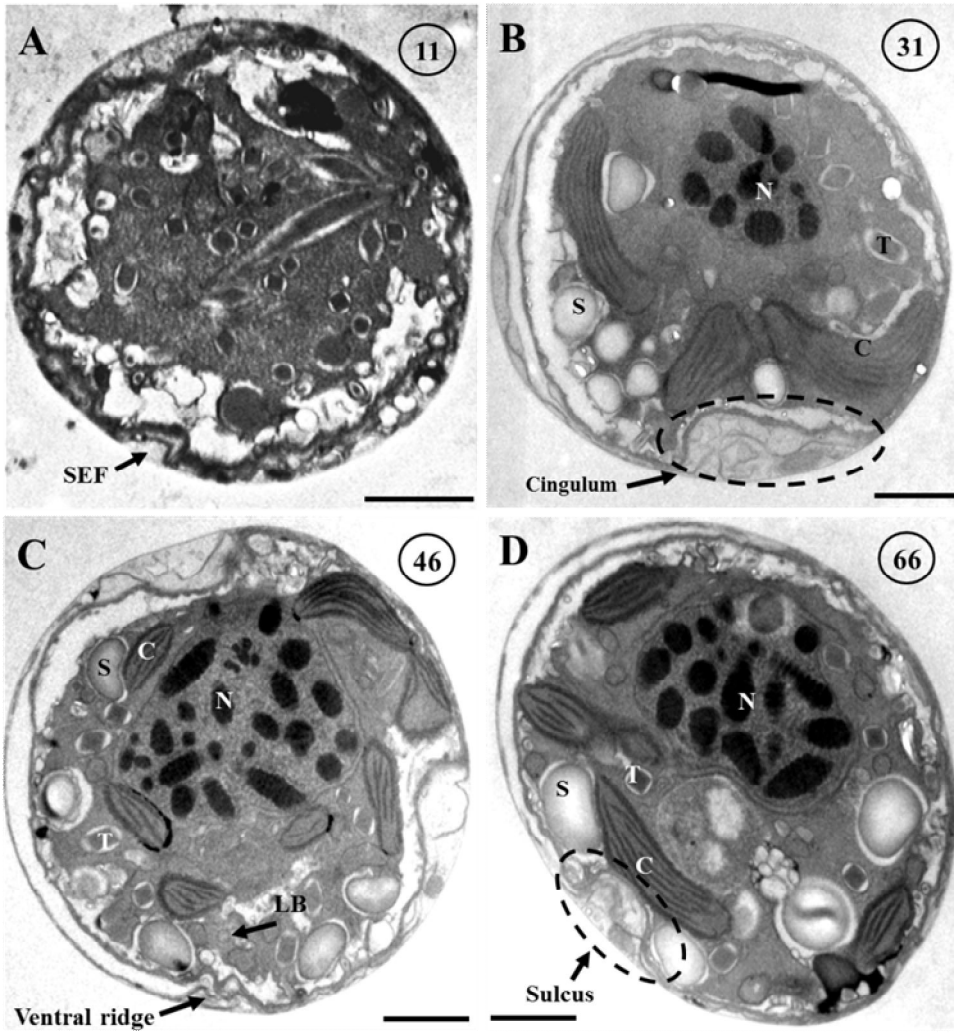

Fig. 3.7 Micrographs of *Paragymnodinium shiwhaense* n. gen., n. sp. taken using transmission electron microscopy. The numbers A-11 to A-66 indicate the layers in serial sections. C, chloroplast; LB, longitudinal basal body; N, nucleus; S, starch; SEF, sulcal extension-like furrow; T, trichocyst. Scale bars = 2 μm.

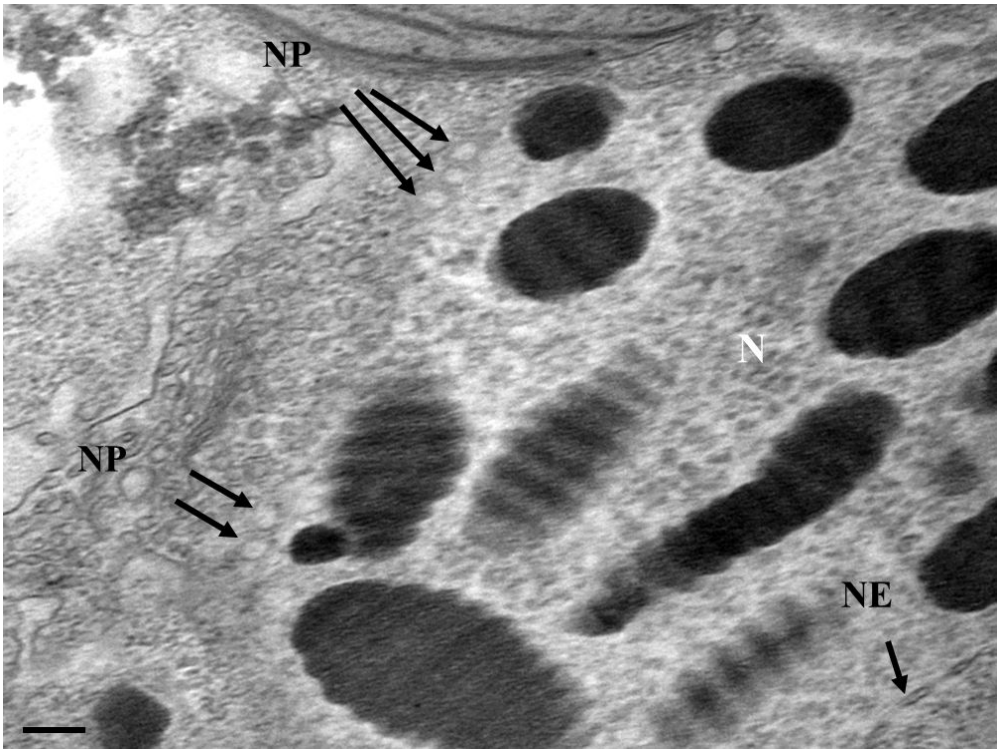

Fig. 3.8 *Paragymnodinium shiwhaense* n. gen., n. sp. Transversely sectioned micrograph of *P. shiwhaense* n. gen., n. sp., taken using transmission electron microscope, showing nuclear pores (NP) in the nuclear envelope (NE). Scale bars = 0.2 μm.

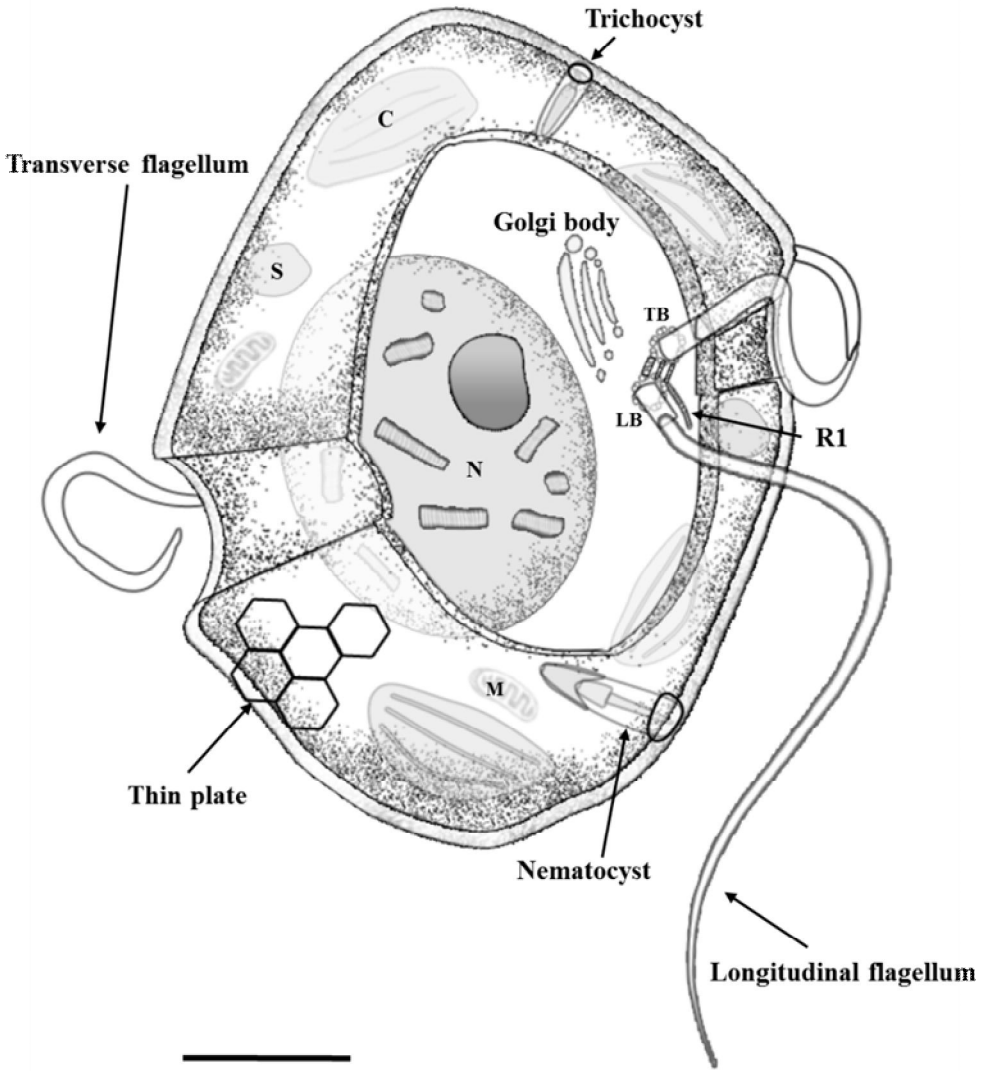

Fig. 3.9 *Paragymnodinium shiwhaense* n. gen., n. sp. Diagrammatic drawing of *P. shiwhaense* n. gen., n. sp., based mainly on serially sectioned transmission electron microscope (i.e. serial sections were approximately 70 nm thick, total of 105 sections) from the apex to the antapex and SEM. C, chloroplast; LB, longitudinal basal body; N, nucleus; M, mitochondria; R1, root 1; S, starch; TB, transverse basal body. Scale bars = 2 μm.

The length of the OP was ~0.3 μm. The width of the OP at the top was 0.2 μm, becoming wider (ca. 0.4 μm) toward the PB. The PB was 0.8 μm long, 0.2 μm wide near the OP, but 0.8 μm wide in the middle. The PB, which was covered by a capsule, contained a fibrous strand (FS), ~0.8 μm long and ~0.15 μm wide, and a posterior chamber (PC). Taeniocysts and posterior vacuoles connected to nematocysts were not observed (Fig. 3.14-3.15). Also, there was no stylet within the nematocysts. The number of nematocysts in one sectional layer was 3-6 (Fig. 3.15G-K). The length and width of the nematocysts were ~1.2 μm and ~0.8 μm, respectively. This dinoflagellate has a peduncle, which was observed between the ventral ridge and the left side the cingulum (Fig. 3.16A-C). Transverse TEM serial sections showed a microtubular strand that represented a retracted peduncle. The peduncle and the ventral ridge were located near the LB (Fig. 3.16C). The vesicle situated at the right side of the ridge was usually somewhat hook-shaped. Numerous mitochondria were found near the nucleus and amphiesima (Fig. 3.16D). Near the nucleus, there was a Golgi apparatus composed of 6-10 stacked cisternae (Fig. 3.16E). Also, a number of starch granules and fibrous vesicles were observed throughout the cytoplasm (Fig. 3.7D, 3.16F). Numerous trichocysts, each ~3 μm long, were located near the surface (Fig. 3.16G). Each chloroplast was bounded by 3 evenly spaced membranes and each lamella comprised two or three thylakoids (Fig. 3.16H). A pyrenoid was absent. Transversal TEM serial sections showed a total of 10-15 chloroplasts per cell. An eyespot was not observed.

The pigments of *P. shiwhaense* satiated with the cryptophyte prey *R. salina* and then starved for 2 weeks were different from those of *R. salina*: *P. shiwhaense* has chlorophyll-*a*, chlorophyll-*c2*, β–carotene, peridinin, diadinoxanthin, and diatoxanthin, while *R. salina* has chlorophyll-*a*, chlorophyll-*c2*, β–carotene, and alloxanthin, but does not have peridinin, diadinoxanthin, and diatoxanthin (Fig. 3.17).

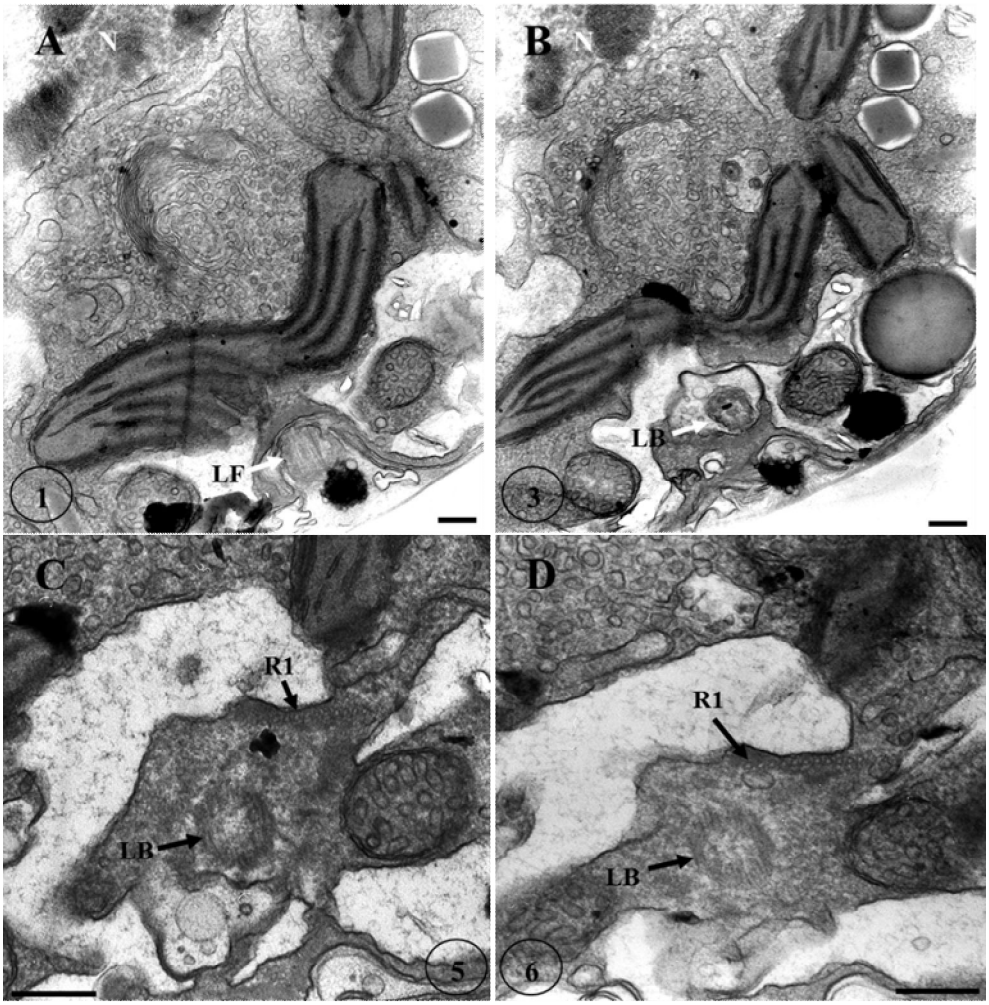

Fig. 3.10 Electron micrographs of serially sectioned *Paragymnodinium shiwhaense* n. gen., n. sp. showing the longitudinal basal body (LB), longitudinal flagellum (LF), nucleus (N), and Root 1 (R1). There was no nuclear fibrous connective between the nucleus and R1. Serial sections were approximately 70 nm thick; the circled number in each micrograph represents the number of a sequential section. Scale bars = 0.2 μm.

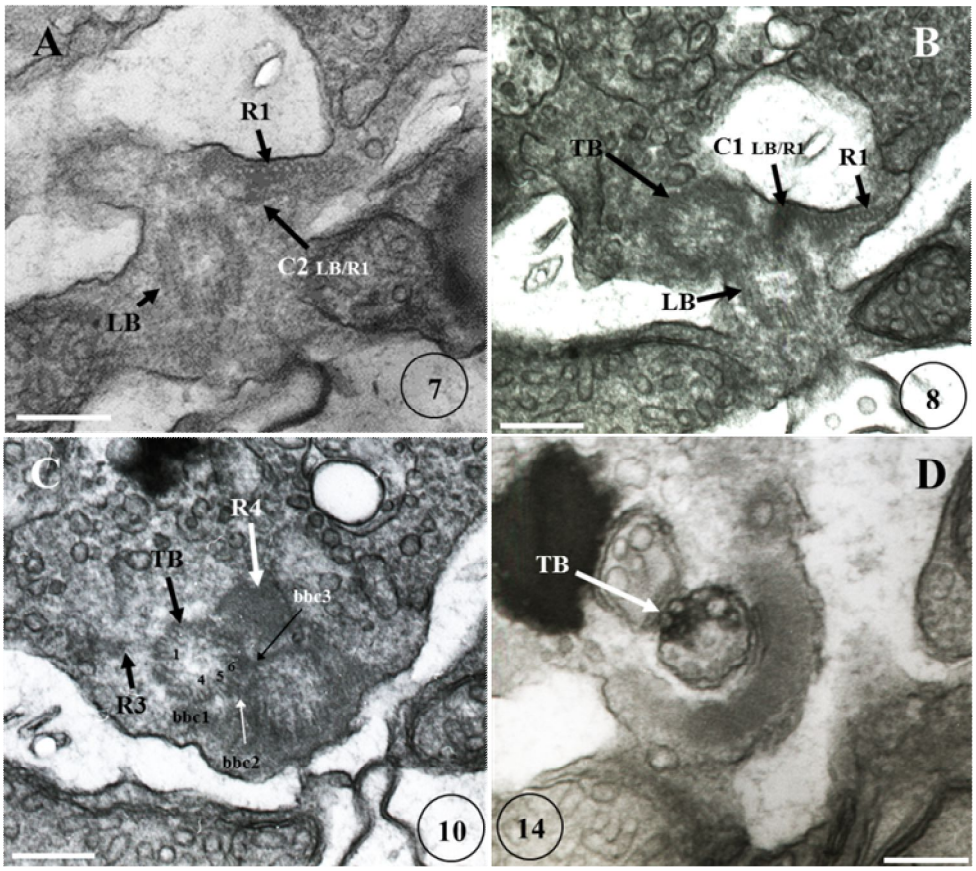

Fig. 3.11 Electron micrographs of serially sectioned *Paragymnodinium shiwhaense* n. gen., n. sp. showing the longitudinal basal body (LB), transverse basal body (TB), Root 1 (R1), Root 3 (R3), $C1_{LB/R1}$ and $C2_{LB/R1}$, and bbc1, 2, 3, which connect the LB and TB. Serial sections were approximately 70nm thick; the circled number in each micrograph represents the number of a sequential section. Scale bars = 0.2 μm.

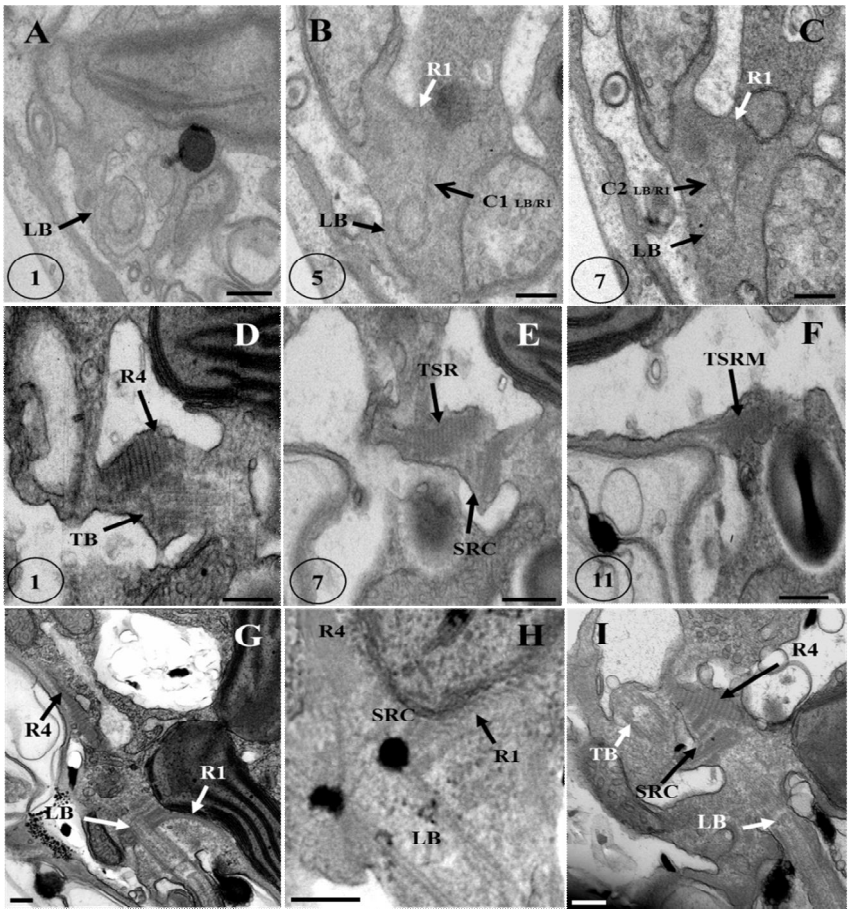

Fig. 3.12 Electron micrographs serially sectioned *Paragymnodinium shiwhaense* n. gen., n. sp. showing the relative positions (angles) of the longitudinal basal body (LB), transverse basal body (TB), Root 1 (R1), $C1_{LB/R1}$ and $C2_{LB/R1}$, and Root 4 (TSR+TSRM), striated root connectives (SRC), transverse striated root (TSR), and transverse striated root microtubule (TSRM). **A-C**. Micrographs showing C1LB/R1 and C2LB/R1, which connect the LB and R1. **D-F**. Micrographs showing the TB, Root 4 (TSR+TSRM), and SRC. **G-I**. Transmission electron microscopic micrographs of *P. shiwhaense* showing the relative positions (angles) of the TB, LB, R1, R4, and SRC. Serial sections were approximately 70 nm thick; the circled number in each micrograph represents the number of a sequential section. Scale bars = 0.2 μm.

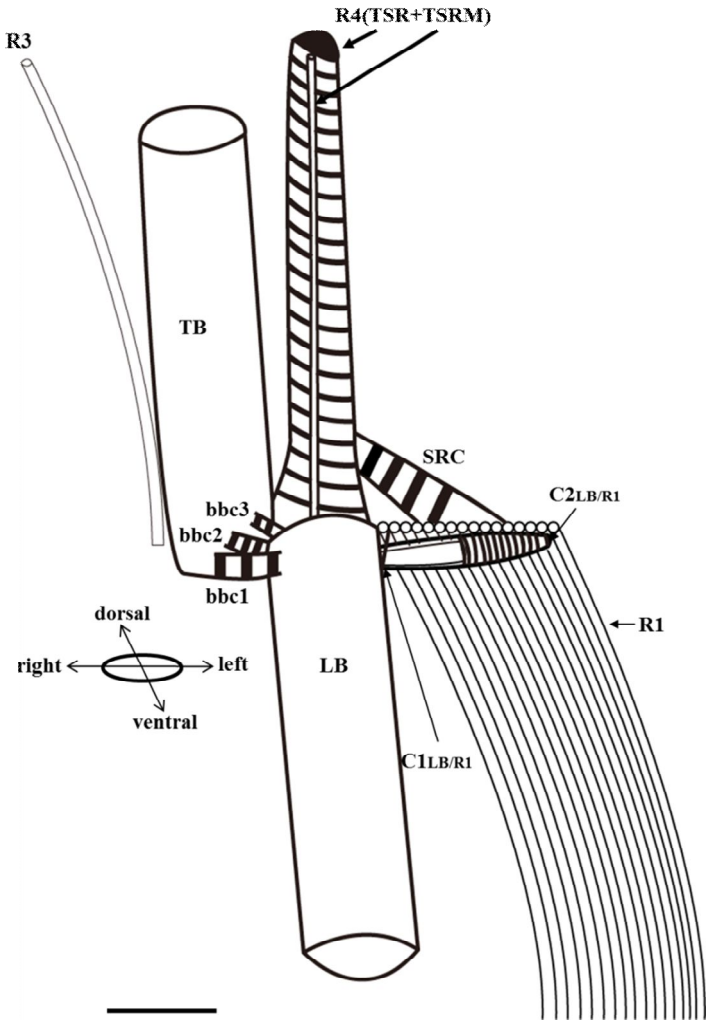

Fig. 3.13 Diagrammatic reconstruction of the flagellar apparatus of *Paragymnodinium shiwhaense*, based mainly on transverse transmission electron microscope serially sectioned layers (70 nm-layer serial section). LB, longitudinal basal body; TB, transverse basal body; R1, root 1; R3, root 3; R4, root 4; SRC, striated root connectives; $C1_{LB/R1}$, connective 1 linking LB and R1; $C2_{LB/R1}$, connective 2 linking LB and R1; bbc1, basal body connective 1; bbc2, basal body connective 2; bbc3, basal body connective 3; TSR, transverse striated root; TSRM, transverse striated root microtubule. Scale bars = 0.2 μm.

3.5.2 Molecular characterization of *Paragymnodinium shiwhaense*

The SSU, ITS 1 and 2, 5.8S, and LSU rDNA sequence (Genbank Accession No. AM408889) of this new isolate comprised 3,361 nucleotides. When properly aligned, the sequence of the SSU rDNA of *P. shiwhaense* was approximately 4% different from that of *Gymnodinium* sp. MUCC284 (AF022196), *Lepidodinium viride* (AF022199), *Gymnodinium catenatum* (AF022193), *Polykrikos hartmannii* (AY421789), *Warnowia* sp. (FJ947040), and *Nematodinium* sp. (FJ947039) the 6 closest species using the SSU rDNA sequence. The sequence of the LSU rDNA was 17-18% different from that of *G. catenatum* (DQ785883), *Lepidodinium chlorophorum* (AF200669), and *Gymnodinium nolleri* (AF200673), the 3 closest species using the LSU rDNA sequence.

The phylogenetic trees based on both SSU and LSU rDNA showed that *P. shiwhaense* belongs to the *Gymnodinium* sensu stricto clade (Fig. 3.18, 3.19). In the phylogenetic trees, *P. shiwhaense* was close to the *Polykrikos* clade but clearly divergent from a Warnowiid clade (including *Warnowia* spp., *Proterythropsis* spp., and *Nematodinium* spp.).

3.5.3 Date and locality of isolation

Our new isolate was found in Shiwha Bay, Korea (35^{o}03` N, 128$^{o}$21` E) on May 25, 2006 when the mixotrophic dinoflagellate *A. carterae* (ca. 150 cells ml^{-1}) and cryptomonads (ca. 3,500 cells ml^{-1}) were abundant and when the water temperature and salinity were 18.8 ^{o}C and 30.4, respectively.

3.5.4 Remarks on culturing and behavior

The new isolate was cultured on *A. carterae*. It did not grow photosynethically. It moved in straight lines or in a helicoidal pattern. Sometimes it suddenly stopped and then went very fast (like a jump).

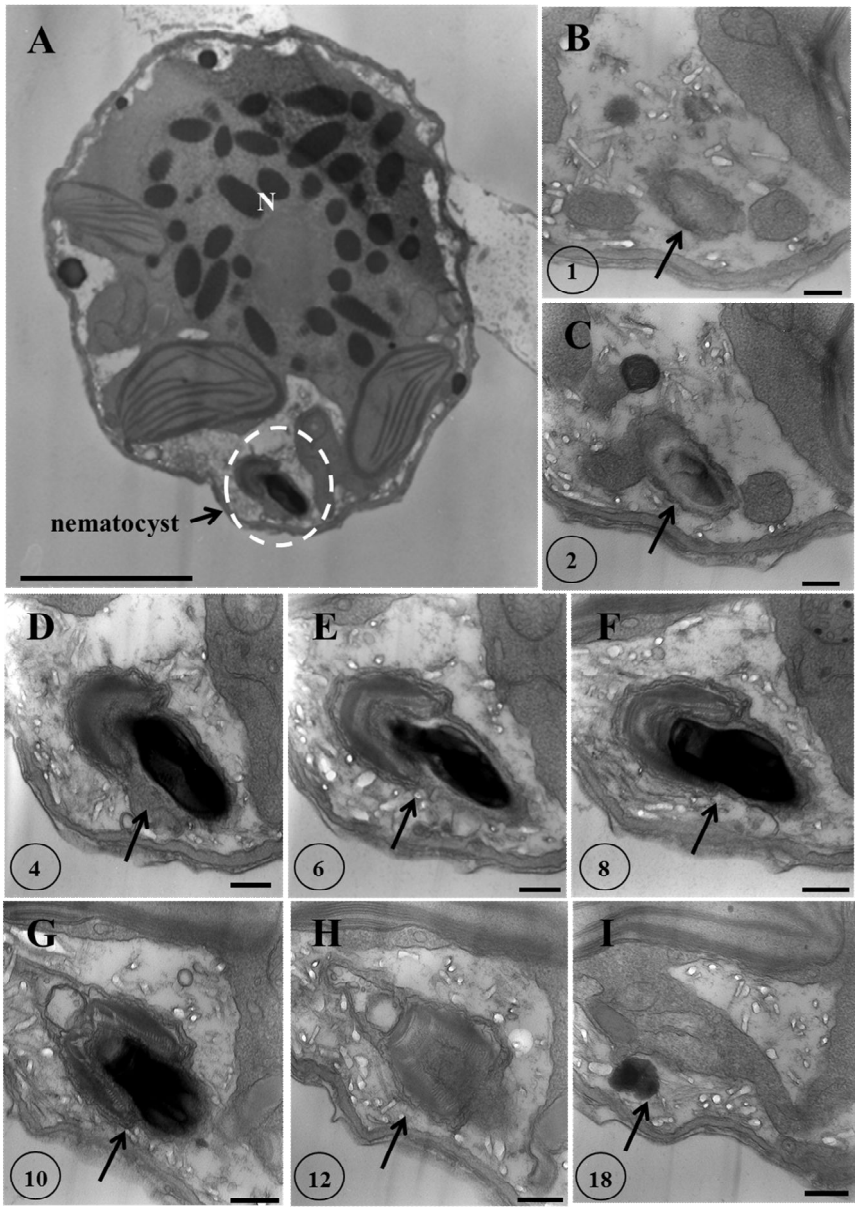

Fig. 3.14 Serially sectioned transmission electron microscope micrographs of *Paragymnodinium shiwhaense* n. gen., n. sp. showing the shape and position of nematocysts (arrows). In the 70-nm-thick cell sections the circled number in each micrograph represents the number of a sequential section. Scale bars = 5 μm (Fig. **A**) and 0.2 μm (Fig. **B-I**).

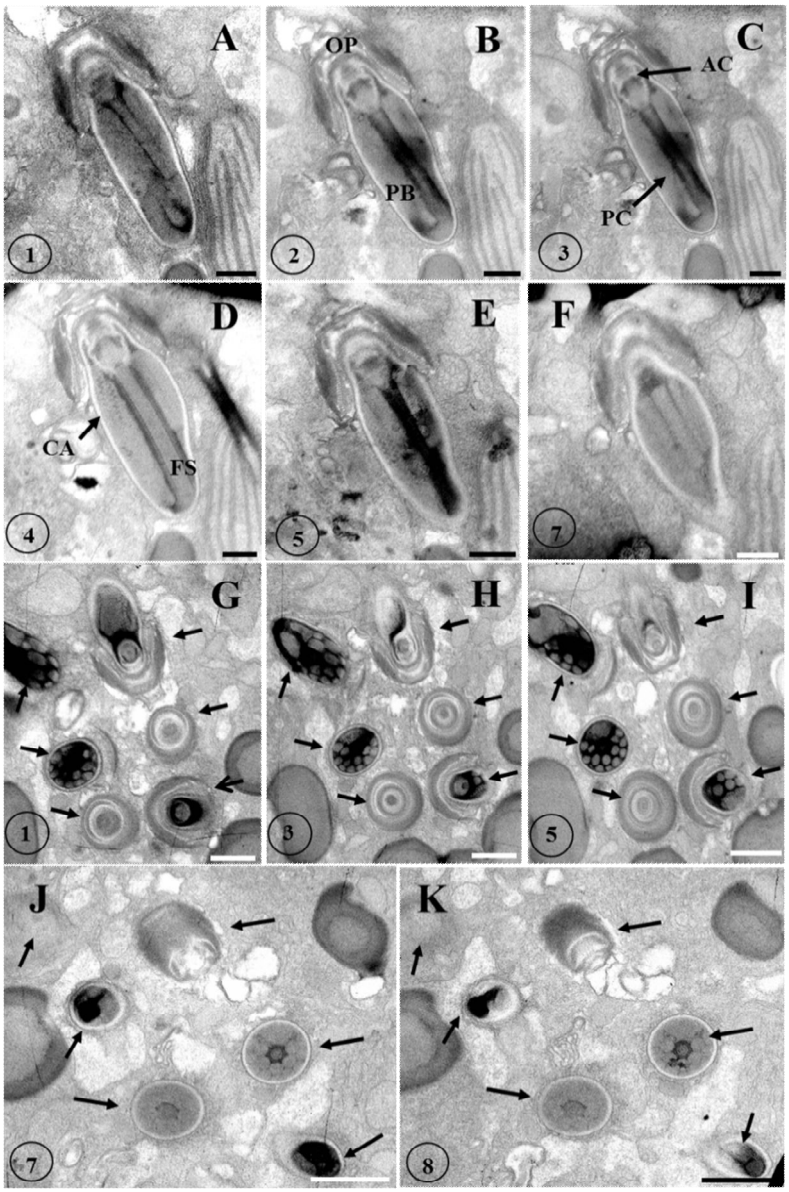

Fig. 3.15 Micrographs of nematocysts of *Paragymnodinium shiwhaense* n.gen., n.sp. **A-F**. The microstructure of a nematocyst with an operculum (OP), anterior chamber (AC), capsule (CA), fibrous strand (FS), posterior body (PB), and posterior chamber (PC). There were no taeniocysts, posterior vacuoles, and stylets outside or inside the nematocysts. **G-K**. Micrographs showing the number of nematocysts (arrows). Scale bars = 0.2 μm.

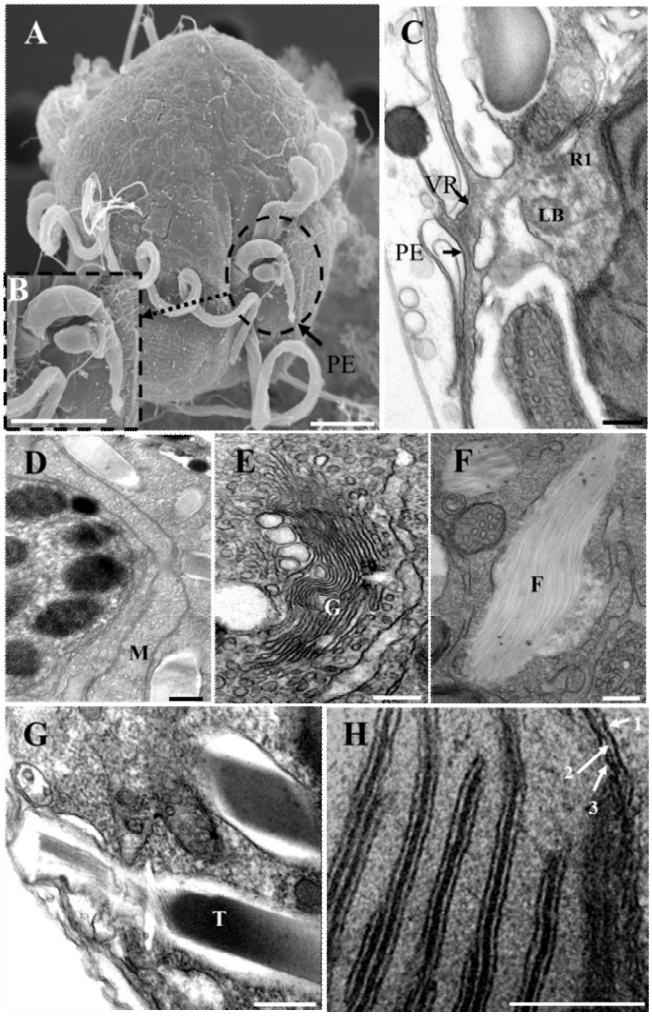

Fig. 3.16 **A-C**. Micrographs of *P. shiwhaense* showing a peduncle (PE) and ventral ridge (VR). **A**. scanning electron micrograph showing a peduncle. **B**. Enlarged from Fig. **A**. **C.** Transmission electron micrograph (TEM) showing a peduncle, ventral ridge, longitudinal basal body (LB), and Root 1 (R1). **D–F.** TEM micrographs showing mitochondrion (M, Fig. **D**), golgi body (G, Fig. **E**), fibrous vesicle (F, Fig. **F**), and trichocyst (T, Fig. **G**). **H.** TEM micrographs showing the chloroplasts bounded by three membranes (arrows with numbers); each lamella possesses two or three thylakoides, but does not have a pyrenoid. Scale bars = 2 μm for Fig. **A, B**, and 0.2 μm for Fig. **C–H.**

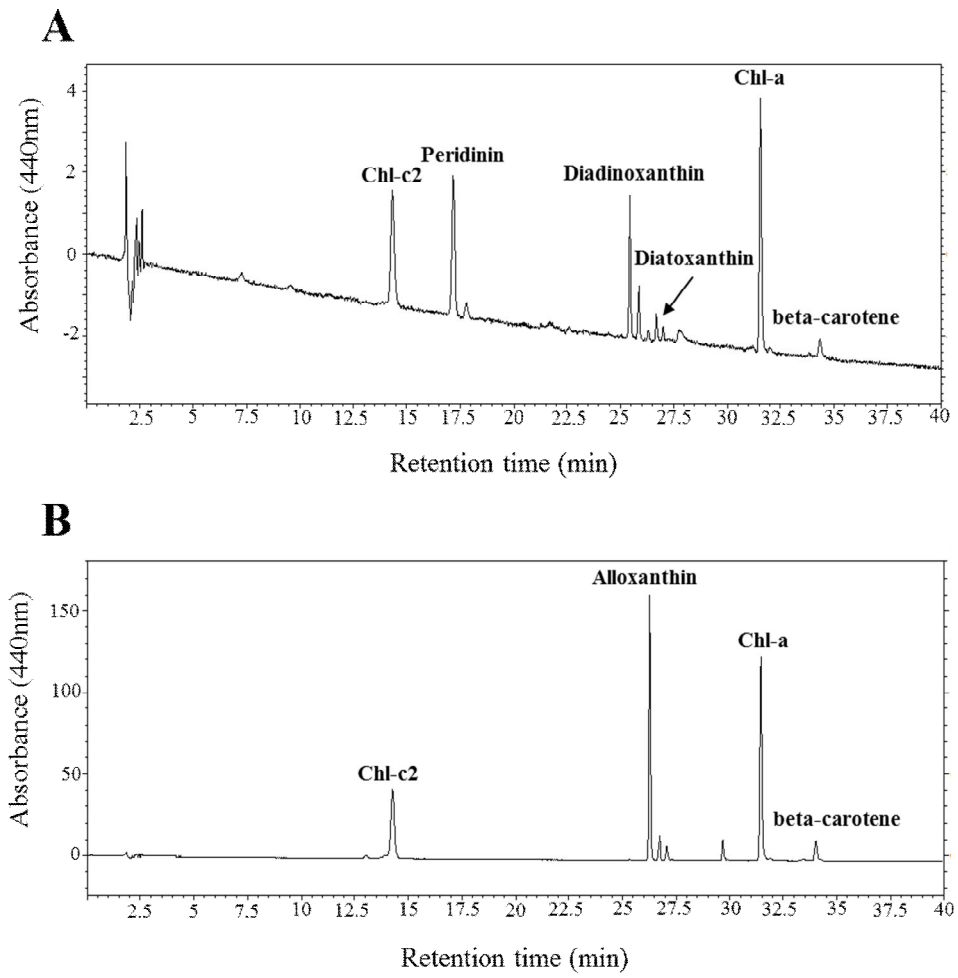

Fig. 3.17 Chromatogram derived by high performance liquid chromatography of the major pigments of *Paragymnodinium shiwhaense* n. gen., n. sp. satiated with the cryptophyte *Rhodomonas salina* and then starved for 2wk (Fig. **A**) compared with that of the prey organism *R. salina* (Fig. **B**).

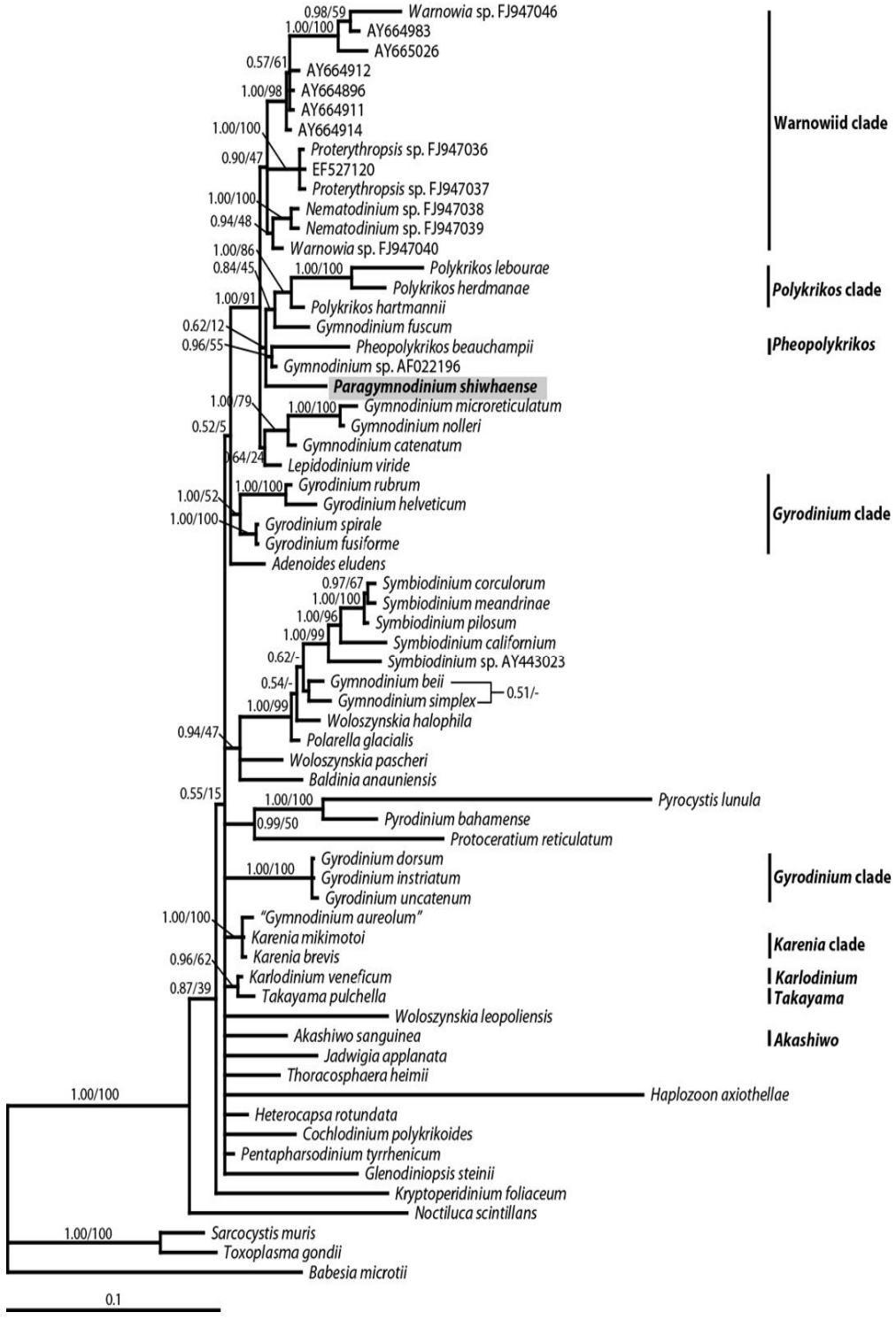
0.98/59
Warnowia sp. FJ947046
1.00/100
AY664983
AY665026
0.57/61
AY664912
1.00/98
AY664896
AY664911
1.00/100
AY664914
Warnowiid clade
0.90/47
Proterythropsis sp. FJ947036
EF527120
Proterythropsis sp. FJ947037
1.00/100
Nematodinium sp. FJ947038
0.94/48
Nematodinium sp. FJ947039
1.00/86
Warnowia sp. FJ947040
0.84/45
1.00/100
Polykrikos lebourae
Polykrikos clade
Polykrikos herdmanae
1.00/91
Polykrikos hartmannii
Gymnodinium fuscum
0.62/12
0.96/55
Pheopolykrikos beauchampii
Pheopolykrikos
Gymnodinium sp. AF022196
Paragymnodinium shiwhaense
1.00/79
1.00/100
Gymnodinium microreticulatum
0.52/5
Gymnodinium nolleri
Gymnodinium catenatum
0.64/24
Lepidodinium viride
1.00/100
Gyrodinium rubrum
1.00/52
Gyrodinium helveticum
Gyrodinium clade
1.00/100
Gyrodinium spirale
Gyrodinium fusiforme
Adenoides eludens
0.97/67
Symbiodinium corculorum
1.00/100
Symbiodinium meandrinae
1.00/96
Symbiodinium pilosum
1.00/99
Symbiodinium californium
0.62/-
Symbiodinium sp. AY443023
0.54/-
Gymnodinium beii
0.51/-
Gymnodinium simplex
1.00/99
Woloszynskia halophila
0.94/47
Polarella glacialis
Woloszynskia pascheri
Baldinia anauniensis
0.55/15
1.00/100
Pyrocystis lunula
0.99/50
Pyrodinium bahamense
Protoceratium reticulatum
Gyrodinium dorsum
1.00/100
Gyrodinium instriatum
Gyrodinium clade
Gyrodinium uncatenum
1.00/100
"Gymnodinium aureolum"
Karenia clade
Karenia mikimotoi
Karenia brevis
0.96/62
Karlodinium veneficum
Karlodinium
0.87/39
Takayama pulchella
Takayama
Woloszynskia leopoliensis
Akashiwo sanguinea
Akashiwo
Jadwigia applanata
Thoracosphaera heimii
1.00/100
Haplozoon axiothellae
Heterocapsa rotundata
Cochlodinium polykrikoides
Pentapharsodinium tyrrhenicum
Glenodiniopsis steinii
Kryptoperidinium foliaceum
Noctiluca scintillans
1.00/100
Sarcocystis muris
Toxoplasma gondii
Babesia microtii
0.1

Fig. 3.18 Consensus Bayesian tree based on 1,618 aligned positions of nuclear SSU rDNA using the TrN + I + G model with *Babesia microti, Sarcocystis muris, Toxoplasma gondii, Noctiluca scintillans* as outgroup taxa. The parameters were as follows: assumed nucleotide frequency with empirical; substitution rate matrix with A-C substitutions=1.0000, A-G = 3.8147, A-T =1.0, C-G = 1.0, C-T = 7.303, G-T = 1.0; proportion of sites assumed to be invariable = 0.3608 and rates for variable sites assumed to follow a gamma distribution with shape parameter = 0.6001. The branch lengths are proportional to the amount of character changes. The numbers above the branches indicate the Bayesian posterior probability (left) and ML bootstrap values (right). Posterior probabilities ≥ 0.5 are shown.

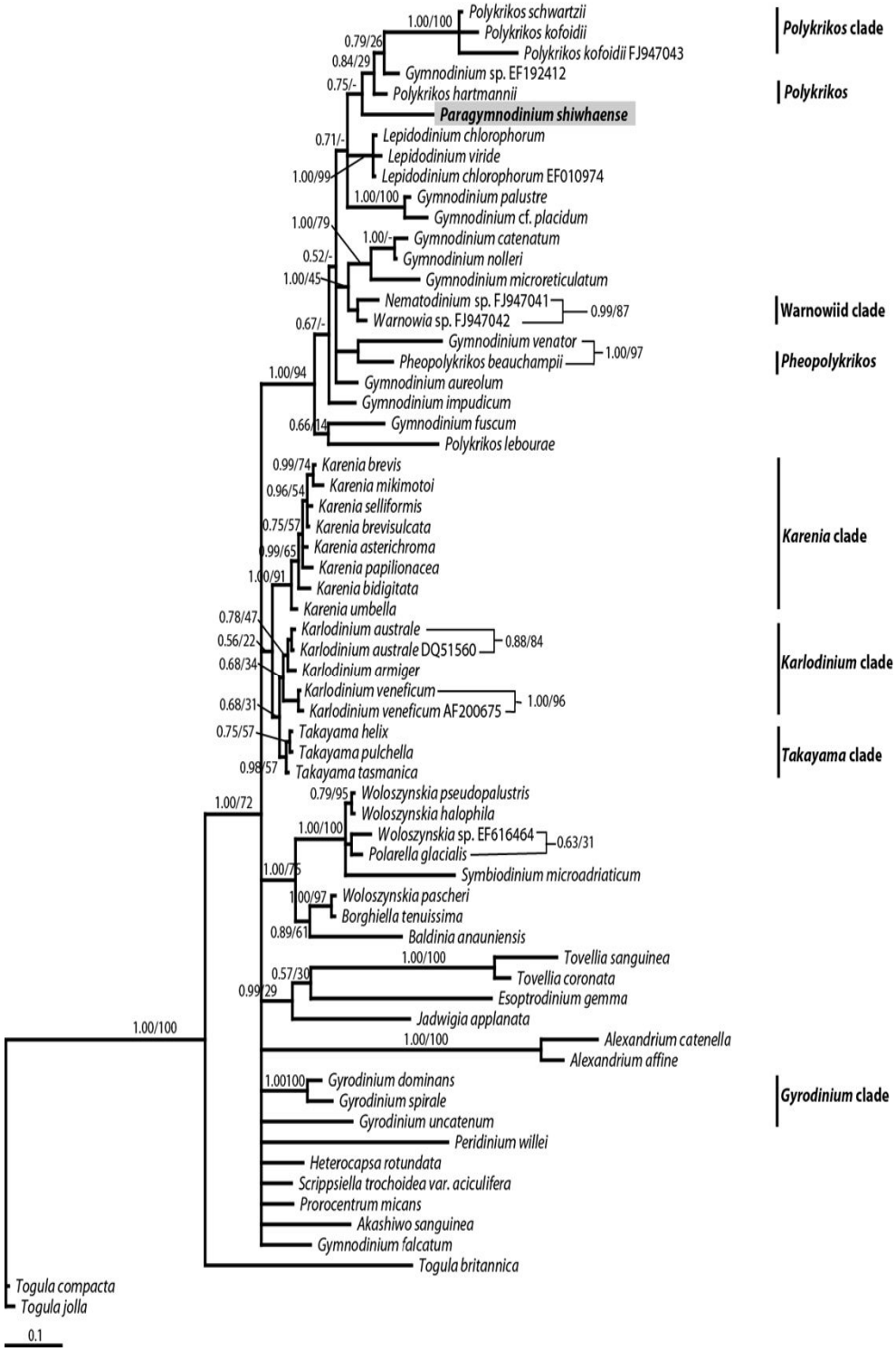
Polykrikos schwartzii
Polykrikos kofoidii
Polykrikos kofoidii FJ947043
Gymnodinium sp. EF192412
Polykrikos hartmannii
Paragymnodinium shiwhaense
Lepidodinium chlorophorum
Lepidodinium viride
Lepidodinium chlorophorum EF010974
Gymnodinium palustre
Gymnodinium cf. placidum
Gymnodinium catenatum
Gymnodinium nolleri
Gymnodinium microreticulatum
Nematodinium sp. FJ947041
Warnowia sp. FJ947042
Gymnodinium venator
Pheopolykrikos beauchampii
Gymnodinium aureolum
Gymnodinium impudicum
Gymnodinium fuscum
Polykrikos lebourae
Karenia brevis
Karenia mikimotoi
Karenia selliformis
Karenia brevisulcata
Karenia asterichroma
Karenia papilionacea
Karenia bidigitata
Karenia umbella
Karlodinium australe
Karlodinium australe DQ51560
Karlodinium armiger
Karlodinium veneficum
Karlodinium veneficum AF200675
Takayama helix
Takayama pulchella
Takayama tasmanica
Woloszynskia pseudopalustris
Woloszynskia halophila
Woloszynskia sp. EF616464
Polarella glacialis
Symbiodinium microadriaticum
Woloszynskia pascheri
Borghiella tenuissima
Baldinia anauniensis
Tovellia sanguinea
Tovellia coronata
Esoptrodinium gemma
Jadwigia applanata
Alexandrium catenella
Alexandrium affine
Gyrodinium dominans
Gyrodinium spirale
Gyrodinium uncatenum
Peridinium willei
Heterocapsa rotundata
Scrippsiella trochoidea var. aciculifera
Prorocentrum micans
Akashiwo sanguinea
Gymnodinium falcatum
Togula britannica
Togula compacta
Togula jolla
0.1
Polykrikos clade
Polykrikos
Warnowiid clade
Pheopolykrikos
Karenia clade
Karlodinium clade
Takayama clade
Gyrodinium clade

Fig. 3.19 Bayesian consensus tree of unarmoured dinoflagellates based 557 aligned positions of nuclear partial LSU rDNA using the TrN + I + G model. The parameters were as follows: assumed nucleotide frequency with equal; substitution rate matrix with A-C substitutions =1.0000, A-G = 3.1151, A-T =1.0, C-G = 1.0, C-T = 6.1349, G-T = 1.0; proportion of sites assumed to be invariable = 0.1893 and rates for variable sites assumed to follow a gamma distribution with shape parameter = 0.7346. The branch lengths are proportional to the amount of character changes. The numbers above the branches indicate the Bayesian posterior probability (left) and ML bootstrap values (right). Posterior probabilities ≥ 0.5 are shown.

3.6 Discussion

Paragymnodinium shiwhaense n. gen., n. sp. has a cell surface similar to many woloszynskioids, with polygonal amphiesmal plates arranged in rows (Table 2.2). According to Lindberg et al. (2005) and Moestrup et al. (2006, 2008), the presence of a row of thin amphiesmal plates in the episome (also referred to as ALP, PEV, or apical groove) is one of the defining characters in woloszynkioid dinoflagellates. For example, the genera *Tovellia* and *Jadwigia* (family Tovelliaceae) and *Biecheleria* have an ALP, and the genus *Borghiella* has a PEV (Moestrup et al. 2008). In contrast, *Baldinia* and *Polarella* do not have an equivalent structure (Hansen et al. 2007b; Montresor et al. 1999). Compared to these genera, *P. shiwhaense* shows no evidence of an ALP, PEV, or apical groove, instead having an extension-like furrow of the sulcus (SEF) from the cingulum to near the apex, which doesn't quite reach the apex. *P. shiwhaense* differs from the genera *Gymnodinium*, *Karlodinium*, *Karenia*, *Lepidodinium*, and *Polykrikos*, all of which have either a horseshoe- or loop-shaped, or a linear apical groove (Table 2.2). In addition to this, *P. shiwhaense* lacks three of the key taxonomic characters that circumscribe the genus *Gymnodinium*, namely the presence of nuclear envelope chambers, a nuclear fibrous connective, and a horseshoe- or loop-shaped apical groove (Daugbjerg et al. 2000). Thus *P. shiwhaense* differs from other dinoflagellate genera so far described and deserves its status as a new genus.

In phylogenetic analyses based on both SSU and LSU rDNA, *P. shiwhaense* was clearly divergent from the Warnowiid clade that contained *Warnowia*, *Proterythropsis*, and *Nematodinium*, but close to the clade formed by the genus *Polykrikos*. Like *P. shiwhaense, Polykrikos hartmannii* (previously *Pheopolykrikos hartmannii*; Hoppenrath et al. 2009b), *P. lebourae,* and *Pheopolykrikos beauchampii* contain both chloroplasts and nematocysts (Hoppenrath and Leander 2007b; Hoppenrath et al. 2009a, 2009b). However, *P. shiwhaense* lacks taeniocysts, posterior vacuoles, and a stylet, evolved features which all other *Polykrikos* species

possess. Given this, *P. shiwhaense* may represent an early divergence away from the *Polykrikos* clade, a conclusion that is supported by its position in the phylogenetic analysis. By comparison, some *Nematodinium* species also have both chloroplasts and nematocysts (Hoppenrath et al. 2009a). However, unlike *P. shiwhaense*, all *Nematodinium* species also possess ocelloids. The nematocysts of *P. shiwhaense* (~1.2 μm in length and ~0.8 μm in width) are considerably smaller than that of *Polykrikos hartmannii* (~9 μm in length and ~2 μm in width), *Nematodinium armatum* (~10 μm in length and ~5 μm in width, Hoppenrath et al. 2009b, Taylor 1987). The smaller body size of *P. shiwhaense* may explain the presence of smaller nematocysts compared to *P. hartmannii* (~60-100 μm in cell length) and *N. armatum* (~ 100 μm in cell length).

Paragymnodinium shiwhaense has a peduncle, a feature that has also been observed in a number of other dinoflagellates, including dinophysioid, gymnodinioid, gonyaulacoid, peridinioid, prorocentroid, and suessioid clades (Calado and Moestrup 1997; Calado et al. 1998; Hansen and Moestrup 1998; Hansen 2001; Jacobson and Andersen 1994; Roberts et al. 1995). The peduncle is hypothesized to serve a role in absorbing material from immobilized prey (e.g. Berge et al. 2008).

Like *Gymnodinium* species and woloszynskoid dinoflagellates, *P. shiwhaense* has peridinin as its major carotenoid. This pigment composition is different from that of *Karenia* spp., *Karlodinium* spp., and *Takayama* spp., which instead have fucoxanthin or its derivatives, and also from *Lepidodinium,* which has chlorophyll-*b* (de Salas et al. 2003; Hansen et al. 2007a). The pigments of *P. shiwhaense* satiated with *R. salina* and then starved for 2 weeks were clearly different from those of *R. salina*. *P. shiwhaense* contained peridinin as its main carotenoid, a pigment that is absent in *Rhodomonas*, establishing that *P. shiwhaense* propagates its own chloroplasts on cell division like species in photosynthetic genera such as *Gymnodinium, Akashiwo,* and *Amphidinium* (de Salas et al. 2003, Jørgensen et al.

2004), and does not rely solely on kleptochloroplasts from its prey.

Paragymnodinium shiwhaense lacks any kind of pyrenoids, which are present in most photosynthetic dinoflagellates. Similarly, the phototrophic dinoflagellate *G. fuscum* is also known to lack pyrenoids (Dodge and Crawford 1969). Our phylogenetic analysis based of SSU sequences suggests that *P. shiwhaense* and *G. fuscum* are relatively closely related, supporting our morphological results that also suggest a close relationship between the two species.

Paragymnodinium shiwhaense lacks a pusule, which is unusual among the unarmoured or thin-walled dinoflagellates. *P. shiwhaense* also lacks eyespot. Eyespot structure is an important phylogenetic marker in dinoflagellates, as there are five different types of eyespots (Lindberg et al. 2005; Moestrup and Daugbjerg 2007). Three of 5 different eyespots have been observed in the woloszynskioids. In Group I, the eyespot comprises a group of pigment globules located outside the chloroplast. The eyespot is located ventrally along the flagellar root R1, near the proximal end of the sulcus (*Woloszynskia coronata***,** *Tovellia sanguinea***,** *Esoptrodinium gemma*, and *Jadwigia applanata*). In group II, the eyespot comprises a system of cisternae containing crystal-like material instead of pigment globules (*Biecheleria pseudopalustris, Biecheleria halophila*, and *Polarella glacialis)*. In group III, the eyespot globules are located within the chloroplast like other common algae (*Borghiella dodgei, Borghiella tenuissima,* and *Baldnia anauniensis*). While individual species could secondarily lose their eyespot, the situation of *P. shiwhaense* outside this clade suggests that it has never possessed one.

Phylogenetic analyses based on both SSU and LSU rDNA sequences consistently place *P. shiwhaense* as a basal branch within the *Gymnodinium* sensu stricto clade. Based on the consistent morphological, genetic, and biochemical (i.e. pigment) divergence of this species from the genus *Gymnodinium* as a whole, I consider it justified to erect the new, separate genus and species *Paragymnodinium shiwhaense* n. gen., n. sp.

Table 2.2 Comparison of *Paragymnodinium* gen. nov with other gymnodinioid and woloszynskioid dinoflagellates

Genus	AG	NC	NFC	AV	Ped	Nem	MCP	Es	Ps	Py
PG	SEF	N	N	Polygonal	Y	Y	P	N	N	N
GYM[1]	Horseshoe	Y	Y	Y or ?	Y or ?	N	P	Y or ?	Y or ?	Y or ?
LEP[2]	Horseshoe	Y	Y	One has body scale or the other does not have	Y or PLS	N	Chl-b*	ESL or N	Y	Y
KARE[3]	Straight	N	N	Y or ?	N	N	F	N or ?	Y or ?	Y or ?
KARL[4]	Straight	N	N	Polygonal or Plug-like	Y or ?	N	F	N or ?	Y or ?	Y or ?
TAK[5]	Sigmoid	N	N	Bubbly, Polygonal or ?	PLS or N	N	F	N or ?	N	Y
POL[6]	Loop	Y or ?	Y or ?	Small polygonal or ?	N	Y	P or ?	N or ?	Y or ?	Y or ?
BAL[7]	Absent	N	N	Polygonal	Y	N	P	Y	Y	Y
BOR[8]	PEV	N	N	Polygonal	N	N	?	Y	Y	N
JAD[9]	ALP	N	N	Polygonal	?	N	?	Y	Y	N
TOV[10]	ALP	N	N	Polygonal	Y or ?	N	?	Y	Y	Y or N
WOL[11]	ALP	N	N	Polygonal	?	N	?	Y	Y or ?	Y or ?

PG: (*Paragymnodinium),* GYM: (*Gymnodinium*)*,* LEP: (*Lepidodinium*)*,* KARE: (*Karenia*)*,* KARL: (*Karlodinium*)*,* TAK: (*Takayama*)*,* POL: *Polykrikos,* BAL: (*Baldinia*), BOR: (*Borghiella*), JAD: (*Jadwigia*), TOV: (*Tovellia***)** WOL: *Woloszynskia*. Y: Observed. N: Not observed. AG: Apical groove. SEF: Sulcal extension-like furrow. ALP: Apical line of narrow plates. PEV: Pair of elongate amphiesmal vesicles. NC: Nuclear envelope chamber. NFC: Nuclear fibrous connective: AV: Amphiesmal vesicles. Ped: Peduncle. PLS: Peduncle-like structure. Nem: Nematocysts: MCP: Major carotenoid pigment. F: Fucoxanthin. P: Peridinin.

**Lepidodinium* spp. have chlorophyll a and b, unlike the other dinoflagellates which posses chlorophyll a and c. Es: Eyespot. ESL: Eyespot-like. Ps: Pusule. Py: pyrenoid.

(1) Daugbjerg et al. (2000), Hansen et al. (2007b), Jørgensen et al. (2004), Tang et al. (2008); (2) de Salas et al. (2003), Hansen et al. (2007a), Honsell and Talarico (2004), Watanabe et al. (1987, 1990); (3) Daugbjerg et al. (2000), de Salas et al. (2004a), Jørgensen et al. (2004); (4) Daugbjerg et al. (2000), de Salas et al. (2005), de Salas et al. (2008), Garces et al. (2006), Jørgensen et al. (2004); (5) de Salas et al. (2003, 2008); (6) Bradbury et al. (1983), Hoppenrath and Leander (2007a, 2007b), Westfall et al. (1983) ; (7) Hansen et al. (2007b), Moestrup and Daugbjerg (2007); (8) Moestrup and Daugbjerg (2007), Moestrup et al. (2008); (9) Lindberg et al. (2005), Moestrup and Daugbjerg (2007), Moestrup et al. (2008); (10) Lindberg et al. (2005), Moestrup et al. (2006, 2008), Moestrup and Daugbjerg (2007); (11) Kremp et al. (2005), Moestrup and Daugbjerg (2007), Moestrup et al. (2008).

Class Dinophyceae (Butschli 1885) Pascher 1914

Order Gymnodiniales Apstein 1909

Family Gymnodiniaceae (Bergh 1881) Lankester 1885

Paragymnodinium n. gen. Kang, Jeong, Moestrup, and Shin

Diagnosis. Dinoflagellates with very thin transparent polygonal amphiesmal vesicles arranged in longitudinal rows. An anterior furrow or line absent, but a furrow extends ventrally from the cingulum to near the apex. Nuclear envelope chambers and nuclear fibrous connective absent. Cells possess chlorophyll-*a* and chlorophyll-*c2*. The major carotenoid is peridinin and cells also contain diadinoxanthin, diatoxanthin, and β–carotene. Cells possess nematocysts and trichocysts, but lacks taeniocysts, posterior vacuoles, and stylet. Mixotrophic.

Etymology: From *para*, Gr. – beside, combined with *Gymnodinium*. Gender: neutral

Type Species. *Paragymnodinium shiwhaense*

Paragymnodinium shiwhaense n. sp.

Diagnosis. Episome somewhat conical, smaller than the hemispherical hyposome. There is a wide and distinctive descending cingulum, which is displaced by 0.2-0.3 x cell length. The sulcus becomes wider toward the antapex. In transverse sections, the episome is almost round, while the hyposome is dorsoventrally slightly flattened. Cell length and width of cells growing photosynthetically 8.4-15.2 μm and 5.2-11.6 μm, respectively, but cells fed with *Amphidinium carterae* 8.4-19.3 μm and 6.1-16.0 μm, respectively. The ratio of cell length to cell width of live cells fed with *A. carterae*, 0.7-1.7, and that of live photosynthetically growing cell, 1.1-1.8. The nucleus was oval and located in the center or dorsal side of the cell. The chloroplasts were located in the cell periphery or near the nucleus. The amphiesmal vesicles were arranged in 16 rows; 6 rows on

the episome, 5 rows in the cingulum, and 5 rows on the hyposome. Peduncle present but eyespot, pusule, and pyrenoid absent.

Etymology. The specific epithet "*shiwhaense*" refers to the location where this species was first collected.

Type locality. Shiwha Bay, Korea (37°18' N, 126° 36'E).

Deposition of type material. A holotype slide as USNM slide 2052403 of cells fixed with 4% (v/v) glutaraldehyde has been deposited in the Protist Type Specimen Slide Collection, US Natural History Museum, Smithsonian Institution, Washington, DC, USA.

Gene sequence. The rDNA gene sequence - GenBank Accession No. AM408889.

Chapter 4: *Gyrodiniellum shiwhaense* n. gen., n. sp., A new planktonic heterotrophic dinoflagellate from the coastal waters of western Korea: Taxonomy

4.1 Abstract

The heterotrophic dinoflagellate *Gyrodiniellum shiwhaense* n. gen., n. sp. is described from live cells and from cells prepared for light, scanning electron, and transmission electron microscopy. Also, sequences of the small subunit (SSU) and large subunit (LSU) of rDNA have been analyzed. The episome is conical, while the hyposome is ellipsoid. Cells are covered with polygonal amphiesmal vesicles arranged in 16 horizontal rows. Unlike other *Gyrodinium*-like dinoflagellates, the apical end of the cell shows a loop-shaped row of five elongate amphiesmal vesicles. The cingulum is displaced by 0.3–0.5 x cell length. Cells that were feeding on the dinoflagellate *Amphidinium carterae* Hulburt were 9.1–21.6 μm long and 6.6–15.7 μm wide. Cells of *G. shiwhaense* contain nematocysts, trichocysts, a peduncle, and pusule systems, but they lack chloroplasts. The SSU rDNA sequence is >3% different from that of the six most closely related species: *Warnowia* sp. (FJ947040), *Lepidodinium viride* Watanabe, Suda, Inouye, Sawaguchi & Chihara, *Gymnodinium aureolum* (Hulburt) Hansen, *Gymnodinium catenatum* Graham, *Nematodinium* sp. (FJ947039), and *Gymnodinium* sp. MUCC284 (AF022196), while the LSU rDNA is 11–12% different from that of *Warnowia* sp., *G. aureolum,* and *Nematodinium* sp. (FJ947041). The phylogenetic trees show that the species belongs in the *Gymnodinium* sensu stricto clade. However, in contrast to *Gymnodinium* spp., cells lack nuclear envelope chambers and a nuclear fibrous connective. Unlike *Polykrikos* spp., cells of which possess a taeniocyst–nematocyst complex, *G. shiwhaense* has nematocysts but lacks taeniocysts. It differs from *Paragymnodinium shiwhaense* Kang, Jeong, Moestrup & Shin by possessing nematocysts with stylets and filaments. *Gyrodiniellum shiwhaense* n. gen., n. sp. furthermore lacks ocelloids, in

contrast to *Warnowia* spp., *Nematodinium* spp., and *Proterythropsis* spp. Based on morphological and molecular data, I suggest that the taxon represents a new species within a new genus.

4.2 Key words

Heterotrophy, LSU, Nematocyst, Peduncle, Protist, SSU, Taxonomy

4.3 Introduction

Heterotrophic dinoflagellates are ubiquitous protists in marine environments and play diverse ecological roles in marine plankton food webs (Jeong 1999; Jeong et al. 2010c; Lessard 1991; Sherr and Sherr 2007); they feed on a diverse array of prey (Hansen 1991; Jeong 1994; Menden-Deuer et al. 2005; Park et al. 2007) and in turn serve as prey for diverse predators (Gransden and Lewitus 2003; Jeong et al. 2004a; Stoecker et al. 2002). To understand the structure and function of the marine ecosystems, it is important to identify heterotrophic dinoflagellates, describe their diversity, and explore their role in marine food webs.

During the last decade, 8 new genera of heterotrophic dinoflagellates have been described: *Cabra* Murray & Patterson (Murray and Patterson 2004), *Cryptoperidiniopsis* Steidinger, Landsberg, Mason, Wolfgang, Vogelbein, Tester & Litaker (Steidinger et al. 2006), *Lessardia* Saldarriaga & Taylor (Saldarriaga et al. 2003), *Luciella* Mason, Jeong, Litaker, Reece & Steidinger (Mason et al. 2007), *Pseudopfiesteria* Litaker, Steidinger, Mason, Shields & Tester (Litaker et al. 2005), *Rhinodinium* Murray, Hoppenrath, Yoshimatsu, Toriumi & Larsen (Murray et al. 2006), *Stoeckeria* Jeong (Jeong et al. 2005b), and *Tyrannodinium* Calado, Craveiro, Daugbjerg & Moestrup (Calado et al. 2009). They are all peridinioid.

Recently, I found a new heterotrophic dinoflagellate in Shiwha Bay, Korea. It has thin amphiesmal plates similar to those of woloszynskioid dinoflagellates.

However, it lacks the Apical Line of narrow Plates (ALP) or the Pair of Elongate amphiesmal Vesicles (PEV) of many woloszynskioids. Instead, it has a loop-shaped apical "acrobase" like *Gymnodinium* spp. However, cells possess nematocysts unlike *Gymnodinium* spp. Such structures are found only in the genus *Paragymnodinium* and in some polykrikoid and warnowiid genera (Greuet 1987; Hoppenrath et al. 2009a, 2009b; Hoppenrath and Leander 2007a, 2007b; Kang et al. 2010; Marshall 1925; Westfall et al. 1983). Below I present a description of the morphology of the flagellate, which I describe as *Gyrodiniellum shiwhaense* n. gen., n. sp. using light microscopy, scanning electron microscopy (SEM), and transmission electron microscopy (TEM), combined with sequencing of the small subunit (SSU) rDNA, the internal transcribed spacers including ITS 1, 5.8S rDNA, and ITS2, and the large subunit (LSU) rDNA, all based on cells established in culture.

4.4 Materials and methods

4.4.1 Collection and culturing of *Gyrodiniellum shiwhaense* n. gen., n. sp.

Plankton samples collected with water samplers were taken from Shiwha Bay, Korea (37° 18' N, 126° 36' E), during September 2009 when the water temperature and salinity were 24.5 ^{o}C and 24, respectively. The samples were filtered gently through a 154-μm Nitex mesh and placed in 6-well tissue culture plates. A clonal culture of *G. shiwhaense* was established following two serial single-cell isolations. The mixotrophic dinoflagellate *Amphidinium carterae* was provided as prey at a concentration of 5,000-8,000 cells ml^{-1}. As the concentration of *G. shiwhaense* increased, cells were transferred to 32, 270, and 500-ml polycarbonate (PC) bottles containing fresh cultures of *A. carterae*. The bottles were filled to capacity with filtered seawater, capped, and placed on a rotating wheel at 0.9 rpm at 20 ^{o}C under an illumination of 20 μmol m^{-2} s^{-1} of cool white fluorescent light in a 14:10 h light–dark cycle. Once dense cultures of *G. shiwhaense* were obtained, they were

transferred daily to 500-ml PC bottles of fresh cultures of *A. carterae* containing ca. 20,000 cells ml^{-1}.

4.4.2 Morphology

The morphology of *Gyrodiniellum shiwhaense* n. gen., n. sp. was examined with a compound microscope, SEM, and TEM. I measured cell length and cell width of live vegetative flagellated cells, some fed *A. carterae* and some starved for 3 d, using an image analysis system on images taken on a compound microscope (Ziess-Axiovert 200M, Carl Zeiss Ltd,. Göttingen, Germany).

For SEM, a 20-ml aliquot of a dense culture of *Gyrodiniellum shiwhaense* was fixed for 1 h with osmium tetroxide (final concentration = 2%, w/v) in seawater. The fixed cells were collected on a 3-μm pore size, polycarbonate membrane filter without additional pressure and rinsed 3 times with distilled water to remove the salt. They were dehydrated in an ethanol series, and dried using a critical point dryer (BAL-TEC, CPD 300, Balzers, Liechtenstein). The dried filters were mounted on a stub and coated with gold-palladium. Cells were viewed with a FE-SEM (S-4800, HITACHI, Hitachinaka, Japan).

For TEM, cells from a dense culture were transferred to a 10-ml tube and fixed in 2.5% (v/v) glutaraldehyde (final concentrations) in culture medium. After 1.5-2 h, the contents of the tube were placed in a 10-ml centrifuge tube and concentrated at 1,610 *g* for 10 min in a Vision Centrifuge VS-5500 (Vision Scientific Company., Bucheon, Korea). A pellet from the tube was subsequently transferred to a 1.5-ml tube and rinsed in 0.2 M sodium cacodylate buffer at pH 7.4. After several rinses in 0.2 M sodium cacodylate buffer, the cells were postfixed for 90 min in 1% (w/v) osmium tetroxide in deionized water. The pellet was then embedded in agar. Dehydration was in a graded ethanol series (50, 60, 70, 80, 90, and 100% ethanol, followed by two changes in 100% ethanol). The material was embedded in Spurr's low-viscosity resin (Spurr 1969). Sections were prepared on a

RMC MT-XL ultramicrotome (Boeckeler Instruments Inc., Tucson, AZ, USA) and stained with 3% (w/v) aqueous uranyl acetate followed by lead citrate. The sections were viewed with a JEOL-1010 transmission electron microscope (JEOL Ltd., Tokyo, Japan).

4.4.3 DNA extraction, PCR amplification, sequencing, and data analysis

Approximately 20 ml of a dense culture of *Gyrodiniellum shiwhaense* n. gen., n. sp. was concentrated by centrifugation at 2,190 *g* for 5-10 min at room temperature, and the pellet was transferred to a 1.5 ml tube and resuspended in Tris-ethylenediaminetetraacetic acid (TE) buffer. Sodium dodecyl sulfate (final conc. 0.5% (w/v)) and proteinase K (final conc. 0.1 mg ml^{-1}) were added, and the mixture was incubated at 37 °C for 1 h. DNA was extracted by adding 800 µl of phenol:chloroform:isoamyl alcohol (25:24:1) to the incubated material and the residual phenol was removed by adding 700 µl of chloroform:isoamyl alcohol (24:1). Extracted DNA was precipitated by adding isopropyl alcohol and washed in cold 70% ethanol. DNA yield was quantified with a spectrophotometer. The extracted DNA was divided into two PCR tubes, and two independent PCR reactions were conducted. The small subunit (SSU) rDNA was amplified using eukaryotic primers (forward: 5′-AAC CTG GTT GAT CCT GCC AGT-3′; reverse: 5′-TGA TCC TTC TGC AGG TTC ACC TAC-3′) and approximately 900 bp of the large subunit (LSU) rDNA were amplified using forward primer Dino 1500F (5'-GTT GTT GCG GTT AAA AAG C-3') and reverse primer LSUB (5'-ACG AAC GAT TTG CAC GTC AG-3'), following Medlin et al. (1988). The 50-µl PCRs were mixed with the following reactants: 1X PCR buffer with 1.5 mM $MgCl_2$, 0.2 mM dNTP, 0.5 µM each primer, 5U of Taq DNA polymerase (Bioneer, Daejeon, Korea), and 200 ng template DNA. The PCR reactions were performed under the following conditions: 1 initial denaturating step of 3 min at 94 °C, 40 cycles of 45 s at 95 °C, 1 min at 55 °C, and 3 min at 72 °C in series, and then 1 extension at 72 °C for 5 min in a GeneAmp PCR System 2700 (Perkin-Elmer, Boston, USA). PCR products were

cloned into the pCR®2.1-TOPO® vector using the TA Cloning® Kit (Invitrogen, Carlsbad, USA). The cloned material was incubated in liquid LB medium at 37 °C overnight. Plasmids were extracted using the AccuPrep® Plasmid Extraction Kit (Bioneer, Daejeon, Korea). The presence of inserts in the plasmids was ascertained by adding *Eco*RI restriction endonuclease (Promega, Madison, USA) into the extracted plasmids. To determine the sequence of internal fragments within the inserts, the reverse primer Euk1209R (5′-GGG CAT CAC AGA CCT G-3′) and ITSR2 (5′-TCC CTG TTC ATT CGC CAT TA-3′) were used. Sequencing the SSU rDNA and LSU rDNA was performed in both directions using an ABI PRISM® 3700 DNA Analyzer (Applied Biosystems, Foster City, USA). All sequences were aligned using the ContigExpress alignment program (InforMax, Frederick, USA).

4.4.4 Sequence availability and phylogenetic analysis

The SSU and LSU rDNA sequences of *Gyrodiniellum shiwhaense* n. gen., n. sp. were added to aligments comprising diverse assemblages of other dinoflagellates available in GenBank (Table 3.1). The sequence for the nuclear SSU rDNA were aligned by eye using the Genetic Data Environment (GDE 2.2) program (Smith et al. 1994), with the alignment based on secondary structure using the nuclear SSU rDNA of *Karenia brevis* (C.C. Davis) G. Hansen & Moestrup (Wuyts et al. 2001) as a guide. The entire conserved areas of the nuclear SSU rDNA genes were readily alignable across taxa and were used for phylogenetic analyses. The sequence for the nuclear LSU rDNA was also aligned manually using the Genetic Data Environment (GDE 2.2) program. For Bayesian analyses, I performed a likelihood ratio test using MODELTEST 3.7 (Posada and Crandall 1998) to determine the best available model for the SSU and LSU rDNA data. The selected models were a TrN+I+ Γ model with a gamma correction for among-site rate variation (SSU; α=0.6944, LSU; α=0.7368) and invariant sites (SSU; I = 0.4378, LSU;I=0.1766). Bayesian analyses were run using an MrBayes 3.1.2 version (Huelsenbeck and Ronquist 2001). Four independent Markov chain Monte Carlo simulations were run simultaneously for 2,000,000 generations and trees were sampled every 1,000

generations and the first 800 trees were deleted to ensure that the likelihood had reached convergence. A majority-rule consensus tree was created from the remaining 1,201 trees in order to examine the posterior probabilities of each clade.

Maximum likelihood. The ML phylogenetic analyses were done using the RAxML 7.0.4 program (Stamatakis 2006) with the general time reversible (GTR) + Γ model. I used 200 independent tree inferences using -# option of the program to identify the best tree. Bootstrap values (MLBS) were calculated using 1,000 replicates and the same substitution model.

4.5 Results

4.5.1 Morphology

The episome is conical with convex sides, and is slightly larger than the ellipsoid hyposome (Fig. 4.1A-B). There is a distinct loop-shaped apical row of amphiesmal vesicles (LAV) (Fig. 4.1B-E, 4.2A, 4.2C). The wide (1.8-4.1 μm), distinct, descending cingulum is displaced by 0.3-0.5 x cell length (Fig. 4.1D). A distinct ventral ridge is located above the right side of the cingulum (Fig. 4.1A, 4.1D, 4.14B). It extends in the antapical direction towards the left, and thus the cingulum and the sulcus form a distinct S-shape in ventral view (Fig. 4.1D). The sulcus extends from the antapex to the episome, forming an extension on the episome. The sulcal extension narrows slightly towards the apex, connecting here to the left end of the apical groove (Fig. 4.1A, 4.1C-D, 4.2A-B). The sulcus widens toward the antapex (Fig. 4.1A, 4.1D, 4.2D).

The ranges (mean $\pm$ standard error, n=92) of cell length and cell width of living cells starved for 3d were 5.9-13.7 μm (10.2$\pm$0.25) and 5.2-10.8 μm (7.7$\pm$0.2), respectively, while live cells fed *Amphidinium carterae* (n=120) measured 9.1-21.6 μm (14.2$\pm$0.27) and 6.6-15.7 μm (11.0$\pm$0.23), respectively. However, the ratio of cell length to cell width of cells starved for 3d (mean $\pm$ standard error = 1.3 $\pm$ 0.03;

range = 1.0-1.8, n=92) was similar to those of cells fed *A. carterae* (mean ± standard error = 1.3 ±0.02; range = 1.1-1.6, n=120).

Cells are covered with hexagonal or pentagonal amphiesmal vesicles (AVs). The length of each side of a hexagonal or pentagonal AV was ~1-2.5 μm. The AVs were arranged in 16 rows: 6 rows on the episome, 5 rows in the cingulum, and 5 rows on the hyposome (Fig. 4.3A, 4.4A-D, 4.5A, 4.6A-D). The total number of AV was ~260. The sulcal extension comprised 7 AVs (Fig. 4.2A-B). Its length was ~5 μm, and the width ~1.5 μm. The loop-shaped row of amphiesmal vesicles (LAV) was composed of 5 AVs [i.e. CR (central ridge) 1-5 in Fig. 4.3C], and surrounded on each side by an indistinct groove (Fig. 4.3A-B). The amphiesmal plates of the apical groove displayed many small knobs: ~ 8, 12, 12, 22, and 18 on CR 1, 2, 3, 4, and 5, respectively (Fig. 4.3C-D, 4.6E). The LAV enclosed an area of 11 AVs (A1-11) (Fig. 4.3C, 4.6E). Of the five horizontal rows of AVs in the cingulum, one row covered the cingulum ceiling (CC), three rows were present in the middle (C1-3), and the last row covered the cingulum floor (CF) (Fig. 4.4B-C, 4.6B). The hyposome comprised five horizontal rows of AVs (Fig. 4.4C-D, 4.5A, 4.6B, 4.6D). Each AV in the hyposome had 5-10 straight lines (SL1-7 in Fig. 4.5A-B). The sulcus comprised ~20 AVs arranged in 4-5 longitudinal rows (S1-S5) (Fig. 4.5C-D).

Longitudinal TEM sections showed the main features of the cell, such as the nucleus (N), Golgi apparatus (G), lipids (L), mitochondria (M), membrane-like lamellae (MLL), nematocysts (NE), fibrous vesicles (F), the pusule system (PS), and trichocysts (T) (Fig. 4.7A-B).

The nucleus, ovoid and located in the right side of the cell, extended from the episome to hyposome (Fig. 4.7A). It contained many chromosomes, each measuring ca. 2 μm x 0.5 μm x 0.5 μm (Fig. 4.7A-B, 4.8A). The length and width of the nucleus were ~1/2 and 1/3 of the whole cell, respectively (Fig. 4.7A).

Table 3.1 List of species used in constructing phylogenetic trees. GenBank accession numbers are listed to the right of each species

Taxon	SSU rDNA Accession no.	LSU rDNA Accession no.
Akashiwo sanguinea		AF260397
Babesia microti	AB219802	
Baldinia anauniensis	EF052682	EF052683
Bernardinium bernardinense		DQ289020
Biecheleria baltica	EF058252	EF205019
Biecheleria cincta		FJ024705
Biecheleria pseudopalustris		AF260402
Biecheleriopsis adriatica		EU857537
Borghiella dodgei		EU126801
Borghiella tenuissima		AY571374
Cochlodinium polykrikoides		EF506627
Cochlodinium fulvescens		AB295051
Gymnodinium aureolum		AF200670
Gymnodinium catenatum		AF200672
Gymnodinium cf. placidum		AF260383
Gymnodinium dorsalisulcum		
Gymnodinium fuscum		AF200676
Gymnodinium impudicum		AF200674
Gymnodinium microreticulatum	AB265964	AY036078
Gymnodinium nolleri	AB265963	AF200673
Gymnodinium palustre		AF260382
Gymnodinium sp.		EF192412 FJ21138
Gymnodinium venator		AY455681
Gyrodinium dominans		AY571370
Gyrodinium dorsum	AF274261	
Gyrodinium fusiforme	AB120002	
Gyrodinium helveticum	AB120004	

Gyrodinium instriatum	AY443015	
Gyrodinium rubrum	AB120003	AY571369
Gyrodinium spirale	AB120001	AY571371
Gyrodinium uncatenum	AF274263	AY916541
Gyrodiniellum shiwhaense	FR720082	FR720082
Heterocapsa rotundata		AF260400
Jadwigia applanata	EF058240	AY950447
Karenia asterichroma		AY590123
Karenia bidigitata		AY947662
Karenia brevis	AJ415518	AF200677
Karenia brevisulcata		AY243032
Karenia mikimotoi	Af022195	AF200678
Karenia papilionacea		AY590124
Karenia selliformis		U92250
Karenia umbella		AY263962
Karlodinium armiger		DQ114467
Karlodinium australe		DQ151559
Karlodinium veneficum	AJ415516	AF200675
Lepidodinium chlorophorum		EF010974
Lepidodinium viride	AF022199	
Nematodinium sp.	FJ947038, FJ947039	FJ947041
Paragymnodinium shiwhaense	AM408889	AM408889
Pelagodinium beii	U41087	
Peridinium willei		AF260384
Pheopolykrikos beauchampii		EF616463
Polarella glacialis	EF417317	AY571373
Polykrikos hartmannii	AY421789	AY526521
Polykrikos herdmanae	DQ975470	
Polykrikos kofoidii		EF192411 FJ947043
Polykrikos lebourae	DQ975472	FJ947044

Polykrikos schwartzii		EF192408
Proterythropsis sp.	FJ947036, FJ947037	
Protodinium simplex	U41086	
Sarcocystis muris	M64244	
Symbiodinium californium	AF225965	
Symbiodinium corculorum	L13717	
Symbiodinium meandrinae	L13718	
Symbiodinium pilosum	X62650	
Symbiodinium sp.	AY443023	
Takayama helix		AY284950
Takayama pulchella	AY800130	U92254
Takayama tasmanica		AY284948
Togula britannica		AY455679
Togula compacta		AY568562
Togula jolla		AY455680
Tovellia coronata		AY950445
Tovellia leopoliensis	AY443025	
Tovellia sanguinea		DQ320627
Toxoplasma gondii	U00458	
Warnowia sp.	FJ947040, FJ947046	FJ947042
Woloszynskia pascheri	EF058253	EF058276
Woloszynskia sp.		EF616464
Uncultured eukaryote	AY664896, AY664911 AY664912, AY664914 AY664983, AY665026	

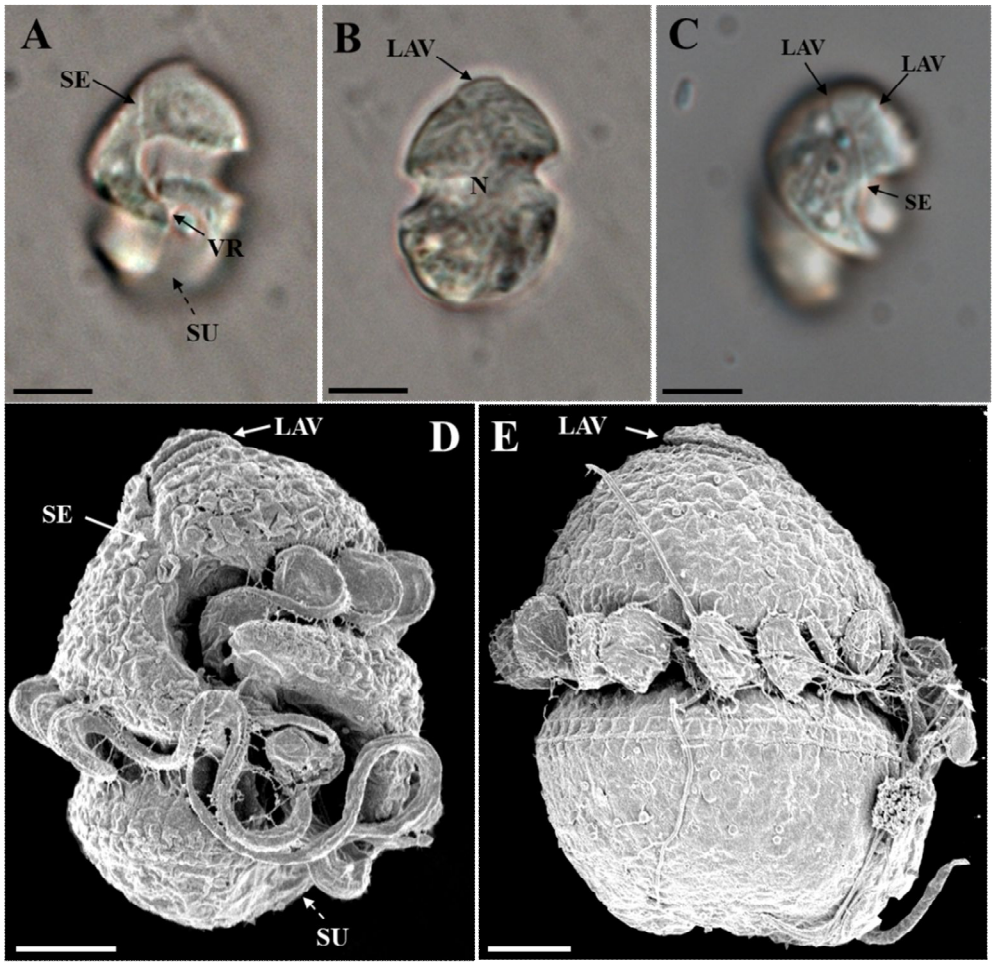

Fig. 4.1 Micrographs of *Gyrodiniellum shiwhaense* n. gen., n. sp. showing the whole cell. **A-C.** Micrographs taken using light microscopy. **A.** Ventral view of cell, showing sulcal extension (SE) onto the episome, the ventral ridge (VR), and the sulcus (SU). **B.** Dorsal view of cell, showing the median position of the cingulum, the large nucleus (N), and the loop-shaped apical row of amphiesmal vesicles (LAV) (arrow). **C.** Lateral view showing LAV and SE. **D, E.** Micrographs taken using scanning electron microscopy. **D.** Ventral view of the cell, showing the conical episome and the ellipsoid hyposome, and illustrating LAV, SE, and SU. **E.** Dorsal view to show the median placement of cingulum, the transverse flagellum, and the LAV. Scale bars = 5μm for Fig. **A-C** and 2μm for Fig. **D, E**.

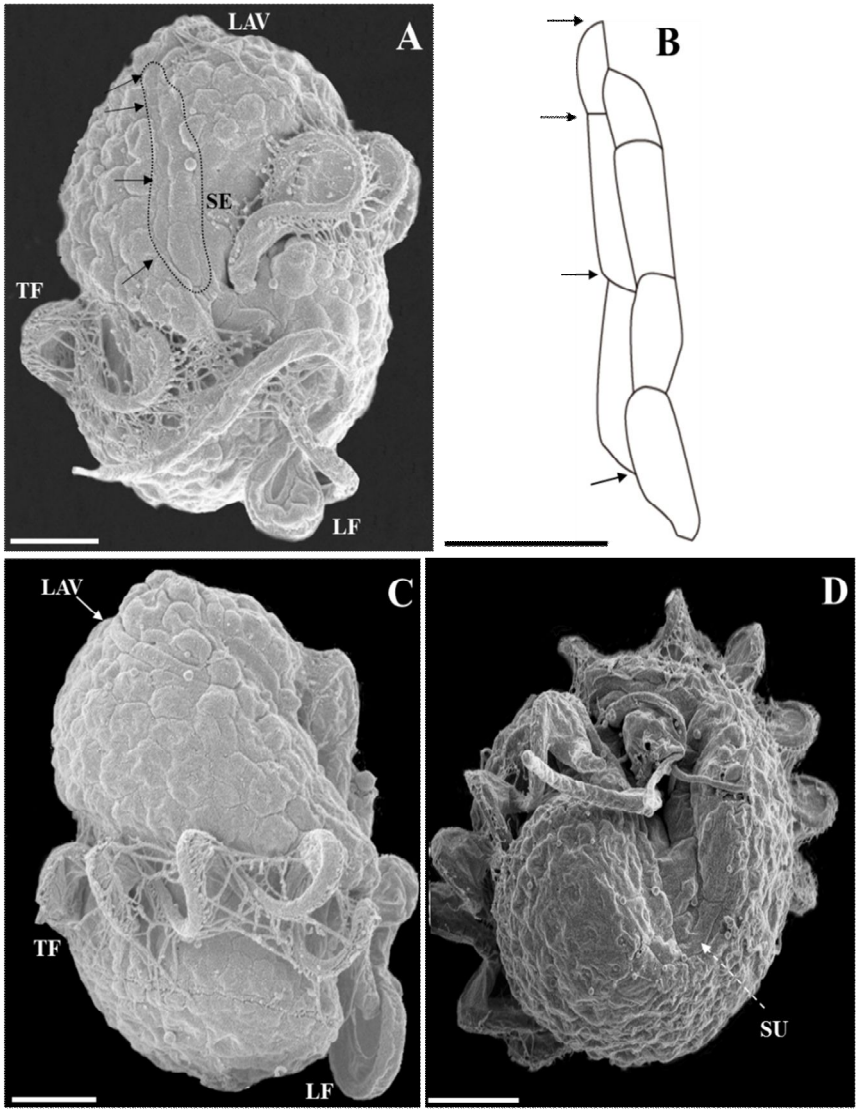

Fig. 4.2 Micrographs of *Gyrodiniellum shiwhaense* n. gen., n. sp. taken using scanning electron microscopy. **A.** Ventral view showing the sulcal extension (SE). The SE contains seven amphiesmal vesicles. Arrows indicate the borders between the amphiesmal vesicles. **B.** Reconstruction of SE with seven amphiesmal vesicles. **C.** Lateral view. **D.** Sulcal view. LAV, loop-shaped apical row of amphiesmal vesicles; LF, longitudinal flagellum; SU, sulcus; TF, transverse flagellum. Scale bars = 2 μm.

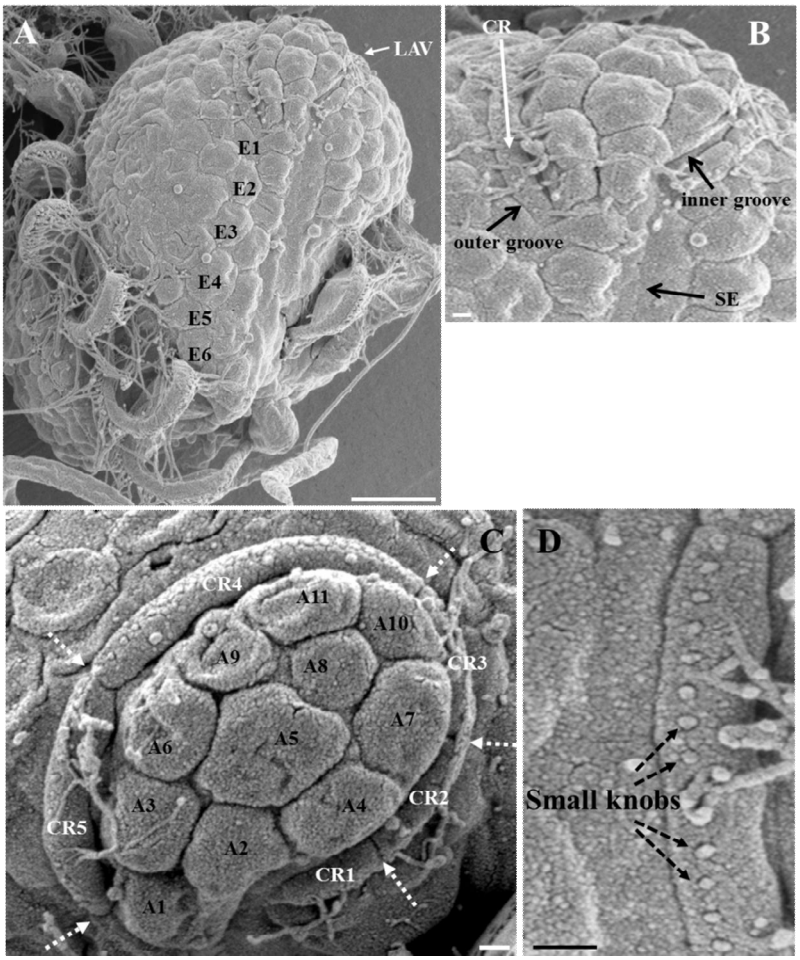

Fig. 4.3 Micrographs of *Gyrodiniellum shiwhaense* n. gen., n. sp. taken using scanning electron microscopy. **A.** Ventral–apical view. Note the presence of vesicles on cell surface arranged in six (E1–E6) latitudinal series and showing the loop-shaped apical row of amphiesmal vesicles (LAV). **B.** The central ridge (CR) of amphiesmal vesicles, sometimes seen to be lined by a narrow groove on each side. SE, sulcal extension. **C.** Micrograph of the amphiesmal vesicles (AVs) within the LAV of *G. shiwhaense*. There are 11 AVs (A1–A11) and the central ridge of 5 AVs (CR1–5). Dashed arrows indicate the point of contact between individual vesicles in the LAV. **D.** Micrograph showing small knobs (dashed arrows). Scale bars = 2 μm for Fig. **A** and 0.2 μm for Fig. **B-D.**

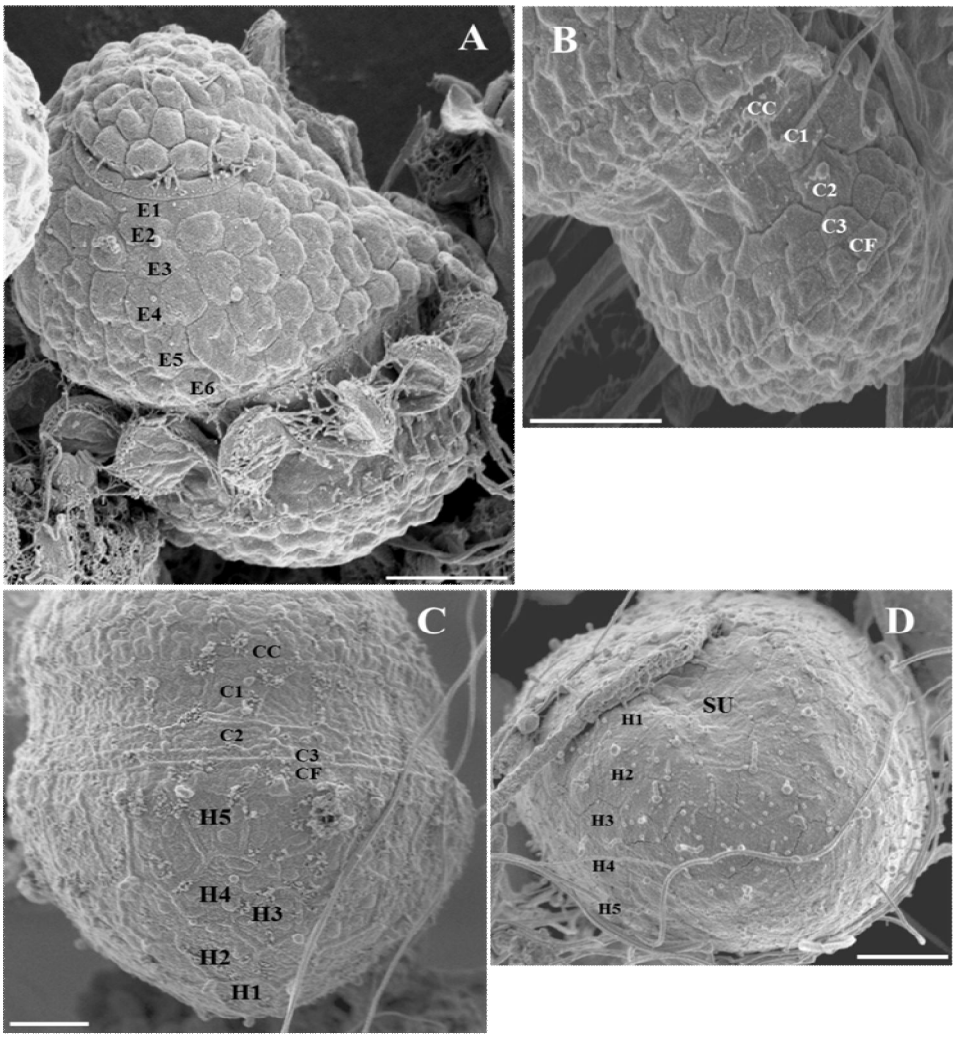

Fig. 4.4 Micrographs of *Gyrodiniellum shiwhaense* n. gen., n. sp. in the scanning electron microscope. **A.** Lateral view of the cell, showing six rows (E1-E6) of amphiesmal vesicles (AVs) on the episome. A narrow groove is visible on the apical side of the anterior loop-shaped structure. **B.** Lateral view of the cell showing five rows (cingulum ceiling [CC], C1-C3, cingulum floor [CF]) of AVs in the cingulum. **C.** Dorsal view of the cell showing five rows (CC, C1-C3, CF) of AVs in the cingulum and five rows (H1-H5) of AVs on the hyposome. **D.** Antapical view showing five rows (H1-H5) of AVs on the hyposome. SU, sulcus. Scale bars = 2 μm.

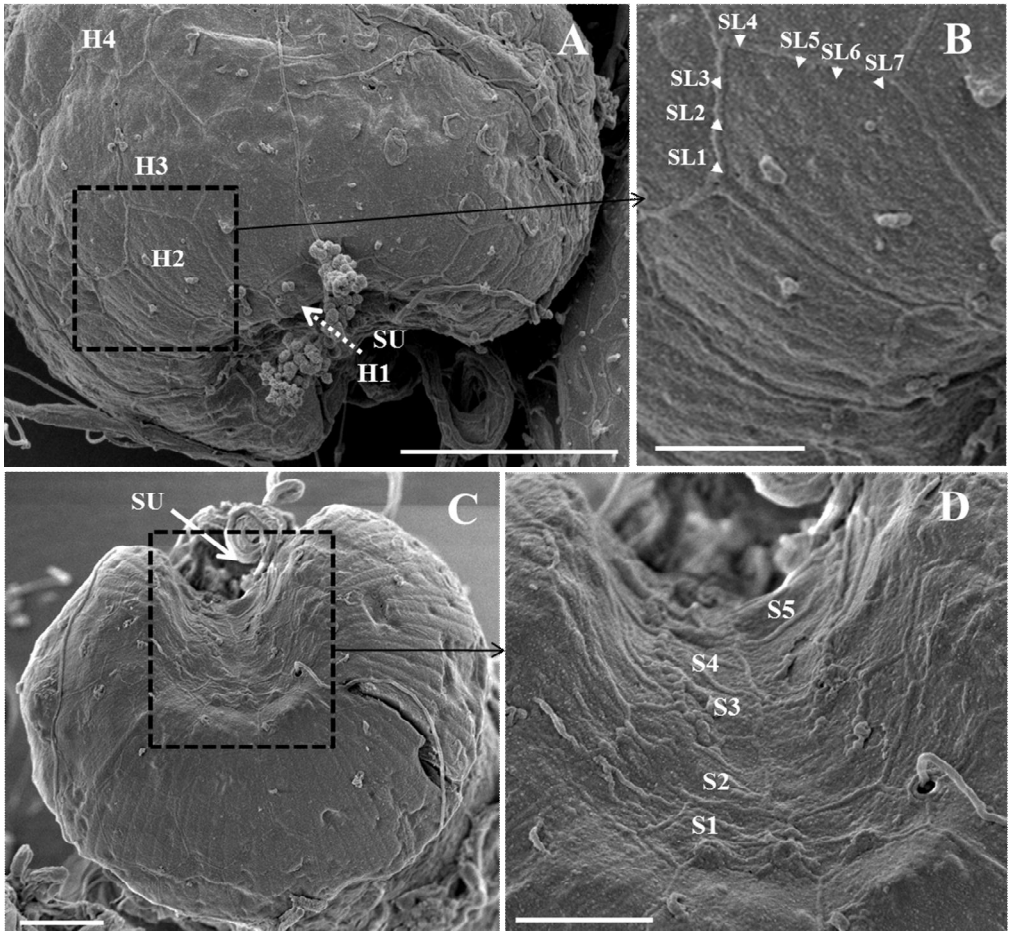

Fig. 4.5 *Gyrodiniellum shiwhaense* n. gen., n. sp. using scanning electron microscopy. **A.** Dorsal view of the hyposome showing four (H1-H4) hyposome amphiesmal vesicles (AVs). **B.** Enlarged part of Fig. **A** showing seven straight lines (SL1–SL7) (arrowheads). **C.** Antapical view. **D.** Enlargement from Fig. **C** showing five rows (S1–S5). SU, sulcus. Scale bars = 2 μm for Fig. **A, C** and 1 μm for Fig. **B, D.**

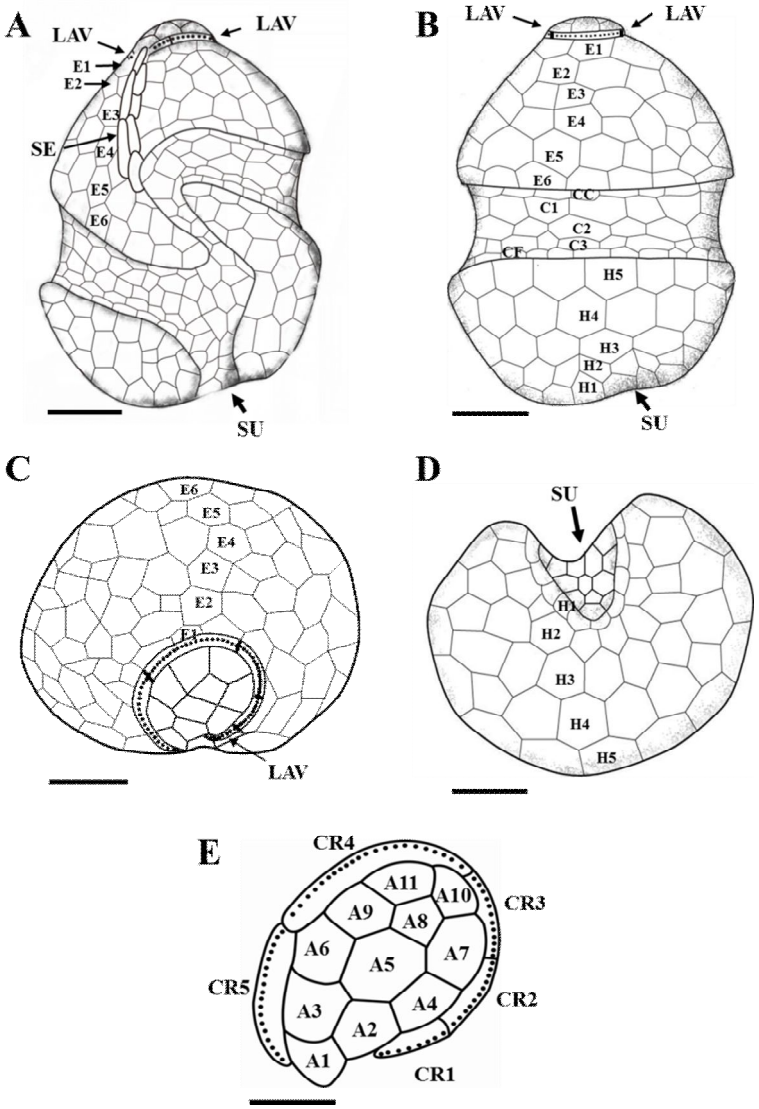

Fig. 4.6 Drawings of *Gyrodiniellum shiwhaense* n. gen., n. sp. to show the external morphology. **A.** Ventral view. **B.** Dorsal view. **C.** Apical view. **D.** Antapical view. **E.** Apical ring surrounding 11 amphiesmal vesicles. CC, cingulum ceiling; CF, cingulum floor; CR, central ridge; LAV, loopshaped apical row of amphiesmal vesicles; SE, sulcal extension; SU, sulcus; "E1–6," "H1–5," "A1–A11," and "CC–CF" indicate episomal, hyposomal, apical, and cingular amphiesmal vesicles, respectively. Scale bars = 2 μm for Fig. **A-D** and 1 μm for Fig. **E.**

The nuclear envelope (NU) possessed typical nuclear pores (NP), while nuclear chambers were absent (Fig. 4.8A-B). Variously-sized flagellar hairs (FH) were present in the perinuclear space (Fig. 4.8A, 4.8C). Inside the FHs, bundles of micro-fibrils were present (Fig. 4.8C). The length and width of the large FHs were ~1.2 μm and ~1.5 μm, respectively, while those of small FHs were ~ 0.1 μm and ~ 0.1 μm, respectively.

The pusule system (PS) was located near the sulcus (Fig. 4.9A). It was ca ~2.5 μm long and comprised a main collecting chamber (C) with associated spherical vesicles (SV) (Fig. 4.9B).

I examined the flagellar apparatus of several cells (Fig. 4.10, 4.11). The flagellar root system comprised a large multi-membered microtubular root (R1), located to the left of the longitudinal basal body (LB) (viewer's right) (Fig. 4.10A); the transverse basal body (TB) was located to the right of the LB (viewer's left) and TB and LB were inserted at an angle of approximately 150 ° to each other (Fig. 4.10B); two fibrous connectives – the C1 (LB/R1) and the C2 (LB/R1) – extended between R1 and adjacent triplets of the LB and R1 (Fig. 4.10D-G). The R2 was not observed; the R3 or transverse microtubular root was located to the right (viewer's left) of the TB (Fig. 4.10C, 4.10H); three basal body connectives (bbc), the bbc1, bbc2, and bbc3, interlinked the two basal bodies (Fig. 4.10H). The R4 consisted of a prominent striated fiber, the transverse striated root (TSR) with an associated single microtubule, the transverse striated root microtubule (TSRM) and was associated with the left proximal part of the TB (Fig. 4.11); the R1 and R4 roots were interlinked by a striated root connective (SRC) (Fig. 4.11B). The pusule system was usually observed near the flagellar appratus (Fig. 4.11A). I examined the space between nucleus and flagellar apparatus in many serial sections (> 50 cells), but no nuclear fibrous connective (NFC) was observed. Also, no eyespot was observed. In addition, a transverse microtubular root extension (TMRE) was not observed (Fig. 4.10-4.12).

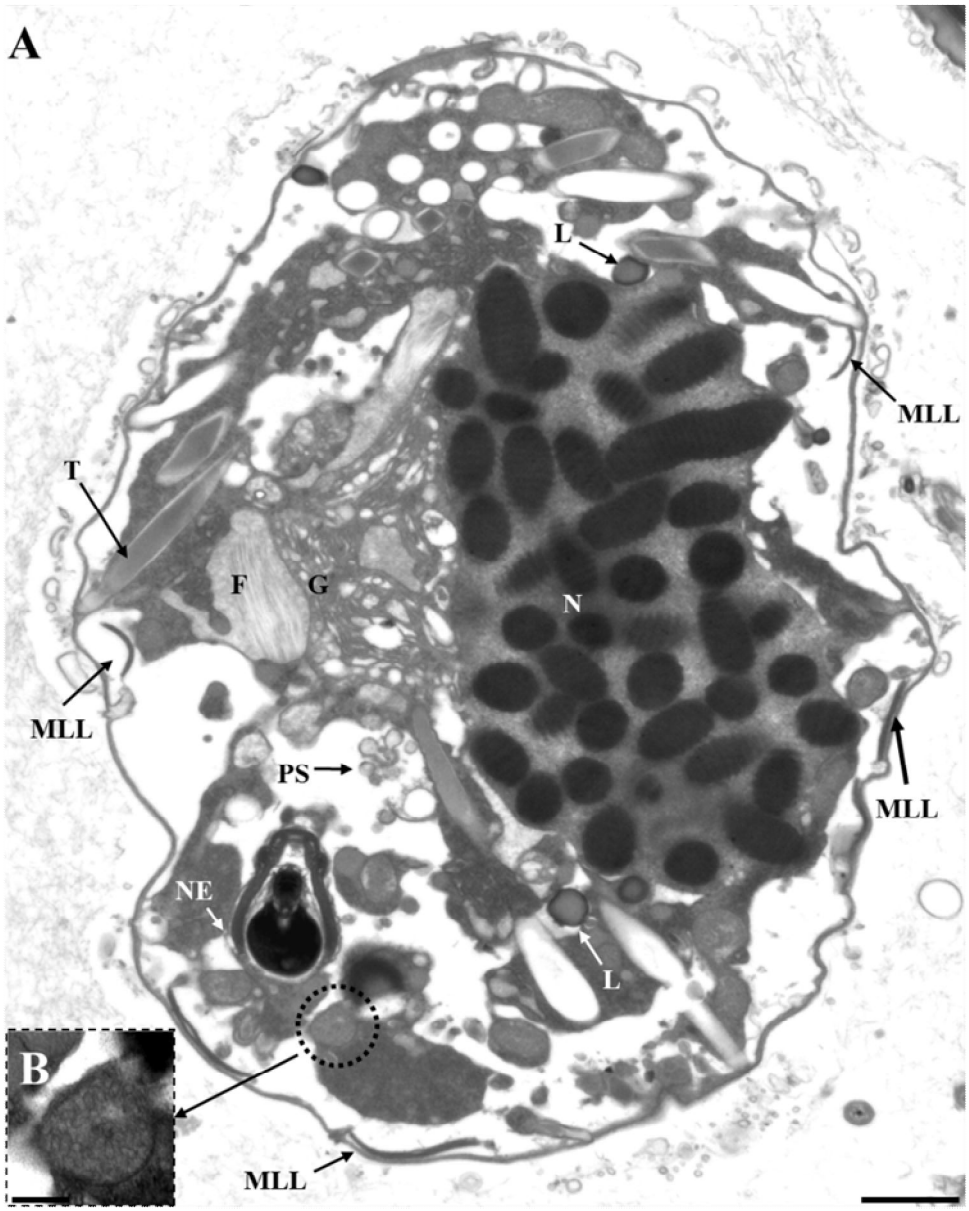

Fig. 4.7 *Gyrodiniellum shiwhaense* n. gen., n. sp. taken using transmission electron microscopy. **A.** Longitudinal section, which shows several organelles inside the protoplasm. **B.** Enlarged from mitochondrion. F, fibrous vesicle; G, Golgi body; L, lipid body; MLL, membrane-like lamellae; N, nucleus; NE, nematocyst; PS, pusule; T, trichocyst. Scale bar = 1 μm for Fig. **A** and 0.2 μm for Fig. **B**.

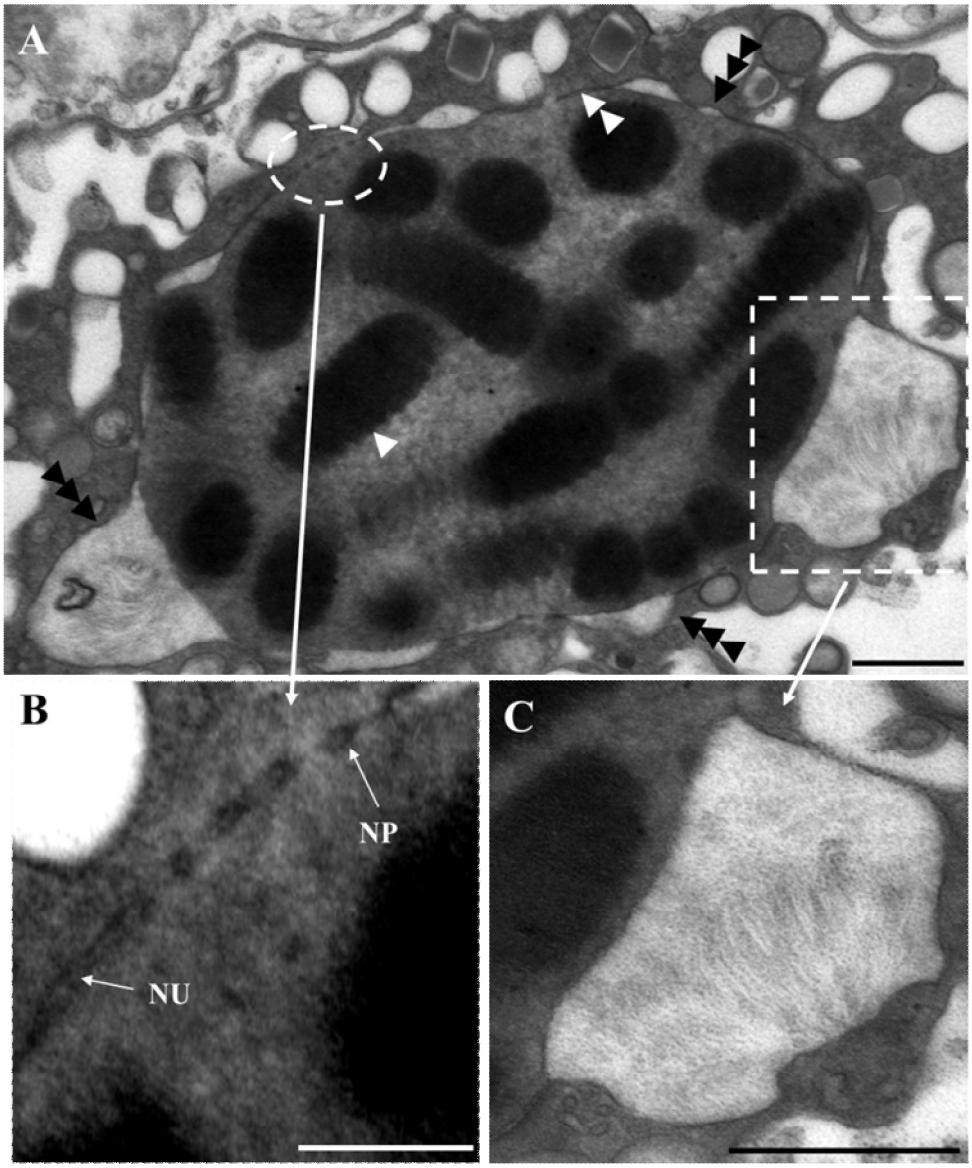

Fig. 4.8 *Gyrodiniellum shiwhaense* n. gen., n. sp., photographed using transmission electron microscopy. **A.** Micrograph showing a nucleus with condensed chromosomes (single arrowhead), nuclear envelope (double arrowhead), and diverse-sized putative flagellar hairs (FHs, triple arrow head). **B.** Enlarged from (**A**) for nuclear envelope (NU) and nuclear pore (NP). **C.** Enlarged from (**A**) for FHs. Scale bars = 0.5 μm for Fig. **A, C** and 0.2 μm for Fig. **B.**

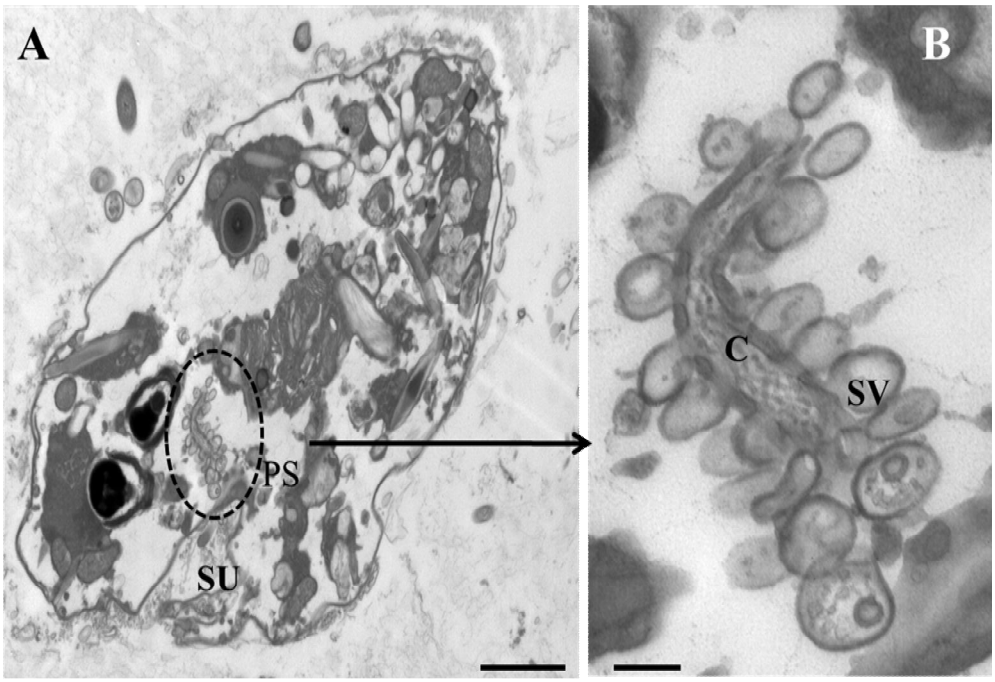

Fig. 4.9 *Gyrodiniellum shiwhaense* n. gen., n. sp., photographed using transmission electron microscopy. **A.** Micrograph showing pusule system (dashed circle). **B.** Enlarged view (**A**). C, collecting chamber; PS, pusule system; SU, sulcus; SV, spherical vesicle. Scale bars = 2 μm for Fig. **A** and 0.2 μm for Fig. **B.**

Several nematocysts were located near the surface (Fig. 4.13). Each nematocyst looked like a light bulb with an anterior operculum (OP), a capsule (CA) and an ovoid posterior chamber (PC) (Fig. 4.13, 4.19A). The length of the OP was ~0.3 μm, while the width at the top was ~0.2 μm, becoming wider (ca. 0.4 μm) toward the PC. The CA contained a stylet (ST) in an inner anterior chamber (AC) and a single filament (FI) in an external PC. The PC was 0.8 μm long, 0.37 μm wide near the OP, but 0.75 μm wide in the middle. The FI was connected to the AC (Fig. 4.13, 4.19A).

Taeniocysts and posterior vacuoles connected to nematocysts were not observed (Fig. 4.13, 4.19A). The complex of FI, PC, and ST is called as the posterior body. When ca. 160 TEM serial sections (70 nm layer serial sections, i.e. ca. 11 μm) from the top to the bottom of 1 *G. shiwhaense* cell were examined, 3 to 5 nematocysts were observed (not shown). The length and width of the nematocysts were ~1.8 μm and ~1.1 μm, respectively.

In SEM many cells displayed a protruded peduncle (PE) located between the exit points of the transverse (TF) and longitudinal flagellum (LF) (Fig. 4.14A). In addition, a ventral ridge (VR) was located at the right side of the PE (Fig. 4.14A-B). In the transversally sectioned TEM photos, the VR was located adjacent to a microtubular strand of the peduncle (MSP), and close to the LB and R1 (Fig. 4.14C). In the longitudinally sectioned TEM photos, the VR was located adjacent to a microtubular strand of the VR (MSVR) and TF (Fig. 4.14D). Based on these SEM and TEM micrographs, it is suggested that the VR may be often associated with elements of the flagellar apparatus and surround the exit point of the PE.

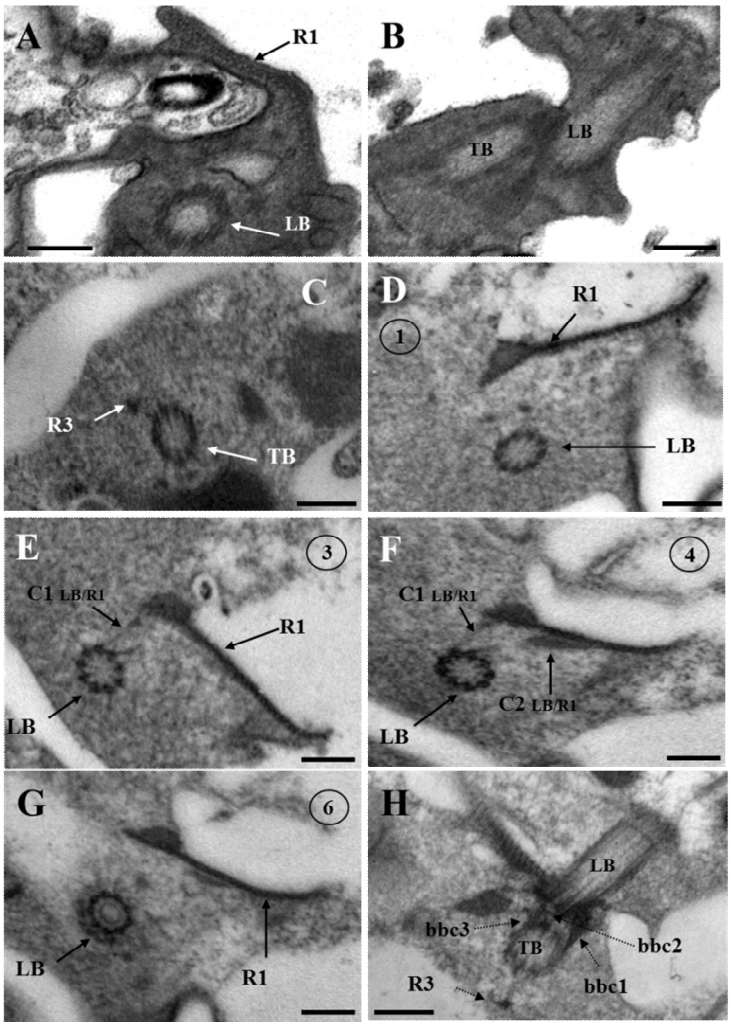

Fig. 4.10 Micrographs showing slightly oblique transverse sections of the flagellar apparatus of *Gyrodiniellum shiwhaense* n. gen., n. sp. **A**. Micrograph showing the multimembered microtubular root (R1) situated to the left of the longitudinal basal body (LB) (viewer's right). **B.** The transverse basal body (TB) and LB. **C.** Micrograph showing TB and Root 3 (R3) (viewer's left). **D-G**. $C1_{LB/R1}$ and $C2_{LB/R1}$ which interconnect the LB and R1; the circled number in each micrograph represents the number of a sequential section. **H.** Micrograph showing the relative positions of the TB, LB, bbc1, bbc2, bbc3, and R3. bbc, basal body connective. Scale bar = 0.2 μm.

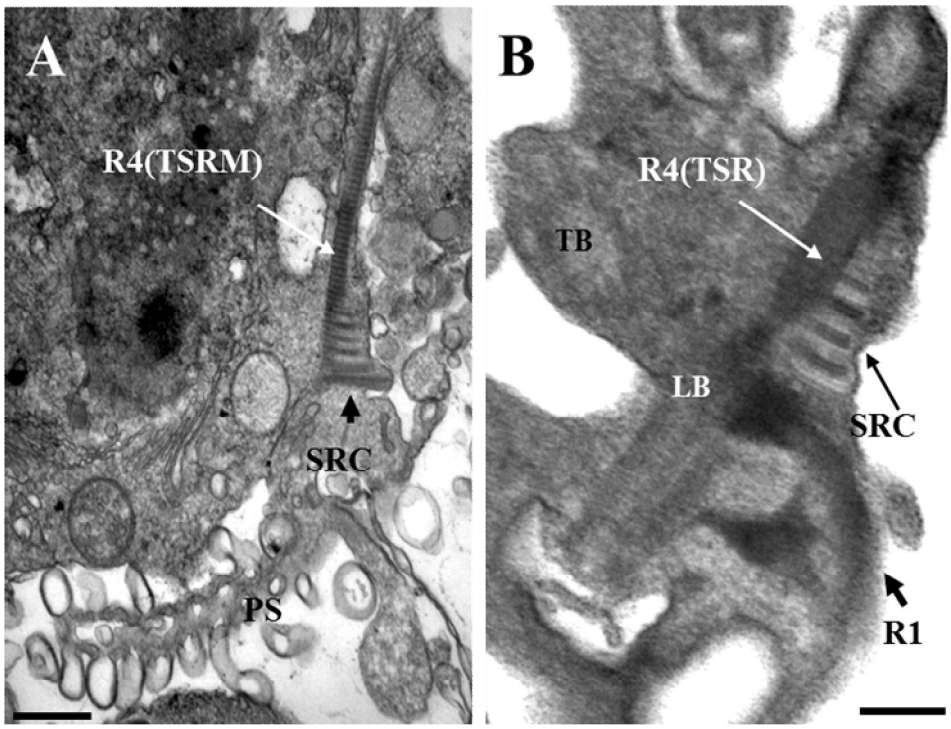

Fig. 4.11 Micrographs showing slightly oblique longitudinal sections of the flagellar apparatus and the relative positions of the longitudinal basal body (LB), transverse basal body (TB), Root1 (R1), Root 4 (transverse striated root+transverse striated root microtubule), striated root connectives (SRC) and pusule system (PS) of *Gyrodiniellum shiwhaense* n. gen., n. sp. **A.** Micrograph showing striated root connective (SRC), transverse striated root microtubule (TSRM), and pusule. **B.** Micrograph showing the transverse basal body (TB), longitudinal basal body (LB), multimembered microtubular root (R1), transverse striated root (TSR), and striated root connective (SRC). Scale bar = 0.2 μm.

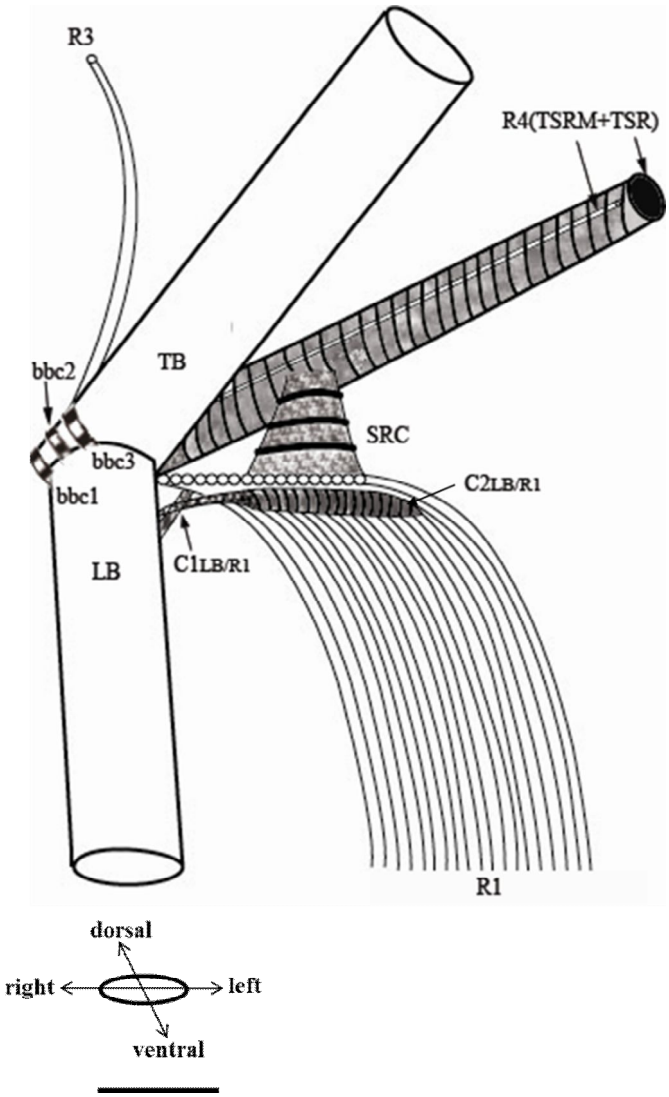

Fig. 4.12 Diagrammatic reconstruction of the flagellar apparatus of *Gyrodiniellum shiwhaense* n. gen., n. sp., based mainly on transverse serial sections (70-nm-thick sections). LB, longitudinal basal body; TB, transverse basal body; R1, root 1; R3, root 3; R4, root 4; SRC, striated root connective; $C1_{LB/R1}$, connective 1 linking LB and R1; $C2_{LB/R1}$, connective 2 linking LB and R1; bbc1, basal body connective 1; bbc2, basal body connective 2; bbc3, basal body connective 3; TSR, transverse striated root; TSRM, transverse striated root microtubule. Scale bars = 0.2 μm.

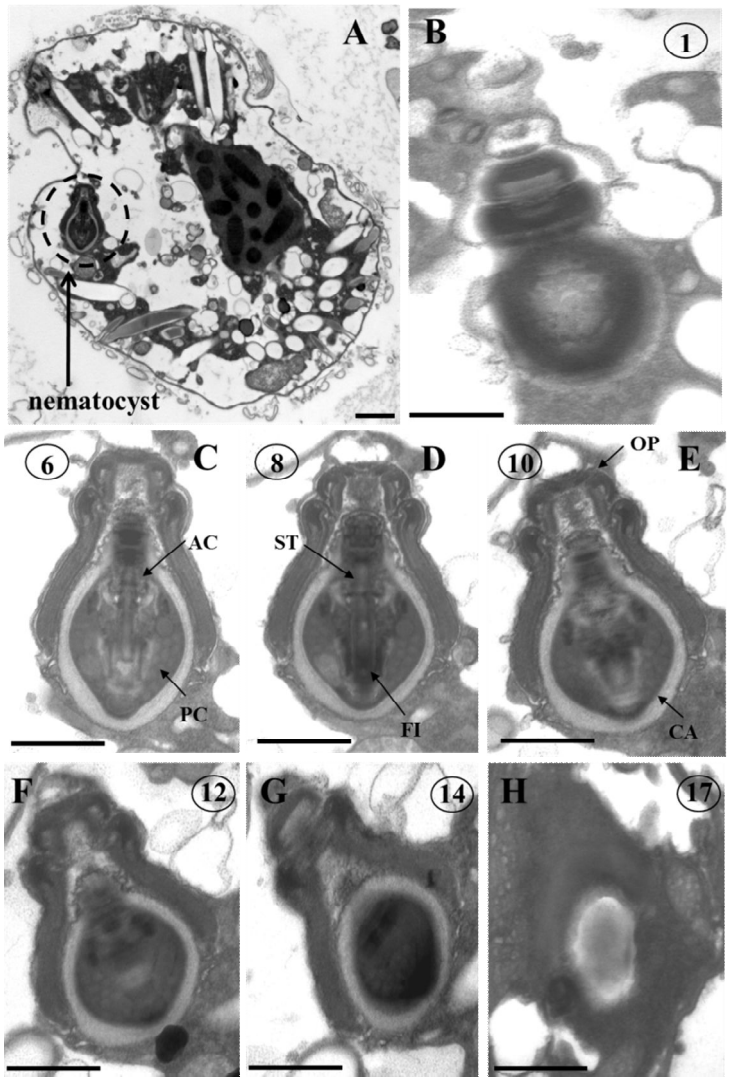

Fig. 4.13 Serial sections of *Gyrodiniellum shiwhaense* n. gen., n. sp. showing shape and position of the nematocysts, using transmission electron microscopy. Sections were 70 nm thick and the circled number in each figure is the section number. Each nematocyst possesses an operculum (OP), anterior chamber (AC), capsule (CA), filament (FI), posterior chamber (PC), and stylet (ST). The complex of FI, PC, and ST is called as the posterior body. There were no taeniocysts or posterior vacuoles. Scale bars = 1 μm for Fig. **A** and 0.5 μm for Fig. **B-H.**

Longitudinal TEM sections additionally showed membrane-like lamellae (MLL) underneath the surface (Fig. 4.15A-C). The length and width of a MLL were ~3 μm and ~0.1 μm, respectively (Fig. 4.15B-C). Numerous trichocysts, each ~4 μm long and ~0.4 μm wide, were located near the surface (Fig. 4.15A, 4.15D). Trichocysts were enveloped by a single membrane and were composed of a column-like body (CB) with a neck ending in an apical cap (Fig. 4.15D).

The morphology of the cell, including the positions of the internal organelles was reconstructed from analysis of ~150 longitudinal TEM serial sections (Fig. 4.16).

4.5.2 Gene sequence of *Gyrodiniellum shiwhaense* n. gen., n. sp. and phylogenetic analysis

The SSU, ITS1, ITS2, 5.8S, and LSU rDNA sequence (Genbank Accession No. FR720082) of this new isolate comprised 3,278 nucleotides. The SSU rDNA of *Gyrodiniellum shiwhaense* was approximately 3% different from that of *Warnowia* sp. (FJ947040), *Lepidodinium viride* (DQ499645), *Gymnodinium aureolum* (AY999082), *Gymnodinium catenatum* (DQ779990), *Nematodinium* sp. (FJ947039), and *Gymnodinium* sp. MUCC284 (AF022196), the 6 most closely related species based on the SSU rDNA sequence. The sequence of the LSU rDNA was 11-12% different from that of *Warnowia* sp. (FJ947042), *G. aureolum* (AF200671), and *Nematodinium* sp. (FJ947041), the 3 closest species using this gene.

The phylogenetic trees based on both SSU and LSU rDNA placed *Gyrodiniellum shiwhaense* in the *Gymnodinium* sensu stricto clade (Fig. 4.17-4.18). In the SSU rDNA tree, *G. shiwhaense* was basal to the *Polykrikos* clade, the *Gymnodinium* clade, and the *Paragymnodinium shiwhaense* and *L. viride*. However, *G. shiwhaense* was clearly separated from a warnowiid clade including *Warnowia* spp., *Proterythropsis* spp., and *Nematodinium* spp..

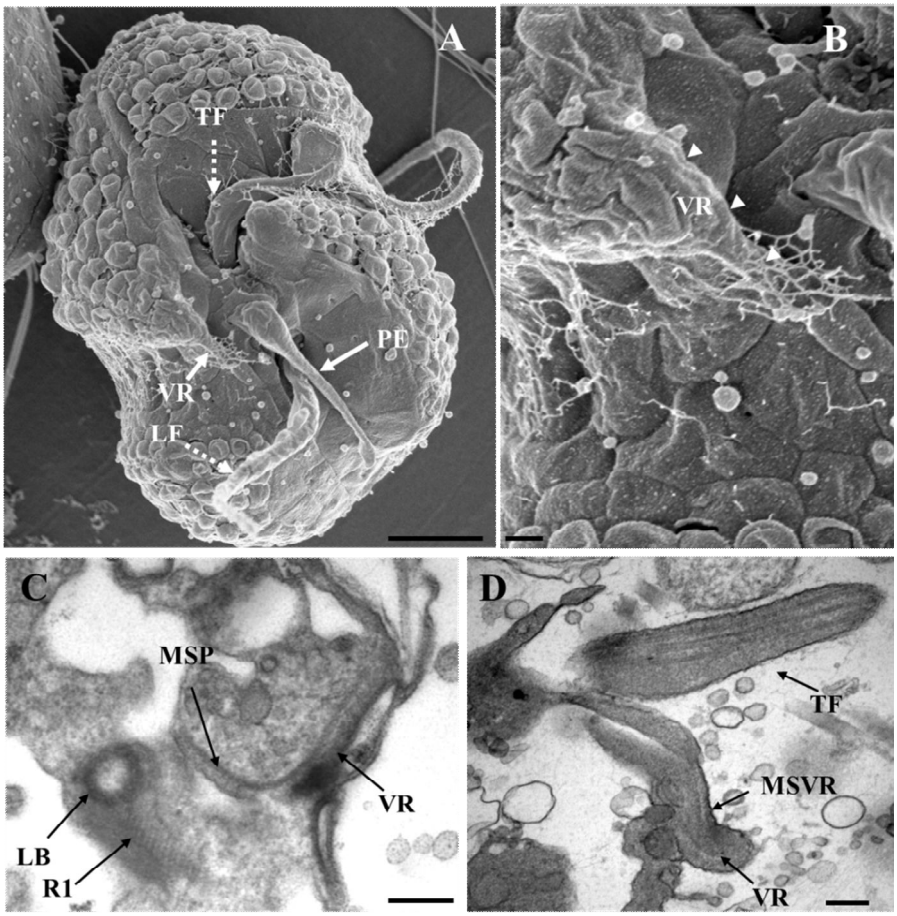

Fig. 4.14 Micrographs of *Gyrodiniellum shiwhaense* n. gen. n. sp. **A, B**. Ventral view. scanning electron microscopic (SEM) photos. **A.** Cells deploying a protruded peduncle (PE), located between the exit points of the transverse (TF) and longitudinal flagellum (LF), and ventral ridge (VR) adjacent to the PE. **B.** A SEM photo enlarged from Fig. **B** shows the VR (arrow heads). **C, D**. Transverse sectioned transmission electron microscopic photos. **C.** A photo showing a microtubular strand of the peduncle (MSP), VR, LB, and root 1 (R1). **D.** A photo showing the positions of VR, a microtubular strand of the VR (MSVR), and TF. Scale bars = 2 μm for Fig. **A**, 0.2 μm for Fig. **B-D.**

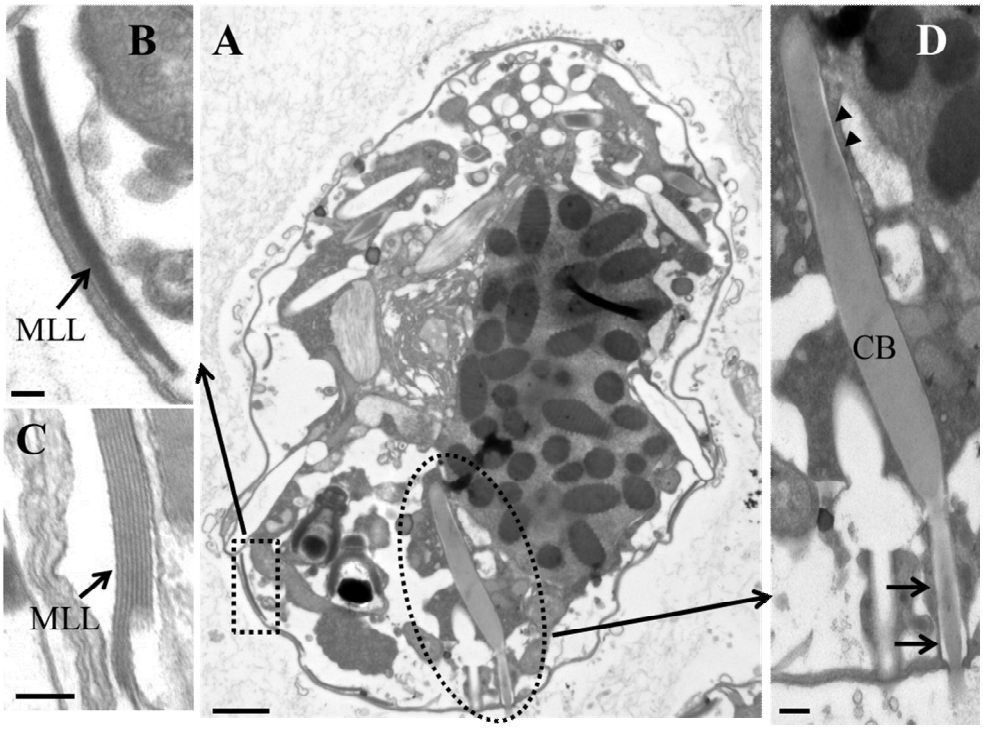

Fig. 4.15 Transmission electron micrographs of *Gyrodiniellum shiwhaense* n. gen., n. sp. showing trichocyst and membrane-like lamellae (MLL). **A.** Cell showing MLL (in dashed box) and trichocysts (in dashed circle). **B**. Enlargement from Fig. **A** showing a MLL. **C**. Striated membrane-like lamellae. **D**. Enlargement from Fig. **A** to show a single membrane (arrowhead), a column-like body (CB), and a neck (arrow) of a trichocyst. Scale bars = 2 μm for Fig. **A**, 0.2 μm for Fig. **D**, and 0.1 μm for Fig. **B, C.**

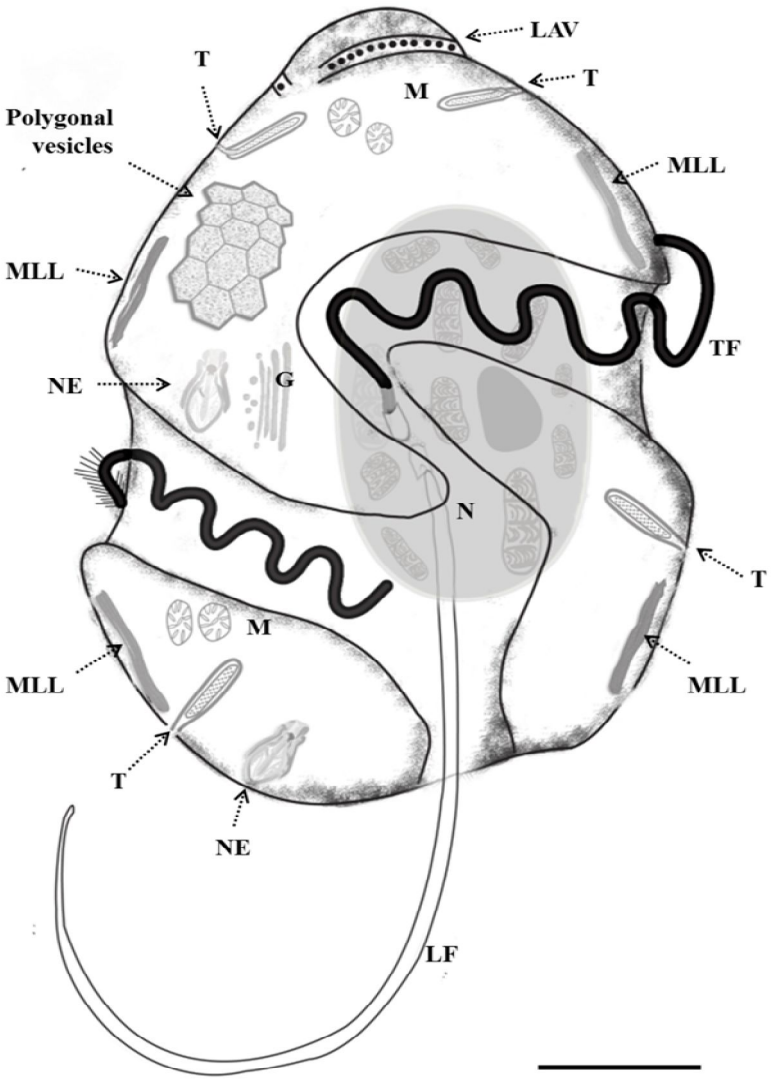

Fig. 4.16 Diagrammatic drawing of *Gyrodiniellum shiwhaense* n. gen., n. sp., based mainly on scanning electron microscopy and on serial sections studied in the transmission electron microscope (total of 150 sections) from the apex to the antapex. G, Golgi body; LAV, loop-shaped apical row of amphiesmal vesicles; LF, longitudinal flagellum; M, mitochondrion; MLL, membrane-like lamellae; N, nucleus; NE, nematocyst; PS, pusule; T, trichocyst; TF, transverse flagellum. Scale bars = 2 μm.

4.5.3 Date and locality of isolation

The new isolate was found in Shiwha Bay, Korea on September 29, 2009 when cryptomonads were abundant (ca. 48,000 cells ml^{-1}) and when the water temperature and salinity were 24.5 ^{o}C and 24, respectively.

4.5.4 Remarks on culturing and behavior

The new isolate was cultured on *A. carterae*. It moved in straight lines or in a helicoidal pattern. It sometimes stopped suddenly and then resumed movement very fast, almost like a jump.

4.6 Discussion

Gyrodiniellum shiwhaense n. gen., n. sp. has a cell surface similar to many woloszynskioid dinoflagellates and the gymnodinioid dinoflagellate *Paragymnodinium shiwhaense*, most of which have polygonal amphiesmal plates arranged in more or less distinct horizontal rows. The number of the AV rows of *G. shiwhaense* (16) was the same as in *P. shiwhaense*, and fell in the range of that in the woloszynskioids (7-29) (Table 3.2). However, among the woloszynskioids, the numbers of the AV rows of only *Borghiella tenuissima* Moestrup, Hansen & Daugberg (14-16) and *Biecheleria pseudopalustris* Moestrup, Lindberg & Daugberg (26-29) were comparable to or greater than that of *G. shiwhaense* (Table 3.2). Thus, the number of the AV rows may not be a critical feature for distinguishing gymnodinioids from woloszynskioids.

Gyrodiniellum shiwhaense n. gen., n. sp. differs from woloszynskioid dinoflagellates and *P. shiwhaense* in the presence of a loop-shaped row of amphiesmal vesicles (LAV) near the apical end of the episome. This part of the cell is considered to be one of the phylogenetically informative parts of the cell in thin-walled dinoflagellates (Table 3.3).

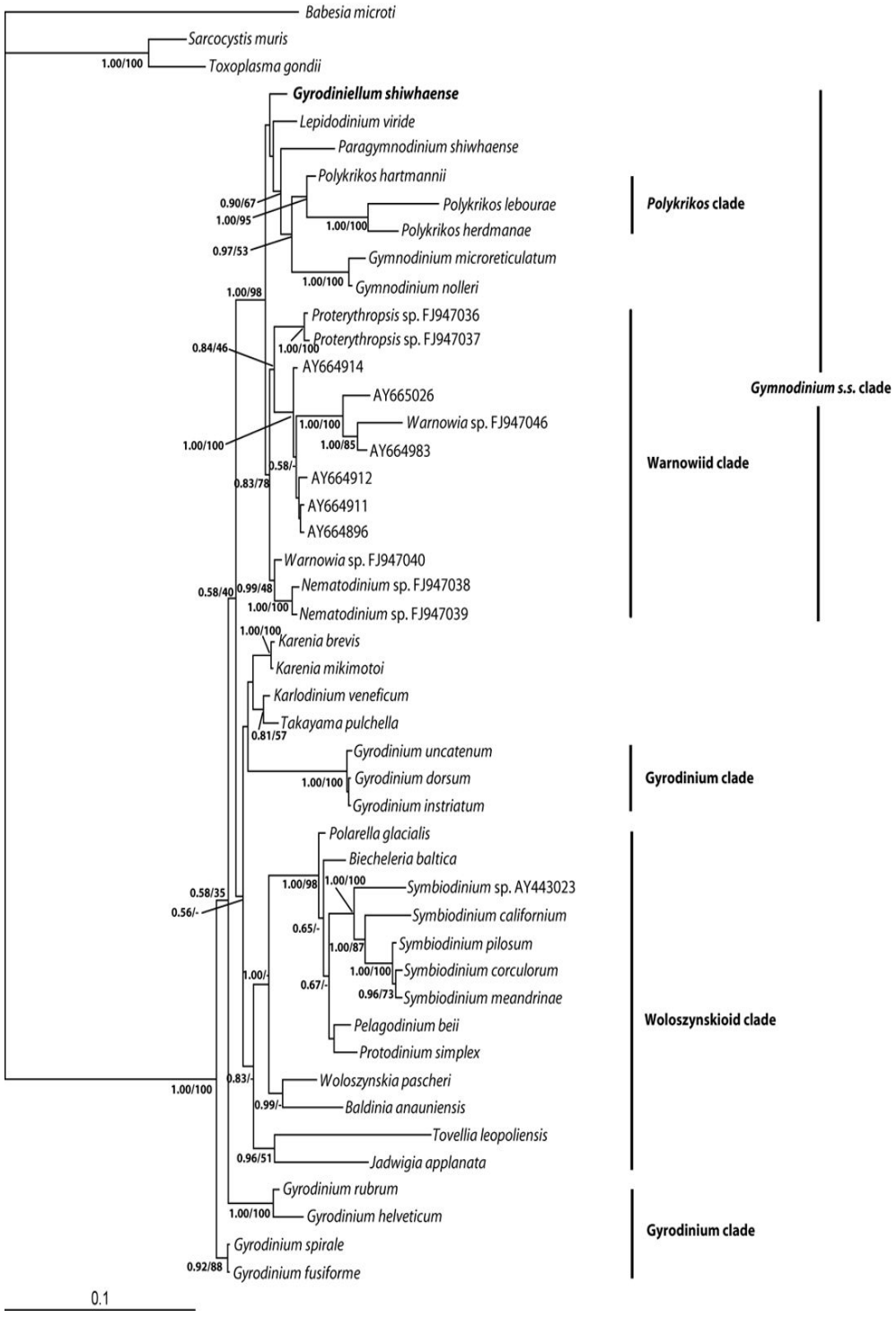
Babesia microti
Sarcocystis muris
1.00/100
Toxoplasma gondii
Gyrodiniellum shiwhaense
Lepidodinium viride
Paragymnodinium shiwhaense
Polykrikos hartmannii
0.90/67
1.00/95
Polykrikos lebourae
1.00/100
Polykrikos herdmanae
0.97/53
Gymnodinium microreticulatum
1.00/100
Gymnodinium nolleri
Polykrikos clade
1.00/98
Proterythropsis sp. FJ947036
0.84/46
1.00/100
Proterythropsis sp. FJ947037
AY664914
AY665026
1.00/100
Warnowia sp. FJ947046
1.00/100
1.00/85
AY664983
0.58/-
0.83/78
AY664912
AY664911
AY664896
Gymnodinium s.s. clade
Warnowiid clade
Warnowia sp. FJ947040
0.58/40
0.99/48
Nematodinium sp. FJ947038
1.00/100
Nematodinium sp. FJ947039
1.00/100
Karenia brevis
Karenia mikimotoi
Karlodinium veneficum
Takayama pulchella
0.81/57
Gyrodinium uncatenum
1.00/100
Gyrodinium dorsum
Gyrodinium instriatum
Gyrodinium clade
Polarella glacialis
Biecheleria baltica
1.00/98
1.00/100
Symbiodinium sp. AY443023
0.58/35
0.56/-
Symbiodinium californium
0.65/-
1.00/87
Symbiodinium pilosum
1.00/-
1.00/100
Symbiodinium corculorum
0.67/-
0.96/73
Symbiodinium meandrinae
Pelagodinium beii
Protodinium simplex
Woloszynskioid clade
0.83/-
1.00/100
Woloszynskia pascheri
0.99/-
Baldinia anauniensis
Tovellia leopoliensis
0.96/51
Jadwigia applanata
Gyrodinium rubrum
1.00/100
Gyrodinium helveticum
Gyrodinium clade
Gyrodinium spirale
0.92/88
Gyrodinium fusiforme
0.1

Fig. 4.17 Consensus Bayesian tree based on 1,618 aligned positions of nuclear small subunit (SSU) rDNA using the TrN+I+G model with *Babesia microti*, *Sarcocystis muris*, and *Toxoplasma gondii* as outgroups. The parameters were as follows: assumed nucleotide frequency with empirical; substitution rate matrix with A–C substitutions= 1.0000, A–G=3.7918, A–T=1.0, C–G=1.0, C–T=6.9738, G–T=1.0; proportion of sites assumed to be invariable=0.4378 and rates for variable sites assumed to follow a gamma distribution with shape parameter=0.6944. The branch lengths are proportional to the number of character changes. The numbers above the branches indicate the Bayesian posterior probability (left) and maximum likelihood bootstrap values (right). Only posterior probabilities ≥ 0.5 are shown. Note the position of *Gyrodiniellum shiwhaense* n. gen., n. sp. (bold).

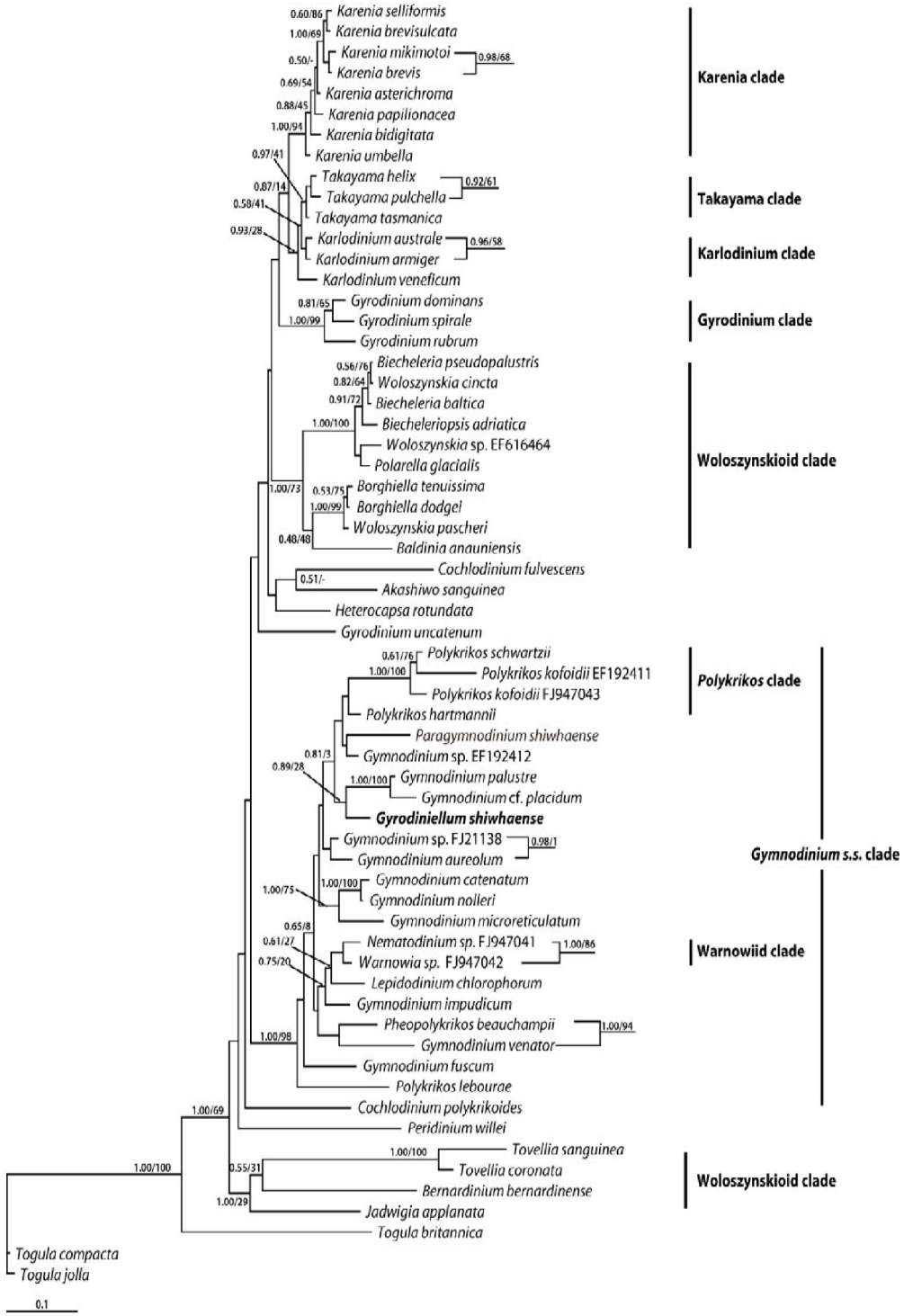
Karenia selliformis
Karenia brevisulcata
Karenia mikimotoi
Karenia brevis
Karenia asterichroma
Karenia papilionacea
Karenia bidigitata
Karenia umbella
Takayama helix
Takayama pulchella
Takayama tasmanica
Karlodinium australe
Karlodinium armiger
Karlodinium veneficum
Gyrodinium dominans
Gyrodinium spirale
Gyrodinium rubrum
Biecheleria pseudopalustris
Woloszynskia cincta
Biecheleria baltica
Biecheleriopsis adriatica
Woloszynskia sp. EF616464
Polarella glacialis
Borghiella tenuissima
Borghiella dodgei
Woloszynskia pascheri
Baldinia anauniensis
Cochlodinium fulvescens
Akashiwo sanguinea
Heterocapsa rotundata
Gyrodinium uncatenum
Polykrikos schwartzii
Polykrikos kofoidii EF192411
Polykrikos kofoidii FJ947043
Polykrikos hartmannii
Paragymnodinium shiwhaense
Gymnodinium sp. EF192412
Gymnodinium palustre
Gymnodinium cf. placidum
Gyrodiniellum shiwhaense
Gymnodinium sp. FJ21138
Gymnodinium aureolum
Gymnodinium catenatum
Gymnodinium nolleri
Gymnodinium microreticulatum
Nematodinium sp. FJ947041
Warnowia sp. FJ947042
Lepidodinium chlorophorum
Gymnodinium impudicum
Pheopolykrikos beauchampii
Gymnodinium venator
Gymnodinium fuscum
Polykrikos lebourae
Cochlodinium polykrikoides
Peridinium willei
Tovellia sanguinea
Tovellia coronata
Bernardinium bernardinense
Jadwigia applanata
Togula britannica
Togula compacta
Togula jolla
0.1
Karenia clade
Takayama clade
Karlodinium clade
Gyrodinium clade
Woloszynskioid clade
Polykrikos clade
Gymnodinium s.s. clade
Warnowiid clade
Woloszynskioid clade

Fig. 4.18 Bayesian consensus tree of unarmoured dinoflagellates based 557 aligned positions of nuclear LSU rDNA using the TrN+I+G model. The parameters were as follows: assumed nucleotide frequency with equal (A=C=G=T=0.25); substitution rate matrix with A–C substitutions=1.0000, A–G=3.1151, A–T=1.0, C–G=1.0, C–T=6.1349, G–T=1.0; proportion of sites assumed to be invariable=0.1893 and rates for variable sites assumed to follow a gamma distribution with shape parameter=0.7346. The branch lengths are proportional to the number of character changes. The numbers above the branches indicate the Bayesian posterior probability (left) and maximum likelihood bootstrap values (right). Only posterior probabilities ≥ 0.5 are shown. Note the position of *Gyrodiniellum shiwhaense* n. gen., n. sp. (bold).

Table 3.2 Comparison of the number of rows of amphiesmal vesicles (AVs) in *Gyrodiniellum shiwhaense*, *Paragymnodinium shiwhaense*, and woloszynskioid dinoflagellates.

Species	Order	episome	cingulum	hyposome	Total	Ref
Gyrodiniellum shiwhaense	Gymnodinioid	6	5	5	16	This study
Paragymnodinium shiwhaense	Gymnodinioid	6	5	5	16	(1)
Baldinia anauniensis	Woloszynskioid	5-6	1	4-5	10-12	(2)
Biecheleria baltica	Woloszynskioid	6	2	4	12	(3)
Biecheleria cincta	Woloszynskioid	4	3	3	10	(9)
Biecheleria pseudopalustris	Woloszynskioid	13-14	3-4	10-11	26-29	(4)
Biecheleriopsis adriatica	Woloszynskioid	4-5	2	4-5	10-12	(5)
Borghiella dodgei	Woloszynskioid	5-6	2	5-6	12-14	(6)
Borghiella tenuissima	Woloszynskioid	7-8	2	5-6	14-16	(6)
Pelagodinium bei	Woloszynskioid	4	1	4	8	(7)
Polarella glacialis	Woloszynskioid	3	2	4	9	(8)
Protodinium simplex	Woloszynskioid	3	3	2	8	(9)
Tovellia coronate	Woloszynskioid	4	1	4	9	(10)
Tovellia sanguinea	Woloszynskioid	3-4	1	3-4	7-9	(11)

Symbiodinium	Woloszynskioid	3	2	2	7	(12)

(1) Kang et al. (2010); (2) Hansen et al. (2007b); (3) Kremp et al. (2005); (4) Moestrup et al. (2009a); (5) Moestrup et al. (2009b); (6) Moestrup et al. (2008); (7) Siano et al. (2010); (8) Montreson et al. (1999); (9) Siano et al. (2009); (10) Lindberg et al. (2005); (11) Moestrup et al. (2006); (12) Hansen and Daugbjerg (2009).

The LAV of *G. shiwhaense* was different from woloszynskioid dinoflagellates, which have (1) a straight apical line of narrow plates (ALP; the genera *Tovellia* Moestrup, Lindberg & Daugberg and *Jadwigia* Moestrup, Lindberg & Daugberg), (2) a pair of elongate amphiesmal vesicles (PEV; the genus *Borghiella*), or (3) an elongate apical vesicle (EAV; the genera *Biecheleria, Biecheleriopsis* and *Symbiodinium* Freudenthal) (Hansen and Daugbjerg 2009; Lindberg et al. 2005; Moestrup et al. 2006, 2008, 2009a, 2009b). The genera *Baldinia* Hansen & Daugbjerg, *Polarella* Montresor, Procaccini & Stoecker, and *Paragymnodinium* do not have an equivalent structure (Hansen et al. 2007b; Kang et al. 2010; Montresor et al. 1999). *Gyrodiniellum shiwhaense* is also different from the genera *Karlodinium* Larsen and *Karenia* Hansen & Moestrup, both of which have a deep linear apical groove (Daugbjerg et al. 2000; de Salas et al. 2004a, 2004b, 2005, 2008; Garces et al. 2006) and the genus *Takayama* de Salas, Bolch, Botes & Hallegraeff which has a sigmoid apical groove. (de Salas et al. 2003, 2008). The shape of the LAV of *G. shiwhaense* is similar to that of the genera *Gymnodinium* Stein, *Lepidodinium* Watanabe, Suda, Inouye, Sawaguchi & Chihara, *Polykrikos* Bütschli, *Nematodinium* Kofoid & Swezy, *Warnowia* Lindemann, and *Proterythropsis* Kofoid & Swezy, all of which belong to the *Gymnodinium s.s.* clade (Daugbjerg et al. 2000; Hansen et al. 2007a; Hoppenrath and Leander 2007a, 2007b; Hoppenrath et al. 2009a). Biecheler (1952) drew a similar structure at the apical end of *Gyrodinium vorax* Biecheler and *Gymnodinium maguellonnense* Biecheler, but according to her drawing it was formed by a single, very long amphiesmal vesicle. Her studies were based on stained cells examined by light microscopy, and whether the ring-shaped “acrobase” in her species comprises one or more amphiesmal vesicles will need to be examined by SEM. The ring-shaped figure, formed by a more or less circular ring of amphiesmal vesicles may prove to be a synapomorphy of the *Gymnodinium-Polykrikos* group (Fig. 4.17). In this respect the group differs from the woloszynskioid and Kareniaceae groups. However, *G. shiwhaense* lacks two of the key taxonomic characters that circumscribe the genus *Gymnodinium*, namely the presence of nuclear envelope

chambers and a nuclear fibrous connective (Daugbjerg et al. 2000). *Gyrodiniellum shiwhaense* is also different from the phototrophic dinoflagellate *Lepidodinium* which has nuclear envelope chambers and the nuclear fibrous connective (Table 3.3). Moreover, *G. shiwhaense* lacks an ocelloid in contrast to the warnowiid dinoflagellates *Nematodinium, Warnowia*, and *Proterythropsis* (e.g. Hoppenrath et al. 2009a).

Cells of *G. shiwhaense, P. shiwhaense*, *Polykrikos* spp., and some warnowiid dinoflagellates possess nematocysts (Table 3.4, Fig. 4.19A-D). However, those of *G. shiwhaense* contain stylets and filaments, which are absent in *P. shiwhaense* (Table 3.3, Fig. 4.19B.). *Gyrodiniellum shiwhaense* differs from *Polykrikos* spp. in that its nematocysts are not connected to a taeniocyst (Bradbury et al. 1983; Greuet 1987; Hoppenrath and Leander 2007a, 2007b; Hoppenrath et al. 2009a, 2009b; Westfall et al. 1983) (Fig. 4.19C). The nematocysts of *Nematodinium* cells differ by possessing an intermediary plug and pedicules, which are absent in *G. shiwhaense* (Fig. 4.19D). Thus, the nematocysts of *G. shiwhaense* represent a unique type.

In the phylogenetic analyses based on SSU rDNA, *Gyrodiniellum shiwhaense* takes up a sister position to a clade comprising the *Polykrikos* clade, the *Paragymnodinium-Lepidodinium* clade, and the *Gymnodinium* clade. If this finding can be substantiated by other studies, several scenarios of evolutionary changes can be imagined, which include acquisition/loss of chloroplasts, modification of nematocysts/taeniocysts, changes in the apical structure, and modification of the nuclear envelope. In the SSU rDNA tree *G. shiwhaense* occupies a sister group relationship to the complex mentioned above, in which ocelloids developed (Hoppenrath et al. 2009a) but some species retained nematocysts (Hoppenrath et al. 2009a).

The diverse-sized fibrous structures observed in the perinuclear space of *G. shiwhaense* are similar to those reported in several other dinoflagellates, and have been interpreted as putative flagellar hairs (Leadbeater 1971).

Table 3.3 Comparison of *Gyrodiniellum shiwhaense* with other gymnodinioid, warnowiid, and woloszynskioid dinoflagellates.

Genus	AS	NC	NFC	AV	PED	NEM	OC	PIS	TRO	Ref
GS	Loop	N	N	Polygonal	Y	Y	N	N	H	This study
PG	SEF	N	N	Polygonal	Y	Y	N	N	M	(1)
NEM	Loop	?	Y or ?	Polygonal	Questionable(?) or engulfment	Y or N	Y	N	M	(2-7)
WAR	Loop	?	?	Polygonal	? or engulfment	N	Y	N	H	(4,6-8)
PRO	Loop	?	?	Polygonal	?	Y	Y	N	H	(4,9)
ERY	Loop	?	?	Polygonal	?	N	Y	Y	H	(3,4,6-13)
POL	Loop	Y or ?	Y or ?	Small polygonal or ?	N	Y	N	N	M	(3,4,7,14-18)
GYM	Loop	Y	Y	Polygonal or ?	Y or ?	N	N	N	M	(19-26)
KARE	Straight Furrow	N	N	Y or ?	N	N	N	N	M	(19,24,27-31)
KARL	Straight Furrow	N	N	Polygonal or Plug-like	Y or ?	N	N	N	M	(19,24,32-35)
LEP	Loop	Y	Y	One has body scale or the other does not have	Y or PLS	N	N	N	M	(36--40)
TAK	Sigmoid	N	N	Bubbly, Polygonal or ?	PLS or N	N	N	N	A	(34,36)
BAL	Absent	N	N	Polygonal	Y	N	N	N	M	(41,42)
BIEA	Single elongate vesicle	N	N	Polygonal	Y or ?	N	N	N	A	(42,43)
BIES	Single elongate vesicle	?	Y	Polygonal	?	N	N	N	M	(42)
BOR	Two elongate vesicles	N	N	Polygonal	N	N	N	N	A	(42-44)

BER	Two elongate vesicles	N	N	?	Y	N	N	N	M	(45)
JAD	Single line of vesicles	N	N	Polygonal	?	N	N	N	A	(42-44, 46)
TOV	Single line of vesicles	N	N	Polygonal	Y or ?	N	N	N	M	(42,43,46-48)

GS: (*Gyrodiniellum shiwhaense*), PG: (*Paragymnodinium),* NEM: (*Nematodinium*), WAR: (*Warnowia*), PRO: (*Proterythropsis*), ERY: (*Erythropsidinium*), POL: (*Polykrikos*), GYM: (*Gymnodinium*), KARE: (*Karenia*), KARL: (*Karlodinium*), LEP: (*Lepidodinium*), TAK: (*Takayama*), BAL: (*Baldinia*), BIEA: (*Biecheleria*), BIES: (*Biecheleriopsis*), BOR: (*Borghiella*), BER: (*Bernardinium*), JAD: (*Jadwigia*), TOV: (*Tovellia*).

Y: Observed. N: Not observed. A: Autotrophic. M: Mixotrophic. H: Heterotrophic. AS: apical structure. AV: amphiesmal vesicles. NC: nuclear envelope chamber. NFC: nuclear fibrous connective. NEM: nematocysts. OC: ocelloid. PIS: piston. PED: peduncle. PLS: peduncle-like structure. SEF: sulcal extension-like furrow. TRO: trophic mode.

(1) Kang et al. (2010); (2) Francis (1967); (3) Greuet (1987); (4) Hoppenrath et al. (2009a); (5) Mornin and Francis (1967); (6) Takayama (1985); (7) Greuet (1987); (8) Greuet (1968); (9) Kofoid and Swezy (1921); (10) Elbrächter (1979); (11) Gómez (2008); (12) Gómez et al. (2009); (13) Greuet (1965); (14) Bradbury et al. (1983); (15) Hoppenrath et al. (2009b); (16) Hoppenrath and Leander (2007a); (17) Hoppenrath and Leander (2007b); (18) Westfall et al. (1983); (19) Daugbjerg et al. (2000); (20) Fariman et al. (2007); (21) Hansen (2001); (22) Hansen and Flaim (2007); (23) Hansen et al. (2000); (24) Jørgensen et al. (2004); (25) Sundström et al. (2009); (26) Tang et al. (2008); (27) Botes et al. (2003); (28) Chang and Ryan (2004); (29) de

Salas et al. (2004a); (30) de Salas et al. (2004b); (31) Haywood et al. (2004); (32) Bergholtz et al. (2005); (33) de Salas et al. (2005); (34) de Salas et al. (2008); (35) Garces et al. (2006); (36) de Salas et al. (2003); (37) Hansen et al. (2007a); (38) Honsell and Talarico (2004); (39) Watanabe et al. (1987); (40) Watanabe et al. (1990); (41) Hansen et al. (2007b); (42) Moestrup et al. (2009b); (43) Moestrup et al. (2009a); (44) Moestrup et al. (2008); (45) Calado et al. (2006); (46) Lindberg et al. (2005); (47) Moestrup et al. (2006); (48) Moestrup et al. (2008).

Table 3.4 Comparison of nematocysts and nematocyst-taeniocyst complex in dinoflagellates.

Name	AC	CA	OP	CH	FI	PB	PC	PVA	ST	TA	LWN	BL	NBL	Ref
Gys	Y	Y	Y	N	Y	Y	Y	N	Y	N	1.8 x 1.1	12.2	0.15	This study
Pas	Y	Y	Y	N	N	Y	Y	N	N	N	1.2 x 0.8	12.4	0.10	(1)
Poh	Y	Y	Y	Y	Y	Y	Y	Y	Y	Y	20 x 2	80	0.25	(2, 3, 4)
Pos	Y	Y	Y	Y	Y	Y	Y	Y	Y	Y	27 x 5	110	0.25	(2, 3, 6)
Pok	Y	Y	Y	Y	Y	Y	Y	Y	Y	Y	26 x 5	75	0.35	(5)
Nea	Y	?	Y	?	Y	Y	Y	?	Y	N	10 x 5	60	0.17	(6, 7)
Prv	?	Y	Y	?	?	?	N	N	Y	N	15 x 6	50	0.30	(8)

Gys: (*Gyrodiniellum shiwhaense*), Pas: (*Paragymnodinium shiwhaense*), Poh: (*Polykrikos hartmannii*), Pos: (*Polykrikos schwartzii*), Pok: (*Polykrikos kofoidii*), Nea: (*Nematodinium armatum*), Prv: (*Proterythropsis vigilans*). AC: anterior chamber, CA: capsule, CH: chute, FI: filament, FS: fibrous strand, OP: operculum, PB: posterior body, PC: posterior chamber, PVA: posterior vacuole, ST: stylet, TA: taeniocyst. LWN: Length and width of a nematocyst or nematocyst-taeniocyst (μm), BL: Body length (μm), NBL: Nematocyst or nematocyst-taeniocyst length /Body length.

(1) Kang et al. (2010); (2) Hoppenrath and Leander (2007a); (3) Hoppenrath and Leander (2007b); (4) Hoppenrath et al. (2009b); (5) Westfall et al. (1983); (6) Greuet (1987); (7) Francis (1967); (8) Marshall (1925). There are no data on *Pheopolykrikos* spp.

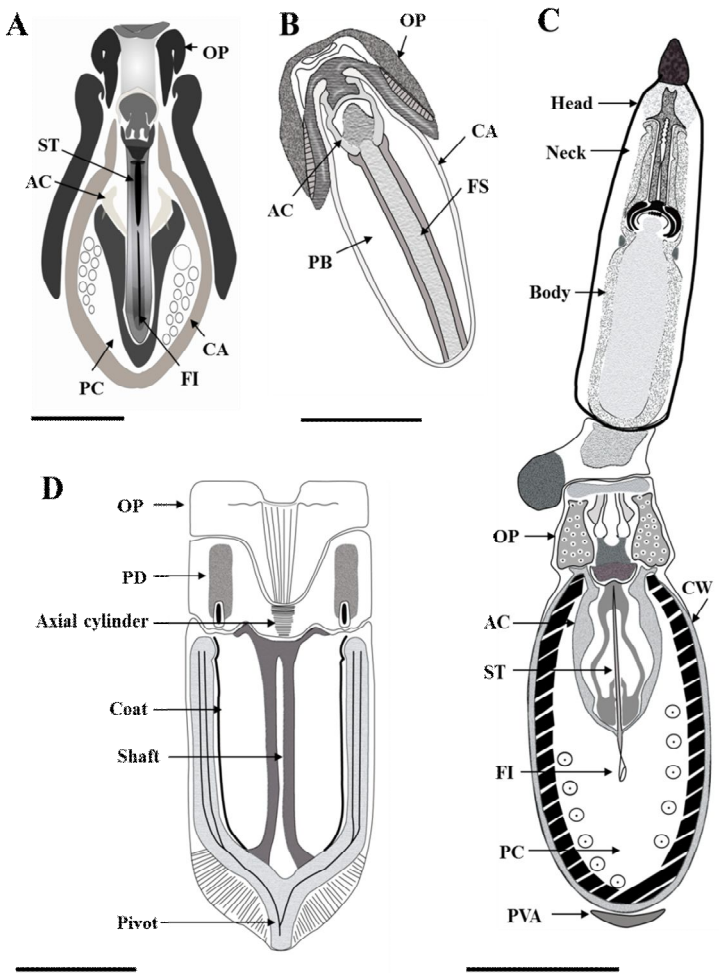

Fig. 4.19 Schematic illustrations showing the organization of nematocysts of *Gyrodiniellum shiwhaense*, *Paragymnodinium shiwhaense*, and *Nematodinium* sp. and the nematocyst-taeniocyst complex of *Polykrikos schwartzii*. **A.** Diagrammatic reconstruction of nematocyst of *G. shiwhaense*, based mainly on serial ultrathin sections in Fig. 4-13. **B.** Nematocyst of *P. shiwhaense* (redrawn from Kang et al. 2010). **C.** Nematocyst-taeniocyst complex of *P. schwartzii* (redrawn from Greuet 1987). **D.** Nematocyst of *Nematodinium* sp. (redrawn from Greuet 1987). AC, anterior chamber; CA, capsule; FI, filament; FS, fibrous strand; OP, operculum; PC, posterior chamber; PD, pedicules; PVA, posterior vacuole; ST, stylet. Scale bars = 0.5 μm for Fig. **A, B** and 5 μm for Fig. **C, D.**

Gyrodiniellum shiwhaense n. gen., n. sp. has membrane-like lamellae (MLL) underneath the surface, which have been reported in the dinoflagellates *Protoperidinium spinulosum* Schiller (Jacobson and Anderson 1992). The length of the MLL of *G. shiwhaense* (~3 μm) is greater than those of *P. spinulosum* (~1.5 μm), but the width of the MLL of *G. shiwhaense* (ca. 0.1 μm) is smaller than ***in*** *P. spinulosum* (0.25 μm). The MLL of *G. shiwhaense* and *P. spinulosum* were located just underneath the surface of cell. The function of the MLL has not been investigated.

Gyrodiniellum shiwhaense possesses a peduncle, a structure that has also been observed in a growing number of dinoflagellates, including dinophysioid, gymnodinioid, gonyaulacoid, peridinioid, prorocentroid, and suessioid clades (Calado and Moestrup 1997; Calado et al. 1998; Jacobson and Andersen 1994; Hansen 2001; Hansen and Moestrup 1998; Roberts et al. 1995). I found that *G. shiwhaense* absorbed material from a captured prey cell as in other peduncle feeders (Jeong et al. 2011b).

The shape of *G. shiwhaense* is similar to that of *Gyrodinium vorax*, which was described by Biecheler (1952), including the shape of the LAV, apical knobs, ventral ridge, and a distinct S-shape in the cingulum and sulcus and the number of the AV rows in the cingulum. However, the cell length and width of *G. shiwhaense* (6-22 μm and 5-16 μm, respectively) are considerably smaller than those of *G. vorax* (30-35 μm and 22-25 μm, respectively). The episome of *G. shiwhaense* is larger than the hyposome, while Biecheler (1952) described the episome of *G. vorax* to be smaller than the hyposome. In addition, the nucleus of *G. shiwhaense* extended from the episome to hyposome, while Biecheler (1952) positioned the nucleus of *G. vorax* only in the episome. The number of the AVs at the apical end and the number of horizontal AVs in the episome and hyposome (11, 6, and 5, respectively) were also much smaller than those of *G. vorax* (ca. 28, 9-11, and 9-10, respectively).

Based on the consistent morphological and genetic divergence of our material compared to other genera, I consider it justified to describe it as a separate genus and species.

Phylum Dinoflagellata (Bütschli 1885) Fensome et al. 1993

Class Dinophyceae Pascher 1914

Order Gymnodiniales Apstein 1909

Family Gymnodiniaceae (Bergh 1881) Lankester 1885

Gyrodiniellum n. gen. Kang, Jeong, and Moestrup

Diagnosis. Dinoflagellate with polygonal amphiesmal vesicles arranged in horizontal rows. A distinct loop-shaped apical ridge is present. Nuclear envelope chambers and nuclear fibrous connective absent. Cells possess nematocysts with stylets and filaments, but lacks taeniocysts and posterior vacuoles. Ocelloids absent. Chloroplast absent. Heterotrophic.

Etymology. The generic epithet "*Gyrodiniellum*" meaning small *Gyrodinium,* refers to its similarity to the genus *Gyrodinium* when seen on the light microscope. Gender: neuter

Type Species. *Gyrodiniellum shiwhaense.* Kang, Jeong, and Moestrup designated here.

Gyrodiniellum shiwhaense n. sp. Kang, Jeong, and Moestrup

Diagnosis. The episome is conical and slightly larger than the ellipsoid hyposome. The cell has a wide and distinctive descending cingulum, which is displaced by 0.3-0.5 x cell length. A distinct ventral ridge is present above the right side of the cingulum. The sulcus extends from the antapex to the episome, becoming slightly narrower towards the apex and connected to the left end of the apical groove at the apex. Cell length and width ranges of living cells unfed were 5-14 μm and 5-11 μm, respectively, but cells fed *Amphidinium carterae* measured 9-

22 μm and 6-16 μm, respectively. The ratio range of cell length to cell width of live cells fed with *A. carterae* was 1.1-1.6, and that of 3-day-starved cells was 1.0-1.8. Nucleus is oval and located in the right side of the cell. The amphiesmal vesicles are arranged in 16 horizontal rows; 6 rows on the episome, 5 rows in the cingulum, and 5 rows on the hyposome. A loop-shaped apical row of 5 amphiesmal vesicles, bearing 8-22 small knobs, surrounds 11 other amphiesmal vesicles. Peduncle, trichocysts and pusule system present, but eyespot and pyrenoid absent.

Etymology. The specific name "*shiwhaense*" refers to the location where this species was first collected.

Type locality. Shiwha Bay, Korea (37° 18' N, 126° 36' E).

Deposition of type material. A holotype slide as USNM slide 2056302 of cells fixed with 2% (w/v) osmium tetroxide has been deposited in the Protist Type Specimen Slide Collection, US Natural History Museum, Smithsonian Institution, Washington, DC, USA.

Gene sequence. The rDNA gene sequence - GenBank Accession No. FR720082.

Chapter 5: Mixotrophy in the newly described phototrophic dinoflagellate *Biecheleria cincta* (=*Woloszynskia cincta*) from western Korean waters: Taxonomy and ecology

5.1 Abstract

Biecheleria species are dinoflagellates in the order Suessiales inhabiting marine or freshwater environments; their ecophysiology has not been well in vestigated, in particular, their trophic modes have yet to be elucidated. Previo us studies have reported that all *Biecheleria* species are photosynthetic, althou gh their mixotrophic abilities have not been explored. I isolated a dinoflagell ate from coastal waters in western Korea and established clonal cultures of t his dinoflagellate. On the basis of morphology and analyses of the small/larg e subunit rRNA gene (GenBank accession number = FR690459), I identified this dinoflagellate as *Biecheleria cincta* (previously *Woloszynskia cincta*). I fu rther established that this dinoflagellate is a mixotrophic species. I found that *B. cincta* fed on algal prey using a peduncle. Among the diverse prey provi ded, *B. cincta* ingested those algal species that had equivalent spherical diam eters (ESDs) $\leq$12.6 μm, exceptions being the diatom *Skeletonema costatum* a nd the dinoflagellate *Prorocentrum minimum*. However, *B. cincta* did not fee d on larger algal species that had ESDs $\geq$15 μm. The specific growth rates for *B. cincta* increased continuously with increasing mean prey concentration before saturating at a concentration of ca. 134 ng C ml^{-1} (1,340 cells ml^{-1}) when *Heterosigma akashiwo* was used as food. The maximum specific grow th rate (i.e. mixotrophic growth) of *B. cincta* feeding on *H. akashiwo* was 0. 499 d^{-1} at 20 °C under illumination of 20 μE m^{-2} s^{-1} on a 14:10 h light-dar k cycle, whereas its growth rate (i.e. phototrophic growth) under the same li

ght conditions without added prey was 0.040 d^{-1}. The maximum ingestion and clearance rates of *B. cincta* feeding on *H. akashiwo* were 0.49 ng C grazer^{-1} d^{-1} (4.9 cells grazer^{-1} d^{-1}) and 1.9 μl grazer^{-1} h^{-1}, respectively. The calculated grazing coefficients for *B. cincta* on co-occurring *H. akashiwo* were up to 1.1 d^{-1}. The results of the present study suggest that grazing by *B. cincta* can have a potentially considerable impact on prey algal populations.

5.2 Key words

Feeding, growth, HAB, *Heterosigma*, ingestion, peduncle, protist, raphidophyte

5.3 Introduction

Dinoflagellates are among the major components of marine ecosystems (Hansen 1991; Jacobson and Anderson 1986; Jeong 1995; Lessard 1984, 1991; Sherr and Sherr 2007; Terrado et al. 2009). They play diverse roles in marine food webs, feeding on diverse prey items and, in turn, serving as prey for diverse predators (reviewed by Jeong et al. 2010c). In the last decade, several novel dinoflagellates, the cell lengths of which are 5-20 μm, have been identified (e.g. Kang et al. 2010). Although it is very difficult to identify these small dinoflagellates under the light microscope, recent developments in molecular techniques and detailed morphological descriptions using electron microscopes have enabled us to identify small dinoflagellates and describe novel species. As a consequence, the number of newly described small dinoflagellate species is increasing (Calado et al. 2009; Jeong et al. 2005b; Mason et al. 2007; Murray and Patterson 2004; Murray et al. 2006; Saldarriaga et al. 2003; Steidinger et al. 2006). However, the ecophysiology of many of these small dinoflagellates has yet to be explored. Thus, it is difficult to assess the roles played by these organisms in marine ecosystems.

For a long time, dinoflagellate species belonging to the genus *Biecheleria* in the order Suessiales were known only as freshwater forms (Lindberg et al. 2005).

However, in 2009, a new *Biecheleria* species, *Biecheleria cincta* (previously *Woloszynskia cincta*) found in marine environments (Siano et al. 2009). Thus, it is now established that species of *Biecheleria* inhabit both freshwater and marine habitats. *Biecheleria* species have a wide geographical distribution, including Europe (Siano et al. 2009; Woloszynska 1917), the United States (Thompson 1951), India (Shyam and Sarma 1975), and Japan (Takano and Horiguchi 2003). However, the ecophysiology of species in this genus has not been investigated. In particular, their trophic modes have yet to be elucidated. Previous studies had reported that all *Biecheleria* species are photosynthetic, and mixotrophy was unknown (Lindberg et al. 2005). Therefore, it is worthwhile exploring the possibility of mixotrophy in *Biecheleria* species.

Recently, I isolated a dinoflagellate from Shiwha Bay, western Korea, and established a clonal culture of this dinoflagellate. I conducted morphological and genetic analyses using this culture. The large subunit (LSU) rDNA sequence of this dinoflagellate (GenBank accession number = FR690459) was found to be identical to that of *B. cincta* (GenBank accession number = FJ024705), which was isolated from the Gulf of Naples and then newly described by Siano et al. (2009). In addition, the morphology of this dinoflagellate is very similar to that of *B. cincta*. However, I identified certain morphological characteristics that had not been described by Siano et al. (2009). The sequences of small subunit (SSU), ITS1, ITS2, and 5.8S rDNA from the Naples strain have not been reported. Thus, in the present study, I report the morphological and genetic characteristics of the newly isolated Korean strain, including the complete sequences of the rDNA region, and present a phylogenetic tree based on the sequence of SSU rDNA. Furthermore, using the clonal culture of this Korean strain, I examined whether *B. cincta* is able to feed on prey (i.e. establish its trophic mode as exclusively autotrophic or mixotrophic). In addition, I observed its feeding behavior using different types of microscope and highresolution video microscopy in order to determine the feeding mechanisms and the prey species from among the diverse algal species provided. I also conducted

experiments to determine the effects of prey concentration on the growth and ingestion rates of *B. cincta* using the raphidophyte *Heterosigma akashiwo*, which I identified as the optimal prey in preliminary tests, as a function of prey concentration, and those when feeding on five other edible prey species at a single prey concentration at which the growth and ingestion rates of *B. cincta* feeding on *H. akashiwo* were saturated. The maximum mixotrophic growth rate of *B. cincta* feeding on *H. akashiwo* at 20 °C under illumination of 20 μE m^{-2} s^{-1} on a 14:10 h light-dark cycle was compared to that of several other reported mixotrophic dinoflagellates feeding on their optimal prey under the same light conditions (Jeong et al. 2004b, 2010b). In addition, I estimated the grazing coefficients attributable to *B. cincta* feeding on *H. akashiwo* using the ingestion rate data obtained from laboratory experiments and the abundances of predators and prey in the field. The results of the present study provide a basis for understanding the feeding mechanism and ecological roles of *Biecheleria* spp. in marine planktonic food webs.

5.4 Materials and methods

5.4.1 Experimental organisms

The mixotrophic dinoflagellates *Cochlodinium polykrikoides* and *Lingulodinium polyedrum* were grown at 20 °C in enriched f/2 seawater medium (Guillard and Ryther 1962) under continuous illumination of 50 μE m^{-2} s^{-1} provided by cool white fluorescent lights, whereas the other phytoplankton species were grown under an illumination of 20 μE m^{-2} s^{-1} provided by cool white fluorescent lights on a 14:10 h light–dark cycle (Table 4.1). *Cochlodinium polykrikoides* and *L. polyedrum* did not grow well under illumination on a light–dark cycle. The mean equivalent spherical diameter (ESD) ± standard deviation was measured using an electronic particle counter (Coulter Multisizer II; Coulter Corporation, Miami, FL). The carbon content of phytoplankton was estimated from cell volume according to Menden-Deuer and Lessard (2000).

For the isolation and culture of *B. cincta* (GenBank accession number = FR690459), plankton samples collected using water samplers were taken from Shiwha Bay, Korea, during June 2009 when the water temperature and salinity were 22 °C and 29.3, respectively. These samples were screened gently through a 154 μm Nitex mesh and placed in six-well tissue culture plates. A clonal culture of *B. cincta* was established by two serial single-cell isolations. *Heterosigma akashiwo* at 10,000-15,000 cells ml^{-1} was provided as prey. As the concentration of *B. cincta* increased, the *B. cincta* culture was sequentially transferred to 32, 270, and finally 500 ml polycarbonate (PC) bottles containing fresh *H. akashiwo*. The bottles were again filled to capacity with freshly filtered seawater, capped, and placed on a rotating wheel at 0.9 rpm at 20 °C under an illumination of 20 μE m^{-2} s^{-1} on a 14:10 h light–dark cycle. Once dense cultures of B. cincta had been obtained, they were transferred daily to 500ml PC bottles of fresh prey at ~ 20,000 cells ml^{-1}.

5.4.2 Morphology of *Biecheleria cincta*

The morphology of live cells and cells preserved in 4% (v/v) glutaraldehyde were examined using a light microscope. The length and width of live cells fed *H. akashiwo* and those starved for 2 d were measured with the aid of a digital camera (Zeiss AxioCam MRc5; Carl Zeiss Ltd., Go¨ttingen, Germany). For scanning electron microscopy (SEM), a 20-ml aliquot of a dense culture of *B. cincta* was fixed for 1 h in osmic acid at a final concentration of 2% (w/v) in seawater. The fixed cells were collected on a PC membrane filter (pore size = 3 μm) without applying additional pressure and rinsed 3 times with distilled water to remove the salt. The cells were dehydrated in an ethanol series and finally dried using a critical point dryer (CPD 300; BAL-TEC, Balzers, Germany). The dried filters were mounted on a stub and coated with gold–palladium. Cells were viewed using a field-emission scanning electron microscope (S-48001EDS, HORIBA: EX-250; Hitachi, Hitachinaka, Japan) and photographed using a digital camera. For transmission electron microscopy (TEM), cells from a dense culture were

transferred to a 50-ml tube and fixed in 4% (v/v) glutaraldehyde in culture medium. After 1.5-2 h, the entire contents of the tube were placed in a 50-ml centrifuge tube and concentrated at 1,610 g for 10 min in a Vision Centrifuge (VS-5500; Vision Scientific Co., Bucheon, Korea). The pellet from the tube was then transferred to a 1.5-ml tube and rinsed with 0.2M sodium cacodylic acid at pH 7.4. After several rinses in the medium, the cells were postfixed in 1% (w/v) osmium tetroxide in deionized water. The pellet was then embedded in agar. Subsequently, the pellet was dehydrated using a graded ethanol series (i.e. 50%, 60%, 70%, 80%, 90%, and 100% ethanol, followed by two 100% ethanol steps). The material was embedded in Spurr's. low-viscosity resin (Spurr 1969). Sections were obtained using an RMC MT-XL ultramicrotome (Boeckeler Instruments Inc., Tucson, AZ) and stained with 3% (w/v) aqueous uranyl acetate followed by 2% (w/v) lead citrate. The sections were observed using a JEOL- 1010 electron microscope (JEOL Ltd., Tokyo, Japan).

5.4.3 DNA extraction, PCR amplification, sequencing, and data analysis

Approximately 20 ml of a dense culture of *B. cincta* were concentrated by centrifugation at 2,190 × *g* for 5-10 min at room temperature, and the pellet was transferred to a 1.5-ml tube and resuspended in Tris-ethylenediaminetetraacetic acid (TE) buffer. Sodium dodecyl sulfate at a final concentration of 0.5% (w/v) and proteinase K at a final concentration of 0.1 mg ml^{-1} were added, and the mixture was incubated at 37 °C for 1 h. DNA was extracted by adding 800 µl of phenol:chloroform:isoamyl alcohol (25:24:1) to the incubated material, and the residual phenol was removed by adding 700 µl of chloroform:isoamyl alcohol (24:1). Extracted DNA was precipitated by adding isopropyl alcohol and washed in cold 70% ethanol. DNA yield was quantified using a spectrophotometer. The extracted DNA was divided into two PCR tubes, and two independent PCR reactions were conducted. The small subunit (SSU) rDNA was amplified using the forward eukaryotic primer 5′-AAC CTG GTT GAT CCT GCC AGT-3′ and the reverse eukaryotic primer 5′-TGA TCC TTC TGC AGG TTC ACC TAC-3′ and

approximately 900 bp of the large subunit (LSU) rDNA were amplified using forward primer D1R (5′-ACC CGC TGA ATT TAA GCA TA-3′) and reverse primer 1483R (5′-GCT ACT ACC ACC AAG ATC TGC-3′), following Medlin et al. (1988). The 50-µl PCR mixtures contained the following reactants: 1× PCR buffer containing 1.5 mM $MgCl_2$, 0.2 mM dNTPs, 0.5 µM of each primer, 5 U of Taq DNA polymerase (Bioneer, Daejeon, Korea), and 200 ng template DNA. The PCR reactions were performed under the following conditions in a GeneAmp PCR System 2700 (Perkin-Elmer, Boston, USA): a single initial denaturing step of 3 min at 94 °C; 40 cycles of 45 s at 95 °C, 1 min at 55 °C, and 2 min at 72 °C; and then a single extension at 72 °C for 5 min. PCR products were cloned into a pCR®2.1-TOPO® vector using the TA Cloning® Kit (Invitrogen, Carlsbad, USA). The cloned material was incubated overnight in liquid LB medium at 37 °C. Plasmids were extracted using an AccuPrep® Plasmid Extraction Kit (Bioneer, Daejeon, Korea). The presence of inserts in the plasmids was ascertained by adding *Eco*RI restriction endonuclease (Promega, Madison, USA) to the extracted plasmids. To determine the sequence of internal fragments inside the inserts, the reverse primers Euk1209R (5′-GGG CAT CAC AGA CCT G-3′) and ITSR2 (5′-TCC CTG TTC ATT CGC CAT TA-3′) were used. Sequencing of the SSU rDNA and LSU rDNA was performed using an ABI PRISM® 3700 DNA Analyzer (Applied Biosystems, Foster City, USA). All sequences were aligned using the ContigExpress alignment program (InforMax, Frederick, USA).

5.4.4 Sequence availability and phylogenetic analysis

The sequences for the nuclear SSU rDNA were aligned using the Genetic Data Environment (GDE 2.2) program (Smith et al. 1994) by eye, with the alignment based on secondary structure using the nuclear SSU rDNA of *Karenia brevis* (C.C. Davis) G. Hansen & Ø. Moestrup (Wuyts et al. 2001) as a guide (Table 4.1). The entire conserved areas of the nuclear SSU rDNA genes were readily alignable across taxa and were used for phylogenetic analyses. For Bayesian analyses, I performed a likelihood ratio test using MODELTEST 3.7 (Posada and

Crandall 1998) to determine the best available model for the SSU rDNA data (Table 4.2). The selected models were a TrN+I+Γ model with a gamma correction for among-site rate variation (α = 0.6022) and invariant sites (I = 0.3567). Bayesian analyses were run using MrBayes version 3.1.1 (Huelsenbeck and Ronquist 2001). Four independent Markov chain Monte Carlo runs were performed simultaneously for 2,000,000 generations, and trees were sampled every 1,000 generations; the first 800 trees were deleted to ensure that the likelihood had reached convergence. A consensus tree with 50% majority rule of the 1,200 trees was obtained while constructing trees, thereby resulting in uniform Bayesian posterior probabilities (BPP) across all data sets.

Maximum likelihood (ML) phylogenetic analyses were performed using the RAxML 7.0.3 program (Stamatakis 2006) with the general time reversible (GTR) + Γ model. The # option of the program was used to identify the best tree from among 200 independent tree inferences. Bootstrap values (MLBS) were calculated from 1,000 replicates using the same substitution model.

5.4.5 Prey species

Experiment 1 was designed to investigate whether *B. cincta* is able to feed on any of the target algal species provided (Table 4.2). The initial concentration of each algal prey species offered was similar in terms of carbon biomass. If a particular prey species failed to result in ingestion, additional higher prey concentrations were provided, to ensure failure to observe ingestion was not a function of prey concentration alone. A dense culture of − 15,000 cells $ml^{-1}$of *B. cincta* growing mixotrophically on *H. akashiwo* in f/2 medium and under a 14:10 h light–dark cycle using cool white fluorescent light at 20 µE m^{-2} s^{-1} was transferred to single 1-l PC bottles containing f/2 medium when *H. akashiwo* was undetectable. This culture was maintained in f/2 medium for 2 d under illumination at 20 µE m^{-2} s^{-1} on a 14:10 h light–dark cycle. Three 1-ml aliquots were then removed from the bottle and examined using a light microscope to determine *B. cincta* concentration.

Table 4.1 List of species used in constructing phylogenetic trees. Genbank accession numbers are listed to the right of each species.

Taxon	SSU rDNA Accession no.
Akashiwo sanguinea	AJ415513
Alexandrium catenella	AJ535392
Amphidinium carterae	AF274251
Amyloodinium ocellatum	DQ490258
Babesia microti	AB219802
Baldinia anauniensis	EF052682
Biecheleria baltica	EF058252
Biecheleria cincta KOREA	FR690459
Ceratium furca	AJ276699
Cochlodinium polykrikoides	AY421782
Cryptoperidiniopsis brodyi	DQ991380
Dinophysis acuminata	AB073117
Gymnodinium aureolum	AF172713
Gymnodinium catenatum	AB265962
Gymnodinium fuscum	AF022194
Gyrodinium fusiforme	AB120002
Gyrodinium spirale	AB120001
Heterocapsa rotundata	AF274267
Heterocapsa triquetra	DQ887501
Heterosigma akashiwo	AY788936
Isochrysis galbana	GQ118682
Jadwigia applanata	EF058240
Karenia brevis	AJ415518
Karenia mikimotoi	Af022195
Karlodinium veneficum	AJ415516
Lepidodinium viride	AF022199

Luciella masanensis	EU048552
Paragymnodinium shiwhaense	AM408889
Pelagodinium beii	U41087
Pfiesteria piscicida	DQ991382
Pfiesteria shumwayae	AY245694
Pheopolykrikos beauchampii	DQ371295
Polarella glacialis	GQ375263
Polykrikos hartmannii	AY421789
Prorocentrum minimum	Y16238
Protodinium simplex	U41086
Proterythropsis sp.	FJ947037
Sarcocystis muris	M64244
Scrippsiella trochoidea	AF274277
Symbiodinium californium	AF225965
Symbiodinium corculorum	L13717
Symbiodinium meandrinae	L13718
Symbiodinium pilosum	X62650
Stoeckeria algicida	AJ841809
Takayama pulchella	AY800130
Teleaulax amphioxeia	AJ007287
Toxoplasma gondii	U00458
Warnowia sp.	FJ947040
Woloszynskia leopoliensis	AY443025
Woloszynskia pascheri	EF058253

Table 4.2 Taxa, sizes, and concentration of prey species offered as food to *Biecheleria cincta* in Expt 1.

Species	ESD (±SD)	Initial prey concentration (cells ml^{-1})	Feeding by *B. cincta*
Diatoms			
Skeletonema costatum	5.9 (1.1)	150,000	N
Prymnesiophytes			
Isochrysis galbana	4.8 (0.2)	150,000	Y
Cryptophytes			
Teleaulex sp.	5.6 (1.5)	100,000	Y
Rhodomonas salina	8.8 (1.5)	50,000	Y
Rhaphidophytes			
Heterosigma akashiwo	11.5 (1.9)	30,000	Y
Euglenophytes			
Eutreptiella gymnastica	12.6 (1.0)	15,000	Y
Mixotrophic dinoflagellates			
Heterocapsa rotundata (T)	5.8 (0.4)	100,000	Y
Amphidinium carterae (NT)	9.7 (1.6)	30,000	Y
Prorocentrum minimum (T)	12.1 (2.5)	15,000-20,000	N
Heterocapsa triquetra (T)	15.0 (4.3)	15,000-20,000	N
Scrippsiella trochoidea (T)	22.8 (2.7)	10,000-20,000	N
Cochlodinium polykrikoides (NT)	25.9 (2.9)	1,000-3,000	N
Prorocentrum micans (T)	26.6 (2.8)	1,000-3,000	N
Akashiwo sanguinea (NT)	30.8 (3.5)	1,000-3,000	N
Gonyaulax polygramma (T)	32.5 (5.4)	1,500-3,000	N

Alexandrium tamarense (T)	32.6 (2.7)	1,000-3,000	N
Lingulodinium polyedrum (T)	38.2 (3.6)	1,000-3,000	N

To confirm no ingestion by the predators on some prey species, additional higher prey concentrations were provided. Mean equivalent spherical diameter (ESD, μm) ± standard deviation of the mean was measured by an electronic particle counter (Coulter Multisizer II, Coulter Corporation, Miami, Florida, USA). n > 2000 for each species. The abundances of the predator for each target prey were 2,000-5,000 cells ml^{-1}.

T, Thecate. NT, Non-thecate. Y, *B. cincta* observed to feed on a living food cell; N, *B. cincta* was observed not to feed on a living food cell.

For observing the ingestion of algal prey under a light microscope and/or an epifluorescence microscope, the initial concentrations of *B. cincta* and each target algal species were established as described above. Triplicate 80-ml PC bottles with mixtures of *B. cincta* and target prey and duplicate predator control bottles containing *B. cincta* only were set up for each target algal species. The bottles were filled to capacity with freshly filtered seawater, capped, and then placed on a vertically rotating plate rotating at 0.9 rpm and incubated at 20 °C under a 14:10 h light–dark cycle with cool white fluorescent light at 20 μE m^{-2} s^{-1}. After 6, 12, 24, and 48 h of incubation, a 5-ml aliquot was removed from each bottle and transferred to a 20-ml bottle. Aliquots of 0.2 ml were placed on slides and then covered with coverslips. Under these conditions, the *B. cincta* cells were alive, but almost motionless. The protoplasms of >200 *B. cincta* cells were carefully examined using a light microscope and/or an epifluorescence microscope (Zeiss-Axiovert 200M; Carl Zeiss Ltd.) at a magnification of 100-400X to determine whether *B. cincta* was able to feed on the target prey species. Pictures showing the ingested cells of each target algal species inside a *B. cincta* cell were taken at a magnification of 400-1,000X using digital cameras attached to these microscopes. For observations using TEM, approximately 8.1×10^5 to 2.7×10^6 cells of each target algal species were added to each of three 270-ml PC bottles, each of which contained *B. cincta* at a concentration of 8,000-10,000 cells ml^{-1}. One "target prey only" control bottle and one *B. cincta* control bottle without added prey were set up for each experiment. The bottles were placed on a vertically rotating plate rotating at 0.9 rpm and incubated at 20 °C under a 14:10 h light-dark cycle with cool white fluorescent light at 20 μE m^{-2} s^{-1}. At the beginning and after 2-d incubation periods, the contents of one experimental bottle from each interval were distributed into five 50-ml centrifuge tubes and then concentrated at 1,610 × *g* for 10 min. The 5 pellets from the 5 centrifuge tubes were then transferred into 1.5-ml tubes and fixed for 1.5 h in 4% (w/v) glutaraldehyde in culture medium. The processes of rinsing, dehydration, sectioning, and taking TEM photos were conducted as described above.

5.4.6 Feeding mechanisms

Expt. 2 was designed to investigate the feeding behavior of *B. cincta* when a unialgal diet of the following organisms was provided as prey: the prymnesiophyte *Isochrysis galbana*, the cryptophytes *Teleaulax* sp. and *Rhodomonas salina*, the raphidophyte *H. akashiwo*, the euglenophyte *Eutreptiella gymnastica*, and the mixotrophic dinoflagellate *Amphidinium carterae*. Feeding by *B. cincta* on these prey species had been established in Expt. 1. The initial concentrations of predator and prey were the same as in Expt. 1.

The initial concentrations of *B. cincta* and the target algal species were established using an autopipette to deliver a predetermined volume of culture with a known cell density to the experimental bottles. One 80-ml PC bottle with mixtures of *B. cincta* and algal prey was set up for each target algal species. The bottle was filled to capacity with freshly filtered seawater, capped, and then mixed well. After a 1-min incubation, a 1-ml aliquot was removed from the bottle and transferred to a 1-ml Sedgwick-Rafter chamber (SRC). The behavior of >60 *B. cincta* cells for each target prey species was monitored under a light microscope and/or an epifluorescence microscope at a magnification of ×100 to ×630. All feeding processes were observed, from the time a prey cell was captured to the time when it was engulfed by the predator. A series of photographs showing the feeding process for a *B. cincta* cell were taken using a video analyzing system (Sony DXC-C33; Sony Co., Tokyo, Japan) mounted on an epifluorescence microscope at a magnification of ×100 to ×630. After *B. cincta* was provided with *H. akashiwo* as prey, I measured the time lag (n = 4) between the deployment of the tow filament and peduncle of *B. cincta* and the time (n = 4) for a prey cell to be completely ingested by a *B. cincta* cell after the predator had deployed its peduncle to the prey cell.

5.4.7 Comparison of growth and ingestion rates for edible prey at single prey concentrations

Expt 3 was designed to compare the growth and ingestion rates of *B. cincta* when *A. carterae*, *E. gymnastica, H. akashiwo*, *I. galbana, R. salina,* and *Teleaulax* sp. were provided at a single prey concentration (Table 4.3). It was confirmed in Expt 1 that these prey species are consumed by *B. cincta*.

A dense culture of ~15,000 cells ml^{-1} of *B. cincta* growing mixotrophically on *H. akashiwo* in f/2 medium and under illumination of 20 µE m^{-2} s^{-1} on a 14:10 h light-dark cycle was transferred to one 1-l PC bottle containing f/2 medium when *H. akashiwo* was undetectable. This culture was maintained in f/2 medium for 2 d under illumination of 20 µE m^{-2} s^{-1} on a 14:10 h light-dark cycle, and then transferred to another 1-l PC bottle containing target prey at a low prey concentration. After approximately 1-2 d incubation, when the target prey was undetectable, the culture was transferred to another 1-l PC bottle. Three 1-ml aliquots from the bottle were examined using a compound microscope to determine the concentrations of *B. cincta* cells and the cultures were then used in further experiments.

The initial concentrations of *B. cincta* and each target prey were established using an autopipette to deliver predetermined volumes of known cell concentrations to the bottles. Triplicate 42-ml PC experimental bottles containing mixtures of predator and prey, triplicate prey control bottles containing prey only, and triplicate predator control bottles containing only predator were set up for each target prey. To make the water conditions similar, the water of a predator culture was filtered through a 0.7-µm GF/F filter and then added to the prey control bottles in the same amount as the volume of the predator culture added to the experiment bottles for each predator-prey combination. Next, 5 ml of f/2 medium were added to all the bottles, which were then filled to capacity with freshly filtered seawater and capped. To determine the predator and prey concentrations at the beginning of the experiment and the prey concentrations after 2 d, a 5-ml aliquot was removed from each bottle and fixed with 5% (v/v) Lugol's solution, and all or >300 predator and

prey cells in three 1-ml SRCs were enumerated. Prior to taking subsamples, the condition of *B. cincta* and its prey was assessed using a dissecting microscope. The bottles were filled again to capacity with freshly filtered seawater, capped, and placed on a rotating wheel at 0.9 rpm at 20 °C under illumination of 20 μE m^{-2} s^{-1} on a 14:10 h light-dark cycle. The dilution of the cultures associated with refilling the bottles was taken into consideration when calculating the growth and ingestion rates.

The specific growth rate of *B. cincta*, μ (d^{-1}), was calculated as follows:

$$\mu = \frac{\mathrm{Ln}\,(W_t / W_0)}{t} \qquad (1)$$

,

where W_0 is the initial concentration of *B. cincta* and W_t is the final concentration after time t. The time was 2 d.

The ingestion and clearance rates were calculated using the equations of Frost (1972) and Heinbokel (1978). The incubation times used for calculating the ingestion and clearance rates were the same as those for estimating the growth rate.

5.4.8 Effects of prey concentration

Expt. 4 was designed to investigate the effects of prey concentration on the growth and ingestion rate of *B. cincta*. I measured the growth, ingestion, and clearance rates of *B. cincta* on *H. akashiwo* (carbon content per cell = 0.1 ng C) as a function of prey concentration.

A dense culture of ~15,000 cells ml^{-1} of *B. cincta* growing mixotrophically on *H. akashiwo* in f/2 medium and under illumination of 20 μE m^{-2} s^{-1} on a 14:10 h light-dark cycle was transferred to one 1-l PC bottle containing f/2 medium when *H. akashiwo* was undetectable. This culture was maintained in f/2 medium for 2 d under illumination of 20 μE m^{-2} s^{-1} on a 14:10 h light-dark cycle and then

transferred to another 1-l PC bottle. Three 1-ml aliquots from the bottle were examined using a compound microscope to determine the cell concentrations of *B. cincta*, and the cultures were then used to conduct experiments.

The initial concentrations of *B. cincta* and *H. akashiwo* were established as described above. Triplicate 42-ml PC experimental bottles containing mixtures of predator and prey, triplicate prey control bottles containing prey only, and triplicate predator control bottles containing predators only were set up for each predator-prey combination. To ensure uniform water conditions, I used the same procedure as used in Expt. 3. Next, 5 ml of f/2 medium were added to all the bottles, which were then filled to capacity with freshly filtered seawater and capped. To determine the actual initial predator and prey densities (cells ml^{-1}) at the beginning of the experiment (i.e. *H. akashiwo* and *B. cincta* = 30/7, 80/15, 270/26, 930/49, 2860/79, 9440/178, and 29460/281, respectively) and the final predator and prey densities after a 2-d incubation, 5-ml aliquots were removed from each bottle and fixed with 5% Lugol's solution, and all *B. cincta* cells and all or >300 prey cells in three 1-ml SRCs were enumerated. Prior to taking the subsamples, the condition of *B. cincta* and its prey was assessed under a dissecting microscope. The bottles were filled again to capacity with f/2 medium, capped, placed on a vertically rotating plate rotating at 0.9 rpm, and incubated at 20 °C under a 14:10 h light-dark cycle with cool white fluorescent light at 20 μE m^{-2} s^{-1}. A light intensity of 20 μE m^{-2} s^{-1} was used so that I could compare our data with those on the growth and ingestion rates of several other mixotrophic dinoflagellates fed on the same prey under the same light conditions (summarized by Burkholder et al. 2008; Jeong et al. 2010c). The dilution of the cultures associated with refilling the bottles was taken into consideration when calculating the growth and ingestion rates.

The specific growth rate of *B. cincta*, μ (d^{-1}), was calculated as described above. Data for *B. cincta* growth rate were fitted to the following equation:

$$\mu = \frac{\mu_{max} \quad (x - x')}{K_{GR} + (x - x')} \qquad (2)$$

,

where μ_{max} = the maximum growth rate (d^{-1}), x = prey concentration (cells ml^{-1} or ng C ml^{-1}), x' = threshold prey concentration (i.e. the prey concentration where $\mu = 0$), and K_{GR} = the prey concentration sustaining ½ μ_{max}. Data were iteratively fitted to the model using DeltaGraph® (SPSS Inc., Chicago, IL, USA).

Ingestion and clearance rates for 2 d were calculated using the equations of Frost (1972) and Heinbokel (1978). Ingestion rate data were fitted to a Michaelis-Menten equation as follows:

$$IR = \frac{I_{max} \quad (x)}{K_{IR} + (x)} \qquad (3)$$

where I_{max} is the maximum ingestion rate (cells $predator^{-1}$ d^{-1} or ng C $predator^{-1}$ d^{-1}), x is the prey concentration (cells ml^{-1} or ng C ml^{-1}), and K_{IR} is the prey concentration sustaining ½ I_{max}.

5.4.9 Potential grazing impact

By combining field data on the abundances of the predator and the target prey with the ingestion rates of the predator feeding on the prey obtained in the present study, I estimated the grazing coefficients attributable to *B. cincta* on co-occurring *H. akashiwo*. Data on the abundances of *B. cincta* and the co-occurring *H. akashiwo* used in this estimate were obtained by analyzing the water samples taken from Shiwha Bay, Korea, in 2008 using real-time PCR for *B. cincta* and cell counting for *H. akashiwo*.

The grazing coefficients (g, d^{-1}) were calculated using the following formula:

$$g = CR \times PC \times 24, \qquad (4)$$

where CR (ml predator^{-1} h^{-1}) is the clearance rate of *B. cincta* on a target prey at a given prey concentration and PC is the predator concentration (cells ml^{-1}). The CR values were calculated as follows:

$$CR = IR/x, \quad (5)$$

where IR (i.e. cells eaten by predator^{-1} h^{-1}) is the ingestion rate of *B. cincta* on the target prey and x (cells ml^{-1}) is the prey concentration. These CR values were corrected using Q_{10} = 2.8 (Hansen et al. 1997) because the in situ water temperature and the temperature used in the laboratory for this experiment (20 °C) were sometimes different.

5.4.10 Swimming speed

A dense culture of ~15,000 cells ml^{-1} of *B. cincta*, maintained as described above, was transferred to a 500-ml PC bottle. An aliquot from the bottle was added to a 50-ml cell culture flask and allowed to acclimate for 30 min. A video camera was focused on a field (i.e., observed as one circle) in a cell culture flask under a dissecting microscope at 20 °C and swimming *B. cincta* cells were recorded at a magnification of ×50 using a video analyzing system (SV-C660; Samsung, Seoul, Korea) and captured using a CCD camera (KP-D20BU; Hitachi, Tokyo, Japan). The mean and maximum swimming velocities were analyzed for all swimming cells observed for the first 10 min. The average swimming speed was calculated on the basis of the linear displacement of cells in 1 s during single-frame playback. The swimming speeds of 30 cells were measured.

5.5 Results

5.5.1 Morphology and rDNA sequences of the Korean strain of *Biecheleria cincta*

The morphology of this strain is similar to that of the Naples strain described by Siano et al. (2009). The cells of this Korean strain are almost spherical with a

distinct and descending cingulum, which is displaced by 0.2-0.4 × cell length (Fig. 5.1A-B, 5.1D-E). The sulcus becomes wider toward the antapex (Fig. 5.1A, 5.1F, 5.2D-E). The central part of the cell is filled with a large nucleus (N) (Fig. 5.1B). The chloroplasts (C) are brownish yellow and located at the cell periphery (Fig. 5.1B-C).

Cells are covered with hexagonal or pentagonal amphiesmal vesicles (AVs) (Fig. 5.1D-G, Fig. 5.2). The AVs are arranged in 10-12 latitudinal rows: 4 to 5 latitudinal rows on the episome (E1, E2, E3, and E4 in Fig. 5.1D or E1, E2, E3, E4, and E5 in Fig. 5.1E), 3 latitudinal rows on the cingulum (C1, C2, and C3 in Fig. 5.1E, 5.1G), and 3 to 4 latitudinal rows on the hyposome (H1, H2, and H3 in Fig. 5.1F or H1, H2, H3, and H4 in Fig. 5.1G). The total number of AVs is ~140. The apical furrow apparatus is rather short, and comprises a narrow elongate apical vesicle (EAV), approximately 2-2.5 μm, which extends from the mid-ventral side of the episome over the apex to the dorsal side (Fig. 5.1D-E, 5.2A). The finger-like protrusion (FLP) on the right side of the episome extends to the intercingular-sulcal region (Fig. 5.1E).

The EAV is ornamented with a central row of approximately 30 small knobs (Fig. 5.2A-B). Six rounded depressions (RD1-RD6) in rows bordering the cingulum were observed (Fig. 5.2A, 5.2C). The number of rows varies from 5 to 6 near the sulcus and decreases gradually in number toward the dorsal side, finally becoming a single row (Fig. 5.2A, 5.2C-E). The sulcus becomes wider toward the antapex and comprises ~10 AVs arranged in 3 to 4 longitudinal rows (Fig. 5.1F, 5.2D-E). The peduncle (PE) was observed on SEM (5.2D-E). Thin TEM sections showed the eyespot (5.4B).

The length and width of cells that grew photosynthetically and were then fixed with 5% (v/v) acidic Lugol's solution (n = 60) were 8.2-13.8 μm (mean ± standard error = 11.2 ± 0.15) and 6.9-13.2 μm (10.1 ± 0.2), respectively, whereas cells fed with *H. akashiwo* and then fixed with 5% acidic Lugol's solution (n = 60)

measured 9.9-17.2 μm (14.1 ± 0.2) and 9.2-15.8 μm (12.7 ± 0.2), respectively. The ratio of cell length to cell width of cells fed on *H. akashiwo* (mean ± standard error = 1.1 ± 0.01; range = 1.0-1.4, n = 60) was the same as that of cells starved for 2 d (mean ± standard error = 1.1 ± 0.01; range = 1.0-1.5, n = 60).

The SSU, ITS1, ITS2, 5.8S, and LSU rDNA sequences, a total of 3,132 bp of this Korean strain of *B. cincta* (GenBank FR690459) were analyzed. The LSU rDNA sequence of the Korean strain is identical to that of the Naples strain (GenBank FJ024705). The SSU rDNA sequence of the Korean strain is 1% different from that of *Biecheleria baltica* (previously *W. halophila*; GenBank EF058252) and 3% different from that of *Polarella glacialis* (GenBank GQ375263) and *Pelagodinium bei* (previously *Gymnodinium beii*; GenBank U41087), the 3 closest species. The SSU rDNA sequence of the Naples strain has not been reported. Thus, the phylogenetic trees based on the SSU rDNA sequences of dinoflagellates show that this dinoflagellate is a sister species to *B. baltica* (Fig. 5.3).

In the phylogenetic trees based on SSU rDNA sequences, most species belonging to the family Suessiaceae and all species in the family Pfiesteriaceae reported to date have a feeding tube, the peduncle (Fig. 5.3). In contrast, all species in the families Polykrikaceae and Warnowiaceae examined to date are engulfment feeders. However, some species in the family Gymnodiniaceae (e.g., *Paragymnodinium shiwhaense*) are peduncle feeders, whereas others (e.g., *C. polykrikoides*) are engulfment feeders.

5.5.2 Prey species

Among the diverse prey provided, *B. cincta* ingested the algal species that had equivalent spherical diameters (ESDs) ≤12.6 μm (e.g., *I. galbana*, *Teleaulax* sp., *R. salina*, *H. akashiwo*, *Heterocapsa rotundata*, *A. carterae*, and *E. gymnastica*), exceptions being the diatom *S. costatum* and the dinoflagellate *P. minimum* (Table 4.2). TEM photographs, taken before and after edible algal prey had been provided,

clearly showed that *B. cincta* contained ingested algal prey cells inside its protoplasm (Fig. 5.4, 5.5). However, *B. cincta* did not feed on larger algal species having an ESD ≥15 μm (e.g., the dinoflagellates *Heterocapsa triquetra*, *Scrippsiella trochoidea*, *Cochlodinium polykrikoides*, *Prorocentrum micans*, *Akashiwo sanguinea*, *Gonyaulax polygramma*, *Alexandrium tamarense*, and *Lingulodinium polyedrum*) and *S. costatum* and *P. minimum* (Table 4.2).

5.5.3 Feeding behavior

Biecheleria cincta fed on its algal prey using a peduncle after anchoring the prey with a tow filament (Fig. 5.6). The distances between the predator cell and the prey cell were 13-22 μm when the predator attached the tow filament to the prey cell; however, this distance was reduced to a value similar to the prey cell length before the peduncle was deployed. The time lag (mean ± standard error, n = 4) between the deployment of the tow filament and that of the peduncle was 12.5 ± 1.3 s for *H. akashiwo* prey. The prey materials were transferred inside the predator cell through the peduncle. The time (mean ± standard error, n = 4) for an *H. akashiwo* prey cell to be completely fed on by a *B. cincta* cell after the predator had deployed its peduncle to the prey cell was 603 ± 48 s. The other edible prey species examined in the present study were ingested by *B. cincta* cells in a manner similar to that for *H. akashiwo* prey.

5.5.4 Comparison of growth and ingestion rates at a single prey concentration

I measured the growth and ingestion rates of *B. cincta* feeding on 6 edible prey species at a single prey concentration (Table 4.3). When the mean prey concentration was 1,990-3,330 ng C ml^{-1}, the specific growth rate (i.e. mixotrophic growth) of *B. cincta* feeding on *I. galbana* (0.086 d^{-1}) was not significantly different from that without added prey (0.033 d^{-1}; autotrophic growth) ($p > 0.1$, 2-tailed *t*-test), whereas that when feeding on *E. gymnastica* (0.117 d^{-1}) was higher than that without added prey ($p < 0.05$, 1-tailed *t*-test).

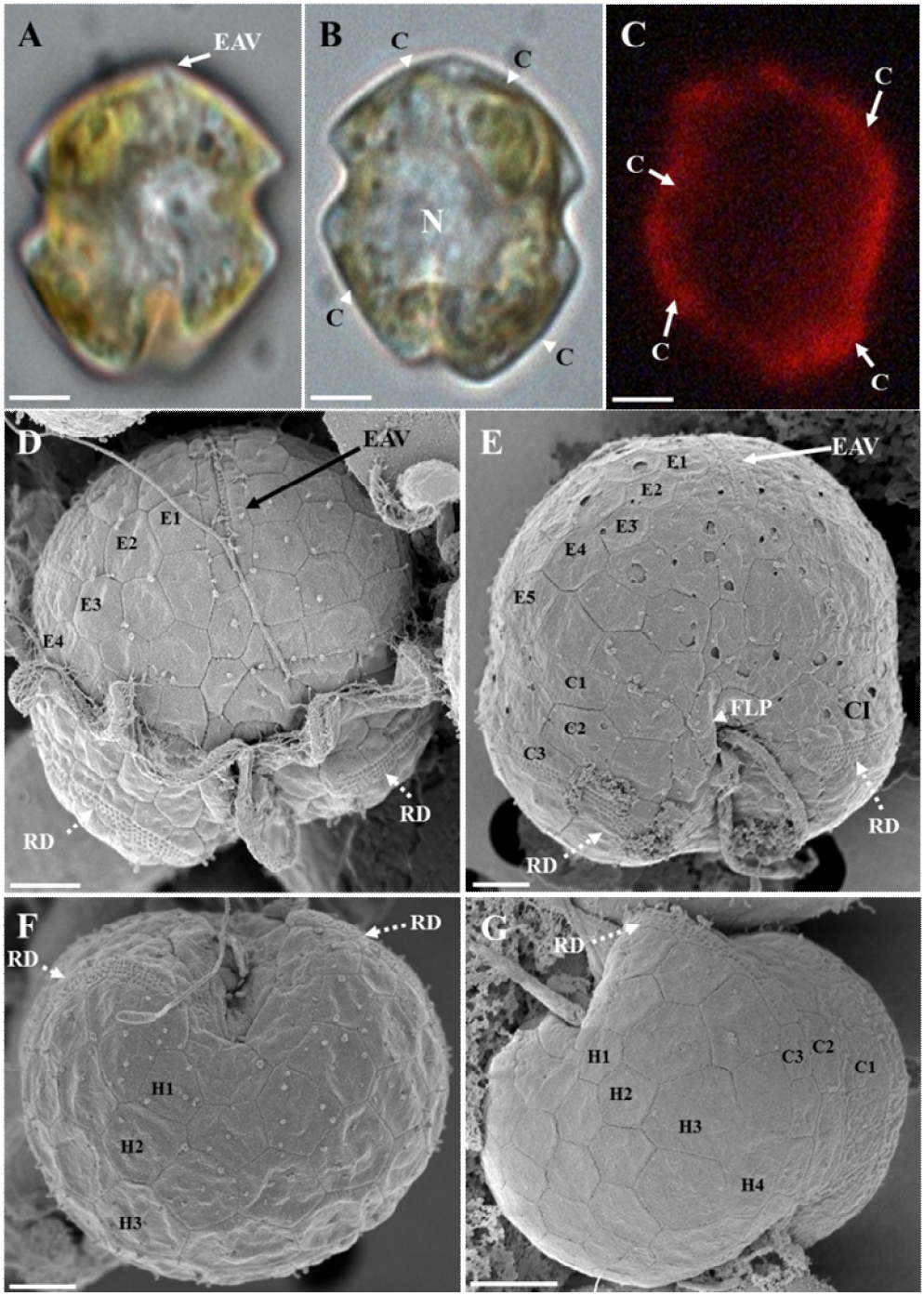
A
EAV
B
C
C
N
C
C
C
C
C
C
C
C
D
EAV
E1
E2
E3
E4
RD
RD
E
EAV
E1
E2
E3
E4
E5
C1
C2
C3
FLP
CI
RD
RD
F
RD
RD
H1
H2
H3
G
RD
H1
H2
H3
H4
C3
C2
C1

Fig. 5.1 Micrographs of *Biecheleria cincta* isolated from Shiwha Bay, Korea. **A-C**. Micrographs taken with a light microscope (**A, B**) and epifluorescence microscope (**C**). **A.** Ventral view. EAV, elongate apical vesicles (arrow). **B.** Dorsal view. The brownish yellow chloroplasts (C) (arrowheads), located at the cell periphery, and the nucleus (N) in the central part of the cell. **C.** Dorsal view. Cell visualized by epifluorescence microscopy, showing the presence of several irregularly shaped chloroplasts (C) (arrows) located at the cell periphery. **D-G.** Micrographs taken using a scanning electron microscope. **D**, **E.** Ventral view. Some cells had four latitudinal series of vesicles on the episome (E1–E4 in **D**), whereas the other cells had 5 (E1–E5 in **E**). All cells had three latitudinal series of vesicles on the cingulum (C1–C3). CI, cingulum; FLP, finger-like protrusion; RD, rounded depressions. **F, G.** Antapical view. Some cells had three latitudinal series of vesicles on the hyposome (H1–H3 in **F**), whereas the other cells had four (H1–H4 in **G**). All scale bars = 2 μm.

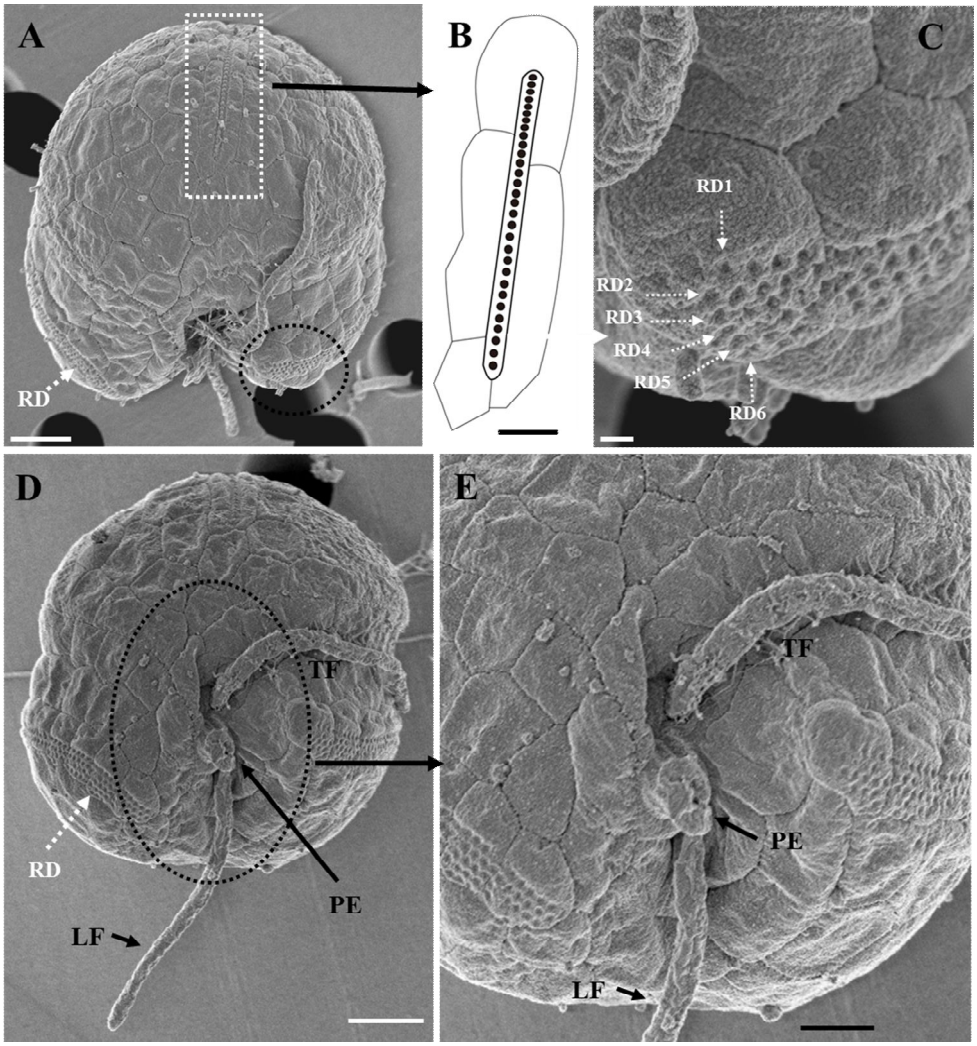

Fig. 5.2 Micrographs of *Biecheleria cincta* taken using a scanning electron microscope and drawing of the elongate apical vesicles (EAV). **A.** Apical view showing the EAV. **B**. Drawing of the EAV. The ventral part of the EAV showing the long and narrow central plate ornamented with knobs. **C.** Rounded depressions (RD1-RD6) in rows bordering the cingulum. **D.** Micrographs showing a peduncle (PE). **E.** Enlarged from Fig. **D**. LF: longitudinal flagellum. TF: transverse flagellum. Scale bars = 0.2 μm for Fig. **C**, 0.5 μm for Fig. **B**, 1 μm for Fig. **E**, and 2 μm for Fig. **A, D.**

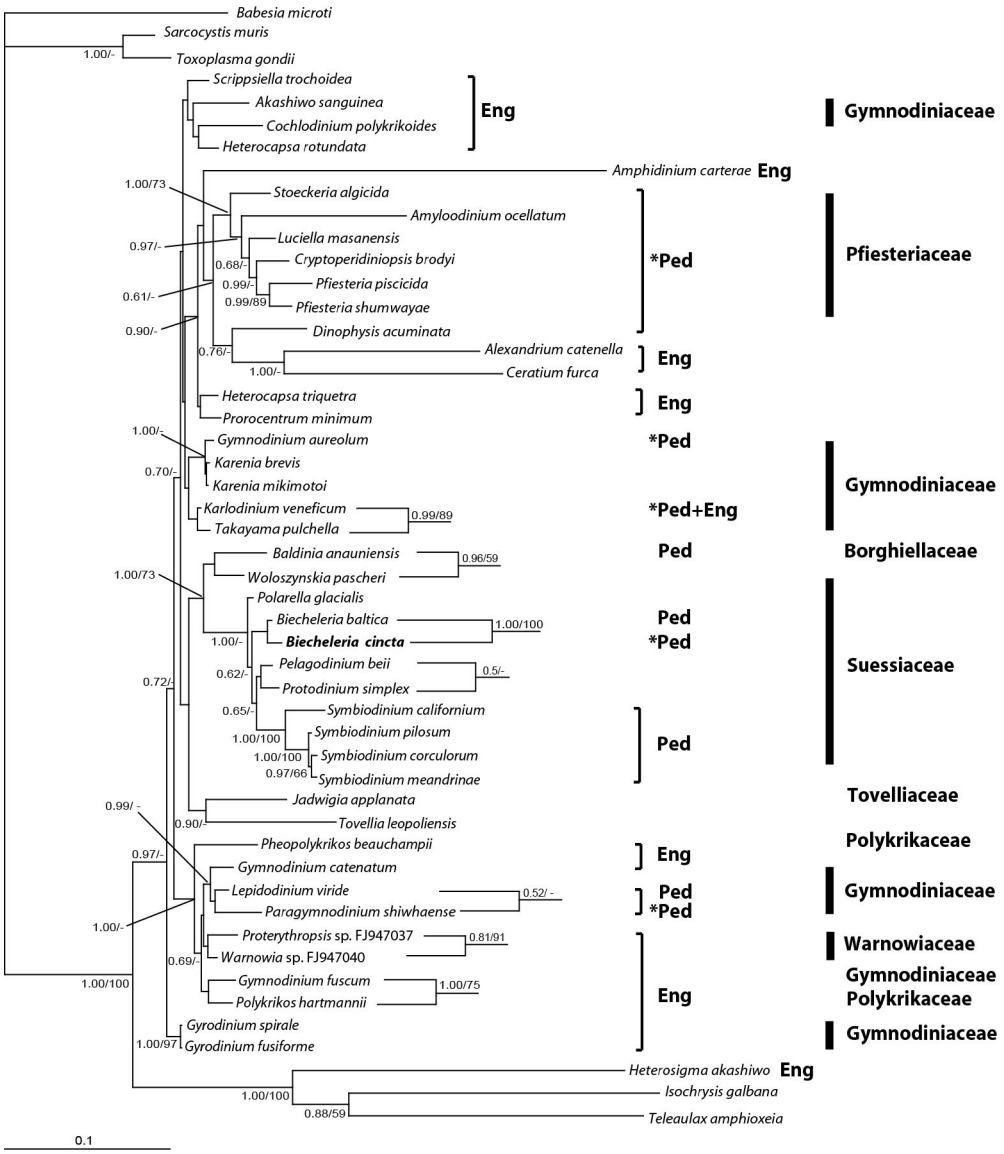

Fig. 5.3 Bayesian consensus trees based on the small subunit (SSU) rDNA data of dinoflagellates, showing the position of *Biecheleria cincta* (bold). Maximum likelihood (ML) tree based on 1,709 aligned positions of nuclear SSU rDNA with *Babesia microti, Sarcocystis muris,* and *Toxoplasma gondii* as outgroup taxa. The parameters were as follows: assumed nucleotide frequency with empirical; substitution rate matrix with A-C substitutions = 1.0000, A-G = 2.8996, A-T =1.0,

C-G = 1.0, C-T = 5.8078, and G-T = 1.0; proportion of sites are assumed to be invariable = 0.3567 and rates for variable sites assumed to follow a gamma distribution with shape parameter = 0.6022. The branch lengths are proportional to the amount of character changes. The numbers above the branches indicate the Bayesian posterior probability (left) and ML bootstrap values (right). Posterior probabilities ≥0.5 are shown. In feeding mechanisms, Ped: peduncle has been reported, but use of the peduncle has not been observed. *Ped: peduncle has been reported and use of the peduncle has been observed. Eng: engulfment feeder.

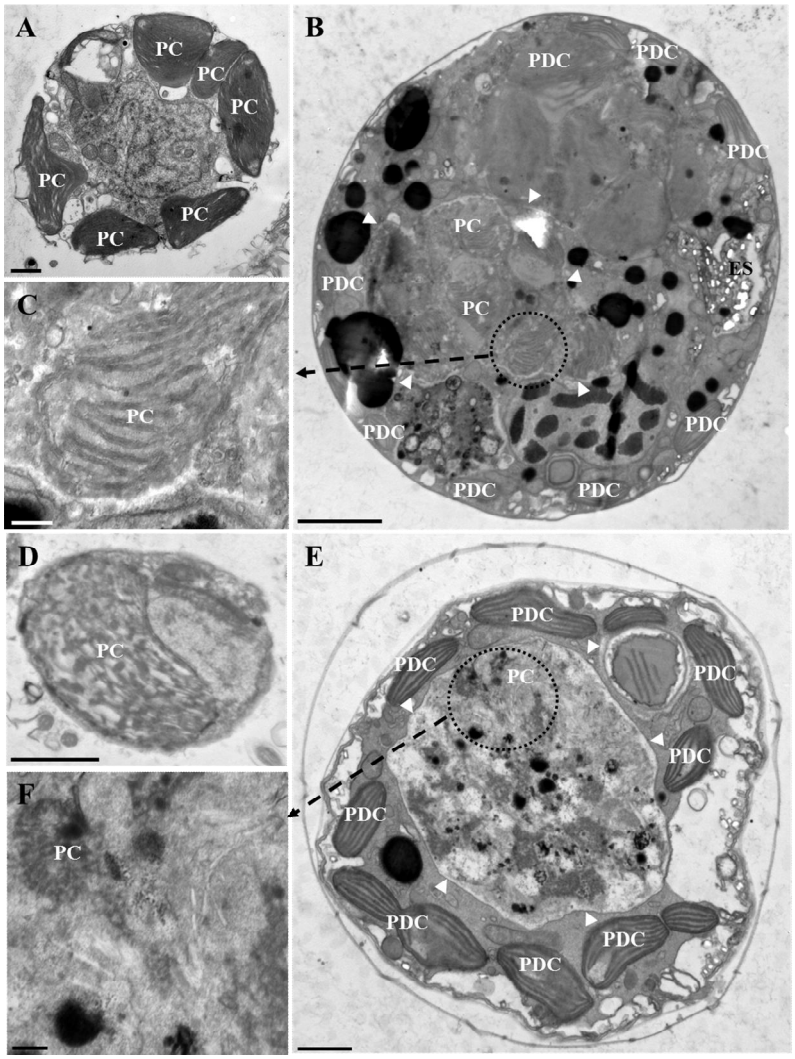

Fig. 5.4 The feeding by *Biecheleria cincta* on *Heterosigma akashiwo* and *Teleaulex* sp. Photomicrographs were taken using a transmission electron microscope. **A.** A *H. akashiwo* cell not ingested. **B.** A *B. cincta* cell with an ingested *H. akashiwo* cell (inside dashed circle). Micrograph showing the eyespot (ES) inside the protoplasm. **C.** Enlarged from (**B**). **D.** A *Teleaulex* sp. cell not ingested. **E.** A *B. cincta* cell with an ingested *Teleaulex* sp. cell (inside dashed circle). **F.** Enlarged from (**E**). PC, prey's chloroplast; PDC, predator's chloroplast. Scale bars = 1 μm for (**A**, **B**, **D**, **E**), 0.5 μm for (**C**), and 0.1 μm for (**F**).

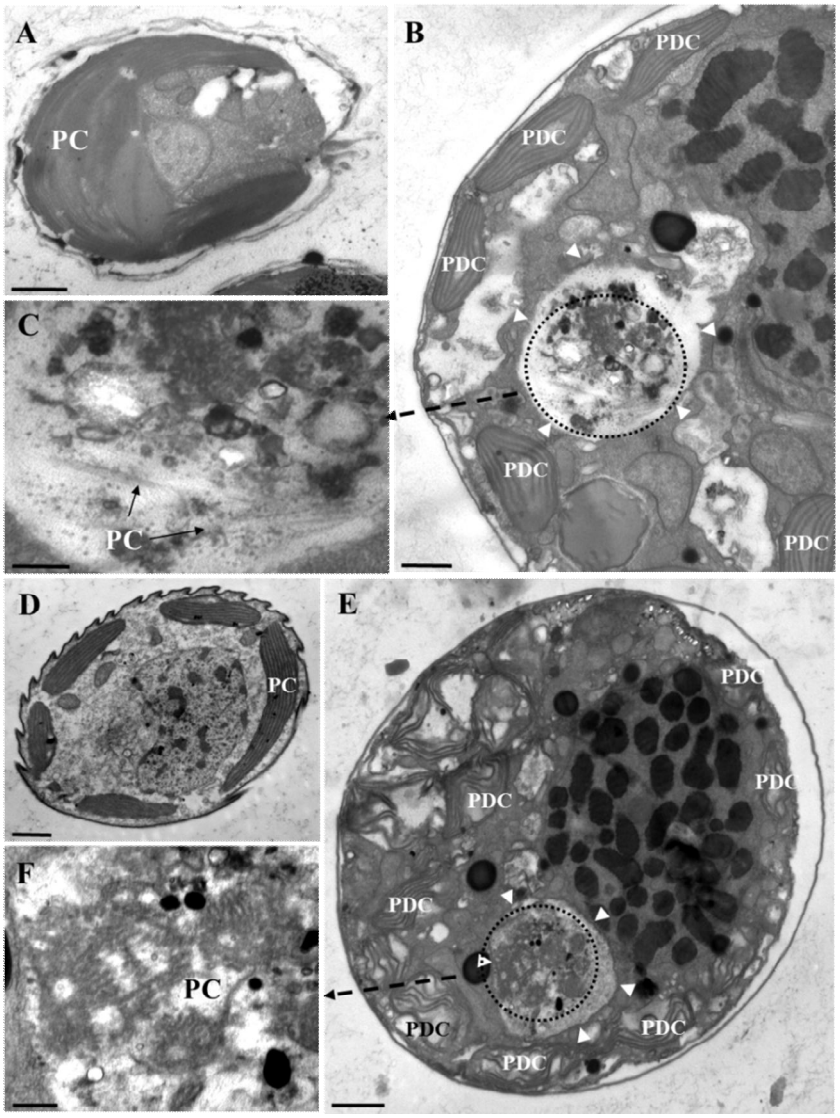

Fig. 5.5 The feeding by *Biecheleria cincta* on *Isochrysis galbana* and *Eutreptiella gymnastica*. Photomicrographs were taken using a transmission electron microscope. **A.** An *I. galbana* cell not ingested. **B.** A *B. cincta* cell with an ingested *I. galbana* cell (inside dashed circle). **C.** Enlarged from (**B**). **D.** An *E. gymnastica* cell not ingested. **E.** A *B. cincta* cell with an ingested *E. gymnastica* cell (inside dashed circle). **F.** Enlarged from (**E**). PC, prey's chloroplast; PDC, predator's chloroplast. Scale bars = 1 μm for (**D, E**), 0.5 μm for (**A, B**), and 0.2 μm for (**C, F**).

When the mean prey concentration was ca. 1,460-1,610 ng C ml^{-1}, the specific growth rate (i.e. mixotrophic growth) of *B. cincta* feeding on *H. akashiwo* (0.475 d^{-1}) was significantly higher than that when feeding on *R. salina* (0.265 d^{-1}), *A. carterae* (0.229 d^{-1}), or *Teleaulax* sp. (0.157 d^{-1}), ($p < 0.01$, one-tailed *t*-test). The ingestion rate of *B. cincta* feeding on *H. akashiwo* (0.41 ng C $grazer^{-1}$ d^{-1}) was significantly higher than that when feeding on the other prey species (0-0.19 ng C $grazer^{-1}$ d^{-1}) ($p < 0.05$, one-tailed *t*-test). The ingestion rate of *B. cincta* feeding on *I. galbana* was not detected (Table 4.3).

Both the growth and ingestion rates of *B. cincta* feeding on the 6 edible prey species were not significantly correlated with prey size [$p > 0.1$, linear regression analysis of variance (ANOVA); Fig. 5.7A and 5.7B]. However, the growth rates of *B. cincta* feeding on the 6 edible prey species were significantly correlated with the ingestion rates for these species ($p < 0.05$; Fig. 5.7C).

5.5.5 Effects of prey concentration

With increasing mean prey concentration, the specific growth rates of *B. cincta* increased rapidly with increasing mean prey concentration before saturating at ~134 ng C ml^{-1} (1,340 cells ml^{-1}) when fed *H. akashiwo* (Fig. 5.8). When the data were fitted to Eq. (2), the maximum specific growth rate (i.e. mixotrophic growth) of *B. cincta* on *H. akashiwo* was 0.499 d^{-1} at 20 °C under illumination of 20 μE m^{-2} s^{-1} on a 14:10 h light-dark cycle. Its growth rate (i.e. autotrophic growth) under the same light conditions without added prey was 0.040 d^{-1}.

With increasing mean prey concentration, the ingestion rates of *B. cincta* feeding on *H. akashiwo* increased rapidly at prey concentrations ≤ ~134 ng C ml^{-1} (1,340 cells ml^{-1}), but increased more slowly at higher prey concentrations (Fig. 5.9). When the data were fitted to Eq.

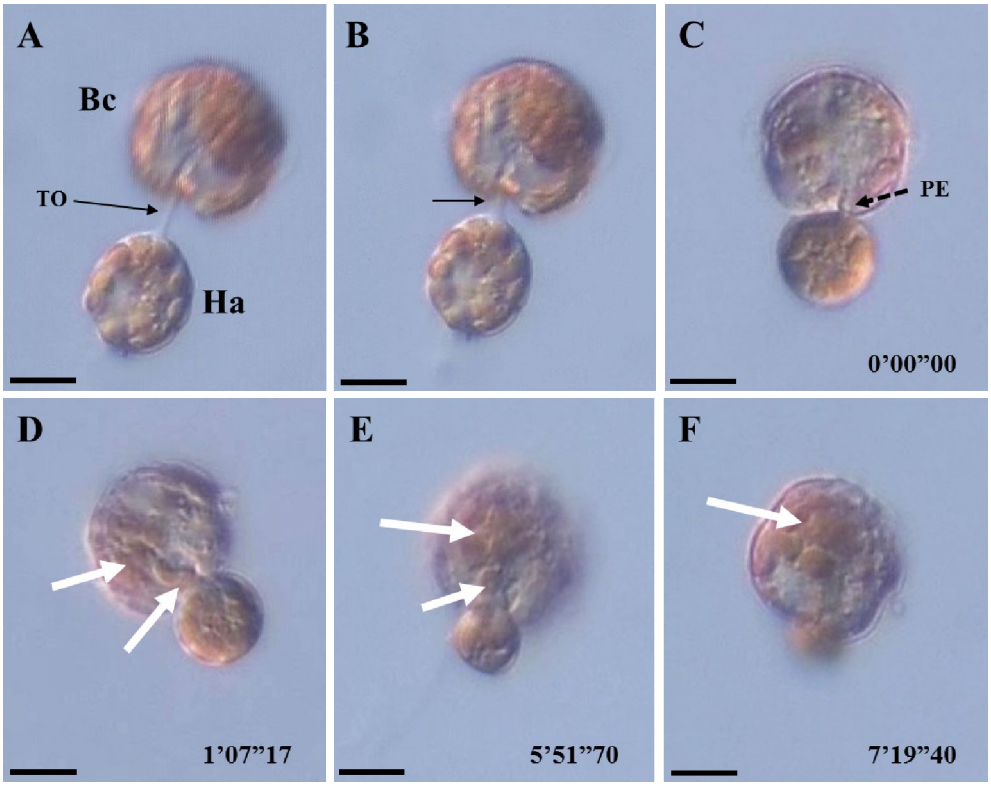

Fig. 5.6 Feeding process of *Biecheleria cincta* (Bc) on *Heterosigma akashiwo* (Ha). **A.** *B. cincta* capturing a *H. akashiwo* cell using a tow filament (TO). **B.** The distances between the predator cell and the prey cell are reduced before the peduncle is deployed. **C-F.** *B. cincta* sucking prey materials through the peduncle (PE) (black dashed arrow). *B. cincta* containing prey materials (white arrow). The prey and predator cells in (**A** and **B**) are the same cells; similarly, those in (C-F) are the same cells. Scale bar = 5 μm.

Table 4.3 Comparison in growth (GR, d^{-1}) and ingestion rates (IR, ng C $predator^{-1}d^{-1}$) [means (± standard errors), n=3] of *Biecheleria cincta* on 6 edible prey species at single mean prey concentrations (MPC, ng C ml^{-1}). Cryptophyte (CR), dinoflagellate (DN), prymnesiphyte (PR), raphidophyte (RA), euglenophyte (EU). ESD: Equivalent spherical diameter (μm).

Prey species	ESD	MPC	GR	IR
Isochrysis galbana (PR)	4.8	3,330 (78)	0.086 (0.025)	0.00 (0.00)
Teleaulex sp. (CR)	5.6	1,510 (66)	0.157 (0.017)	0.19 (0.06)
Rhodomonas salina (CR)	8.8	1,350 (27)	0.265 (0.004)	0.16 (0.06)
Amphidinium carterae (DN)	9.7	1,610 (29)	0.229 (0.012)	0.09 (0.03)
Heterosigma akashiwo (RA)	11.5	1,460 (16)	0.475 (0.033)	0.41 (0.04)
Eutreptiella gymnastica (EU)	12.6	1,990 (24)	0.117 (0.011)	0.12 (0.02)
Control (without added prey)		0	0.033 (0.018)	

(3), the maximum ingestion rate of *B. cincta* feeding on *H. akashiwo* was 0.49 ng C grazer^{-1} d^{-1} (4.9 cells grazer^{-1} d^{-1}) and K_{IR} was 132 ng C ml^{-1} (1,320 cells ml^{-1}). The specific ingestion rate (IR) of *B. cincta* on *H. akashiwo* was 0.093 h^{-1}.

The maximum clearance rate and maximum volume-specific clearance rate of *B. cincta* feeding on *H. akashiwo* was 1.9 µl grazer^{-1} h^{-1} and 1.5 × 10^{6} h^{-1}, respectively.

5.5.6 Potential grazing impact

The grazing coefficients for *B. cincta* feeding on co-occurring *H. akashiwo* in water samples taken from Shiwha Bay, Korea, in 2008 (n = 14), when the abundances of *H. akashiwo* and *B. cincta* were 6-2,138 cells ml^{-1} and 0.1-113 cells ml^{-1}, respectively, were 0.001-1.102 d^{-1} (Fig. 5.10).

5.5.7 Swimming speed

The range of swimming speeds for *B. cincta* starved for 1 to 2 d was 144-378 µm s^{-1} (average swimming speed ± SE = 265 ± 11 µm s^{-1}, n = 30).

5.6 Discussion

5.6.1 *Biecheleria cincta* isolated from Korean waters

This is the first report of *Biecheleria cincta* (previously *Woloszynskia cincta*) from a locality other than the Gulf of Naples, Italy (Siano et al. 2009). The size and shape of this strain are very similar to that of the Naples strain described by Siano et al. (2009). The length and width of cells of the Korean strain that had grown photosynthetically and were then fixed with 5% acidic Lugol's solution (8-14 µm and 7-13 µm, respectively) are similar to those of the Naples strain (9-15 µm and 9-13 µm, respectively) (Siano et al. 2009). However, I found that the Korean strain had 4 or 5 latitudinal rows of amphiesmal vesicles (AVs) on the episome and 3 or 4

rows on the hyposome. Siano et al. (2009) reported that the numbers of latitudinal rows of AVs on the episome and hyposome of the Naples strain were only 4 and 3, respectively. Thus, I suggest that the numbers of latitudinal rows on the episome and hyposome are 4 to 5 and 3 to 4, respectively. A difference of 1 to 2 latitudinal rows is common in the woloszynskioid dinoflagellates (Siano et al. 2009, 2010). Six rounded depressions (RDs) in rows bordering the cingulum were observed in the present study. The presence of RDs was also reported by Siano et al. (2009), although the exact number of RDs was not stated. In addition, the present article describes, for the first time, the feeding tube (the peduncle) and eyespot in this species.

5.6.2 Prey species and feeding mechanism

The present study is also the first to reveal that *B. cincta* is a mixotrophic dinoflagellate. Accordingly, mixotrophy should be considered when exploring the ecophysiology of this species. In view of this discovery, it is likely that the other species in the genus *Biecheleria* are also mixotrophic. The present study revealed that *B. cincta* is able to feed on prey belonging to diverse taxa, including a prymnesiophyte, cryptophyte, raphidophyte, euglenophyte, and mixotrophic dinoflagellates. Recently, Yoo et al. (2013) discovered that *B. cincta* serve as prey in marine food web. Thus, *B. cincta* is likely to transfer materials from diverse prey species to organisms at higher trophic levels in marine food webs (Fig. 5.11).

The type of algal prey that *B. cincta* was able to feed on in the present study is almost the same as that of the mixotrophic dinoflagellates *C. polykrikoides, G. impudicum*, and *P. minimum* that engulf prey cells through the sulcus or suture (Jeong et al. 2004b) and the mixotrophic dinoflagellates *G. aureolum* and *P. shiwhaense* that feed on prey cells using a peduncle (Jeong et al. 2010b; Yoo et al. 2010). Therefore, in the case of co-occurrence of *B. cincta* and the above mentioned mixotrophic dinoflagellates, there might be competition for common algal prey species.

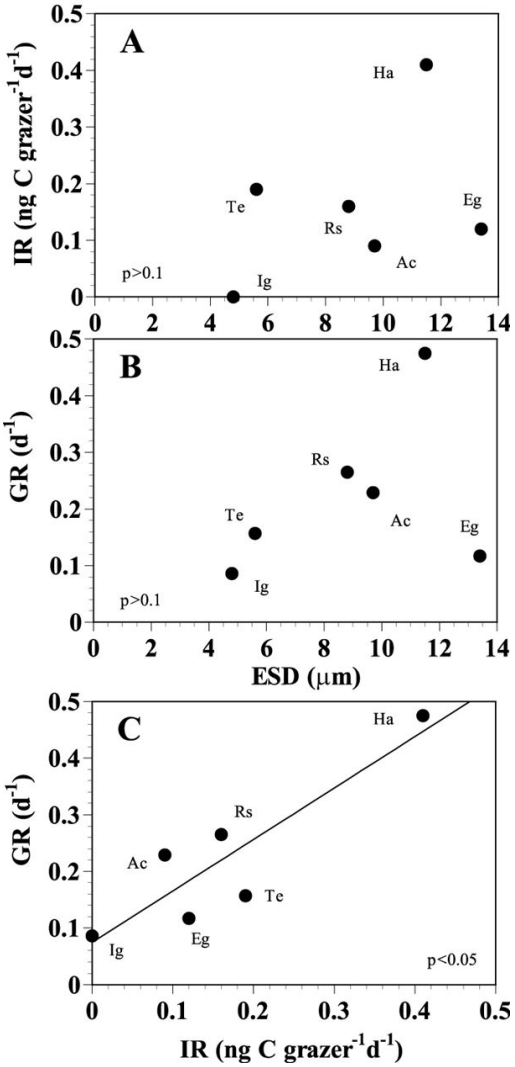

Fig. 5.7 The ingestion rate (IR; **A**) and growth rate (GR; **B**) of *Biecheleria cincta* feeding on 6 edible prey species as a function of prey size (equivalent spherical diameter, μm) and the GR as a function of the IR (**C**) as in Table 4-3. The *p* values in (**A**) and (**B**) are >0.1, whereas that in (**C**) is <0.05 [linear regression analysis of variance (ANOVA)]. The equation of the curve in (**C**), GR = 0.91 (IR) + 0.075, and r^2 = 0.791, Ac: *Amphidinium carterae*, Eg: *Eutreptiella gymnastica*, Ha: *Heterosigma akashiwo*, Ig: *Isochrysis galbana*, Rs: *Rhodomonas salina*, Te: *Teleaulax* sp..

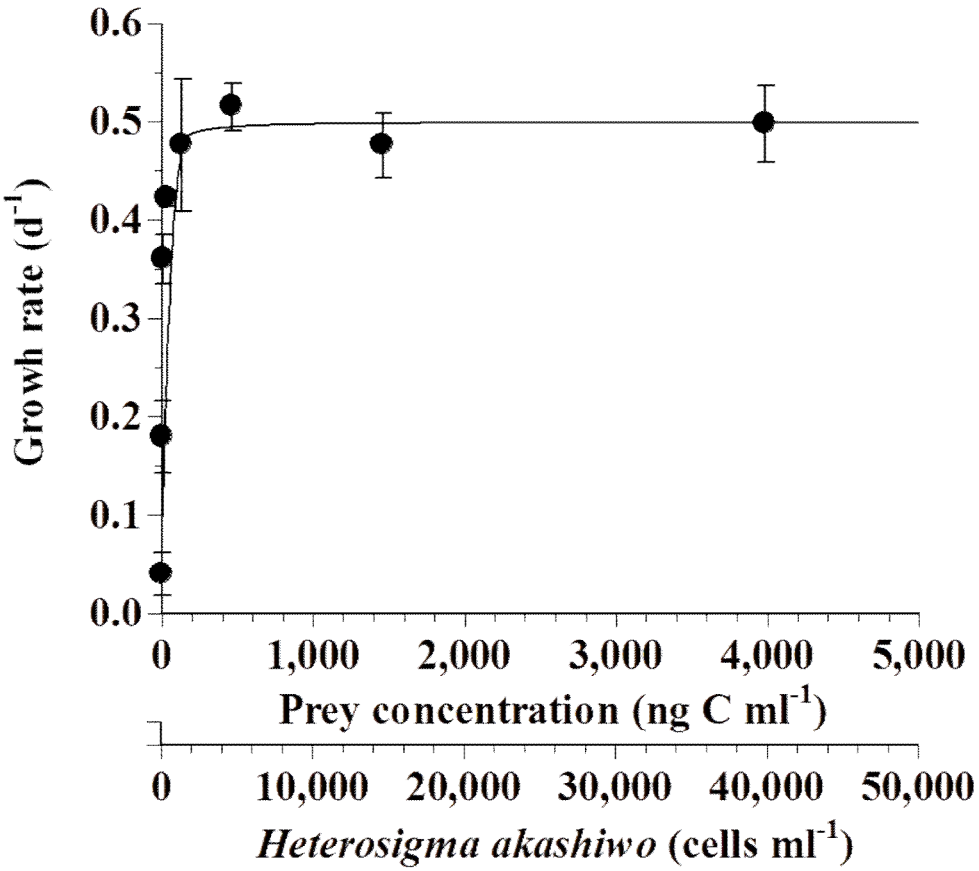

Fig. 5.8 Specific growth rates of *Biecheleria cincta* feeding on *Heterosigma akashiwo* as a function of mean prey concentration (x, ng C ml^{-1}). Symbols represent treatment means ± 1 standard error (SE). The curve is fitted by a Michaelis-Menten equation [Eq. (2)] using all the treatments in the experiment. Growth rate (GR, d^{-1}) = 0.499 [(x + 0.37)/(5.3 + (x + 0.37))], r^2 = 0.897.

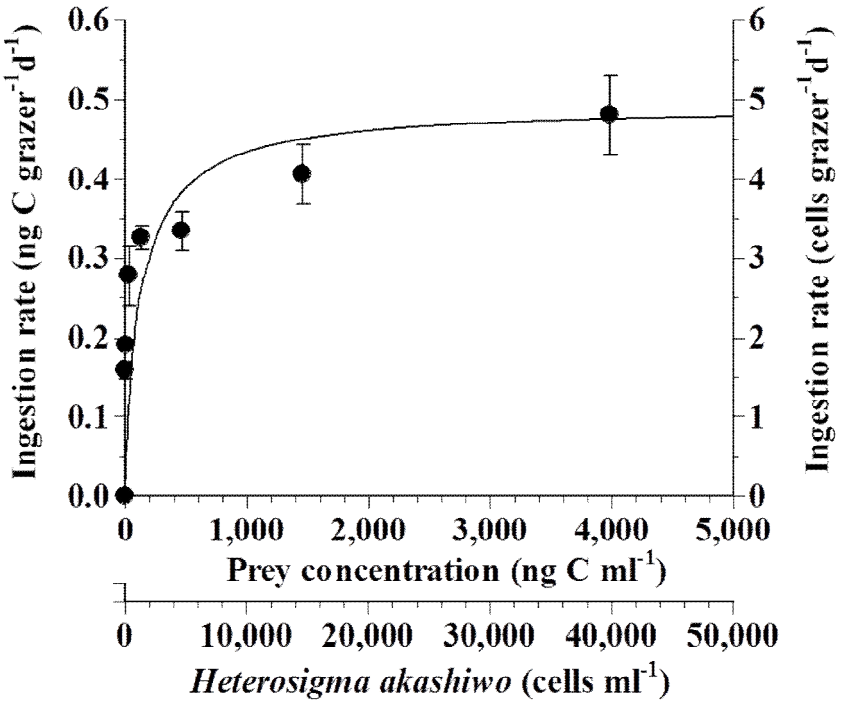

Fig. 5.9 Ingestion rates of *Biecheleria cincta* feeding on *Heterosigma akashiwo* as a function of mean prey concentration (x, ng C ml^{-1}). Symbols represent treatment means ± 1 standard error (SE). The curve is fitted by a Michaelis-Menten equation [Eq. (3)] using all the treatments in the experiment. Ingestion rate (IR, ng C grazer^{-1} d^{-1}) = 0.49 [x/(132 + x)], r^2 = 0.645.

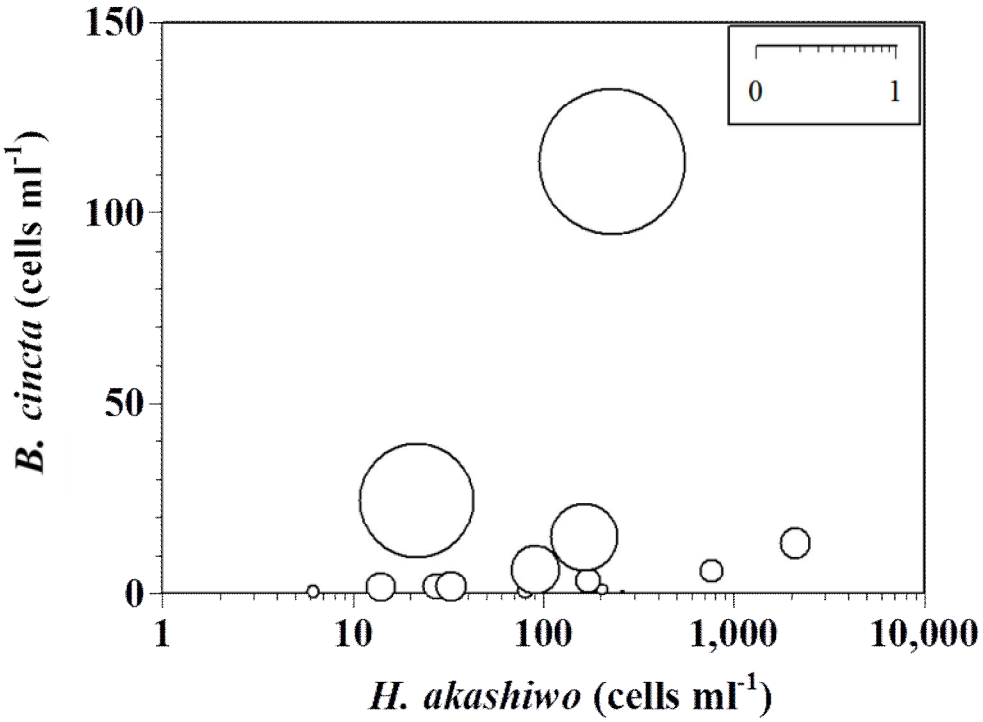

Fig. 5.10 Calculated grazing coefficients (g, d^{-1}) for *Biecheleria cincta* feeding on co-occurring *Heterosigma akashiwo* (see text for calculation). n = 14.

It is relatively easy to identify *C. polykrikoides, G. impudicum*, and *P. minimum* in fixed samples under the light microscope, but almost impossible, due to their small size and similar morphology, to identify *G. aureolum*, *P. shiwhaense*, and *B. cincta*. Thus, molecular techniques, such as real-time PCR and DNA probes, are necessary to initially identify and quantify the abundance of the latter dinoflagellates, before exploring the relative contribution of grazing by these 6 mixotrophic dinoflagellates on the population of common algal prey in marine planktonic food webs.

Biecheleria cincta feeds on algal prey using a peduncle. The mixotrophic dinoflagellates *G. aureolum*, *P. shiwhaense*, *Karlodinium armiger*, and the heterotrophic dinoflagellates *Pfiesteria piscicida, Stoeckeria algicida,* and *Luciella masanensis* also feed on algal prey using a peduncle (Berge et al. 2008; Burkholder and Glasgow 1997; Jeong et al. 2005a, 2006, 2007, 2010c; Yoo et al. 2010). Therefore, the use of the peduncle among the mixotrophic and heterotrophic dinoflagellates with a cell length of 10-30 μm appears to be common. The peduncle feeders are able to feed on larger prey than the engulfment feeders having similar sizes. Therefore, the peduncle enables small dinoflagellates to feed on prey species with a wider size range compared to similar-sized engulfment-feeding dinoflagellates.

In the phylogenetic trees based on the sequence of SSU rDNA, most species belonging to the family Suessiaceae and all species in the family Pfiesteriaceae reported to date have a peduncle, whereas all species in the Polykrikaceae and Warnowiaceae are engulfment feeders. Thus, on the basis of the dinoflagellates reported to date, it is suggested that feeding mechanisms (i.e., peduncle feeding and engulfment feeding) may be family-specific characteristics at least in these 3 families (i.e. Pfiesteriaceae, Polykrikaceae, and Warnowiaceae). However, some species in the Gymnodiniaceae (e.g., *G. aureolum* and *P. shiwhaense*) are peduncle feeders, whereas others (e.g., *C. polykrikoides*) are engulfment feeders. Thus,

feeding mechanism may not be a characteristic of the families Gymnodiniaceae and Suessiaceae. There are several species (i.e. *Biecheleria baltica, Biecheleria pseudopalustris Lepidodinium viride, Symbiodinium natans*) in which the presence of a peduncle has been observed on TEM photos, but actual use of the peduncle has not been observed (Moestrup et al. 2009a, Hansen et al. 2007a, Hansen and Daugbjerg 2009). Thus, it would be worthwhile examining whether the peduncle is a functional or vestigial structure in these species. Like *G. aureolum*, *K. armiger*, and *P. shiwhaense*, *B. cincta* does not feed on the small diatom *Skeletonema costatum*, upon which *P. piscicida* and *L. masanensis* are able to feed (Berge et al. 2008; Jeong et al. 2006, 2007, 2010b; Yoo et al. 2010; Table 4.4). Thus, these peduncle-feeding mixotrophic dinoflagellates do not appear to have peduncles that are sufficiently strong to penetrate the frustules of diatoms, whereas the peduncle-feeding heterotrophic dinoflagellates appear to have strong peduncles.

Lack of chemical signals or surface molecules may also cause no feeding. Thus, it is worthwhile to explore this topic. *Skeletonema costatum* is one of the most common diatoms (Borkman and Smayda 2009); therefore, when *S. costatum* predominates in phytoplankton assemblages, the abundance of the peduncle-feeding mixotrophic dinoflagellates is expected to be low, whereas that of the peduncle-feeding heterotrophic dinoflagellates is expected to be high.

The time of ~600 s for an *H. akashiwo* prey cell to be completely fed on by a *B. cincta* cell after the predator has deployed its peduncle to the prey cell is considerably longer than the 129 s taken by *S. algicida* (Jeong et al. 2005a). This suggests that the digestive enzymes of *B. cincta* as a mixotrophic dinoflagellate may be less efficient than those of the heterotrophic *S. algicida*. Alternatively, *B. cincta* may be less efficient than *S. algicida* at sucking materials from its prey. However, whereas *B. cincta* is able to feed on diverse prey, *S. algicida* is known to feed only on *H. akashiwo* (Jeong et al. 2005a). Thus, *B. cincta* may have a more diverse array of digestive enzymes than *S. algicida*.

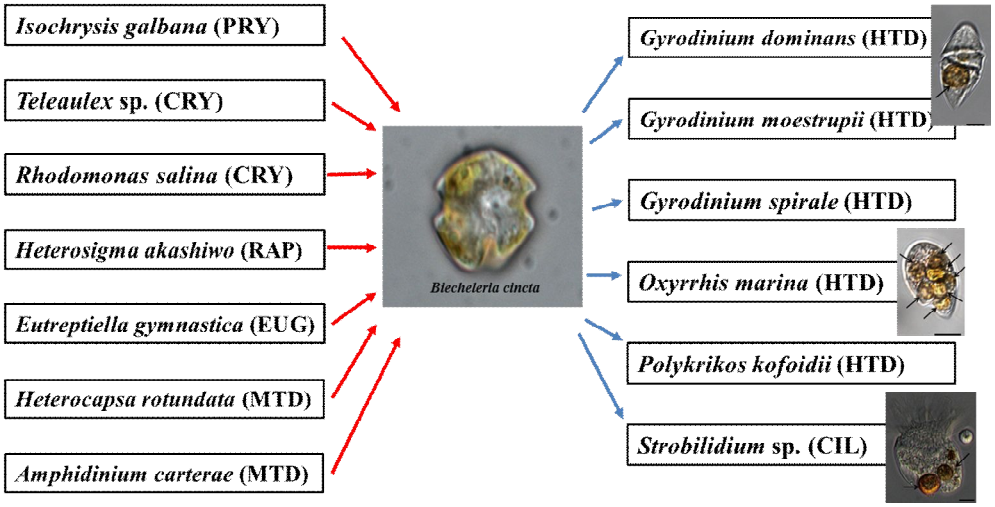

Fig. 5.11 The prey and predators of *Biecheleria cincta* so far reported. The red-colored arrows (routes) emerging from *B. cincta* lead to the variety of prey all point to *B. cincta*, while the blue-colored arrows (routes) emerging from *B. cincta* lead to the diverse predator species. (CIL: ciliates, CRY: cryptophytes, EUG: euglenophytes, HTD: heterotrophic dinoflagellates, MTD: mixotrophic dinoflagellates, PRY: prymnesiophytes, RAP: raphidophyte).

5.6.3 Comparison of growth and ingestion rates for the 6 edible prey species

The growth rates (i.e. mixotrophic growth) of *B. cincta* feeding on *H. akashiwo, R. salina*, *A. carterae*, *Teleaulax* sp., and *E. gymnastica* were significantly higher than those without added prey (i.e. autotrophic growth). However, the growth rate of *B. cincta* on *I. galbana* was not significantly different from that without added prey. In addition, the ingestion rate of *B. cincta* on *I. galbana* was not detectable using the bottle incubation method. Thus, this evidence suggests that phagotrophy in *B. cincta* clearly increases its growth rate when feeding on 5 of the 6 edible prey species offered. Neither the growth rate nor the ingestion rate of *B. cincta* on the 6 edible prey species was significantly correlated with prey size. Thus, there may be other factors affecting the growth and ingestion rates of *B. cincta* feeding on algal prey. When the mean prey concentrations were similar, the growth and ingestion rates of *B. cincta* feeding on *H. akashiwo* were significantly higher than those when feeding on the other algal prey. *Heterosigma akashiwo* is a common red tide organism, known to be harmful to other plankton and fish (Chang et al. 1990; Hiroishi et al. 2005; Yu et al. 2010), and has often caused large-scale fish mortalities in the waters of many countries (Bourdelais et al. 2002; Honjo 1993; Rensel et al. 2010). Reactive oxygen species, neurotoxin, and mucus have been suggested to be responsible for gill tissue damage, the ultimate cause of fish death (Bowers et al. 2006; Edvardsen and Imai 2006; Marshall et a1. 2003). Therefore, reducing levels of the harmful alga *H. akashiwo* using *B. cincta* may reduce the mortality of marine organisms and losses in the aquaculture industry. *Heterosigma akashiwo* was the optimal prey among examined prey species for the heterotrophic dinoflagellates *Oxyrrhis marina* and *S. algicida* (Jeong et al. 2003, 2005a). However, to date, there have been no mixotrophic dinoflagellates for which *H. akashiwo* has been determined to be the optimal algal prey. Thus, *B. cincta* is the first reported mixotrophic dinoflagellate whose optimal algal prey is *H. akashiwo*.

The growth rates of *B. cincta* feeding on the 6 edible prey species were significantly correlated with their ingestion rates. Thus, the conversion of ingested prey to growth may be similar for this predator feeding on these different species.

5.6.4 Effect of prey concentration

Both the growth and ingestion rates of *B. cincta* feeding on a unialgal diet of *H. akashiwo* were affected by prey concentration. In the literature, there are reports of 7 mixotrophic dinoflagellates for which ingestion and growth rates have been measured under illumination of 20 $\mu E\ m^{-2}\ s^{-1}$ on a 14:10 h light-dark cycle, as in *B. cincta* (Table 4.5).

I compared the maximum ingestion rate, specific ingestion rate (ingested carbon/body carbon), swimming speed, maximum growth rate, and maximum mixotrophic growth rate minus autotrophic growth rate (i.e. mixotrophic growth – autotrophic growth) of these 7 mixotrophic dinoflagellates feeding on their optimal prey [i.e. *H. akashiwo* for *B. cincta*, *Lingulodinium polyedrum* for *Fragilidium* cf. *mexicanum*, and *Teleaulax* sp. (ESD = 5.6 μm) for the others]. The maximum ingestion rate of *B. cincta* feeding on *H. akashiwo* obtained under illumination of 20 $\mu E\ m^{-2}\ s^{-1}$ on a 14:10 h light-dark cycle (0.49 ng C $grazer^{-1}\ d^{-1}$) was comparable to that of *P. shiwhaense* (0.38 ng C $grazer^{-1}\ d^{-1}$), but considerably higher than that of *G. aureolum, Prorocentrum donghaiense,* or *P. micans* (0.03-0.06 ng C $grazer^{-1}\ d^{-1}$) (Table 4.5). However, the rate was considerably lower than that for *F.* cf. *mexicanum* feeding on optimal prey under the same conditions (7 ng C $grazer^{-1}\ d^{-1}$).

The maximum ingestion rates of the 7 mixotrophic dinoflagellates feeding on optimal prey were significantly correlated with predator size ($p < 0.01$, linear regression analysis of variance (ANOVA); Fig. 5.12A).

Table 4.4 Comparison in prey species and the maximum growth and ingestion rates of the peduncle feeding mixtotrophic (MTD) and heterotrophic dinoflagellates (HTD).

Prey species / Predator	ESD	Bc	Ga	Ps	Ka	Lm	Sa	Pp
Prymnesiophytes								
Isochrysis galbana	4.8	Y	Y	Y	Y	Y	N	Y
Diatoms								
Skeletonema costatum	5.9	N	N	N		Y	N	Y
Thalassiosira weissflogii	11.8				Y			
Thalassiosira rotula	29.3		N	N		Y	N	Y
Nitzschia navis-varingica	18.2				N			
Cryptophytes								
Unidentified cryptophyte (*Teleaulax* sp.)	5.6	Y	Y	Y		Y	N	Y
Teleaulax amphioxeia	7.3				Y			
Rhodomonas salina	8.8	Y	Y	Y	Y	Y	N	Y
Rhaphidophytes								
Heterosigma akashiwo	11.5	Y	Y	Y	Y	Y	Y	Y
Chattonella ovata	40.0		N	N		Y	N	Y
MTDs								
Heterocapsa rotundata	5.8	Y	Y	Y	Y	Y	N	Y

Amphidinium carterae	9.7	Y	Y	Y		Y	N	Y
Prorocentrum minimum	12.1	N	N	N	Y	N	N	N
Heterocapsa triquetra	15.0	N	N	N	Y	N	N	N
Scrippsiella trochoidea	22.8	N	N	N		N	N	N
Cochlodinium polykirkoides	25.9	N	N	N		Y	N	Y
Prorocentrum micans	26.6	N	N	N	Y	N	N	N
Akashiwo sanguinea	30.8	N	N	N	Y	Y	N	Y
Gyrodinium instriatum	31.2				Y			
Gonyaulax polygramma	32.5	N	N	N		N	N	N
Alexandrium catenella	32.6		N	N		N	N	N
Gymnodinium catenatum	33.9		N	N		N	N	N
Lingulodinium polyedrum	38.2	N	N	N		N	N	N
MGR		0.499	0.169	1.097	0.650	1.460	1.630	1.740
MIR		0.5	0.1	0.4	1.0	2.6	0.8	4.3
*Reference		(1)	(2)	(3)	(4)	(5)	(6)	(7)

(1) This study; (2) Jeong et al. (2010b); (3) Yoo et al. (2010); (4) Berge et al. (2008); (5) Jeong et al. (2007); (6) Jeong et al. (2005a); (7) Jeong et al. (2006).

ESD (Equivalent spherical diameter, μm); Bc: *Biecheleria cincta* (MTD); Ga: *Gymnodinium aureolum* (MTD); Ps: *Paragymnodinium shiwhaense* (MTD); Ka: *Karlodinium armiger* (MTD); Lm: *Luciella masanensis* (HTD); Sa: *Stoeckeria algicida* (HTD); Pp: *Pfiesteria piscicida* (HTD); MGR (maximum growth rate in d^{-1}), MIR (maximum ingestion rate in ng C $predator^{-1}$ d^{-1}), Blank: Not tested.

However, when *F.* cf. *mexicanum* was omitted, the maximum ingestion rates of the remaining 6 mixotrophic dinoflagellates were not significantly correlated with predator size ($p > 0.1$). In addition, the specific ingestion rates of *B. cincta* and *P. shiwhaense* feeding on their optimal prey (0.083-0.093 h^{-1}) were higher than that of *F.* cf. *mexicanum* (0.033) or the other dinoflagellates (0.001-0.005 h^{-1}) (Fig. 5.12B). The specific ingestion rates of the mixotrophic dinoflagellates feeding on optimal prey were also not significantly correlated with predator size ($p > 0.1$; Fig. 5.12B). *Gymnodinium aureolum*, which has relatively low maximum and specific ingestion rates, feeds on prey using a peduncle similar to *B. cincta* and *P. shiwhaense* (Jeong et al. 2010b). Thus, this evidence suggests that there may be factors other than predator size and feeding mechanisms that affect the maximum ingestion rates of these mixotrophic dinoflagellates.

The maximum mixotrophic growth rate or maximum mixotrophic growth rate minus autotrophic growth rate (M-A GR) of the 7 above mentioned mixotrophic dinoflagellates feeding on their optimal prey observed under illumination of 20 μE m^{-2} s^{-1} on a 14:10 h light-dark cycle were likewise not significantly correlated with predator size ($p > 0.1$; Fig. 5.12C-D). The M-A GR of *P. shiwhaense* was highest, followed by that of *B. cincta* and *F.* cf. *mexicanum*. The M-A GR of the mixotrophic dinoflagellates was not significantly correlated with maximum ingestion rate or specific ingestion rate ($p > 0.1$, Fig. 5.12E-F). The maximum mixotrophic growth rate and M-A GR of *P. shiwhaense* feeding on *Teleaulax* sp. were considerably higher than those of *B. cincta* feeding on *H. akashiwo*, whereas the maximum ingestion rate and specific ingestion rate of the former dinoflagellate were slightly lower than those of the latter dinoflagellate. Possible explanations for this observed pattern are as follows: (1) the nutritional value of *Teleaulax* sp. may be considerably higher than that of *H. akashiwo*; and/or (2) *B. cincta* may expend more energy on handling, ingesting, and/or digesting *H. akashiwo* than does *P. shiwhaense* when preying on *Teleaulax* sp. The maximum swimming speed of 860 μm s^{-1} of *P.*

shiwhaense is considerably higher than the 380 μm s^{-1} of *B. cincta* (Fig. 5.13). Thus, *P. shiwhaense* is likely to expend more energy on swimming than *B. cincta*. However, the proportion of total energy expended on swimming in protists with sizes of 1-30 μm is known to be <10% when the swimming speed is ≤1,000 μm s^{-1} (Crawford 1992). Thus, for *P. shiwhaense* and *B. cincta* predators, energy expended on handling, ingesting, and/or digesting a prey cell may be higher than that expended on swimming. This is a topic that will be worthwhile exploring in greater depth.

At a light intensity of 20 μE m^{-2} s^{-1}, the ratio of maximum mixotrophic growth relative to autotrophic growth (RMA) for *B. cincta* feeding on its optimal prey was considerably higher than that for *G. aureolum*, *H. triquetra, P. donghaiense,* and *P. micans* (i.e. 12.5 vs 1.4-1.9) (Table 4.5).

In addition, the maximum mixotrophic growth rates of *P. shiwhaense* and *F.* cf. *mexicanum* were positive, whereas their autotrophic growth rates were negative. Thus, this evidence suggests that phagotrophy in mixotrophic dinoflagellates makes a greater contribution to energy requirements than photosynthesis in the following sequence: *P. shiwhaense* > *F.* cf. *mexicanum* and *B. cincta* > *G. aureolum*, *H. triquetra*, *P. donghaiense*, and *P. micans*.

At a light intensity of 20 μE m^{-2} s^{-1}, the growth rates of *B. cincta, F.* cf. *mexicanum*, and *P. shiwhaense* without added prey were negative or almost zero, whereas those of *G. aureolum*, *H. triquetra*, *P. donghaiense*, and *P. micans* were positive (Fig. 5.11C). Therefore, in natural environments, the abundances of the former dinoflagellates are likely to fluctuate with wide ranges as opportunistic species (i.e., abundant when suitable prey is abundant, and rare when prey is rare), whereas those of the latter dinoflagellates are unlikely to do so.

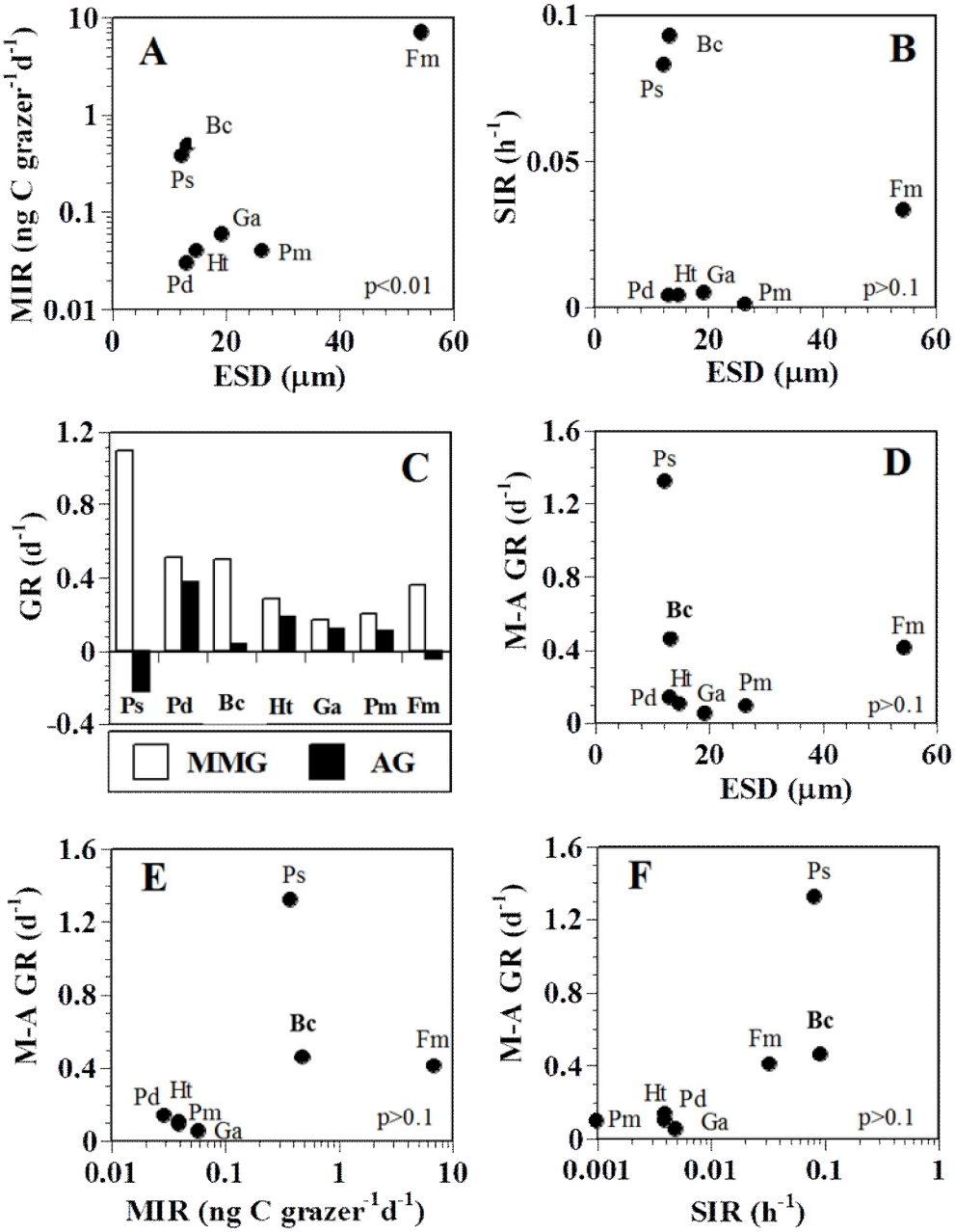

Fig. 5.12 Maximum ingestion rate (MIR, **A**), specific ingestion rate (SIR, **B**), maximum mixotrophic growth rate (MMG, **C**) and autotrophic growth rate as control (AG, **C**), and maximum mixotrophic growth rate minus autotrophic growth

rate (M-A GR = MMG-AG, **D**) of 7 mixotrophic dinoflagellates feeding on their optimal prey (*Heterosigma akashiwo* for *Biecheleria cincta*, *Lingulodinium polyedrum* for *Fragilidium* cf. *mexicanum*, and *Teleaulax* sp. for the other mixotrophic dinoflagellate predators) as a function of equivalent spherical diameter (ESD, μm), obtained under illumination of 20 μE m^{-2} s^{-1} on a 14:10 h light-dark cycle. M-A GR's of 7 mixotrophic dinoflagellates feeding on optimal prey species as a function of MIR (**E**) and SIR (**F**). See the text for the details of statistical tests. Bc: *Biecheleria cincta,* Fm: *Fragilidium* cf. *mexicanum*, Ga: *Gymnodinium aureolum*, Ht: *Heterocapsa triquetra,* Pd: *Prorocentrum donghaiense*, Pm: *Prorocentrum micans*, Ps: *Paragymnodinium shiwhaense.*

The maximum growth rate of *B. cincta* feeding on *H. akashiwo* obtained in the present study was considerably lower than that observed for the heterotrophic dinoflagellates *O. marina*, *P. piscicida*, and *S. algicida* feeding on the same prey under the same conditions (Table 4.6). The lower maximum ingestion rate of *B. cincta* feeding on *H. akashiwo* than that of these other heterotrophic dinoflagellates is likely to be responsible for the lower growth rate. However, the maximum growth rate of the heterotrophic dinoflagellate *Gyrodinium dominans* feeding on *H. akashiwo* is considerably lower than that of *B. cincta*. Thus, during blooms dominated by *H. akashiwo*, the sequence of the abundances of these dinoflagellates is expected to be as follows: *O. marina*, *P. piscicida*, and *S. algicida* > *B. cincta* > *G. dominans*. It will be worthwhile exploring this order during *H. akashiwo* blooms in natural environments.

5.6.5 Grazing impact

The grazing coefficients for *B. cincta* feeding on co-occurring *H. akashiwo* determined in the present study were up to 1.1 d^{-1} (i.e., up to 67% of the *H. akashiwo* populations was removed by *B. cincta* populations in 1 d). The results of the present study suggest that grazing by *B. cincta* may sometimes have a considerable impact on the populations of co-occurring *H. akashiwo*. Thus, feeding by *B. cincta* on *H. akashiwo* may sometimes prevent an outbreak and/or accelerate the decline of harmful blooms dominated by their prey. In order to understand the population dynamics of *B. cincta* and *H. akashiwo* and the bloom dynamics of harmful alga, it is necessary to gain an understanding of the daily variations in the abundances of *B. cincta* and *H. akashiwo*.

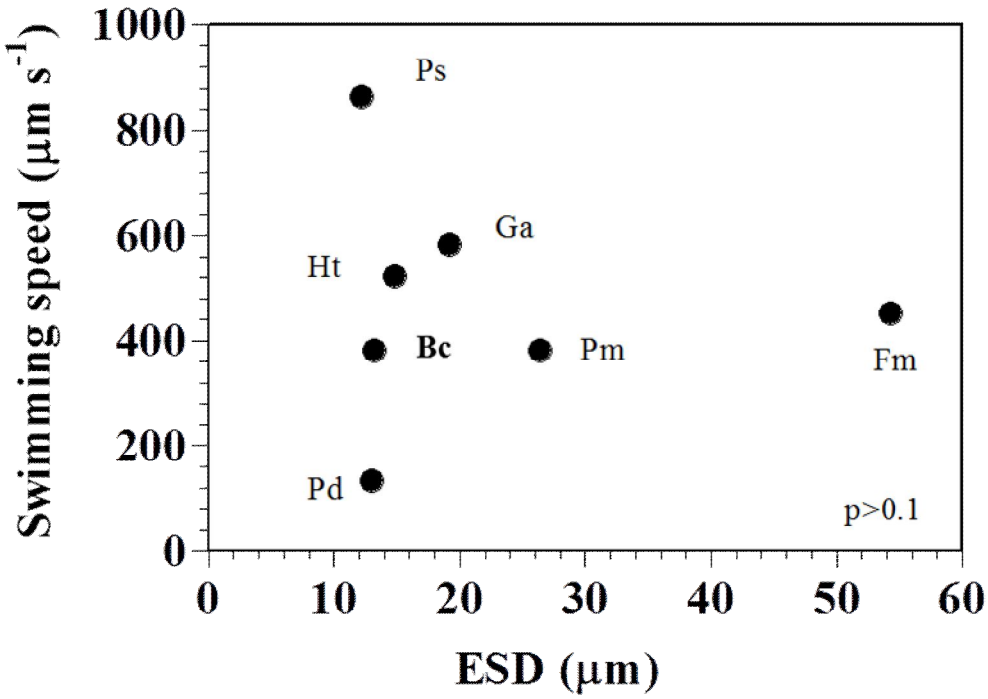

Fig. 5.13 Maximum swimming speed of 7 mixotrophic dinoflagellates feeding on their optimal prey species as a function of equivalent spherical diameter (ESD, μm), obtained under illumination of 20 μE m^{-2} s^{-1} on a 14:10 h light-dark cycle. The *p* value is >0.1, linear regression analysis of variance (ANOVA). Bc: *Biecheleria cincta,* Fm: *Fragilidium* cf. *mexicanum*, Ga: *Gymnodinium aureolum*, Ht: *Heterocapsa triquetra,* Pd: *Prorocentrum donghaiense*, Pm: *Prorocentrum micans*, Ps: *Paragymnodinium shiwhaense.*

Table 4.5 Optimal prey, maximum mixotrophic growth (MGR), ingestion (MIR), and clearance rates (MCR) of each mixotrophic dinoflagellate predator species at the light intensity of 20 μE m^{-2} s^{-1}

Predator	ESD	Optimal prey	ESD	T	MMG	AG	M-A	RMA	MIR	MCR	MSS	Ref
Paragymnodinium shiwhaense	12.4	*Teleaulax* sp.	5.6	20	1.097	-0.224	1.32		0.38	0.70	860	(1)
Prorocentrum donghaiense	13.2	*Teleaulax* sp.	5.6	20	0.510	0.375	0.14	1.4	0.03	0.04	130	(2)
Biecheleria cincta	13.4	*Heterosigma akashiwo*	11.5	20	0.499	0.040	0.46	12.5	0.49	1.90	380	(3)
Heterocapsa triquetra	15.0	*Teleaulax* sp.	5.6	20	0.283	0.184	0.10	1.5	0.04	0.05	520	(2)
Gymnodinium aureolum	19.4	*Teleaulax* sp.	5.6	20	0.169	0.120	0.05	1.4	0.06	0.003	580	(4)
Prorocentrum micans	26.6	*Teleaulax* sp.	5.6	20	0.197	0.106	0.09	1.9	0.04	0.05	380	(2)
Fragilidium cf. *mexicanum*	54.5	*Lingulodinium polyedrum*	37.9	22	0.360	-0.050	0.41		7.00	6.00	450	(5)

(1) Yoo et al. (2010); (2) Jeong et al. (2005d); (3) This study; (4) Jeong et al. (2010b); (5) Jeong et al. (1999b).

ESD, equivalent spherical diameter (μm); T, temperature (^{o}C); light intensity, 20 μE/m^2/s; MMG, maximum mixotrophic growth rate (d^{-1}); AG, autotrophic growth rate (d^{-1}); *M-A* GR, MMG-AG; RMA, MMG/AG; MIR, maximum ingestion rate (ng C/predator/d); MCR, maximum clearance rate (μl/predator/h); MSS, maximum swimming speed (μm/s).

Table 4.6 The maximum growth, ingestion, and clearance rates of mixotrophic and heterotrophic dinoflagellate predators on *Heterosigma akashiwo* which was the optimal or suboptimal prey for the predators.

Predator	ESD	FM	T	MGR	MIR	MCR	Ref
Biecheleria cincta (MTD)	13.4	PD	20	0.499	0.5	1.9	(1)
Pfiesteria piscicida (HTD)	13.5	PD	20	1.100	0.8	0.1	(2)
Stoeckeria algicida (HTD)	13.9	PD	20	1.630	0.8	3.7	(3)
Oxyrrhis marina (HTD)	15.6	DE	20	1.430	1.3	0.3	(4)
Gyrodinium dominans (HTD)	20.0	DE	24	0.150	NA	NA	(5)

(1) This study; (2) Jeong et al. (2006); (3) Jeong et al. (2005a); (4) Jeong et al. (2003); (5) Nakamura et al. (1995). MTD: Mixotrophic dinoflagellate. HTD: Heterotrophic dinoflagellate. ESD: Equivalent spherical diameter (μm). FM: Feeding mechanism. DE: Direct engulfment. PD: Peduncle. PL: Pallium. RPP: ratio of predator to prey ESD. T: Temperature (^{o}C). MGR: Maximum growth rate (d^{-1}). MIR: Maximum ingestion rate (ng C $predator^{-1}$ d^{-1}). MCR: Maximum clearance rate (μl h^{-1}). NA: Not available.

Chapter 6. Overall conclusion

This study shows that the frequency of red tide events and the red tide causative species in Shiwha bay before and after the construction of the huge tidal power plant changed. In addition, I established 2 new dinoflagellate genera, *Paragymnodinium* and *Gyrodiniellum*, Furthermore; this study reveals that a newly described phototrophic dinoflagellate *Biecheleria cincta* is a mixotrophic dinoflagellate which is able to feed on diverse prey species. The results of this study may contribute to better understanding the structure and function of marine ecosystems in general aspects. In addition, this study may provide new findings in taxonomy and ecophysiology and stimulus on research on evolution of dinoflagellates and cnidarians.

The results of Chapter 2 shows that relaxation of water circulation in Shiwha bay after the construction of the tidal power plant in 2011 switched red-tide causative species from phototrophic dinoflagellates to diatoms. Exchange of seawater between the inside and outside of the dike through the tidal power plant may have resulted in this change in the causative species. Ten huge turbines of the tidal power plant are likely to generate turbulent waters. Theoretically, all the waters inside the Shiwha Bay pass the turbines at the speed of 12-13 m s^{-1} every two days and become turbulent flow. The dinoflagellates *Akashiwo sanguinea*, *Cochlodinium polykrikoides*, and *Lingulodinium polyedrum* had negative growth at the $\varepsilon > 0.05$ cm^{-2} s^{-3}, while the diatoms *Chaetoceros* and *Psedonitzshia* had positive growth at similar ε. Therefore, an increase in turbulence may have been responsible for the change in the red-tide causative species from phototrophic dinoflagellates to diatoms. In addition, some phototrophic dinoflagellates and flagellates may acquire phosphorus from prey because inorganic phosphorus concentrations for the growth of phototrophic dinoflagellates and small flagellates during red tides may be limited, whereas inorganic nitrogen concentrations were likely unlimited. The maximum grazing coefficients of the heterotrophic dinoflagellates feeding on red-tide

causative taxa including cryptophytes, *Eutreptiella gymnastica*, *P. minimum*, and *S. costatum* were considerable. In conclusion, this study may be a nice example showing that the artificial construction can alter the frequency and dominant species of red tides. It may provide a guide for predicting red tide occurrences in environmental assessment for an artificial construction in coastal areas.

The results of Chapter 3 show that *Paragymnodinium shiwhaense* is a new species in the new genera in the family family Gymnodiniaceae. *P. shiwhaense* shows no evidence of an ALP, PEV, or apical groove, instead having an extension-like furrow of the sulcus (SEF) from the cingulum to near the apex, which doesn't quite reach the apex. In addition, *P. shiwhaense* lacks three of the key taxonomic characters that circumscribe the genus *Gymnodinium*, namely the presence of nuclear envelope chambers, a nuclear fibrous connective, and a horseshoe- or loop-shaped apical groove. In phylogenetic analyses based on both SSU and LSU rDNA, *P. shiwhaense* was clearly divergent from the Warnowiid clade that contained *Warnowia*, *Proterythropsis*, and *Nematodinium*, but close to the clade formed by the genus *Polykrikos*. Like *P. shiwhaense, Polykrikos hartmannii*, *P. lebourae,* and *Pheopolykrikos beauchampii* contain both chloroplasts and nematocysts. However, *P. shiwhaense* lacks taeniocysts, posterior vacuoles, and a stylet, evolved features which all other *Polykrikos* species possess. Given this, *P. shiwhaense* may represent an early divergence away from the *Polykrikos* clade, a conclusion that is supported by its position in the phylogenetic analysis. In conclusion, in this thesis, I establish the 24th genus in the family and open researches related to this dinoflagellate incuding eco-physiology, evolution, nematocysts, and maybe commercial uses. Furthermore, this study shows that Shiwha Bay is a place in which diverse dinoflagellates including new species and genera are present. Moreover, *Paragymnodinium* n. gen. is the first discovered dinoflagellate genus which has both nematocysts and peduncle. The nematocysts are toxic stings and the peduncle is a feeding tube. Thus, combination of the peduncle with nematocysts may increase efficiency in capturing and ingesting prey cells.

The results of Chapter 4 show that *Gyrodiniellum shiwhaense* is a new species in the new genus. It differs from woloszynskioid dinoflagellates and Kareniaceae dinoflagellates in the presence of a loop-shaped row of amphiesmal vesicles (LAV) near the apical end of the episome. In addition, *G. shiwhaense* lacks two of the key taxonomic characters that circumscribe the genus *Gymnodinium*, namely the presence of nuclear envelope chambers and a nuclear fibrous connective. *Gyrodiniellum shiwhaense* is also different from the phototrophic dinoflagellate *Lepidodinium* which has nuclear envelope chambers and the nuclear fibrous connective. Moreover, unlike *Polykrikos* spp., cells of which possess a taeniocyst–nematocyst complex, *G. shiwhaense* has nematocysts but lacks taeniocysts. It differs from *Paragymnodinium shiwhaense* by possessing nematocysts with stylets and filaments. *G. shiwhaense* furthermore lacks ocelloids, in contrast to *Warnowia* spp., *Nematodinium* spp., and *Proterythropsis* spp. Thus *G. shiwhaense* differs from other dinoflagellate genera so far described and deserves its status as a new genus. In the phylogenetic analyses based on SSU rDNA, *Gyrodiniellum shiwhaense* takes up a sister position to a clade comprising the *Polykrikos* clade, the *Paragymnodinium-Lepidodinium* clade, and the *Gymnodinium* clade. If this finding can be substantiated by other studies, several scenarios of evolutionary changes can be imagined, which include acquisition/loss of chloroplasts, modification of nematocysts/taeniocysts, changes in the apical structure, and modification of the nuclear envelope. In the SSU rDNA tree *G. shiwhaense* occupies a sister group relationship to the complex mentioned above, in which ocelloids developed but some species retained nematocysts. In conclusion, in this thesis, I establish the 25th genus in the family and provide an interesting heterotrophic dinoflagellate which has a nematocyst and peduncle.

Chapter 5 is the first report of *Biecheleria cincta* from a locality other than the Gulf of Naples, Italy. In addition, this study is a first to report the presence of eyespots type E in this species. Eyespot type E consists of seve ral layers of brick-like units delimited by membranes and characterizes the fa

mily Suessiaceae. This thesis adds to the number of detailed ultrastructural d escriptions of Suessiaceae, allowing for a more clear view of the ultrastructur al characteristics typical of Suessiaceae. The present study first reported that *B. cincta* is a mixotrophic dinoflagellate. The results of this study may stimu late further investigation to test whether the other species in the genus *Biech eleria* is also mixotrophic or not. *Heterosigma akashiwo* is a common red tid e organism, known to be harmful to other plankton and fish. The growth rat e of *B. cincta* feeding on *H. akashiwo* was significantly higher than these wi thout added prey. In addition, the results of the present study suggest that gr azing by *B. cincta* may sometimes have a considerable impact on the populat ions of co-occurring *H. akashiwo*. Thus, feeding by *B. cincta* on *H. akashiw o* may sometimes prevent an outbreak and/or accelerate the decline of harmf ul blooms dominated by their prey and reduce the mortality of marine organi sms and losses in the aquaculture industry. In addition, *B. cincta* is able to f eed on prey belonging to diverse taxa, including prymnesiophytes, cryptophyt es, raphidophytes, euglenophytes, and mixotrophic dinoflagellates. Recently, Y oo et al. (2013) discovered that *B. cincta* serve as prey in marine food web. Thus, *B. cincta* is likely to transfer materials from diverse prey species to o rganisms at higher trophic levels in marine food webs. The results of the pre sent study provide a basis for understanding the feeding mechanism and ecol ogical roles of *Biecheleria* spp. in marine planktonic food webs.

The results of my studies will provide a basis on understanding red tide dynamics in the waters where artificial construction is established. Several areas in the world have been suggested to establish tidal power plants to obtain regeneration energy. Thus, changes in the red-tide causative species before and after the construction of a tidal power plant in this study may give a cue to reduce harmful red tides in waters where a tidal power plant is planned to be established.

It is difficult to identify dinoflagellates < 20 μm in size because they are too

small to examine their morphological characterizations. Due to genetic analyses, whetehr these small dinoflagellates are new species or not. In this study, I established two dinoflagellate species < 20 μm in size, *Paragymnodinium shiwhaense* and *Gyrodiniellum shiwhaense* and identified a small dinoflagellate *Biecheleria cincta*. This study may give help in establishing new small dinoflagellate species or genus.

Both *Paragymnodinium shiwhaense* and *Gyrodiniellum shiwhaense* which have nematocysts are positioned basal of a clade of the dinoflagellates *Polykrikos* spp. which have nematocyst-taeniocyst complex. Moreover, *P. shiwhaense* and *G. shiwhaense* have single cells, while *Polykrikos* spp. have pseudocolonies. Thus, the results of this study may stimulate researches on evolution from single cells to pseudocolonies in dinoflagellates.

Many phototrophic dinoflagellates which were previously thought to be exclusively autotrophic have been revealed to be mixotrophic. However, mixotrophy has been revealed in ca. 5% of the phototrophic dinoflagellates. This study reveals that *Biecheleria cincta* is also mixotrophic and thus adds a mixotrophic dinoflagellate species in the list.

I hope this study to stimulate researches on red tides, responses by marine ecosystems to diverse scaled environmental changes, finding new species, and utilization of dinoflagellates in the future.

Bibliography

Alexander, S., Ehrlich, P. R., Goulder, L., Lubchenco, J., Matson, P. A., Mooney, H. A., Postel, S., Schneider, S. H., Tilman, D. & Woodwell, G. M. 1997. Ecosystem services: benefits supplied to human societies by natural ecosystems (Vol. 2). Washington (DC): Ecological Society of America.

Allen, W. E. 1949. Data Files, 1917-1949. Accession No. 81-19. Scripps Institution of Oceanography Archives. University of California, San Diego.

Apstein. 1909. Die pyrocysteen der plankton-expedition. *Ergeb. Plankton Exped. Humboldt-Stift.,* 4: 1-27.

Arin, L., Marrasé, C., Maar, M., Peters, F., Sala, M. & Alcaraz, M. 2002. Combined effects of nutrients and small-scale turbulence in a microcosm experiment. I. Dynamics and size distribution of osmotrophic plankton. *Aquat. Microb. Ecol.,* 29: 51-61.

Bae, Y. H., Kim, K. O. & Choi, B. H. 2010. Lake Sihwa tidal power plant project. Ocean Engineering. 37: 454-463.

Baek, S. H., Ki, J. S., Katano, T., You, K., Park, B. S., Shin, H. H., Shin, K., Kim, Y. O. & Han, M. S. 2011. Dense winter bloom of the dinoflagellate *Heterocapsa triquetra* below the thick surface ice brackish lake Shihwa, Korea. *Phycol. Res.,* 59: 273-285.

Balkis, N. 2003. Seasonal variations in the phytoplankton and nutrient dynamics in the neritic waters of Büyükçekmece Bay, Sea of Marmara. *J. Plankton Res.,* 25: 703-717.

Ballantine, D. 1956. Two new marine species of *Gymnodinium* isolated from the Plymouth area. *J. Mar. Biol. Ass.,* 35: 467-474.

Banse, K. 1982. Cell volumes maximal growth rates of unicellular algae and ciliates, and the role of ciliates in the marine pelagial. *Limnol. Oceanogr.,* 27: 1059-1071.

Berge, T., Hansen, P. J. & Moestrup, Ø. 2008. Feeding mechanism, prey specificity and growth in light and dark of the plastidic dinoflagellate *Karlodinium armiger*. *Aquat. Microb. Eco.,* 50: 279-288.

Bergh, R. S. 1881. Bidrag til cilioflagellaternes naturhistorie. Forelobige meddelelser. *Dansk Naturhist. For. Kjobenhavn. Vid. Medd. Ser. 4.,* 3: 60-76.

Bergholtz, T., Daugbjerg, N. & Moestrup, Ø. 2005. On the identity of *Karlo dinium veneficum* and description of *Karlodinium armiger* sp. nov. (Din ophyceae), based on light and electron microscopy, nuclear-encoded LS U rDNA, and pigment compsition. *J. phycol.,* 42: 170-193.

Biecheler, B. 1952. Recherches sur les Pe´ridiniens. *Bull. Biol. France Belg.,* 36 (suppl): 1-149.

Black, E. A., Whyte, J. N. C., Bagshaw, J. W. & Ginther, N. G. 1991. The effects of *Heterosigma akashiwo* on juvenile *Oncorhynchus tshawytscha* and its implications for fish culture. *J. Appl. Ichthyol.,* 7: 168-175.

Bockstahler, K. R. & Coats, D. W. 1993. Grazing of the mixotrophic dinoflagellate *Gymnodinium sanguineum* on ciliate populations of Chesapeake Bay. *Mar. Biol.,* 116: 477-487.

Borkman, D. G. & Smayda, T. 2009. Multidecadal (1959–1997) changes in *Skeletonema* abundance and seasonal bloom patterns in Narragansett Bay, Rhode Island, USA. *J. Sea Res*., 61: 84-94.

Botes, L., Sym, S. D. & Pitcher, G. C. 2003. *Karenia cristata* sp. nov. and *Karenia bicuneiformis* sp. nov. (Gymnodiniales, Dinophyceae): two new *Karenia*

species from the South African coast. *Phycologia,* 42: 563-571.

Bourdelais, A. J., Tomas, C. R., Naar, J., Kubanek, J. & Baden, D. G. 2002. New fish-killing alga in coastal Delaware produces neurotoxins. *Environ. Health Perspect.,* 110: 465-470.

Bowers, H. A., Tomas, C. R., Tengs, T., Kempton, J. W., Lewitus, A. J. & Oldach, D. W. 2006. Raphidophyceae (Chadefaud ex Silva) systematics and rapid identification: sequence analyses and realtime PCR assays. *J. Phycol.,* 42: 1333-1348.

Bradbury, P. C., Westfall, J. A. & Townsend, J. W. 1983. Ultrastructure of the dinoflagellate *Polykrikos*. II. The nucleus and its connections to the flagellar apparatus. *J. Ultrastruct. Res.,* 85: 24-32.

Burkholder, J. M. & Glasgow, H. B. Jr. 1995. Interactions of a toxic estuarine dinoflagellate with microbial predators and prey. *Arch Protistenkd*., 145: 177-188.

Burkholder, J. M. & Glasgow, H. B. Jr. 1997. Trophic controls on stage transformations of a toxic ambush-predator dinoflagellate. *J. Eukaryot. Microbiol*., 44: 200-205.

Burkholder, J. M., Glibert, P. M. & Skelton, H. M. 2008. Mixotrophy, a major mode of nutrition for harmful algal speeies in eutrophic waters. *Harmful Algae,* 8: 77-93.

Bütschli. 1885. O. Bütschli, Erster Band. Protozoa. *In*: Klassen und Ordnungen des Thier-Reichs, wissenschaftlich dargestellt in Wort und Bild, Winter, Leipzig, p. 865-1088.

Calado, A. J., Craveiro, S. C., Daugbjerg, N. & Moestrup, Ø. 2006. Ultrastructure and LSU rDNA-based phylogeny of *Esoptrodinium gemma* (Dinophyceae),

with notes on feeding behavior and description of the flagellar base area of a planozygote. *J. Phycol.,* 42: 434-452.

Calado, A. J., Craveiro, S. C., Daugbjerg, N. & Moestrup, Ø. 2009. Description of *Tyrannodinium* gen. nov., a freshwater dinoflagellate closely related to the marine *Pfiesteria*-like species. *J. Phycol.,* 45: 1195-1205.

Calado, A. J., Craveiro, S. C. & Moestrup, Ø. 1998. Taxonomy and ultrastructure of a freshwater, heterotrophic *Amphidinium* (Dinophyceae) that feeds on unicellular protists. *J. Phycol.,* 34: 536-554.

Calado, A. J. & Moestrup Ø. 1997. Feeding in *Peridiniopsis berolinensis* (Dinophyceae): new observations on tube feeding by an omnivorous, heterotrophic dinoflagellate. *Phycologia,* 36: 47-59.

Carvalho, W. F., Minnhagen, S. & Granéli, E. 2008. *Dinophysis norvegica* (Dinophyceae), more a predator than a producer. *Harmful Algae,* 7: 174-183.

Cembella, A. D., Antia, N. J. & Harrison, P. J. 1984. The utilization of inorganic and organic phosphorus compounds as nutrients by eukaryotic microalgae: a multidisciplinary perspective: part I. CRC Crit. *Rev. Microbiol.*, 10: 317-391.

Chang, F. H., Anderson, C. & Boustead, N. C. 1990. First record of a *Heterosigma* (Raphidophyceae) bloom with associated mortality of cagereared salmon in Big Glory Bay, New Zealand. *J. Mar. Freshwater Res.*, 24: 461-469.

Chang, F. H. & Ryan, K. G. 2004. *Karenia concordia* sp. nov. (Gymnodiniales, Dinophyceae), a new nonthecate dinoflagellate isolated from the New Zealand northeast coast during the 2002 harmful algal bloom events. *Phycologia,* 43: 552-562.

Chen, D. & Jirka, G. H. 1998. Linear instability analysis of turbulent mixing layers and jets in shallow water layers. *J. Hydraul. Res*., 36: 815-830.

Cheng, Y. S., Mcdonald, J. D., Kracko, D., Irvin, C. M., Zhou, Y., Pierce, R. H., Henry, M. S., Bourdelaisa, A., Maar, J. & Baden, D. G. 2005. Concentration and particle size of airborne toxic algae (brevetoxin) derived from ocean red tide events. *Environ. Sci. Technol.*, 39: 3443-3449.

Choi, J. K., Lee, E. H., Noh, J. H. & Huh, S. H. 1997. The study on the phytoplankton bloom and primary productivity in Lake Shihwa and adajcent coastal areas. *The Sea*, 2: 78-86 (in Korean, with English abstract).

Clough, J. & Strom, S. 2005. Effects of *Heterosigma akashiwo* (Raphidophyceae) on protist grazers: laboratory experiments with ciliates and heterotrophic dinoflagellates. *Aquat. Microb. Ecol*., 39: 121-134.

Conover, D. 1980. Practical nonparametric statistics. 2nd ed. John Wiley and Sons, New York, N.Y. 493pp.

Conway, H. L. & Harrison, P. J. 1977. Marine diatoms grown in chemostats under silicate or ammonium limitation. 4. Transient response of *Chaetoceros debilis, Skeletonema costatum*, and *Thalassiosira gravida* to a single addition of the limiting nutrient. *Mar. Biol*., 43: 33-43.

Conway, H. L., Harrison, P. J. & Davis, C. O. 1976. Marine diatoms grown in chemostats under silicate or ammonium limitation. 2. Transient response of *Skeletonema costatum* to a single addition of limiting nutrient. *Mar. Biol.*, 35: 187-199.

Crawford, D. W. 1992. Metabolic cost of motility in planktonic protists: theoretical considerations on size scaling and swimming speed. *Microb. Ecol.*, 24: 1-10.

Daugbjerg, N., Hansen, G., Larsen, J. & Moestrup, Ø. 2000. Phylogeny of some major genera of dinoflagellates based on ultrastructure and partial LSU rDNA sequence data, including the erection of 3 new genera of unarmoured

dinoflagellates. *Phycologia,* 39: 302-317.

de Salas, M. F., Bolch, C. J. S., Botes, L., Nash, G., Wright, S. W. & Hallegraeff, G. M. 2003. *Takayama* gen. nov. (Gymnodiniales, Dinophyceae), a new genus of unarmoured dinoflagellates with sigmoid apical grooves, including the description of two new species. *J. Phycol*., 39: 1233-1246.

de Salas, M. F., Bolch, C. J. S. & Hallegraeff, G. M. 2004a. *Karenia umbella* sp. nov. (Gymnodiniales, Dinophyceae), a new potentially ichthyotoxic dinoflagellate species from Tasmania, Australia. *Phycologia,* 43: 166-175.

de Salas, M. F., Bolch, C. J. S. & Hallegraeff, G. M. 2004b. *Karenia asterichroma* sp. nov. (Gymnodiniales, Dinophyceae), a new dinoflagellate species associated with finfish aquaculture mortalities in Tasmania, Australia. *Phycologia,* 43: 624-631.

de Salas, M. F., Bolch, C. J. S. & Hallegraeff, G. M. 2005. *Karlodinium australe* sp. nov. (Gymnodiniales, Dinophyceae), a new potentially ichthyotoxic unarmoured dinoflagellate from lagoonal habitats of south-eastern Australia. *Phycologia,* 44: 640-650.

de Salas, M. F., Laza-Martinez, A. & Hallegraeff, G. M. 2008. Novel unarmored dinoflagellate from the toxigenic family Kareniaceae (Gymnodiniales): five new species of *Karlodinium* and one new *Takayama* from the australian sector of the southern ocean. *J. Phycol*., 44: 241-257.

Dodge, J. D. & Crawford, R. M. 1969. The fine structure of *Gymnodinium fuscum* (Dinophyceae). *New Phytol.,* 68: 613-618.

Doremus, C. 1982. Geochemical control of dinitrogen fixation in the open ocean. *Biol. Oceanogr*., 1: 429-436.

ECOHAB, 1995. The Ecology and Oceanography of Harmful Algal Blooms. A

National Research Agenda. Woods Hole Oceanographic Institute, Woods Hole, MA, pp. 1-66.

Edvardsen, B. & Imai, I. 2006. The ecology of harmful prymnesiophytes and raphidophytes. In: Grane´li, E. & Turner, J. T. (ed.), The Ecology of Harmful Algae. Springer, Berlin. p. 67–80.

Elbrächter, M. 1979. On the taxonomy of unarmoured dinophytes (Dinophyta) from the Northwest African upwelling region.*"Meteor" Forsch.-Ergebnisse,* 30: 1-22.

Eppley, R. W. Rogers, J. N. & McCarthy, J. J. 1969. Half-saturation constants for uptake of nitrate and ammonium by marine phytoplankton. *Limnol. Oceanogr.,* 14: 912-920.

Estrada, M. & Berdalet, E. 1998. Effects of turbulence on plankton. *In* D.M. Anderson, A.D. Cembella and G.M. Hallegraeff [eds.] Physiological ecology of harmful algal blooms. NATO ASI Series, Serie G, Vol. 41, Springer, Berlin. pp. 601-618.

Fan, C., Glibert, P. M. & Burkholder, J. M. 2003. Characterization of the affinity for nitrogen, uptake kinetics, and environmental relationships for *Prorocentum minimum* in natural blooms and laboratory cultures. *Harmful Algae*, 2: 283-299.

Fariman, G., de Salas, M. F., Negri, A. P. & Bolch, C. J. S. 2007. Morphology and phylogeny of *Gymnodinium trapeziforme* sp. nov. (Dinophyceae): a new dinoflagellate from the southeast coast of Iran that forms microreticulate resting cysts. *Phycologia,* 46: 644-656.

Fensome, R. A., Taylor, F. J. R, Norris, G., Sargeant, W. A. S., Wharton, D. I. & William, G. L. 1993. A classification of living and fossil dinoflagellates.

micropaleontology, Special Publication No. 7. Sheridan Press, Hanover. 1-351 p.

Fermin, E. G, Figueiras, F. G., Arbones, B. & Villarino, M. L. 1996. Short-time scale development of a *Gymnodinium catenatum* population in the Ria de Vigo (NW Spain). *J. Phycol.*, 32: 212-221.

Francis, D. 1967. On the eyespot of the dinoflagellate, *Nematodinium*. *J. Exp. Biol.,* 47: 495-501.

Franks, P. J. S. 2005. Plankton patchiness, turbulent transport and spatial spectra. *Mar. Ecol. Prog. Ser.*, 294: 295-309.

Frost, B. W. 1972. Effects of size and concentration of food particles on the feeding behavior of the marine planktonic copepod *Calanus pacificus*. *Limnol. Oceanogr.,* 17: 805-815.

Gómez, F. 2008. *Erythropsidinium* (Gymnodiniales, Dinophyceae) in the Pacific Ocean, a unique dinoflagellate with an ocelloid and a piston. *Eur. J. Prostistol.,* 44: 291-298.

Gómez, F, López-García, P. & Moreira, D. 2009. Molecular phylogeny of the ocelloid bearing dinoflagellates *Erythropsidinium* and *Warnowia* (Warnowiaceae, Dinophyceae). *J. Eukaryot. Microbiol.,* 56: 440-445.

Gransden, S. G. & Lewitus, A. J. 2003. Grazing of two euplotid ciliates on the heterotrophic dinoflagellates *Pfiesteria piscicida* and *Cryptoperidiniopsis* sp. *Aquat. Microb. Ecol.,* 33: 303-308.

Greuet, C. 1965. Structure fine de l'ocelle d'*Erythropsis pavillardi* Hertwig, Péridinien Warnowiidae Lindemann. *C. R. Acad. Sc. Paris,* 261: 1904-1907.

Greuet, C. 1968. Organisation ultrastructurale de l'ocelle de deux Péridiniens

Warnowiidae, *Erythropsis pavillardi* Kofoid et Swezy et *Warnowia pulchra* Schiller. *Protistologica,* 4: 209-230.

Greuet, C. 1987. Complex organelles. In: Taylor, F. J. R. (ed.), The Biology of Dinoflagellates. Botanical Monographs. Blackwell Sci. Publ., Oxford. p. 119-142.

Guillard, R. R. L. & Ryther, J. H. 1962. Studies of marine planktonic diatoms. I. *Cyclotella nana* Hustedt and *Detonula confervacea* (Cleve) Grun. *Can. J. Microbiol.,* 8: 229-239.

Hansen, G. 2001. Ultrastructure of *Gymnodinium aureolum* (Dinophyceae): toward a further redefinition of *Gymnodinium sensu stricto. J. Phycol.,* 37: 612-623.

Hansen, G., Botes, L. & de Salas, M. F. 2007a. Ultrastructure and large subunit rDNA sequences of *Lepidodinium viride* reveal a close relationship to *Lepidodinium chlorophorum* comb. nov. (= *Gymnodinium chlorophorum*). *Phycol. Res.,* 55: 25-41.

Hansen, G. & Daugbjerg, N. 2009. *Symbiodinium natans* sp nov.: a free-living dinoflagellate from Tenerife (northeast-Atlantic Ocean). *J. Phycol.,* 45: 251-263.

Hansen, G., Daugbjerg, N. & Henriksen, P. 2007b. *Baldinia anauniensis* gen. et sp. nov.: a 'new' dinoflagellate from Lake Tovel, N. Italy**.** *Phycologia,* 46: 86-108.

Hansen, G. & Flaim, G. 2007. Dinoflagellates of the Trentino Province, Italy. *J. Limnol.,* 66: 107-141.

Hansen, G. & Moestrup, Ø. 1998. Fine-structural characterization of *Alexandrium catenella* (Dinophyceae) with special emphasis on the flagellar apparatus. *Eur. J. Phycol.,* 33: 281-291.

Hansen, G., Moestrup, Ø. & Roberts, K. R. 2000. Light and electron microscopical observations on the type species of *Gymnodinium, G. fuscum* (Dinophyceae). *Phycologia*, 39: 365-376.

Hansen, P. J. 1991. *Dinophysis*-a planktonic dinoflagellate genus which can act both as a prey and a predator of a ciliate. *Mar. Ecol. Prog. Ser.,* 69: 201-204.

Hansen, P. J., Bjornsen, P. K. & Hansen, B. W. 1997. Zooplankton grazing and growth: scaling within the 2-2,000-μm body size range. *Limnol. Oceanogr.,* 42: 687-704.

Haywood, A. J., Steinger, K. A., Truby, E. W., Bergquist, P. R., Bergquist, P. L., Adamson, J. & MacKenzie, L. 2004. Comparative morphology and molecular phylogenetic analysis of three new species of the genus *Karenia* (Dinophyceae) from New Zealand. *J. Phycol*., 40: 165-179.

Heinbokel, J. F. 1978. Studies on the functional role of tintinnids in the Southern California Bight. I. Grazing and growth rates in laboratory cultures. *Mar. Biol*., 47: 177-189.

Herndon, J. & Cochlan, P. 2007. Nitrogen utilization by the raphidophyte *Heterosigma akashiwo*: growth and uptake kinetics in laboratory cultures. *Harmful Algae*, 6: 260-270.

Hiroishi, S., Okada, H., Imai, I. & Yoshida, T. 2005. High toxicity of the novel bloom-forming species *Chattonella ovata* (Raphidophyceae) to cultured fish. *Harmful Algae*, 4: 783-787.

Holling, C. S., Schindler, D. W., Walker, B. W. & Roughgarden, J. 1995. Biodiversity in the functioning of ecosystems: an ecological synthesis. *Biodiversity loss: economic and ecological issues*, 44-83.

Honer, R. A., Garrison, D. L. & Plumley, F. G. 1997. Harmful algal blooms and red

tide problems on the U. S. west coast. *Limnol. Oceanogr.*, 42: 1076-1088.

Honjo, T. 1993. Overview on bloom dynamics and physiological, ecology of *Heterosigma akashiwo*. In: Smayda, T. J. & Shimizu, Y. (ed.), Toxic Phytoplankton Blooms in the Sea. Elsevier, New York. p. 33–41.

Honsell, G. & Talarico, L. 2004. *Gymnodinium chlorophorum* (Dinophyceae) in the Adriatic Sea: electron microscopical observations. *Bot. Mar.,* 47: 152-166.

Hoppenrath, M., Bachvaroff, T. R., Handy, S. M., Delwiche, C. F. & Leander, B. S. 2009a. Molecular phylogeny of ocelloid-bearing dinoflagellates (Warnowiaceae) as inferred from SSU and LSU rDNA sequences. *BMC. Evol. Biol.,* 9: 116-130.

Hoppenrath, M. & Leander, B. S. 2007a. Character evolution in polykrikoid dinoflagellates. *J. Phycol*., 43: 366-377.

Hoppenrath, M. & Leander, B. S. 2007b. Morphology and phylogeny of the pseudocolonial dinofagellates *Polykrikos lebourae* and *Polykrikos herdmanae* n. sp. *Protist,* 158: 209-227.

Hoppenrath, M., Yubuki, N., Bachvaroff, T. R. & Leander, B. S. 2009b. Re-classification of *Pheopolykrikos hartmannii* as *Polykrikos* (Dinophyceae) based partly on the ultrastructure of complex extrusomes. *Europ. J. Protistol.,* 46: 29-37.

Hu, H., Zhang, J. & Chen, W. 2011. Competition of bloom-forming marine phytoplankton at low nutrient concentrations. *J. Envron. Sci.*, 23: 654-663.

Huang, C. & Qi, Y. 1997. The abundance cycle and influence factors on red tide phenomena of *Noctiluca scintillans* (Dinophyceae) in Dapeng Bay, the South China Sea. *J. Plankton Res.*, 19: 303-318.

Huelsenbeck, J. P. & Ronquist, F. 2001. MrBayes: Bayesian inference of phylogeny. *Bioinformatics,* 17: 754-755.

Imai, I., Itakura, S., Matsuyama, Y. & Yamaguchi, M. 1996. Selenium requirement for growth of a novel red tide flagellate *Chattonella verruculosa* (Raphidophyceae) in culture. *Fish. Sci.*, 62: 834-835.

Iwataki, M., Kawami, H. & Matsuoka, K. 2007. *Cochlodinium fulvescens* sp. nov. (Gymnodiniales, Dinophyceae), a new chain-forming unarmored dinoflagellate from Asian coasts. *Phycol. Res.,* 55: 231-239.

Jacobson, D. M. & Anderson, D. M. 1986. Thecate heterotrophic dinoflagellates: Feeding behavior and mechanisms. *J. Phycol*., 22: 249-258.

Jacobson, D. M. & Anderson, D. M. 1992. Ultrastructure of the feeding apparatus and myonemal system of the heterotrophic dinoflagellate *Protoperidinium spinulosum*. *J. Phycol*., 28: 69-82.

Jacobson, D. M. & Andersen, R. A. 1994. The discovery of mixotrophy in photosynthetic species of *Dinophysis* (Dinophyceae): light and electron microscopical observations of food vac uoles in *Dinophysis acuminata, D. norvegica* and two heterotrophic dinophysoid dinoflage llates. *Phycologia,* 33: 97-110.

Jeong, H. J. 1994. Predation by the heterotrophic dinoflagellate *Protoperidinium* cf. *divergens* on copepod eggs and early naupliar stages. *Mar. Ecol. Prog. Ser*., 114: 203-208.

Jeong, H. J. 1995. The interactions between microzooplanktonic grazers and dinoflagellates causing red tides in the open coastal waters off southern California. Disseration. University of California, San Diego. 139 p. Available on microfilm from University of Michigan, Accession Number 223882.

Jeong, H. J. 1999. The ecological roles of heterotrophic dinoflagellates in marine planktonic community. *J. Eukaryot. Microbiol.,* 46: 390-396.

Jeong, H. J. 2011. Mixotrophy in red tide algae raphidophytes. *J. Eukaryot. Microbiol.*, 58: 215-222.

Jeong H. J., Ha J. H., Park J. Y., Kim J. H., Kang N. S., Kim S., Kim J. S., Yoo Y. D. & Yih W. H. 2006. Distribution of the heterotrophic dinoflagellate *Pfieteria piscicida* in Korean waters and its consumption of mixotrophic dinoflagellates, raphidophytes, and fish blood cells. *Aquat. Microb. Ecol.,* 44: 263-278.

Jeong, H. J., Ha, J. H., Yoo, Y. D., Park, J. Y., Kim, J. H., Kang, N. S., Kim, T. H., Kim, H. S. & Yih, W. H. 2007. Feeding by the *Pfiesteria*-like heterotrophic dinoflagellate *Luciella masanensis*. *J. Eukaryot. Microbiol.*, 54: 231-241.

Jeong, H. J., Kim, J. S., Kim, J. H., Kim, S. T., Seong, K. A., Kim, T. H., Song, J. Y. & Kim, S. K. 2005a. Feeding and grazing impact by the newly described heterotrophic dinoflagellate *Stoeckeria algicida* on the harmful alga *Heterosigma akashiwo*. *Mar. Ecol. Prog. Ser*., 295: 69-78.

Jeong, H. J., Kim, J. S., Park, J. Y., Kim, J. H., Kim, S. H., Lee, I. H., Lee, S. H., Ha, J. H. & Yih, W. H. 2005b. *Stoeckeria algicida* n. gen., n. sp. (Dinophyceae) from the coastal waters off southern Korea: morphology and small subunit ribosomal DNA gene sequence. *J. Eukaryot. Microbiol.,* 52: 382-390.

Jeong, H. J., Kim, J. S., Yoo, Y. D, Kim, S. T, Kim, T. H., Park, M. G, Lee, C. H., Seong, K. A., Kang, N. S. & Shim, J. H. 2003. Feeding by the heterotrophic dinoflagellate *Oxyrrhis marina* on the red-tide raphidophyte *Heterosigma akashiwo*: a potential biological method to control red tides using mass-cultured grazers. *J. Eukaryot. Microb*., 50: 274-282.

Jeong, H. J., Kim, T. H., Yoo, Y. D., Yoon, E. Y., Kim, J. S., Seong, K. A., Kim, K. Y. & Park, J. Y. 2011a. Grazing impact of heterotrophic dinoflagellates and ciliates on common red-tide euglenophyte *Eutreptiella gymnastica* in Masan Bay, Korea. *Harmful Algae*, 10: 576-588.

Jeong, H. J., Lee, K. H., Yoo, Y. D., Kang, N. S. & Lee, K. 2011b. Feeding by the newly described, nematocyst-bearing heterotrophic dinoflagellate *Gyrodiniellum shiwhaense*. *J. Eukaryot. Microbiol.*, 58: 511-524.

Jeong, H. J., Park, J. Y., Nho, J. H., Park, M. O., Ha, J. H., Seong, K. A., Chang, J., Seong, C. N., Lee, K. Y. & Yih, W. H. 2005c. Feeding by the red-tide dinoflagellates on the cyanobacterium *Synechococcus*. *Aquat. Microb. Ecol*., 41: 131-143.

Jeong, H. J., Seong, K. A., Kang, N. S., Yoo, Y. D., Nam, S. W., Park, J. Y., Shin, W. G., Glibert, P. M. & Johns, D. 2010a. Feeding by raphidophytes on the cyanobacterium *Synechococcus*. *Aquat. Microb. Ecol.*, 58: 181-195.

Jeong, H. J., Shim, J. H., Lee, C. W., Kim, J. S. & Koh, S. M. 1999a. Growth and grazing rates of the marine planktonic ciliate *Strombidinopsis* sp. on red-tide and toxic dinoflagellates. *J. Euk. Microb.,* 46: 69-76.

Jeong, H. J., Shim, J. H., Kim, J. S., Park, J. Y., Lee, C. W. & Lee, Y. 1999b. The feeding by the thecate mixotrophic dinoflagellate *Fragilidium* cf. *mexicanum* on red tide and toxic dinoflagellate. *Mar. Ecol. Prog. Ser.,* 176: 263-277.

Jeong, H. J., Yoo, Y. D., Kang, N. S., Lim, A. S., Seong, K. A., Lee, S. Y., Lee, M. J., Lee, K. H., Kim, H. S., Shin, W., Nam, S. W., Yih, W. & Lee, K. 2012. Heterotrophic feeding as a newly identified survival strategy of the dinoflagellate *Symbiodinium*. *Proc. Natl. Acad. Sci.,* 109: 12604-12609.

Jeong, H. J., Yoo, Y. D., Kang N. S., Rho, J. R., Seong, K. A., Park, J. W., Nam, G. S. & Yih, W. H. 2010b. Ecology of *Gymnodinium aureolum*. I. Feeding in western Korean water. *Aquat. Microb. Ecol.,* 59: 239-255.

Jeong, H. J., Yoo, Y. D., Kim, J. S., Kang, N. S. & Kim, T. H. 2010c. Growth, feeding and ecological roles of the mixotrophic and heterotrophic dinoflagellates in marine planktonic food webs. *Ocean. Sci, J.*, 45: 65-91.

Jeong, H. J., Yoo, Y. D., Kim, J. S., Kang, N. S., Kim, T. H. & Kim, J. H. 2004a. Feeding by the marine planktonic ciliate *Strombidinopsis jeokjo* on common heterotrophic dinoflagellates. *Aquat. Microb. Ecol.,* 36: 181-187.

Jeong, H. J., Yoo, Y. D., Kim, J. S., Kim, T. H., Kim, J. H., Kang, N. S. & Yih, W. H. 2004b. Mixotrophy in the phototrophic harmful alga *Cochlodinium polykrikoides* (Dinophycean): prey species, the effects of prey concentration and grazing impact. *J. Eukaryot. Microb*., 51: 563-569.

Jeong, H. J., Yoo, Y. D., Kim, S. T. & Kang, N. S. 2004c. Feeding by the heterotrophic dinoflagellate *Protoperidinium bipes* on the diatom *Skeletonema costatum*. *Aquat. Microb. Ecol.,* 36: 171-179.

Jeong, H. J., Yoo, Y. D., Lee, K. H., Kim, T. H., Seong, K. A., Kang, N. S., Lee, S. Y., Kim, J. S., Kim, S. & Yih, W. H. 2013a. Red tides in Masan Bay Korea in 2004–2005: I. Daily variations in the abundance of red-tide organisms and environmental factors. *Harmful Algae*, 30: S75-S88.

Jeong, H. J., Yoo, Y. D., Lim, A. S., Kim, T. & Lee, K. 2013b. Raphidophyte red tides in Korean waters. *Harmful Algae*, 30: S41-S52.

Jeong, H. J., Yoo, Y. D., Park, J. Y., Song, J. Y., Kim, S. T., Lee, S. H., Kim, K. Y. & Yih, W. H. 2005d. Feeding by the phototrophic red-tide dinoflagellates: five

species newly revealed and six species previously known to be mixotrophic. *Aquat. Microb. Ecol*., 40: 133-155.

Jeong, H. J., Yoo, Y. D., Seong, K. A., Kim, J. H., Park, J. Y., Kim, S. H., Lee, S. H., Ha, J. H. & Yih, W. H. 2005e. Feeding by the mixotrophic dinoflagellate *Gonyaulax polygramma*: mechanisms, prey species, the effects of prey concentration, and grazing impact. *Aquat. Microb. Ecol.,* 38: 249-257.

Jirka, G. H. 2001. Large scale flow structures and mixing processes in shallow flows. *J. Hydraul. Res.*, 36: 567-573.

Jørgensen, M. F., Murray, S. & Daugbjerg, N. 2004. *Amphidinium* revisited I. Redefinition of *Amphidinium* (Dinophyceae) based on cladistic and molecular phylogenetic analyses. *J. Phycol.,* 40: 351-365.

Juhl, A. R., Velazquez, V. & Latz, M. I. 2000. Effect of growth conditions on flow-induced inhibition of population growth of a red-tide dinoflagellate. *Limnol. Oceanogr*., 45: 905-915.

Kamiyama, T. & Matsuyama, Y. 2005. Temporal changes in the ciliate assemblage and consecutive estimates of their grazing effect during the course of a *Heterocapsa circularisquama* bloom. *J. Plankton Res.,* 27: 303-311.

Kang, N. S., Jeong, H. J., Moestrup, Ø. & Park, T. G. 2011a. *Gyrodiniellum shiwhaense* n. gen., n. sp., A new planktonic heterotrophic dinoflagellate from the coastal waters off western Korea: morphology, pigments, and ribosomal DNA gene sequence. *J. Eukaryot. Microbiol*., 58: 284-309.

Kang, N. S., Jeong, H. J., Moestrup, Ø., Shin, W. G., Nam, S. W., Park, J. Y., De Salas, M. F., Kim, K. W. & Noh, J. H. 2010. Description of a new planktonic mixotrophic dinoflagellate *Paragymnodinium shiwhaense* n. gen., n. sp. from the coastal waters off western Korea: morphology, pigments, and ribosomal

DNA gene sequence. *J. Eukaryot. Microbiol.*, 57: 121-144.

Kang, N. S., Jeong, H. J., Yoo, Y. D, Yoon, E. Y., Lee, K. H., Lee, K. & Kim, K. H. 2011b. Mixotrophy in the newly described phototrophic dinoflagellate *Woloszynskia cincta* from western Korean waters: Feeding mechanism, prey species, and effect of prey concentration. *J. Eukaryotic Microbiol.,* 58: 152-170.

Kim, H. G. 1997. Recent harmful algal blooms and mitigation strategies in Korea. *Ocean Res.*, 19: 185-192.

Kim, H. G. 1998. Harmful algal blooms in Korean coastal waters focused on three fish killing dinoflagellates. In: Kim, H. G., Lee, S. G., Lee, C. K., editors. Harmful Algal Blooms in Korea and China. Pusan: National Fisheries Research and Development Institute. p. 1-20.

Kim, J. S. 2001. The temporal and spatial distributions of the mixotrophic dinoflagellates off the SaeManKeum Area, ChenBuk, Korera, and effect of turbulence on red-tide dinoflagellates. Department of Oceanography, Kunsan National University, Korea. (in Korean, with English abstract)

Kim, J. S. & Jeong., H. J. 2004. Feeding by the heterotrophic dinoflagellates *Gyrodinium dominans* and *G. spirale* on the red-tide dinoflagellate *Prorocentrum minimum. Mar. Ecol. Prog. Ser.,* 280: 85-94.

Kiørboe, T. & Saiz, E. 1995. Planktivorous feeding in calm and turbulent environments with emphasis on copepods. *Mar. Ecol. Prog. Ser.*, 122: 133-145.

Kishi, M. & Ikeda, S. 1986. Population dynamics of ‘red tide’ organisms in eutrophicated coastal waters-numerical experiment of phytoplankton bloom in the East Seto Inland sea, Japan. *Ecol. Model.*, 31: 145-174.

Kofoid, C. A. & Swezy, O. 1921. The free-living unarmored Dinoflagellata. Berkeley, University of California Press; Memoirs of the University of California, 5: 1-559.

Kononen, K. 1992. Dynamics of the toxic cyanobacterial blooms in the Baltic Sea. *Finn. Mar. Res.,* 261: 3-36.

Korea Meterorogical Administration (KMA). http://web.kma.go/kr.

Kremp, A., Elbrachter, M., Schweikert, M., Wolny, J. L. & Gottschling, M. 2005. *Woloszynskia halophila* (Biecheler) comb. nov.: A bloom-forming cold-water dinoflagellate co-occurr ing with *Scrippsiella hangoei* (Dinophyceae) in the Baltic Sea. *J. Phycol*., 41: 629-642.

Lankester, E. R. 1885. Protozoa. In: Baynes, T. S., (ed.), The Encyclopedia Britannica, 9th ed. JM Stoddard Co. Ltd., Philadelphia, Pennsylvania. 19: 831-865.

Leadbeater. B. S. C. 1971. The intracellular origin of flagellar hairs in the dinoflagellate *Woloszynskia micra* Leadbeater & Dodge. *J. Cell Sci*., 9: 443-451.

Lessard, E. J. 1984. Oceanic heterotrophic dinoflagellates: distribution, abundance and role as microzooplankton. Disseration. University of Rhode Island. 166 p. Available on microfilm from University of Michigan, Accession Number 993020.

Lessard, E. J. 1991. The trophic role of heterotrophic dinoflagellates in diverse marine environments. *Mar. Microb. Food Webs,* 5: 49-58.

Li, A., Stoecker, D. K. & Coats, D. W. 2000. Mixotrophy in *Gyrodinium galatheanum* (Dinophyceae): responses to light intensity and inorganic nutrients. *J. Phycol.,* 36: 33-45.

Lindberg, K., Moestrup, Ø. & Daugbjerg, N. 2005. Studies on woloszynskioid dinoflagellates I: *Woloszynskia coronata* re-examined using light and electron microscopy and partial LSU rDNA sequences, with description of *Tovellia* gen. nov and *Jadwigia* gen. nov. (Tovelliaceae fam. nov.). *Phycologia,* 44: 416-440.

Litaker, R. W., Steidinger, K. A., Mason, P. L., Landsberg, J. H., Shields, J. D., Reece, K. S., Haas, L. W., Vogelbein, W. K., Vandersea, M. W., Kibler, S. R. & Tester, P. A. 2005. The reclassification of *Pfiesteria shumwayae* (Dinophyceae): *Pseudopfiesteria*, gen. nov. *J. Phycol.*, 41: 643-651.

Lomas, M. W. & Glibert, P. M. 2000. Comparison of nitrate uptake, storage, and reduction in marine diatoms and flagellates. *J. Phycol.*, 36: 903-913.

MacKenzie, L. 1991. Toxic and noxious phytoplankton in Big Glory Bay, Stewart Island, New Zealand. *J. Appl. Phycol.*, 3: 19-34.

Marshall, J. A., Nichols, P. D., Hamilton, B., Lewis, R. J. & Hallegraeff, G. M. 2003. Ichthyotoxicity of Chattonella marina (Raphidophyceae) to damselfish (Acanthochromis polycanthus): the synergistic role of reactive oxygen species and free fatty acids. *Harmful Algae*, 2: 273- 281.

Marshall, S. M. 1925. On *Proterythropsis vigilans*, n. sp. *Q. J. microsc. Sci.,* 69: 177-184.

Mason, P. L., Litaker, R. W., Jeong, H. J., Ha, J. H., Reece, K. S., Vogelbein, W. K., Stokes, N. A., Park, J. Y., Steidinger, K. A., Vandersea, M. W., Kibler, S., Tester, P. A. & Vogelbein, W. K. 2007. Description of a new genus of *Pfiesteria*-like dinoflagellate, *Luciella* gen.nov. (Dinophyceae), including two new species: *Luciella masanensis* sp. nov. and *Luciella atlantis* sp. nov. *J. Phycol.,* 43: 799-810.

Menden-Deuer, S. & Lessard, E. 2000. Carbon to volume relationships for dinoflagellates, diatoms, and other protist plankton. *Limnol. Oceanogr*., 45: 569-579.

Menden-Deuer, S., Lessard, E. J., Satterberg, J. & Grunbaum, D. 2005. Growth rates and starvation survival of three species of the pallium-feeding, thecate dinoflagellate genus *Protoperidinium*. *Aquat. Microb. Ecol*., 41: 145-152.

Medlin, L., Elwood, H. J., Stickel, S. & Sogin, M. L. 1988. The characterization of enzymatically amplified eukaryotic 16S-like rRNA-coding regions. *Gene,* 71: 491-499.

Moestrup, Ø. & Daugbjerg, N. 2007. On dinoflagellate phylogeny and classification. *In*: Brodie, J. & Lewis, J. (ed.), Unravelling the Algae: The Past, Present, and Future of Algae Systematics. Systematics Association Special Volumes, Vol 75. CRC Press, Boca Raton, Florida, p. 215-230.

Moestrup, Ø., Hansen, G. & Daugbjerg, N. 2008. Studies on woloszynskioid dinoflagellates III: On *Borghiella* gen. nov., and *B. dodgei* sp. nov., a cold-water species from Lake Tovel, N. Italy, and on *B. tenuissima* comb. nov. (syn. *Woloszynskia tenuissima*). *Phycologia,* 47: 54-78.

Moestrup, Ø., Hansen, G., Daugbjerg, N., Flaim, G. & D'Andrea, M. 2006. Studies on woloszynskioid dinoflagellates II: On *Tovellia sanguinea* sp. nov., the dinoflagellate species responsible for the reddening of Lake Tovel, N. Italy. *Eur. J. Phycol.,* 41: 47-65.

Moestrup, Ø., Lindberg, K. & Daugbjerg, N. 2009a. Studies on woloszynskioid dinoflagellates IV: the genus *Biecheleria* gen. nov. *Phycol. Res.,* 57: 203-220.

Moestrup, Ø., Lindberg, K. & Daugbjerg, N. 2009b. Studies on woloszynskioid

dinoflagellates V. Ultrastructure of *Biecheleriopsis* gen. nov., with description of *Biecheleriopsis adriatica* sp. nov. *Phycol. Res.,* 57: 221-237.

Montresor, M., Procaccini, G. & Stoecker, D. K. 1999. *Polarella glacialis* gen. et sp. nov. (Dinophyceae): Suessiaceae are still alive! *J. Phycol.,* 35: 186-197.

Mornin, L. & Francis, D. 1967. The fine structure of *Nematodinium armatum*, a naked dinoflagellate. *J. Microscopie,* 6: 759-772.

Murray, S. & Patterson, D. J. 2004. *Cabra matta*, gen. nov., sp. nov., a new benthic, heterotrophic dinoflagellate. *Eur.J. Phycol.,* 39: 229-234.

Murray, S., Hoppenrath, M., Preisfeld, A., Larsen, J., Yoshimatsu, S. A., Toriumi, S. & Patterson, D. J. 2006. Phylogenetics of *Rhinodinium broomeense* gen. et sp. nov., a peridinoid, sand-dwelling dinoflagellate (Dinophyceae). *J. Phycol.,* 42: 934-942.

Nakamura, Y., Suzuki, S. & Hiromi, J. 1995. Population dynamics of heterotiophic dinoflagellates during a *Gymnodinium mikimotoi* red tide in the Seto Inland Sea. *Mar. Ecol. Prog. Ser.,* 125: 269-277.

National Fisheries Research and Development Institute (NFRDI), 2012. Data on red tides. http://www.nfrdi.re.kr/redtideinfo (in Korean).

Omand, M. M., Leichter, J. J., Franks, P. J. S., Guza, R. T., Lucas A. J. & Feddersen. F. 2011. Physical and biological processes underlying the sudden surface appearance of a red tide in the nearshore. *Limnol. Oceanogr.*, 56: 787-801.

Paasche, E. 1973. Silicon and the ecology of marine plankton diatoms. II. Silicate-uptake kinetics in five diatom species. *Mar. Biol.*, 19: 262-269.

Park, J. Y., Jeong, H. J., Yoo, Y. D. & Yoon, E. Y. 2013. Mixotrophic dinoflagellate red tides in Korean waters: Distribution and ecophysiology. *Harmful Algae*,

30: S28-S40.

Park, T. G., Christopher, J. S., Bolch, C. J. S. & Hallegraeff, G. M. 2007. Larval *Crassostrea* bivalve and *Artemia* brine shrimp bioassays to assess toxicity and micropredation by the heterotrophic dinoflagellates *Cryptoperidiniopsis brodyi* and *Pfiesteria piscicida* from Australian waters. *J. Plankton Res.,* 29: 791-801.

Park, T. G., Park, G. H., Park, Y. T., Kang, Y. S., Bae, H. M., Kim, C. H., Jeong, H. J. & Lee, Y. 2009. Identification of the dinoflagellate community during *Cochlodinium polykrikoides* (Dinophyceae) blooms using amplified rDNA melting curve analysis and real-time PCR probes. *Harmful Algae*, 8: 430-440.

Pascher, A. 1914. Über Flagellaten und Algen. *Deutsche Botanische Gesellschaft,* 32: 136-160.

Porter, K. G. & Feig, Y. S. 1980. The use of DAPI for identifying and counting aquatic microflora. *Limnol. Oceanogr.*, 25: 943-948.

Posada, D. & Crandall, K. A. 1998. Modeltest: testing the model of DNA substitution. *Bioinformatics,* 14: 817-818.

Potvin, E., Jeong, H. J., Kang, N. S., Tillmann, U. & Krock, B. 2012. First report of the photosynthetic dinoflagellate genus *Azadinium* in the Pacific Ocean: morphology and molecular characterization of *A*. cf. *poporum*. *J. Eukaryot. Microbiol.*, 59: 145-156.

Reid, P. C. 1980. Toxic dinoflagellates and tidal power generation in the Bay of Fundy, Canada. *Mar. Pollut. Bull.*, 11: 47-51.

Rensel, J. E, Haigh, N. & Tynan, T. J. 2010. Fraser River Sockeye Salmon marine survival decline and harmful blooms of *Heterosigma akashiwo*. *Harmful Algae*, 10: 98-115.

Reynolds, C. S. 1994. The role of fluid motion in the dynamics of phytoplankton in lakes and rivers. In: Giller, P.S., Hildrew, A.G., Raffaelli, D.G. (Eds.), Aquatic Ecology. Scale, Pattern and Process. British Ecological Society. Blackwell Science Oxford, UK, pp. 147-187.

Roberts, K. R., Heimann, K. & Wetherbeer. 1995. The flagellar apparatus and canal structure in *Prorocentrum micans* (Dinophyceae). *Phycologia,* 34: 313-322.

Saldarriaga, J. F., Leander, B. S., Taylor, F. J. R. & Keeling, P. 2003. *Lessardia elongata* gen. et. sp. nov. (Dinoflagellata, Peridiniales, Podolampaceae) and the taxonomic position of the genus *Roscoffia*. *J. Phycol.,* 39: 368-378.

Seong, K. A., Jeong, H. J., Kim, S., Kim, G. H. & Kang, J. H. 2006. Bacterivory by co-occuring red-tide algae, heterotrophic nanoflagellates, and ciliates. *Mar. Ecol. Prog. Ser.*, 322: 85-97.

Sherr, E. B. & Sherr, B. F. 2007. Heterotrophic dinoflagellates: a significant component of microzooplankton biomass and major grazers of diatoms in the sea. *Mar. Ecol. Prog. Ser.,* 352: 187-197.

Shin, J. K., Kim, D. S. & Cho, K. J. 2000a. Dynamics of water environment factors and phytoplankton before and after inflow of seawater in Shihwa Reservoir. *J. Korean Environ. Sci. Soc.,* 9: 115-123. (in Korean, with English abstract).

Shin, J. K., Kim, D. S. & Cho, K. J., 2000b. Dynamics of inorganic nutrients and phytoplankton in Shihwa Reservoir. *Korean J. Limnol.*, 33: 109-118. (in Korean, with English abstract).

Shyam, R. & Sarma, Y. S. R. K. 1975. *Woloszynskia stoschii* and *Gymnodinium indicum*, two new freshwater dinoflagellates from India: morphology, reproduction and cytology. *Plant Syst. Evol.*, 124: 205-212.

Siano, R., Kooistra, W. H. C. F., Montresor, M. & Zingone, A. 2009. Unarmoured

and thin-walled dinoflagellates from the Gulf of Naples, with the description of *Woloszynskia cincta* sp. nov. (Dinophyceae, Suessiales). *Phycologia,* 48: 44-65.

Siano, R., Montresor, M., Probert, I., Not, F. & Vargas, C. d. 2010. *Pelagodinium* gen. nov. and *P. béii* comb. nov., a dinoflagellate symbiont of planktonic foraminifera. *Protist,* 161: 385-399.

Smalley, G. W., Coats, D. W. & Adam, E. J. 1999. A new method for using fluorescent microspheres to determine grazing rates on ciliates by the mixotrophic dinoflagellate *Cerutium furca. Aquut. Microb. Ecol.,* 17: 167-179.

Smayda, T. J. 1997. Harmful algal blooms: Their ecophysiology and general relevance to phytoplankton blooms in the sea. *Limnol. Oceanogr*., 42: 1137-1153.

Smayda, T. J. 2002. Turbulence, watermass strafication and harmful algal blooms: an alternative view and frontal zones as “pelagic seed banks”. *Harmful algae,* 1: 95-112.

Smith, S. W., Overbeek, R., Woese, C. R., Gilbert, W. & Gillevet, P. M. 1994. The genetic data environment an expandable GUI for multiple sequence analysis. *CABIOS,* 10: 671-675.

Spurr, A. R. 1969. A low viscosity epoxy resin embedding medium for electron microscopy. *J. Ultrastruct. Res*., 26: 31-42.

Stamatakis, A. 2006. RAxML-VI-HPC: maximum likelihood-based phylogenetic analyses with thousands of taxa and mixed models. *Bioinformatics*, 22: 2688-2690.

Steidinger, K. A. 1983. A re-evaluation of toxic dinoflagellate biology and ecology.

Prog. Phycol. Res., 2: 147-278.

Steidinger, K. A., Landsberg, J. H., Mason, P. L., Vogelbein, W. K., Tester, P. A. & Litaker, R. W. 2006. *Cryptoperidiniopsis brodyi* gen. et sp. nov. (Dinophyceae), a small lightly armored dinoflagellate in the Pfiesteriaceae. *J. Phycol.,* 42: 951-961.

Stoecker, D., Tillmann, U. & Granéli, E. 2006. Phagotrophy in harmful algae. *In*: Granéli E, Turner J (ed.) Ecology of Harmful Algae, Series: Ecological Studies Vol. 189, Springer Verlag, Heidelberg, p. 177-187.

Stoecker, D. K., Li, A., Coats, D. W., Gustafson, D. E. & Nannen, M. K. 1997. Mixotrophy in the dinoflagellate *Prorocentrum minimum*. *Mar. Ecol. Prog. Ser.,* 152: 1-12.

Stoecker, D. K, Parrow, M. W, Burkholder, J. M. & Glasgow, H. B. Jr. 2002. Grazing by microzooplankton on *Pfiesteria piscicida* cultures with different histories of toxicity *Aquat. Microb. Ecol.,* 28: 79-85.

Stoecker, D. K. & Sanders, N. K. 1985. Differential grazing by *Acartia tonsa* on a dinoflagellate and a tintinnid. *J. Plankton Res.,* 7: 85-100.

Sundström, A. M., Kremp, A., Daugbjerg, N., Moestrup, Ø., Ellegaard, M., Hansen, R. & Hajdu, S. 2009. *Gymnodinium corollarium* sp. nov. (Dinophyceae)- a new cold-water dinoflagellate responsible for cyst sedimentation events in the Baltic Sea. *J. Phycol.* 45: 938-952.

Takano, Y. & Horiguchi, T. 2003. A phylogenetic study of freshwater dinoflagellate. In: Matsuoka, K., Yoshida, M. & Iwataki, M. (eds), Seventh International Conference on Modern and Fossil Dinoflagellates, Nagasaki 21–25 September 2003. Book of Abstracts. Nagasaki University, Nagasaki, Japan. p. 115.

Takayama, H. 1985. Apical grooves of unarmored dinoflagellates. *Bull. Plankton Soc. Jpn.,* 32: 129-140.

Tang, Y. Z., Egerton, T. A., Kong, L. & Marshall, H. G. 2008. Morphological variation and phylogenetic Analysis of the dinoflagellate *Gymnodinium aureolum* from a tributary of Chesapeake Bay. *J. Eukaryot. Microbiol*., 55: 91-99.

Taylor, F. J. R. 1987. The Biology of Dinoflagellates. Blackwell, Boston, p. 126-134.

Terrado, R., Vincent, W. F. & Lovejoy, C. 2009. Mesopelagic protists: diversity and succession in a coastal Arctic ecosystem. *Aquat. Microb. Ecol.*, 56: 25-39.

Thomas, W. H. & Gibson, C. H. 1990. Effects of small-scale turbulence on microalgae. *J. Appl. Phycol.*, 2: 71-77.

Thomas, W. H., Vernet, M. & Gibson, C. H. 1995. Effects of small-scale turbulence on photosynthesis, pigmentation, cell division, and cell size in the marine dinoflagellate *Gonyaulax polyedra* (Dinophyceae). *J. phycol.*, 31: 50-59.

Thompson, R. H. 1951. A new genus and new records of freshwater Pyrrhophyta in the Desmokontae and Dinophyceae. *Lloydia*, 13: 277-299.

Tomas, C. R. 1979. *Olisthodiscus leteus* (Chrysophyceae). Ⅲ. Uptake and utilization of nitrogen and phosphorus. *J. Phycol.*, 15: 5-12.

Tsutsumi, H., Okamura, E., Ogawa, M., Takahashi, T., Yamaguchi, H., Montani, S., Kohashi, N., Adachi, T. & Komatsu, T. 2003. Studies of the cross section of water in the innermost area of Ariake Bay with the recent occurrence of hypoxic water and red tide. *Oceanogr. Japan*., 12: 291-305.

Tynan, C. T. 1993. The effects of small-scale turbulence on dinoflagellates. Disseration. Scripps Institution of Oceanography. University of California,

San Diego. 227 p.

Watanabe, M. M., Takeda, Y., Sasa, T., Inouye, I., Suda, S., Sawaguchi, T. & Chihara, M. 1987. A green dinoflagellate with chlorophylls a and b morphology fine structure of the chloroplast and chlorophyll composition. *J. Phycol.,* 23: 382-389.

Watanabe, M. M., Suda, S., Inouye, I., Sawaguchi, T. & Chihara, M. 1990. *Lepidodinium viride* gen. et sp. nov. (Gymnodiniales, Dinophyta), a green dinoflagellate with chlorophyll A- and B-containing endosymbiont. *J. Phycol.,* 26: 741-751.

Welch, P. S. 1948. Limnological methods. The Blaikston Co., Philadelphia. 381 p.

Westfall, J. A., Bradbury, P. C. & Townsend, J. W. 1983. Ultrastructure of the dinoflagellate *Polykrikos*. I. Development of the nematocyst-taeniocyst complex and morphology of the site for extrusion. *J. Cell Sci*., 63: 245-261.

Woloszynska, J. 1917. Neue Peridineen-arten nebst Bemerkungen Überden Bau der HÜlle bei *Gymno*- und *Glenodinium. Bulletin Internationalde l'Académie des Sciences de Cracovie. Classe des Sciences Mathématiques et Naturelles, Série B, Sciences Naturelles* 1917: 114-122.

Wuyts, J., De Rijk, P., Van de Peer, Y., Winkelman, T. & DeWachter, R. 2001. The european large subunit ribosomal RNA database. *Nucleic Acid Res.,* 29: 175-177.

Xingyu, S., Liangmin, H., Jianlin, Z., Honghui, H., Tao, L. & Qiang, S. 2009. Harmful algal blooms (HABs) in Daya Bay, China: an in situ study of primary production and environmental impacts. *Mar. Poll. Bul.*, 58: 1310-1318.

Yang, Z. B., Hodgkiss, I. J. & Hansen, G. 2001. *Karenia longicanalis* sp. nov.

(Dinophyceae): a new bloom-forming species isolated from Hong Kong, May 1998. *Botanica Marina,* 44: 67-74.

Yih, W., Kim, H. S., Jeong, H. J., Myung, G. & Kim, Y. G. 2004. Ingestion of cryptophytes cells by the marine photosynthetic ciliate *Mesodinium rubrum*. *Aquat. Microb. Ecol.*, 36: 165-170.

Yih, W., Myung, G., Yoo, Y. D., Kim, Y. G. & Jeong, H. J. 2005. Semiweekly variation of spring phytoplankton community in relation to the freshwater discharges from Keum River estuarine weir, Korea. *The Sea*, 10: 154-163. (in Korean, with English abstract).

Yoo, Y. D., Yoon, E. Y., Kang, N. S. & Jeong, H. J. 2013. Growth and ingestion rates of heterotrophic dinoflagellates and a ciliate on the mixotrophic dinoflagellate *Biecheleria cincta*. *Algae*, 28: 343-354.

Yoo, Y. D., Jeong, H. J., Kang, N. S., Song, J. Y., Kim, K. Y., Lee, K. T. & Kim, J. H. 2010. Feeding by the newly described mixotrophic dinoflagellate *Paragymnodinium shiwhaense*: feeding mechanism, prey species, and effect of prey concentration. *J. Eukaryot. Microbiol.,* 57: 145-158.

Yoo, Y. D., Jeong, H. J., Kim, M. S., Kang, N. S., Song, J. Y., Shin, W. G., Kim, K. Y. & Lee, K. T. 2009. Feeding by phototrophic red-tide dinoflagellates on the ubiquitous marine diatom *Skeletonema costatum*. *J. Eukaryot. Microbiol.,* 56: 413-420.

Yoo, Y. D., Jeong, H. J., Shim, J. H., Park, J. Y., Lee, K. J., Yih, W., Kweon, H. K., Pae, S. J. & Park, J. K. 2002. Outbreak of red tides in the coastal waters off the southern Saemankeum areas, Jeonbuk, Korea. 1. Temporal and spatial variations in phytoplankton community in the summer-fall of 1999. *The Sea*, 7: 129-139.

Yoon, E. Y., Kang, N. S. & Jeong, H. J. 2012. *Gyrodinium moestrupii* n. sp., A new planktonic heterotrophic dinoflagellate from the coastal waters of western Korea: morphology and ribosomal DNA gene sequence. *J. Eukaryot. Microbiol.,* 59: 571-586.

Yu, J., Yang, G. & Tian, J. 2010. The effects of the harmful alga *Heterosigma akashiwo* on cultures of *Schmackeria inopinus* (Copepoda, Calanoida). J. Sea Res., 64: 287-294.

Zapata, M., Rodriguez, F. & Garrido, J. L. 2000. Separation of chlorophylls and carotenoids from marine phytoplankton: a new HPLC method using a reversed phase C8 column and pyridine containing mobile phases. *Mar. Ecol. Prog. Ser.*, 195: 29-45.

Zar, J. H. 1999. Biostatistical analysis, 4th edition.. Prentice Hall, Upper Saddle River, NJ.

국문초록

적조는 수중의 식물플랑크톤이 대량 증식 또는 집적되어 바닷물의 수색을 변색되는 현상으로 어패류, 해양 포유류의 대량 폐사를 야기하고, 때때로 해양 미소생태계의 균형을 파괴시킨다. 특정한 지역에서의 적조 동태와 적조로 인한 경제적 영향을 이해하기 위해서는, 적조 원인종을 정확히 동정 해야하고, 그들의 풍도를 조사하여야 한다. 게다가, 이전에 보고 되지 않은 종이라면, 그들의 분류 연구와 함께 생태생리에 대한 연구를 수행하여야 한다.

제한된 물의 흐름과 육상으로부터 높은 농도에 영양염이 공급되는 하구역이나 만은 적조 발생에 좋은 지역이다. 그러나, 물리적으로 거대한 난류가 발생되는 지역이나 물의 혼합이 잘 일어나는 지역에서는 적조의 발생을 억제하기도 한다. 시화호는 제한된 물의 흐름, 높은 영양염 유입, 난류와 물의 혼합에 의한 적조 발생의 영향을 연구하기에는 좋은 연구 지역이다. 시화 방조제는 총 길이가 12.7-km로 1994년에 완공되었다. 시화 방조제에는 길이 100m 배수갑문을 통해 매일 시화 방조제 안쪽과 바깥쪽에 물이 순환되고 있지만, 방조제로 인해 물의 흐름이 제한되어 있고, 그로 인해 조석 간만의 차가 3−5m로 줄어들었다. 그러나, 시화호 방조제 중앙에 위치한 세계 최대 규모의 조력발전소가 2011년에 완공되었고 밀물 때의 낙차를 이용한 단류식 창조 발전으로 터빈을 통해 물이 순환되고 있다.

시화호에서의 적조 동태를 이해하기 위하여, 조력발전소 설립 전·후 적조 발생과 발전소를 통한 물의 흐름의 변화에 따른 영향을 알아보고자 물리, 화학, 생물학적 특성을 3개 고정 정점에서 2008년 5월부터 2012년 7월까지 매달 현장 시료 채집과 측정을 통해 분석 하였다

(Chapter 2). 연구기간 동안, 시화호에서 와편모류를 순수 분리하여 단독 배양체 확립에 성공하였고, 단종 배양체를 이용하여 형태/유전자적 분류 분석을 통해 두개의 신속 *Paragymnodinium*과 *Gyrodiniellum*을 수립하였다 (Chapter 3과 4). 게다가, 한국 연안에서 발견되지 않은 *Biecheleria cincta*를 시화호에서 발견하였고 그들의 생태생리학에 대해 연구하였다 (Chapter 5). *Biecheleria cincta*는 다양한 먹이를 섭식하는 혼합영양성 와편모류로 밝혀졌다. 본 논문의 종합적인 결과는 시화호에서 발생하는 적조 동태를 이해하는데 기초 자료를 제공할 것으로 판단된다.

Chapter 2에서는 적조 발생과 물의 흐름의 변화에 따른 영향을 알아봤다. 물의 순환물의 흐름이 제한된 정점 1 (시화호 안쪽)은 배수갑문을 통해 시화호 내측과 외측에 물이 교환되는 정점 3에 비해 광영양성 와편모류종들에 의해 적조가 더욱 빈번하게 발생하였다. 2011년 조력 발전소 건설된후에 적조 원인종이 광 영양성 와편모류 (*Gymnodinium aureolum*, *Heterocapsa rotundata*, *Heterocapsa triquetra*, *Karlodinium veneficum*, *Paragymnodinium shiwhaense*, *Prorocentrum minimum*)에서 규조류 (*Chaetoceros* spp., *Skeletonema costatum*, *Thalassiosira* spp.)로 변화되었다. 조력 발전소 가동으로 인해 생긴 시화호 안쪽과 바깥쪽의 물의 순환이 적조 원인종의 변화를 가져왔을 것이다. 연구 기간 동안 무기 질소 농도는 광 영양성 와편모류종과 작은 편모조류들의 성장에 대해서 제한 요소가 아니였지만 무기인 농도는 이들의 성장에 제한 요소였다. 그래서 일부 광 영양성 와편모류종과 편모조류들은 먹이 섭식을 통해서 인을 공급받을 것으로 판단된다. 종속영양성 와편모류 (*Pfiesteria piscicida*, *Gyrodiniellum shiwhaense*, *Gyrodinium dominans, Gyrodinium moestrupii*, *Protoperidinium bipes*)가 적조 원인종 (Cryptophytes, *Eutreptiella gymnastica*, *P. minimum*, *S. costatum*)을 섭식하였을 때 0.14-0.77 h^{-1}이였다. 그러므로, 종속영양성 원생생물들은 시화호에서 적조 원인종의

군집과 함께 출현하였을 때 상당한 포식압을 끼치는 것으로 나타났다.

Chapter 3에서는 광 영양성 신속 와편모류를 수립하였다. 광 영양성 와편모류 *Paragymnodinium shiwhaense*의 형태적 특징을 분석하고 기술하기 위해 생 시료와 고정 시료을 이용하여 광학현미경, 주사/투과 전자현미경을 사용하여 정확한 분류을 실시했다. 또한, SSU, ITS1, 5.8S, ITS2, D1-D3 LSU rDNA 지역의 염기 서열 분석과 엽록소를 분석하였다. 상각은 conical과 하각은 hemispherical의 모양을 보였고, 세포의 세포벽은 다각형의 amphiesmal vesicles로 이루어져 있었으며 16줄로 이루어져 있었다. *P. shiwhaense*는 속 (genus) 수준의 분류키가 되는 apical groove나 apical line plates를 가지고 있지 않고, 대신에 sucal extension-like furrow를 가지고 있었다. 먹이인 *Amphidinium carterae*를 섭식하였을때의 길이와 폭은 8.4-19.3과 6.1-16.0 μm 였다. 또 다른 속 수준의 분류키인 nuclear envelope chamber이나 nuclear fibrous connective (NFC)이 관찰되지 않았다. *P. shiwhaense*는 엽록체, 자포 (nematocysts), 모포 (trichocysts), 섭식 빨때 (peduncle), 안점 (eyespots), 피레노이드 (pyrenoids)가 관찰 되었지만, 수낭(pusule)은 관찰되지 않았고 이 종의 주 색소는 peridinin으로 나타났다. *P. shiwhaense*의 SSU rDNA (GenBank AM408889) 염기서열을 통해 다른 종과 비교 분석한 결과 가장 가까운 근연종인 *Gymnodinium aureolum*, *Lepidodinium viride*, *Gymnodinium catenatum*과 4% 차이를 보였고, LSU rDNA는 *G. catenatum*, *Lepidodinium chlorophorum*, *Gymnodinium nolleri*과 17-18% 차이를 보였다. 또한 *P. shiwhaense*는 분류계통학적 계통도 분석 결과 *Gymnodinium* sensu stricto clade에 속한 것으로 나타났다. 하지만, *Gymnodinium* sensu stricto clade에 속해 있는 *Gymnodinium* spp. and *Lepidodinium* spp.과 달리 nuclear envelope chambers, NFC, apical groove를 가지고 있지 않아 그 들 속들과 차이를 보였다. Nemetocyst를 가지고 있다고 보고된 속은 *Polykrikos*, *Warnowia*, *Nematodinium*, *Proterythropsis*가 보고됐다. *Polykrikos* spp.의 자포

기관은 taeniocyst-nematocyst complex로 이루어져 있지만 *P. shiwhaense*는 taeniocysts 기관이 없이 자포로만 구성되어 있어 *Polykrikos* spp.과 차이점을 보였다. 또한 자포 기관을 가지고 있는 *Warnowia* spp.와 *Nematodinium* spp.과 달리 *P. shiwhaense*는 ocelloids (안구)를 가지고 있지 않았다. 그러므로 형태/분자적 분류 분석 결과를 토대로 *P. shiwhaense*는 신속/신종이라 판단된다.

Chapter 4에서는 종속영양성 신속 와편모류를 수립하였다. 종속영양성 와편모류인 *Gyrodiniellum shiwhaense*의 형태적 특징을 분석하고 기술하기 위해 생 시료와 고정 시료을 이용하여 광학현미경, 주사/투과 전자현미경을 사용하여 정확한 분류을 실시했다. 또한, SSU, ITS1, 5.8S, ITS2, D1-D3 LSU rDNA 지역의 염기 서열 분석을 실시했다. 상각은 conical 모양을 보였고 하각은 ellipsoid였다. 세포의 세포벽은 다각형의 amphiesmal vesicles로 이루어져 있었으며 16줄로 이루어져 있었다. *Gyrodinium*-like종들 (타원형)과 달리, loop-shaped 형태의 apical groove를 가졌다. 먹이인 *Amphidinium carterae*를 섭식하였을때의 길이와 폭은 9.1-21.6과 6.6-15.7 μm였다. *G. shiwhaense*는 자포, 모포, 빨대 섭식 기관, 수낭를 가졌지만, 엽록체는 관찰되지 않았다. *G.. shiwhaense*의 SSU rDNA 염기서열을 통해 다른 종과 비교 분석한 결과 가장 가까운 근연종은 *Warnowia* sp., *Lepidodinium viride*, *Gymnodinium aureolum*, *Gymnodinium catenatum*, *Nematodinium* sp., *Gymnodinium* sp.으로 >3% 차이를 보였고, LSU rDNA는 가장 가까운 근연종인 *Warnowia* sp., *G. aureolum, Nematodinium* sp. 등과 11-12% 차이를 보였다. 분류계통학적 계통도를 분석한 결과 *G. shiwhaense*는 *Gymnodinium* sensu stricto clade에 속했지만 *Gymnodinium* sensu stricto clade에 속해 있는 *Gymnodinium*, *Lepidodinium*과 달리 nuclear envelope chambers와 nuclear fibrous connective를 가지고 있지 않아서 이들 속들과 차이점을 보였다. 지금까지 nemetocyst를 가지고 있다고 보고된 속은 *Paragymnodinium*,

Polykrikos, *Warnowia*, *Nematodinium*, *Proterythropsis*등으로 *Gyrodiniellum*은 이들 속들과 자포 구조의 차이점을 보였다. *Polykrikos*의 자포는 taeniocyst–nematocyst의 복합체 구조를 가지고 있으나, *G. shiwhaense*는 taeniocysts를 가지고 있지 않았고, *G. shiwhaense*는 *Paragymnodinium shiwhaense*과 달리 자포 기관속에 stylets과 filaments이 관찰됐다. 마지막으로, 자포 기관을 가지고 있는 *Warnowia* spp., *Nematodinium* spp., *Proterythropsis* spp.과 달리 *G. shiwhaense*는 ocelloids의 구조가 관찰되지 않았다. 그러므로 형태/유전자적 분류 분석 결과를 토대로 *G. shiwhaense*는 신속/신종으로 판단된다.

Chapter 5에서는 한국에서 발견되지 않았던 광 영양성 와편모류인 *Biecheleria cincta*의 생태생리에 대해 연구를 수행했다. Suessiales 목에 속하는 *Biecheleria* 종들은 해양과 담수에서 서식하는데 생태생리에 대한 연구 및 그들의 영양 방식에 대한 연구도 미흡한 실정이다. 이전 연구에서는 모든 *Biecheleria* 종들은 광합성을 한다고 보고되었지만 혼합영양성에 대해서는 연구가 되어지지 않았다. 시화호에서 와편모류를 순수분리하여 단종 배양체를 확립하였고, 단종 배양체를 형태/유전자적 분류 분석을 통해 *Biecheleria cincta* (=*Woloszynskia cincta*)로 판단하였다. 또한, *B. cincta*가 혼합 영양성 와편모류라고 밝혔다. *B. cincta*은 빨대 섭식기관을 이용하여 먹이를 섭식하였고, 다양한 분류군의 먹이를 공급하였을 때 *B. cincta*는 먹이의 크기 (Equivalent spherical diameter; ESD)가 12.6 ㎛보다 작은 먹이는 섭식할 수 있었지만 (*Skeletonema costatum, Prorocentrum minimum*)는 제외, ESD가 15 ㎛보다 큰 먹이는 섭식하지 않는 것으로 나타났다. *B. cincta*가 *Heterosigma akashiwo*를 섭식하였을 때 *H. akashiwo* 농도가 포화농도 ca. 134 ng C ml^{-1} (1,340 cells ml^{-1})로 될 때까지 *B. cincta* 성장률이 계속 증가하였다. *B. cincta*가 광도가 20 µE m^{-2} s^{-1} 에서 광합성시 최대 성장률은 0.040 d^{-1}이었으나, 먹이인 *H. akashiwo*를 섭식하였을 때 *B. cincta*의 최대 성장률은 0.499 d^{-1} 로 나타났다. 또한, *B. cincta*가

침편모류인 *H. akashiwo*를 섭식하였을 때 최대 섭식율과 여과율은 0.49 ng C grazer^{-1} d^{-1} (4.9 cells grazer^{-1} d^{-1})와 1.9 μl grazer^{-1} h^{-1}였다. 실험실에서 측정한 섭식율을 이용하여 현장에서 *B. cincta*와 *H. akashiwo*가 동시에 출현하였을 때 포식압을 구한결과 1.1 d^{-1}로 나타났다. 이와 같은 결과 혼합영양성 와편모류인 *B. cincta*는 먹이 생물 군집에 상당한 포식압을 끼치는 것으로 나타났다.

결론적으로, 본 연구 결과는 조력 발전소 가동으로 인해 생긴 시화호 안쪽과 바깥쪽의 물의 순환이 적조 원인종의 변화를 가져왔을 가능성이 있다고 제안하고, 신속 와편모류 발견은 생태생리, 진화, 산업적 이용 연구 측면에서 기초 자료를 제공될 것으로 기대하며, 크기가 작은 (<20μm) 광 영양성 와편모류 *Biecheleria cincta*의 혼합영양 능력의 발견은 해양 생태계 내에서 크기가 작은 혼합 영양성 와편모류의 생태학적 역할에 대한 이해를 높일 것으로 생각된다.

Keywords: 생태, 유해조류 대발생, 생리, 원생생물, 적조, 분류

Student Number: 2005-23246